



Kundegorski, Mikolaj Edmund (2025) *Quantitative analysis of the collective movement and migratory behaviour of Atlantic salmon*. PhD thesis.

<https://theses.gla.ac.uk/84996/>

Copyright and moral rights for this work are retained by the author

A copy can be downloaded for personal non-commercial research or study, without prior permission or charge

This work cannot be reproduced or quoted extensively from without first obtaining permission from the author

The content must not be changed in any way or sold commercially in any format or medium without the formal permission of the author

When referring to this work, full bibliographic details including the author, title, awarding institution and date of the thesis must be given

Enlighten: Theses

<https://theses.gla.ac.uk/>
research-enlighten@glasgow.ac.uk

Quantitative analysis of the collective movement and migratory behaviour of Atlantic salmon

Mikolaj Edmund Kundegorski

Submitted in fulfilment of the requirements for the
Degree of Doctor of Philosophy

School of Mathematics & Statistics
College of Science and Engineering
University of Glasgow



September 2024

In memory of my grandfathers Edmund Nowacki and Kazimierz Kundegorski.

Abstract

The migration of Atlantic salmon (*Salmo salar*) is a complex ecological process of great importance to conservation and ecosystem management. Despite a rapid decline in the Atlantic salmon population, little is known about the fine-scale behaviour of juvenile migration to the sea, which occurs in an environment under strong anthropogenic pressure and results in high mortality.

Juvenile salmon migration involves large quantities of small animals travelling underwater through a complex riverine landscape. It is difficult to study, but recent advances in tracking technology and mathematical methods now allow the behaviour and ecology of downstream migrating salmon to be explored in depth.

This thesis reviews recent advances in the study of Atlantic salmon, and develops further the mathematical and computational methods of movement ecology. These help in forming hypotheses about how the fish behave, leading to laboratory experiments that focus on their responses to flow conditions, social influences during obstacle navigation, and the behavioural differences between wild and hatchery-reared individuals.

Impounded waters pose a challenge for migrating smolts due to the lack of strong flow to provide directional cues. In laboratory experiments, I established the baseline flow values that prompt a behavioural response in salmon smolts, necessary for the design of river structures. In another experiment, I showed evidence of collective decision-making in navigating obstacles during movement in an experimental flume. This finding emphasises the density-dependent factors in migration success and necessitates further study of the collective behaviour of this species that have thus far been mostly under-explored. I also show clear differences in behaviour of hatchery animals compared to wild ones, providing guidance on the usability of hatchery smolts in further studies and design of river infrastructure.

Modern machine learning methods allow improved analysis of data in many contexts. Improvements to visual tracking of fish based on deep-learning models are presented, allowing for detailed analysis of movement in laboratory and field experiments where

video cameras are becoming ever more prevalent. In this thesis, I present a new visual tracking method that is tailored to correctly predict the movement of animals and tested on simulated data inspired by common movement models.

The Bayesian modelling framework of Approximate Bayesian Computation is leveraged to analyse movement patterns from acoustic telemetry data. This simulation-based method combines the hypotheses about the fine-scale movement with computational methods that allow efficient parallelisation on GPU-accelerated hardware.

This thesis provides insights into the migratory behaviour of Atlantic salmon smolts, with significant implications for conservation efforts, ecological engineering applications, and the design of effective river infrastructure. The findings emphasise the necessity of considering social behaviours and the differences between wild and hatchery fish in both modelling and practical implementations to aid in the preservation of this important species.

Acknowledgements

I would like to sincerely thank my supervisors Colin Torney, Colin Adams and Shaun Killen for making this exciting project possible and guiding me along the way.

Nicol McCallum, Matt Newton, Krzysztof Stanik and Witold Kundegorski deserve great thanks for the technical work put into building and running the behavioural experiments. I'm grateful for scientific and literary help provided by Hannele Honkanen, Peter Koene, Jenn Gaskell, Adrian Bowman, Chas Nelson and Grégoire Payen de La Garanderie.

Declaration

I hereby declare that the material presented in this thesis is the result of original research, conducted by the author between October 2018 and September 2024, under the supervision of Professor Colin Torney, Professor Shaun Killen, and Professor Colin Adams. This work has not been submitted in whole or in part for consideration towards the fulfilment of any other degree or qualification in this, or any other university.

Place and Date

Signature

Contents

1	Introduction	13
1.1	Ecology and biology of salmon	13
1.1.1	Atlantic salmon (<i>Salmo salar</i>)	14
1.1.2	Brown trout (<i>Salmo trutta</i>)	15
1.1.3	Arctic charr (<i>Salvelinus alpinus</i>)	15
1.1.4	Pacific salmon, genera <i>Oncorhynchus</i>	16
1.1.5	Ecology of salmon	16
1.1.5.1	Downstream migration	18
1.1.5.2	Collective behaviour	20
1.1.5.3	Importance of salmon	21
1.1.6	Threats to salmon population	23
1.1.6.1	Effect of changing temperatures	24
1.1.6.2	Habitat degaradation and farming	25
1.1.6.3	Barriers	26
1.1.6.4	Predation	28
1.1.7	Studying Atlantic salmon	29
1.1.7.1	Direct Observation	29
1.1.7.2	Catching	29
1.1.7.3	Electrofishing	30
1.1.7.4	Radio tags	30
1.1.7.5	Acoustic telemetry	31
1.1.7.6	Sonars	32
1.1.7.7	Direct Experimentation	33
1.2	Quantitative movement ecology	34
1.2.1	Ecological research	34
1.2.2	Mathematical modelling of animal movement	35

1.2.2.1	Lagrangian modelling	36
1.2.2.2	Eulerian Approach	39
1.2.2.3	State-space models	40
1.2.3	Collective behaviour	42
1.2.3.1	Mechanisms of collective behaviour	42
1.2.3.2	Modelling collective behaviour	43
1.2.3.3	Empirical studies of collective behaviour	44
1.2.3.4	Quantifying social and environmental factors	44
1.3	Modern mathematical methods in biology and ecology research	45
1.3.1	Changing Data Landscape	46
1.3.2	Machine learning	48
1.3.2.1	Supervised learning	48
1.3.2.2	Applications of Machine learning in Ecology	52
1.3.2.3	Unsupervised learning	53
1.4	Applications in the context of salmon migration	55
1.4.1	Outline of this thesis	57
2	Defining the water flow cues for navigation in migrating Atlantic salmon smolts	59
2.1	Abstract	59
2.2	Introduction	60
2.3	Methods	62
2.4	Results	66
2.5	Discussion	68
3	Predicting complex movement of multiple animals in simulated video recordings	72
3.1	Introduction	72
3.1.1	Motivation	72
3.1.2	Contribution	78
3.1.3	Background: Visual tracking of animals	79
3.1.3.1	Overview	79
3.1.3.2	Localisation	79
3.1.3.3	Image recognition	81
3.1.3.4	Track Linking	85
3.1.3.5	Modern Tracking	86

3.1.3.6	Tracking in biology and ecology research	89
3.2	Methods	90
3.2.1	Detection of animals	91
3.2.2	Predicting object position with the Kalman Filter	93
3.2.2.1	Application of Kalman filter to image plane movement tracking	94
3.2.2.2	Formulation of Kalman-based methods	94
3.2.3	Deep Predictor	94
3.2.4	Simulated movement data	97
3.2.4.1	Training	99
3.2.4.2	Summary of test scenarios	99
3.2.4.3	Comparison methods	101
3.3	Results	102
3.4	Discussion	105
4	Collective decision making in laboratory experiment of smolt down- stream migration	112
4.1	Introduction	112
4.1.1	Preceding work	115
4.2	Experimental Setup	116
4.2.1	Salmon smolts	116
4.2.2	Artificial stream	116
4.2.3	Choice chamber	118
4.2.4	Camera setup	119
4.2.5	Video processing	121
4.2.6	Extraction of data for quantitative results	122
4.2.7	Trials	125
4.3	Modelling framework	125
4.3.1	Model Formulation	125
4.3.2	Covariates	127
4.3.2.1	Consideration of random effects	128
4.3.3	Model selection	128
4.4	Results	131
4.4.1	Observations	131
4.4.2	Frequency analysis of channel choices	132

4.4.3	Model interpretation	134
4.4.3.1	Comparison without trails with low-from differential	136
4.5	Discussion	136
5	Individual-based modelling of salmon downstream migration using ABC	140
5.1	Introduction	140
5.1.1	Telemetry	141
5.1.2	Approximate Bayesian Computation	143
5.1.2.1	Sample rejection ABC	145
5.1.2.2	Sequential Monte Carlo ABC	146
5.2	Methods	146
5.2.1	Spey river migration data	146
5.2.2	Simulation of river migration	147
5.2.2.1	Simulation	148
5.2.2.2	Model implementation	153
5.2.3	Design of summary statistic	154
5.2.3.1	Detector based statistics	155
5.2.3.2	General statistics	156
5.2.3.3	Normalisation of the statistics	156
5.2.3.4	Distance function	157
5.2.4	ABC modelling	158
5.2.5	Validation on simulated data	160
5.3	Results	162
5.3.1	Target parameter recovery	162
5.3.2	Quantile distribution	165
5.3.3	Example of parameter recovery from real system	169
5.4	Conclusions	171
6	Conclusions	175
6.1	Future work	179

List of Figures

1.1	Charismatic Atlantic salmon smolts.	14
1.2	Schematics of HMM and SSM models	40
2.1	Frequency response to flow reversal	68
2.2	Minimum flow velocity required for flow reversal	68
3.1	Challenges in animal tracking	74
3.2	Anaerobic burst swimming in fish	77
3.3	Convolutional Neural Networks	82
3.4	Simplified architecture of YOLO detector	84
3.5	Schematic of Deep Predictor	96
3.6	2D model of animal appearance	98
3.7	Time series plot and histogram of the movement model used for training .	100
3.8	Examples of movement patterns used for Deep Predictor training	101
3.9	Simple testing scenario A of track prediction	104
3.10	Comparison of track predictors	104
3.11	Complex testing scenario Z of track prediction with 3 animals	105
3.12	Simple testing scenario B of track prediction	107
3.13	Complex testing scenario Z of track prediction with 20 animals and identical appearance	108
3.14	Comparison of Deep Predictor with same and different appearance of objects	109
4.1	Experimental setup of the artificial stream at SCENE	117
4.2	Schematic of the choice chamber	119
4.3	Histogram of swimming directions of tracked fish	123
4.4	Illustration of tracked fish approaching the choice chamber	124
4.5	Comparison of BIC score for models with different formulation of influence variable	129

4.6	Comparison of BIC score for different complexity models	131
4.7	Illustration of different observations of group movement in the experiment with a choice chamber.	132
4.8	Frequency of channel choices for farmed and while fish	133
4.9	Interaction plot of the best-performing model	136
5.1	Map of the the river Spey	148
5.2	Number of registrations at different receivers on the river Spey	149
5.3	Difference in registration time between fish	149
5.4	ABC inference schematic	150
5.5	Schematic of the smolt migration movement simulation	150
5.6	Time series plot of the movement simulation	153
5.7	Summary statistic without normalisation	158
5.8	Normalised summary statistic	159
5.9	Absolute error of parameter recovery in ABC modelling	163
5.10	Relative error of parameter recovery in ABC modelling	164
5.11	Comprehensive results of posterior estimation on RiverShort model.	165
5.12	Comprehensive results of posterior estimation on SynthSpey model with social interaction.	166
5.13	Recovered posterior distribution and quantiles of repeated distributions for parameter vector θ_A^\dagger	168
5.14	Predicted posterior of parameter values from telemetry data on the river Spey	170

List of Tables

2.1	Fish Behavioural Responses to Flow Changes	65
3.1	Parameters of scenarios used for training of Deep Predictor	99
3.2	Parameters of evaluation scenarios	100
3.3	Results of average IoU of each method	103
3.4	Results breakdown by scenario and number of animals	106
4.1	Fish used in choice chamber experiment	117
4.2	Flow measures for all scenarios in the experiment.	126
4.3	Description of covariates used for statistical modelling.	127
4.4	AIC, BIC and Log Likelihood for different models	130
4.5	Frequency of fish choices in the choice chamber experiment	133
4.6	Ratio of non-influenced fish	134
4.7	Logistic Regression Coefficients Ordered by Z-value	135
5.1	Parameters used in the simulation	152
5.2	Hyper-parameters of RiverShort and SynthSpey simulations	154
5.3	Summary of receiver parameters for RiverShort model	154
5.4	Summary of receiver parameters for SynthSpey model	155
5.5	Results table for parameters μ and α	167
5.6	Results table for parameters β and λ	169
5.7	Results table for parameters P_{surv} and γ	169

Chapter 1

Introduction

1.1 Ecology and biology of salmon

Migration is observed in all major branches of the animal kingdom and describes different forms of long-term movement between habitats (Dingle and Drake, 2007). Atlantic salmon *Salmo salar* is one of the species that undergo extraordinary physiological and behavioural transformations to shift between completely different habitats (McCormick et al., 1998). Its remarkable migration from freshwater to the sea and back again offers an interesting and instructive life history. Studying its adaptations to environmental changes and its ecological role can provide profound insights into our understanding of ecosystems (Aas et al., 2011).

Salmonids (*Salmonidae*) are a captivating family of cold-water, ray-finned fish that are intricately linked to their habitats and have significant interactions with humans. As these environments undergo changes due to human activities, the vulnerability and value of this fish family increase (Thorstad et al., 2021).

There are seven species of fish commonly named salmon - one in the Atlantic - *Salmo salar*, the lead character of this thesis, and six Pacific cousins, Chinook (*Oncorhynchus tshawytscha*), Chum (*Oncorhynchus keta*), Coho (*Oncorhynchus kisutch*), Masu (*Oncorhynchus masou*), Pink (*Oncorhynchus gorbuscha*) and Sockeye (*Oncorhynchus nerka*). Even though there are important differences (Hansen and Quinn, 1998) in general, the basic behaviour and life history of species of salmon are similar. Other members of the family that share many similarities are known as trout (both in the *Salmo* and *Oncorhynchus* genera) and charr (genus *Salvelinus*) (Klemetsen et al., 2003).

1.1.1 Atlantic salmon (*Salmo salar*)

Atlantic salmon is primarily an anadromous fish that hatches in the fast-flowing streams of cold Northern European and North American rivers, where it remains for one or more years (McCormick et al., 1998). Before reaching sexual maturity, it undergoes significant behavioural and physiological transformations to migrate to the North Atlantic feeding grounds, where it stays for years before migrating back to spawn in its natal streams (Rikardsen et al., 2021).



Figure 1.1: Charismatic Atlantic salmon smolts from River River Gryffe in a flume after the experiments described in Chapter 4.

It hatches in oligotrophic water of fast-flowing riffles and spends the first months as *fry* establishing a feeding territory in the river near its siblings before developing into *parr* a fresh-water form. Depending on feed availability and other factors, after a number of years, usually two or three in Scottish populations (Malcolm et al., 2019), the parr begins changing to a sea-ready form, *smolt*, in a process called *smolting*. This process usually starts in Autumn and completes at the end of migration in late spring and is believed to be regulated by changes in the daylight cycle (photoperiod), increases in water temperature, and water discharge. In appearance, smolts are more silvery, and physiological changes allow them to live in salty water. They are more social than parr and favour strong flowing water, which will then lead them all the way to the seas where they will live

as adult fish. Salmon grows considerably at sea, from over 10 cm as a juvenile fish to over half a metre. Scottish salmon initiates migration back to its natal streams usually after a year, but for other populations, that can be up to eight years (Klemetsen et al., 2003). The mortality rate during both downstream and upstream migration, known as the *run*, is highly variable (reported between 3% and 64% during downstream riverine migration (Thorstad et al., 2012b)). Additionally, the timing of the *run* may influence fish survival afterwards (McCormick et al., 1998). The fish which make it back to their natal site breed, lay eggs, and often die there, providing nutrients for new life to carry on. Sometimes, studying other salmonid species offers clearer insights into life histories due to shared habitats (Klemetsen et al., 2003). Research on salmon frequently includes other ecosystem species, partly because common methodologies and mechanisms apply to multiple species (Adams et al., 2022b; Honkanen et al., 2017; Enders et al., 2007). The rest of this section introduces trout, charr, and Pacific salmon—the closest cousins of Atlantic salmon.

1.1.2 Brown trout (*Salmo trutta*)

Brown trout is the most common sympatric species with Atlantic salmon. Their habitat as juveniles is often the same, and they are found migrating in the rivers also at the same time (Milner et al., 2003). In general, Brown trout is a fish that has been introduced worldwide by humans. The review by Klemetsen et al. (2003) informs us that, like salmon, it is polymorphic and exhibits varied life histories. It spawns in freshwater but can reside and thrive in salt and brackish waters (estuaries). It has both non-anadromous and migrant populations, some travelling as far as the North Sea (Euzenat et al., 1999). It is adept at colonising a wide variety of water systems due to its variability in size, growth rate, feeding strategies, and habitat choice. It normally lives in rivers and lakes, but in the case of environmental shifts, it can move to brackish estuarine waters or even spawn there (for example, in the Baltic) (Limburg et al., 2001). It exhibits ontogenetic habitat shifts, often within one geographical area, depending on its size and developmental rates. Its appearance (phenotype) varies widely between habitats (Koene et al., 2020). It requires the right (but broad) temperature range and good water quality, living in environments ranging from small streams to large rivers, lakes, and coastal waters. It spawns on stones and gravel in running water like salmon. The size of a mature fish ranges from 20g in populations staying in small streams to kilograms in piscivorous and migrant populations (Klemetsen et al., 2003).

1.1.3 Arctic charr (*Salvelinus alpinus*)

Ecology and phenotype variation in Arctic charr are unique. It lives in the northernmost parts of the globe (a circumpolar species distribution), with the most northern habitat of both anadromous and freshwater species (Klemetsen et al., 2003). It is found in cold, glaciated lakes, where it is often the only fish species. It is now absent from southern glacial lakes, possibly due to temperature, eutrophication (increased nutrients and reduced oxygen availability), and potential competition with other fish species. There are many anadromous and some riverine populations, though charr generally lives in oligotrophic and ultraoligotrophic lakes (Wilson et al., 2004). It can be found in deep lakes (recorded up to 220m in Loch Ness, Scotland).

Extraordinarily, adult charr can weigh between 3 grams and 12 kg, with variously sized populations found in sympatry (Klemetsen et al., 2003). Its colouring shows wide variation, partly depending on the environment but most likely genetic for assortative mating. It demonstrates pronounced ontogenetic habitat shifts at higher densities and loss of differentiation when the density decreases. It often spawns in lakes but migrates between different lakes in the same river system (Maitland, 1995).

It is an important species for studying phenotypic plasticity and speciation due to its presence in recently glaciated lakes. These relatively new habitats, created around 10,000 years ago by receding glaciers, provide a variety of unexploited niches, promoting rapid diversification. It exhibits many morphs in different colours, morphologies, and life histories, adapting different feeding strategies and colonising different niches within the same geographical area. It is believed that this diversity results from both ontogenetic polymorphism and genetic variations (Adams, 1999).

1.1.4 Pacific salmon, genera *Oncorhynchus*

Even though Pacific salmon are not as closely related to Atlantic salmon as brown trout or charr they share the name “salmon” due to many similarities in their behaviour. Research shows that the basic biology of these species is the same, allowing some conclusions to be drawn between different populations (Hansen and Quinn, 1998). Their life histories are very similar, with the key difference being that all Pacific salmon species are semelparous, dying after spawning, whereas Atlantic salmon can spawn multiple times and even migrate back to the sea. Most *Oncorhynchus* species are classified as least concern in terms of conservation status (Rand, 2010), with large upstream runs of adult fish well studied in large North American rivers (Schindler et al., 2003). They are also also subject to

commercial and sport fishing, activities that are already limited for Atlantic salmon, a near-threatened species receiving increasing protection (see Section 1.1.6).

1.1.5 Ecology of salmon

Atlantic salmon exhibit a wide range of life histories, from non-anadromous freshwater populations (mostly associated with large lakes, but also a few rivers) to anadromous populations where fish spend up to 5 years at sea (Hansen and Quinn, 1998). Freshwater-only populations occur in areas separated from the seas due to physical barriers but also in sympatry with anadromous populations. In freshwater, females can mature at a length as small as 10 cm. Mature non-anadromous salmon in large lakes have been observed at lengths of over 50 cm, similar to anadromous populations, mainly due to the availability of food (Klemetsen et al., 2003).

Freshwater *parr* prefer fluvial to lacustrine habitats, overlapping with those of trout (Armstrong et al., 2003) but in different seasons migrate locally in the rivers depending on the availability of food, competition, and predators (McCormick et al., 1998). In case of displacement (e.g., due to a flood), they can even rear in lakes.

Juvenile salmon are diurnal for most of the year, switching to nocturnal during the winter. Even though parr are somewhat adapted to feeding in low-level illumination, their feeding efficiency decreases with darkness (Fraser and Metcalfe, 1997). It seems that the change in periods of activity relates to their reduced feeding needs during the winter, a desire to avoid the dangers of ice formation and increased risk of predation during the day.

Complex habitats are sometimes assumed to be preferable, however, observations of Atlantic salmon parr (Kemp et al., 2005a) in experimental flumes with and without complex boulder cover help to understand the trade-offs of various habitats for the life of the fish. A more complex environment might not necessarily increase population density (or, equivalently, decrease territory size). The effect can be complex due to increased flow complexity and decreased foraging opportunities from drifting food, along with increased susceptibility to predation in shallower holding stations.

Parr exhibits a hierarchical structure with a highly polarised food acquisition strategy, meaning that, when possible, some fish will monopolise the best access to resources Adams et al. (1998). After developing into smolts, they migrate to the sea mostly in late spring/early summer between the first and the eighth year, but some populations migrate in the autumn. Section 1.1.5.1 focuses on that crucial period.

Salmon can spend as little as a few months at sea, keeping to a small area (for instance, in the Baltic Sea) or travel far into feeding grounds in the North Atlantic, usually spending

up to 5 years there (Bacon et al., 2009).

When mature fish have grown at sea sufficiently for a reasonable chance of successful spawning, they will attempt to return to the stream where they hatched. Many studies have confirmed that salmon retain a memory of the chemical composition of water they encounter when smolting in a process called olfactory imprinting (Klemetsen et al., 2003). Recent evidence by Haraldstad et al. (2022) highlights that what occurs is a sequential imprinting of this olfactory information, starting from an early age, and is crucial at the stage of entering the marine environment to enable the correct decision when choosing channels during the upstream run.

They can return for spawning in a synchronised “run” with other fish at the end of autumn, but in the north of Scotland, salmon can enter upstream of the river at any time of the year, up to a year before spawning (Bacon et al., 2009).

The spawning habitat of Atlantic salmon ranges from 0.35 to 0.80 m/s in water flow and 17-76 cm in depth. Although average ranges for temperature, oxygen, etc., are well-documented, understanding variations within and between populations remains challenging (Armstrong et al., 2003). Once female fish arrive at the shallow streams up the river, they create redds, small gravel mounds in which they bury the eggs to a depth of 15-25 cm. During that process, the eggs are fertilised by competing males. Some males develop a hook-like structure in their lower jaw, called a “kype”, during their return from the sea, which helps them establish dominance (Perry et al., 2019). In general, the number of eggs increases with body size, ranging from tens in some freshwater populations to over 17,000. Atlantic salmon are known to spawn consecutively up to five times (e.g., in Newfoundland rivers) and biennially (Klemetsen et al., 2003). Additionally, there are variations with some salmon dying after spawning (semelparous, as with all Pacific salmon), but others migrate back to the sea and are called *kelts* (iteroparous).

Even within anadromous populations, an alternative pathway to migration is sexual maturation in freshwater. Adults that mature in freshwater are typically much smaller, which facilitates the mixing of breeding cohorts and provides a hedge against migration problems. Although the majority of parr that sexually mature do not migrate, Lothian et al. (2024a) indicates that there is not necessarily a developmental conflict between these two strategies, allowing parr that matures sexually in autumn to smolt in the subsequent spring and undergo migration.

The diversity of life histories is most likely what guarantees these fishes’ survival (Adams et al., 2022a). Additionally, they have complex population makeup and hierarchies, as one population can exhibit a variety of life histories. Even in anadromous

populations, there are cases of maturing males and (rarely) females (Klemetsen et al., 2003). As fish can spend different amounts of time at sea, one population can have different-aged fish at spawning, as well as different ages (usually 1-3) at parr migration. There are mechanisms such as faster-growing parr releasing at a smaller age to adjust to potential growth and feeding opportunities.

1.1.5.1 Downstream migration

There are complex environmental and physiological cues that trigger migratory behaviour in salmon parr to motivate them to migrate out of fresh water and not merely move between nearby water bodies (McCormick et al., 1998). For fish to be ready to respond to the changing environment in the springtime, they need sufficient energy reserves. Some can sexually mature in freshwater and compete to reproduce without migrating. The main migration period is in the spring, while less commonly, some populations migrate in the autumn. The migration is marked by the process of smolting that occurs in response to rising temperatures and changes in photoperiod. Most importantly, the migration to the sea requires adaptation to much higher salinity levels, and in order to allow for the quickest and the most successful sea entry, fish undergo physiological changes even before they begin moving (Gorbman et al., 1982). When temperature rises and photoperiod extends, smolts commence their movement with increased water discharge and presence of other migrants (Thorstad et al., 2012b).

Salmon exhibit a diel migration pattern, preferring to travel at night to better avoid predation and spend daylight hours in safer parts of the rivers. Lothian et al. (2018) shows that if they travel during the day, their speed might increase as an alternative survival strategy.

Salmon exhibit various swimming patterns throughout migration. Detailed modelling of Chinook salmon smolts movement by Holleman et al. (2022), in conjunction with a flow profile of a river fragment, allowed for the study of their movements at a fine scale, showing both positive and negative rheotaxis (swimming facing the flow and with the flow), lateral movements, and passive transport.

In situ study juvenile Chinook salmon downstream migration of Vowles et al. (2014) shows fish avoiding high-velocity gradients (accelerating from a natural 0.1 m/s to 1 m/s magnitude) that exceed their swimming capabilities, especially in light conditions. Kemp and Williams (2008) observed wild Chinook salmon smolts (*Oncorhynchus tshawytscha*) passing through a fish byway through one of two culverts equipped with cameras and artificial lighting. This study confirmed some hypotheses about the orientation of fish

during migration (with a preference for swimming tail-first (positive rheotaxis) at night) and showed a preference for a less turbulent channel. Overall, smolts travel faster under light than in darkness and possibly prefer a less complex environment.

Migration through standing waters presents another challenge for smolts. [Honkanen et al. \(2018\)](#) showed that in the waters of Loch Lomond, Scotland, smolts spent extended periods actively swimming but not following the most direct route. Some fish took more than ten times longer to traverse the lake than if they took the direct route. Further analysis of this data in [Lilly et al. \(2022\)](#) shows that smolts indeed explored the loch randomly until reaching a zone near the outflow that provided enough flow cues to find the correct migration direction.

During downstream migration, smolts navigate many obstacles, some man-made. [Haro et al. \(1998\)](#) examined how smolts navigate weirs during their downstream journey under laboratory conditions. Most of the fish maintained positive rheotaxis in the upstream reservoir, but as holding positions became nonviable, they turned with the flow and generally crossed in groups rather than alone, adjusting their orientation to other fish. In those weirs, with a flow of 2.25 m/s, they would sometimes engage in burst swimming out of the current rather than being transported down at an uncomfortably high speed.

Studies analysed in [Thorstad et al. \(2012b\)](#) reveal significant variation in smolt mortality rates during river migration, with 3% mortality reported in the River Conwy in Wales ([Moore et al., 1995](#)) and 64% in the River Eira in Norway ([Thorstad et al., 2012a](#)). The median reported mortality per kilometre of river is 2.3% km⁻¹, with a range of 0.3% to 7.0% km⁻¹. This is lower than the median mortality in river mouths and estuaries, which is 6% km⁻¹ (range 0.6%–36% km⁻¹), potentially influenced by migration delays caused by challenges in the river phase ([McCormick et al., 1998](#)).

There is evidence from a study of juvenile Pacific salmon—Chinook salmon *Oncorhynchus tshawytscha*, coho *O. kisutch*, and sockeye *O. nerka*—that the timing of marine entry is influenced by the lunar cycle and resulting tidal patterns ([DeVries et al., 2004](#)). In this study, an artificial barrier with floodgate passages allowed for the precise registration of the passage of both wild and hatchery fish via PIT tags (method described later in Section 1.1.7.4). The fish attempted to navigate the obstacle primarily during the moon’s apogee (farthest point) or quarter moon—phases where tidal fluctuation and amplitude are the lowest. The influence of the moon phase is mediated not just by changes in the photoperiod at night but also by more nuanced physiological changes in the environment. Other variables, such as tides, illumination, temperature, or salinity, did not affect entry time over the three years of the study, highlighting the subtle and hidden way how the

environment affects salmon behaviour.

The path post-smolts take in seawater remains somewhat enigmatic. Our understanding of their spatial distribution typically derives from catch data. A large study conducted on the west coast of Scotland in the North Sea by [Rodger et al. \(2024\)](#) examined the pathway to the North Atlantic of smolts from 25 rivers in England, Scotland, and Ireland, showing considerable variation within and between populations.

1.1.5.2 Collective behaviour

Some insight into the social aspects of salmon life can be gleaned from traditional observations and catch data. [Berdahl et al. \(2017\)](#) demonstrates how upstream migration is influenced by social interactions. This study uses 20 years of data on Pacific salmon's entry into spawning pools (the last stage of migration). Assuming only environmental and internal factors influence the decision to enter, the timing should follow a Poisson distribution. However, an alternative social model assuming that fish follow one another explains the observed data much better. The same reasoning provides evidence of salmon schooling at sea, based on catch data from a methodical netting study ([Berdahl et al., 2017](#)). It remains challenging to establish whether social coordination occurs when fish decide to migrate back or if another factor causes increased clustering of salmon in the seas.

An observational study by [Vowles et al. \(2014\)](#) of juvenile Chinook salmon in the Columbia River in the USA found that when presented with an obstacle in a form of a channel constriction with an increased flow, they are more likely to school in light when navigating difficulty, while in darkness, they pass individually.

Data from the Moray Firth Tracking Project ([Newton et al., 2021](#)) shows that fish released as part of a larger group (as well as earlier migrants) have the highest probability of successfully reaching the sea.

Hatchery smolts allow for experimentation that is impossible with wild individuals and might provide a crucial proxy to understand more complex behaviours. [Olsén et al. \(2004\)](#) investigated the schooling behaviour of juvenile hatchery smolts to understand what drives group composition, finding that genetic factors take precedence over familiarity, with sibling groups more likely to travel together than fish from the same rearing group. This sibling effect was apparent during the predominant night-time migration.

An analysis of multiple datasets on salmon's upstream success and run size by [Berdahl et al. \(2014\)](#) also shows that as the size of the migrating group of fish decreases, the straying rate increases. This indicates that salmon migrate more often up a stream different than

the one they were born in if the size of the population they come from decreases. It presents an interesting evolutionary mechanism that can increase population resilience to changing environments.

1.1.5.3 Importance of salmon

Atlantic salmon is an iconic species and thus benefits from widespread social interest. It has been an integral part of many cultures in the north of Europe and America ([Ween and Colombi, 2013](#)).

People associate salmon rivers with high water quality and healthy ecosystems ([Kochalski et al., 2022](#)). Extractive ecosystem services (relating to fishing and sustenance) are highly valued in places with existing salmon populations, such as Norway, meaning that people in environments that directly benefit from salmon rivers place a higher value on their preservation. Interactions with salmon through recreational fishing, watching river migration, as well as indirectly through education and river restoration projects, are significant predictors of interest in salmon preservation. In general, [Kochalski et al. \(2022\)](#) shows that there is a strong desire to preserve these resources for future generations, not just for their immediate extractive benefits.

Recreational fishing for salmon is a popular sport, though more recently conservation status puts it under increasing restrictions ([Morton et al., 2016](#)). Atlantic salmon has been a source of food for humans for centuries and still persist as an important element of Indigenous cultures ([Hiedanpää et al., 2020](#)) and has been an important part of the industrialisation of food supply ([Ween and Colombi, 2013](#)).

Salmon farming is a significant and growing industry worldwide ([Torrissen et al., 2011](#)). It has expanded exponentially in the last four decades, especially in Norway, Scotland, Chile, and Canada, starting in the 1970s. In the north of Europe, the lineages most common in farming is Norwegian salmon, bred for over 12 generations to increase the body size ([López et al., 2019](#)).

Despite issues with pollution and antibiotic use, it compares favourably with terrestrial animal meat production. [Torrissen et al. \(2011\)](#) argues that if the issues of sustainable feed for salmon are resolved, for instance, by harvesting seaweed instead of using either unsustainable wild-caught fish or agricultural products that do not provide necessary omega-3 long-chain polyunsaturated fatty acids, salmon will become a sustainable source of protein for humans.

Sea cages where farmed salmon mature in the coastal marine environment can contain up to 200,000 fish. If only because of their scale, the fish farms are a significant problem to

coastal environments that host them. They are a massive source of pollution from excrement and protective antibiotics. Fish concentration provides grounds for the development of pathogens and parasites. [Føre et al. \(2018\)](#) reports that over the last decade, infestation with sea lice (*Lepeophtheirus salmonis*) has become one of the main welfare and health issues in farmed salmon, particularly in Norway and Scotland. For the farms themselves, it represents a significant economic cost due to lost production and delousing operations.

To their ecosystem, salmon provides an important role as both a prey in the freshwater for both avian and aquatic species, as well as a predator in the marine environments. The most unique role, though, relates to the transfer of nutrients from rich oceans to oligotrophic natal areas.

Salmon provide a service of nutrient transport to freshwater streams through their excretory products, gametes, and, ultimately, carcasses. In many ontogenetic habitats of the rivers at high altitudes, these are key for maintaining ecological processes and ecosystem functions ([Samways and Cunjak, 2015](#)). The key nutrients provided by spawning salmon are nitrogen and phosphorus. From gametes and excretion alone, salmon provide enough nutrients to allow for significant growth of biofilm, resulting in increased productivity of microinvertebrate populations necessary to support the rearing of hatched salmon ([Samways and Cunjak, 2015](#)). The nutrients' effect on terrestrial growth and abundance might even affect the songbird communities in line with the biomass of adult salmon returning to the natal streams ([Wagner and Reynolds, 2019](#)).

For the reasons of its complex life history and social importance Atlantic Salmon has been an important species for scientific study.

The gut microbiome of different forms of Atlantic salmon provides an excellent system to study how microbiomes change with the environment ([Llewellyn et al., 2016](#)). In [Llewellyn et al. \(2016\)](#), authors found that the stability of the Operational Taxonomic Unit (OTU) declines with age, evident in returning salmon that exhibit more variable richness and diversity in their microbiomes. Understanding the migration, together with the physiology of salmon, opens the opportunities to study unique ecological interactions.

The conservation of Atlantic salmon remains important for different communities, the coordination of the effort and communication of scientific knowledge are in the spotlight ([Brattland and Mustonen, 2018](#); [Hiedanpää et al., 2020](#); [Flye et al., 2021](#)).

1.1.6 Threats to salmon population

The population of Atlantic salmon has been recently re-assessed by the International Union for Conservation of Nature and Natural Resources (IUCN) for the Red List of Threatened

Species (Darwall and IUCN, 2022). Atlantic salmon is believed to be facing a decline and has been classified as a “near threatened” across all populations of the Atlantic. Its conservation is a complex problem requiring a broad and informed approach (Lennox et al., 2021).

As an animal with a long and complex life history that involves many different habitats and cover thousands of miles, salmon are especially vulnerable to rapid changes in the environment. The selection pressures on migrants might not directly promote the best long-term strategy, for instance fresh water residency, as the migratory instinct is too deeply ingrained. It is worrisome that Atlantic salmon might be caught in an “evolutionary trap”, as evidenced by the sharply decreasing number of returns (Adams et al., 2022a).

Populations of salmon fluctuate over time, which can have complex reasons due to the species’ diverse and complex life history. A long-term data of Atlantic salmon population since 1952 in the catchment of River Foyle in Ireland is analysed by Honkanen et al. (2019) to investigate the strength of density-dependent and independent factors in salmon population dynamics. Density-dependent mechanisms can relate to competition for resources, such that as population size declines, the individuals experience better abundance and growth, increasing their survival—something indeed observed in salmonids. This study explains 32% of the variation in population changes over time, suggesting most of the changes are explained by density-independent mechanisms. These can have more or less pronounced effects at different life stages, but their severity does not decrease with the population size.

I undertake my work in Scotland, where Adams et al. (2022b) reports on the long-term data that comes from catch records in Loch Lomond. The evident fluctuations in population size are more likely to correspond with wider environmental features affecting the stock rather than the periodicity of the generation periods. The body mass of the anadromous trout and salmon declined throughout the second half of the 20th century, while the non-anadromous brown trout population increased markedly. Observed changes to the upstream migration pattern also suggest an increase in salmon that spend more than one year at sea, meaning they need more time to grow.

Diversity is considered a cornerstone of resilience ecology. For Pacific salmon, it has been shown that the diversity of life histories increase the growth rate of populations across longer periods of time (over 5 years), providing a buffer against fluctuations and likely enhancing resilience, even though, in the short run, higher diversity resulted in decreased productivity (Greene et al., 2010).

In terms of conservation, density-dependent factors are most important in freshwater

and density-independent in the oceans. It is believed that the factors responsible for the decline of Atlantic salmon are in the marine environment, but some closings of commercial fisheries and conservation zones have so far not resulted in consistent gains in the productivity of salmon stocks. That is consistent with other marine stocks. In the past, the temperature conditions have improved but without recovery in stocks (Klemetsen et al., 2003).

It is important to note that most of the threats to the species result from human activities affecting populations at different life cycle stages, requiring better understanding and active mitigation (Thorstad et al., 2021). The following sections will focus on the specific threats.

1.1.6.1 Effect of changing temperatures

During spawning and incubation, higher water temperatures can negatively affect stock size and survival. Later on, low water conditions reduce habitat availability for recently hatched salmon and juvenile parr. During seaward migration, higher water discharge increases the chances for successful sea entry of smolts (Thorstad et al., 2012b).

Climate change and resulting ocean warming have been suggested as key drivers of population decline in many species. Soto et al. (2018) analyzed data from salmon from 1980 to 2010 travelling from St. John River on Canada's east coast to compare survival rates at sea of subpopulations that feed on different grounds. They argue that varied warming in the feeding grounds cannot be the principal cause of the more synchronous decline of the population. Analysing salmon growth using historical data from fish scales across Norwegian rivers, Vollset et al. (2022) provides evidence supporting a hypothesis of a step change in the environment of the North East Atlantic. The fish are not growing as much in the sea as they used to, and as a result, the percentage of fish staying longer at sea has changed. The shift in growth rates coincides with the steep increase in the average surface temperature of the Norwegian Sea, a decrease in the proportion of Arctic water, and a decrease in zooplankton abundance. Data from studies of other marine species also show a reduction in size.

1.1.6.2 Habitat degradation and farming

Salmon require good water quality, flow conditions, and the environment providing shelter and foraging opportunities. Habitat restoration is part of conservation efforts but often fails to address the sources of ongoing degradation and environmental issues. The water must be well-oxygenated, free of major pollutants, and free from both chemical pollution

from agriculture and silt ([Armstrong et al., 2003](#)). Agricultural pollution from farmlands is now a major source of degradation of water quality ([Hendry et al., 2003](#)). Additional sources of pollution include salmon and trout farms, often located in the same river systems as the wild stock. The substantial quantities of feed and excrement alter the biological composition of the ecosystems through which the migrating fish pass, making them more susceptible to developing diseases or parasites.

Another significant problem, especially for wild salmon populations that are often in the same areas as the fish farms, is the escapes of the farmed salmon that provide competition in the river system for the wild populations. An additional problem is the maladaptations in the subsequent generations due to interbreeding between wild and farmed salmon ([Fraser et al., 2010](#)). The genetic integrity of many wild populations has now been clearly reduced in areas where salmon farming is present ([Gilbey et al., 2021a](#); [Pritchard, 2023](#)).

There are some positive developments regarding this issue of the farm escapes. Recent work by [Benhaïm et al. \(2020\)](#) shows that triploid fish (i.e. genetically modified for sterility) can have comparable productivity (growth) to the normal diploids, when reared at low temperatures, providing a safer alternative for commercial production.

[Rodger et al. \(2024\)](#) studied the direction of travel of smolts from 25 rivers in England, Scotland, and Ireland, showing that in their migration, they avoid areas that seem to be the optimal route but are developed with salmon farms, providing evidence of the additional cost to the late-stage migration. There are, however, some benefits from the development of commercial salmon rearing. In some regions, the extinct population of wild salmon is reintroduced with hatchery-reared fish. On the River Testebo in Sweden, [Serrano et al. \(2009\)](#) observed that despite designed fish passes, smolts are still guided towards hydropower turbines, with an overall very low migration success (21% and 7% in each year of study). The authors suggest that despite many stocking programs across the Baltic Sea, they are hindered by still inadequate corrections to the river environment ([Serrano et al., 2009](#)).

Hatchery smolts often differ from wild smolts, typically having a larger size and higher energetic states (amount of body lipids and protein). Comparing the threat response of juvenile wild Atlantic salmon with farmed fish [Johnsson et al. \(2001\)](#) showed an effect of domestication that was both environmental as well as genetic, with captive animals' response blunted compared to the wild. The condition factor—a ratio of their length to mass—serves as a good proxy for the energetic state in laboratory experiments with both wild and hatchery smolts, showing further migration distance for lower energetic state fish, despite a slower migration speed ([Persson et al., 2018](#)). As with wild smolts, hatchery

salmon migration success correlates with high water discharge or rapidly increasing at the start of migration—suggesting that both the overall year and the timing of migration are crucial. Laboratory experimentation confirms that a lower energetic state predicts migration success, as it reflects a lack of food and resources in the feeding habitat of the parr (Persson et al., 2019).

In Denmark, a telemetry study shows that well-prepared hatchery-reared salmon can actually have a higher survival rate throughout downstream migration than their wild counterparts. The larger fish in both groups experienced lower mortality during the downstream migration, which explained part of the difference, and further studies are needed, as the wild salmon sample size was relatively small (Flávio et al., 2019).

1.1.6.3 Barriers

Increasing pollution, fish farming, and man-made obstacles are either directly causing mortality or delaying migration and causing it indirectly. As Atlantic salmon undergo not one but two riverine migrations, physical barriers present a particular challenge.

The well-being of humans requires some level of exploitation of the natural environment. Rivers historically always provided a source of energy and water and were tamed to provide safe shelter in the settlements. However, even thoughtful improvements in river management - whether for flood defences, agricultural use or conservation result in the creation of reservoirs with some obstacles to the free flow of water on which anadromous fishes depend.

Fragmentation of rivers is a major problem for migratory fish species. In Europe, there are 0.74 barriers per kilometre, many of which are barriers under two meters in height that are missing from existing records (Belletti et al., 2020). Most work on obstacles to migration focuses on large dams, which in Great Britain constitute only 0.4% of barriers. However, even smaller obstacles represent an added cost to migration and increased mortality risk. In the European Union, a law “Water Framework Directive” requires free passage for migratory fish travelling between areas of the river essential for their life history (Gauld et al., 2013), highlighting an increased focus on conservation.

The fragmentation of rivers with dams and weirs has an obvious effect on the upstream migration of fish. Large fish swimming up the rivers are relatively easy to study in capture and tag studies, compared to juvenile fish, for which, until recently, most telemetry tags were unsafe due to their size. Gauld et al. (2013) looked at the impact of those very common low-head weirs on brown trout (*Salmo trutta*), which are particularly troublesome for smolts during common periods of low water levels, for instance, during summer migration

times.

The conflicting needs of environmentally conscious societies include the proliferation of hydropower plants. Not all water needs to be fed through the turbines of the power plant, and in principle, it is possible to provide a suitable passage for fish migrating both up and down the river. In practice, however, this is a challenging ecological engineering problem that depends not only on the species of fish for which a fish pass is designed but also on the characteristics of the water reservoirs and the hydroelectric machinery. [Brackley et al. \(2018\)](#) compares the damage to Atlantic salmon smolts resulting from direct swim through an Archimedean screw turbine with the passive passage of euthanized fish—to establish a method of estimating the safety of a turbine without resorting to post-factum telemetry data (that suggests up to 10% mortality on the turbines). Such a turbine has a slow revolution of under 30 rpm, which allows actively swimming fish to avoid most of the scale loss (used as a proxy for mortality here), while passive euthanized fish are much more damaged. This highlights the difficulty in designing safe passages for fish.

Particularly challenging are obstacles that not only act as physical barriers but also make it difficult for fish to find the correct passage due to the turbidity of water and hydraulic noise. Such situations are typical of hydroelectric plants with a fish bypass. In study by [Kerr and Kemp \(2018\)](#) migrating brown trout *Salmo trutta* undergo an experiment that shows that higher turbidity of water may mask the velocity gradient. Fish orientation gives clues about whether it finds the accelerating flow and orients downstream or is likely to reject the channel if the flow is too strong or turbulent.

Study of the behaviour of migrating smolts at different facilities in Finland ([Karppinen et al., 2021](#)) shows that every hydroelectric facility encountered by smolts presents a unique problem requiring an individual approach. The characteristics of the reservoir above the dam, its physical structure, and hydroacoustic properties all affect smolt behaviour and subsequent mortality or migration delay. [Stoilova \(2024\)](#) reviews various methods to prevent fish from making incorrect (and potentially lethal) entries at man-made structures. Many different approaches are currently in use, including acoustic, light, electric, mechanical, olfactory, and hydrodynamic barriers, all of which are characterized by trade-offs, with suitability depending on the understanding of the target species and its response to the environment.

[Newton et al. \(2018\)](#) assesses the impact of an obstacle on Atlantic salmon upstream migration based on radio tag data. Adult fish are caught and released downstream of the dam with a fish pass. A telemetry receiver array allows for detection in distinguished areas below and above the obstacle but does not quantify actual movement. The authors find

that the main predictors of successful passage are time spent searching for the pass, fish length, and fat content. This highlights the energetic cost required for successful obstacle navigation during migration.

Another challenge for smolts entering the sea is high-energy coastal waters, either due to strong tides or the presence of turbines from tidal energy projects. It is observed that smolts do not stay to feed in coastal waters, instead moving to the deeper seas with active swimming using appropriate currents (McIlvenny et al., 2021).

Godfrey et al. (2015) examines Scottish salmon swimming in the Atlantic and finds different patterns of diving with the potential for interactions with marine renewable energy developments on the north coast of Scotland, especially among repeat spawners that migrate multiple times. As those developments become more widespread, they are likely to further reduce migration survival.

1.1.6.4 Predation

Investigations reveal that smolts are most vulnerable to predation during the early phase of migration, though there seems to be a large variation between different populations and different years. Avian and piscivorous predation is the main cause of mortality in many rivers (Chavarie et al., 2022; Thorstad et al., 2011).

Mortality in the lake itself can be low, but the confluences of the river, where predatory fish such as pike (*Esox lucius*) aggregate, pose the largest threats. Smolts time their entry to and from the river to be after dusk as a possible predator-avoidance behaviour (Kennedy et al., 2018). It is also suggested that synchronous migration is an antipredatory behaviour that increases survival through overwhelming the predators with large numbers of smolts, leading to a linear increase in survival with the number of migrants when density-dependent and independent factors are accounted for (Finstad and Jonsson, 2001).

The more time fish spent in estuaries and river mouths more it was predated on by harbour seals (*Phoca vitulina*, cetaceans such as bottlenose dolphins (*Tursiops truncatus*), birds such as cormorants (*Phalacrocorax carbo*), and fishes such as Atlantic cod (*Gadus morhua* - as evidenced by the aggregation of many predators during the time of smolts' entry to the sea (Green et al., 2022; Lilly et al., 2024).

1.1.7 Studying Atlantic salmon

1.1.7.1 Direct Observation

Aquatic environments naturally present a bigger challenge for the observation of the behaviour of animals than terrestrial ones. It is possible to observe the upstream run of salmon - especially the bright red sockeye salmon (*Oncorhynchus nerka*)- but this is a rare exception when the fish is both large and navigates obstacles by often jumping above the water line. Most of the time, studying the habitat and behaviour of salmonids in the wild depends on the ability to observe them in challenging conditions. With the development of underwater cameras it is becoming possible to survey some small areas, but the unforgiving lack of light in aquatic environments makes it often unfeasible. There are reasons to attempt that, as even in the case of fish tagged with a positional system (see following sections) and fully mapped habitat, limiting observation to only a few tagged fish might not be representative of their true behaviour.

Specifically, observations in winter with lower light pose a challenge and seasonal bias to direct observation methods such as snorkelling (due to low temperature and possible ice cover). In streams and in the laboratory setting, [Erkinaro et al. \(2018\)](#) examined visual methods for estimating the fish location and quantity compared to precise but time-consuming methods of electrofishing and radio telemetry (described in the following section). The authors report a very low effectiveness of observation both during the day and at night with infrared light. This illustrates the practical difficulties in performing more fine-scaled studies with multiple individuals.

1.1.7.2 Catching

In rivers, data from recreational fishing offers the longest timescales of high-quality population data on fish. [Adams et al. \(2022b\)](#) examined 116 years of catch records, providing confirmation of a long-term decline in the Atlantic salmon stock in Scotland. Such data is all the more valuable if it comes with some measure of catch effort—in this case, the number of angling club members in a given catchment. The earliest attempts to learn about the life history of individuals were based on tagging the fish with coded wires attached to its fins, so on the subsequent catch, the location change and condition of the fish could be measured. Scientific trawler surveys catch coded wire-tagged post-smolts to provide information on where at sea salmon from different river systems feed ([Lilly et al., 2024](#)).

1.1.7.3 Electrofishing

Today, the most common method for assessing stream-dwelling populations of fish like salmon is electrofishing. This involves surveying representative areas methodically with electrodes that induce fish movement towards the operator—either on a boat or wading through shallow water—and immobilises the fish, allowing for their temporary removal from the water for assessment and measurement. In closed environments, multiple passes of the area with the removal of fish from the water (population depletion) allow for a good estimate of species richness and abundance. More recently, this process has been replaced by a less labour-intensive process where a catch-per-unit-effort (CPUE) can be estimated for a reliable estimate of the population without the necessity of population depletion. (Honkanen et al., 2017).

To improve survey data, it is beneficial to understand historical trends and estimate electrofishing efforts through cross-checking abundance between studies and sites. Atlantic salmon electrofishing data from across Scotland has been analyzed to provide a benchmark density of stocks (Malcolm et al., 2019). Modelling the capture probability and density with covariates referring to the location, habitat, and method of sampling allows for a better understanding of the data and expected results across Scotland.

1.1.7.4 Radio tags

PIT (Passive Integrated Transponders) tags are electronic presence tags suited for narrow passages and close proximity detections. The tags that are implanted under the scales of a fish are miniature transmitters that send an electronic code to a receiver as they cross its induction loop - i.e. using the energy provided by the receiver. They are very popular in laboratory experiments due to their small size (under 12 by 3 mm) and the possibility to identify individuals, allowing, for instance, a study of group composition in laboratory conditions (Olsén et al., 2004). They are additionally limited by the frequency of the pulses of the receiver, which is usually 1Hz. In order to allow greater distance and frequency of reporting, the tags need to contain their own battery, making them active tags.

In freshwater, active radio tags have been in use for a long time to study upstream migration, initially starting with larger fish due to the size of the batteries and the size (almost 10cm long) of the tags with a large antenna. Due to the limited range, it often required active tracking (McCleave et al., 1978).

PIT tags and radio telemetry bring substantial improvements where previously only

direct observation would be possible, such as studying the habitat and the behaviour of salmon parr during the winter (Enders et al., 2007). PIT tags require wading in the water to allow a close detection distance from the antenna, whereas radio tags provide a larger detection distance.

Radio tags with motion-sensing capabilities allow the monitoring of adult Atlantic salmon in freshwater spawning grounds as validated with direct video recordings (Karpinen and Erkinaro, 2009). Serrano et al. (2009) used a mix of both acoustic and radio telemetry to track the downstream migration. Radio tags have an advantage in position location but lose signal in deeper water and in increased salinity, where researchers rely on acoustic receivers.

1.1.7.5 Acoustic telemetry

Recent advances in miniaturisation allow for small radio or acoustic transmitters (tags) to be placed on or under fish scales. Radio tags are unsuitable for operation in seawater due to the attenuation of electromagnetic waves in this medium. Hence, salmon migration, which spans both fresh and seawater environments, is commonly surveyed with acoustic tags. Acoustic telemetry works by transmitting encoded acoustic signals that can be picked up by an anchored receiver tens of meters away, allowing presence data to be reported every few seconds from passing fish for many months.

The burden of the tag can be a problem, so there are broad rules to follow to avoid introducing a disadvantage to tagged fish. Different tag sizes were also compared, finding that within a reasonable range of 1.9% to 7.39% of body mass, the precise difference in the tag burden did not matter (Lothian et al., 2024b).

Presented in Lothian et al. (2018) is an example of a telemetry study to understand survival in downstream river migration of Atlantic salmon. By connecting telemetry data with other environmental factors (water discharge, time of day, moon phase), we can understand the factors affecting survival rates, migration timing, and the direction of entry to the sea. This sort of data has limitations for collective behaviour study because very few individuals are released at the same time (limited potential of shoaling), and it is often many days before they reach the first receivers, by which time the fish travelling together might already disperse.

Compared to river migration, the sea phase of it is even less understood. Multiple research teams tagged more than 1900 smolts to understand the migration pathways of Atlantic salmon smolts from tributaries of the Irish Sea. Sets of marine arrays—allowing detection of presence over wide gaps between Scotland and Ireland, as well as a SeaMonitor

remotely controlled vessel, allow gathering data from far in the sea (Green et al., 2022; Lilly et al., 2024). The relatively short time period spent in the Irish Sea suggests that post-smolts choose to get out as fast as they can, swimming actively and not just relying on water flows. Similarly, large telemetry exercise data from the east coast of Scotland, Moray Firth Tracking Project (Newton et al., 2021) shows that fish followed a common migration pathway, swimming actively and using water currents but showing directionality instead of passively following the flow.

Precise placement and calibration of multiple receivers are crucial. One study, Guzzo et al. (2018), shows how we can achieve accuracy comparable with a GPS and temporal resolution close to 1Hz while tracking fish on a small, calm lake covered with a receiver array. However, placing such an array close to an obstacle on a river is more challenging due to the more likely drift of receivers and noise from falling water or mechanical equipment interfering with the acoustic signal from fish tags.

One such trial with Atlantic salmon has been reported by Leander et al. (2020), where two types of acoustic arrays (pulse-position-modulation and phase shift) accuracy was tested near a hydropower facility in Sweden. Such systems are limited by encryption of receiver data on telemetry devices, forcing the use of manufacturer proprietary positioning algorithms and study design adhering to arbitrary requirements.

Better positioning is possible with radio telemetry, and sometimes both types of tags are used (Serrano et al., 2009). Recently, it has become possible to combine fine-scale telemetry with a hydroacoustic profile of the river to study swimming and migration patterns *in situ* (Holleman et al., 2022).

Long-term pop-up satellite archival tags allow for long-term tracking of fish at sea. High-resolution light-based geolocation archival tags are novel and allow studying both vertical and horizontal migration, showing (though on a small sample of six fish) high diversity in paths, habitats, and strategies (Strøm et al., 2018).

Passive and active telemetry has been used by Chavarie et al. (2022) to provide more precise locations of mortality of salmon and discern residency and travelling patterns.

It is easier to study farmed salmon in sea cages due to their size and accessible location. Increasingly, there is a growing concern regarding farmed salmon welfare, which is addressed with more precise real-time monitoring (Føre et al., 2018). The acoustic tags used on commercial farms can track the location in 3D but again require additional processing from device manufacturers, which often brings additional challenges and limitations (Stockwell et al., 2021).

1.1.7.6 Sonars

DIDSON (manufactured by Sound Metrics Corp., Seattle, USA) is the most popular multi-beam sonar, also known as acoustic cameras, which offers fine spatial and temporal resolution, allowing for a bird's-eye view and video-like presentation of objects up to 20 meters underwater. With a framerate over 5 fps and angular resolution of 0.3 degrees, it facilitates observation of fine-scale behaviour.

The automation of video processing and the imaging sonar are utilized by [Handegard and Williams \(2008\)](#), who use DIDSON to track fish following a vessel at sea and employ simple computer vision techniques to automatically extract movement data. They argue that for schools with moderate density, DIDSON is sufficient for behavioural studies, although the smallest group of fish tested were, on average, 24 cm long, which is considerably larger than salmon smolts.

[Tušer et al. \(2014\)](#) studied the precision and potential biases in length measurement of fish observed in laboratory conditions, reporting reasonable detection and sizing for fish down to 20 cm, and highly dependent on the fish's orientation relative to the sonar beam—a factor that is difficult to control outside the laboratory.

The acoustic camera is deployed in the work of [Doehring et al. \(2011\)](#), where it records the movement of juvenile anadromous whitebait during migration at floodgates. In the study, fish measuring approximately 60 mm, are observed in turbid water to analyse the choice and timing of the passage through an obstacle in quantities not possible without direct underwater observation with a sonar. This suggests a promising avenue in future research on salmon, though the cost of the equipment remains an obstacle.

1.1.7.7 Direct Experimentation

An alternative route to understanding behaviour in the wild is to recreate scenarios in a constrained laboratory setup. Combining real-life scenarios with laboratory control, as leveraged by [Kemp et al. \(2005b\)](#), the authors study the reactions of different species and year groups of Pacific salmon to their choice of channel in a natural river divided by an obstacle. They observed evidence of active swimming and various strategies when entering either a constricted or an unconstrained channel of the flume. The two channels, differing in water velocity and turbulence (a choice chamber), facilitate the study of responses to hydraulic stimuli. Downstream migrating smolts are recorded on a video camera during both day and night with infrared illumination. Contrary to previous observational studies, the authors noted that fish travelled both head-first and tail-first at times, actively

swimming. They preferred the choice of a less turbulent water channel and sometimes actively swam upstream out of a channel with low water velocity.

Direct measurement of fish movement in an artificial stream and its modelling in a Lagrangian context is presented by [Tan et al. \(2018\)](#). A flume filled with vertical slots/obstacles had a precise flow profile measured so that the repeated filmed passage of a test fish (silver carp) allowed for a description of its movement with a model driven by response to hydraulic stimuli within some sensory range of the fish. This study, while not involving any collective behaviour, showcases what is possible with well-controlled laboratory settings and modern tracking techniques.

1.2 Quantitative movement ecology

We approach salmon migration in the context of potential collective movement. To choose an appropriate framework for different types of observations, we need to understand the connection between different types of ecological modelling.

1.2.1 Ecological research

Ecology is built on *in situ* observations and testing of the hypothesis about organisms and their interactions. Unlike biology, where a study can be focused on identifying single phenomena through controlled laboratory experimentation, ecologists look for longer spatial and temporal patterns. Some of those patterns will be described as theoretical models long before measurement at the required scale is possible. As data becomes available, those two approaches, observational and theoretical, are reconciled through statistical and mathematical modelling methods ([Codling and Dumbrell, 2012](#)).

Advancements in the capability of sensors have increased data availability, allowing more complex phenomena to be studied but requiring more complex data analysis tools. Increasingly, understanding of nature can only be expressed in the form of rigorous stochastic models ([Schmolke et al., 2010](#)).

A basic ecological model that focuses on a specific species takes into account some measure of the organism's environment, e.g. availability of feed, predation, and habitat quality. Additionally, it can include the structure of the population, intra- and inter-population competition, and seasonality. The simplest models can be stationary and deterministic, while the more advanced ones incorporate temporal and spatial randomness at various scales ([Codling and Dumbrell, 2012](#)).

Beyond modelling single or multiple species interactions, other approaches focus on the spread of diseases (Hampson et al., 2009; Faust et al., 2017) or predicting the changes and disturbances in the ecosystems (King et al., 2015; Mouquet et al., 2015).

Inferring the behaviour of individuals in a population, or the behaviour of the entire population based on individual variation, poses complex questions that bridge behavioural biology and ecology. The common starting point for statistical modelling is a *mean-field* approach where variability is averaged, and the structure and hierarchy underlying it are ignored. This approach can be necessary for the model to have an understandable mechanism and be computationally feasible but matches poorly to the natural environment that is usually heterogeneous (Grünbaum, 2012).

Unlike laboratory experiments, where the established protocol can be followed and sampling and measurements adjusted for the phenomena studied, field observations have unavoidable biases that go beyond the measurement uncertainty. Field sampling protocols are established in the context of specific environment and modelling type (Dengler and Oldeland, 2010). Equipment constraints dictate what can be measured and where, usually within a small part of a wide habitat. The access to the the natural environment is limited geographically, and together with unavoidable temporal constraints can result in a strong convenience sampling bias (Honkanen et al., 2017; Grünbaum, 2012). Missing data points and high measurement error combined with variability and unexpected interference makes the modelling of uncertainty in field studies even more important than in laboratory work (Nakagawa and Freckleton, 2011).

Many ecological questions are posed in a spatial context, and for animals, movement is a key aspect of behaviour. Movement ecology underlies the understanding of habitat use and choice, and this research grows with the development of data acquisition over last decades (Kays et al., 2015).

Previously in Section 1.1.7 I discussed many ways in which historically, salmon have been studied, which also illustrates the breadth and limitations of approaches in spatial and movement ecology of other species and ecosystems (Jacoby and Piper, 2023). Later in Section 1.3.1, I discuss the advances in data gathering, such as the development of imaging techniques, improved telemetry, genetics data and other modern methods over the last two decades drove the step change in quantity and quality of observations (Nathan et al., 2022). With better data, we expect models to not only test binary hypotheses about species in their ecological context but also understand complex phenomena and how they change (Mouquet et al., 2015; Nakagawa and Freckleton, 2011). Modelling at different scales allows understanding of individual and social aspects of behaviour. The following section

presents the fundamentals of modelling of animal movement, that plays a crucial role in wider ecological modelling.

1.2.2 Mathematical modelling of animal movement

Movement is the most obvious and easily quantifiable animal behaviour. Much of the missing knowledge of population dynamics can be filled in by understanding behaviour in the context of animal movement [Morales et al. \(2010\)](#). Behaviours such as feeding or breeding are usually implied by movement across the environment. Movement is also a key aspect of studying migratory species such as salmon.

The first stochastic description of natural movement, the Brownian motion, has been proposed in 1827 by botanist Robert Brown, who observed particles of pollen submerged in fluid. This basic continuous-time random process was later formalised by [Einstein \(1905\)](#) and can be seen as a description of movement where change in position $dx(t)$ is a draw from a Gaussian distribution:

$$dx(t) = d\Psi(t) \sim \mathcal{N}(0, dt), \quad (1.1)$$

which is a *Lagrangian* formulation of movement - with the point of reference being the single individual. Alternatively, the same can be seen in an *Eulerian* context as an equation of diffusion that describes the probability of the appearance of an animal in space averaged over stochastic realisations of the process [1.1](#), its probability distribution function:

$$f(x, t) = \frac{1}{\sqrt{2\pi t}} \exp\left(-\frac{x^2}{2t}\right) \quad (1.2)$$

As a mathematical process, this is known as the Wiener process, and underlines most of the stochastic processes. The generalisation of it comes in the form of Lévy process ([Zaburdaev et al., 2015](#)), that generalise $\Psi(t)$ to be a draw from any stable distribution. Discretised, Equation [1.1](#) describes increment of a position Δx at the n^{th} time step Δt :

$$\Delta x_n \sim \mathcal{N}(0, \Delta t) \quad (1.3)$$

known as **random walk** ([Pearson, 1905](#))

Despite increasing understanding of biological, social and psychological mechanisms in animal behaviour, those fundamentals remain key approaches in the modelling of movement. Brownian motion, the *Lagrangian* formulation, captures the microscopic dynamics

of movement, while *Eulerean* captures the macroscopic state of diffusion. The time scale of observations and computational limitations inform the choice of discrete random-walk-based models. The following sections present examples of different modelling approaches and how additional terms help characterise what is observed in the movement of animals.

1.2.2.1 Lagrangian modelling

The Lagrangian approach in ecological modelling can describe the movement of a single animal through stochastic differential equations (SDEs) that express the movement as a combination of deterministic forces and random fluctuations, also known as the Langevin equation (Zaburdaev et al., 2015). It allows combining the inherent randomness of movement introduced with Brownian motion (or the Wiener process) 1.1 with the most basic mechanisms of some directionality. In principle, those are individual-based models (IBMs) as they focus on a single individual. Different formulations vary with the coordinate system, for the purpose of presentation, we will use the simplest two-dimensional definition following Preisler et al. (2004). We define an incremental step about an animal location $\mathbf{r}(t) = (x(t), y(t))$, at time t in a Cartesian plane as:

$$d\mathbf{r}(t) = \boldsymbol{\mu}(\mathbf{r}(t), t)dt + \mathbf{D}(\mathbf{r}(t), t) \cdot d\boldsymbol{\Psi}(t), \quad (1.4)$$

and in a matrix form as

$$\begin{bmatrix} dx(t) \\ dy(t) \end{bmatrix} = \begin{bmatrix} \mu_x(\mathbf{r}(t), t) \\ \mu_y(\mathbf{r}(t), t) \end{bmatrix} dt + \mathbf{D}(\mathbf{r}(t), t) \cdot \begin{bmatrix} d\Psi_x(t) \\ d\Psi_y(t) \end{bmatrix}, \quad (1.5)$$

where

- vector $\boldsymbol{\mu}(\mathbf{r}(t), t) = \begin{bmatrix} \mu_x(\mathbf{r}(t), t) \\ \mu_y(\mathbf{r}(t), t) \end{bmatrix}$ defines the **drift** component, which is the deterministic part of the movement describing the animal attraction and avoidance at different times and locations.
- The matrix $\mathbf{D}(\mathbf{r}(t), t)$ is the **diffusion matrix** that provides the magnitude of random movement in each direction, mediating the effect of the environment and allowing for correlation between directionality of movement.
- $\boldsymbol{\Psi}(t) = \begin{bmatrix} d\Psi_x(t) \\ d\Psi_y(t) \end{bmatrix}$ represents the increments of random Gaussian process for each dimension.

This generic formulation allows for many complex parametrisations, where parameters of movement change according to complex functions of time and location. In practice, however, the models need to be interpretable to match a hypothesis and able to fit the data to confirm or deny it. The most common cases are the following variations of random walk (Hooten et al., 2017):

- For **uncorrelated/simple random walk** this model is the equivalent to 1.1 with the drift $\boldsymbol{\mu}$ being zero and the diffusion terms independent between dimensions:

$$\begin{bmatrix} dx(t) \\ dy(t) \end{bmatrix} = \begin{bmatrix} D_x & 0 \\ 0 & D_y \end{bmatrix} \begin{bmatrix} d\Psi_x(t) \\ d\Psi_y(t) \end{bmatrix} \quad (1.6)$$

In this case, there is no implied directional preference and movement in one direction does not influence movements in another. Even though it is too simplistic to describe most animal behaviour, it still is a useful null hypothesis to more complex (or non-Gaussian) models (Sakiyama and Gunji, 2013).

- **Correlated random walk** (CRW) contains no drift component ($\boldsymbol{\mu} = 0$), and the diffusion term is usually temporarily correlated. The spatial correlation of the diffusion term is an unlikely case, and usually, CRW is modelled in polar coordinates where the step is defined in terms of its length $s(t)$ and the direction $\alpha(t)$, $r(t) = (s(t), \alpha(t))$. In those coordinates, if $\alpha(t) = d\Psi_\alpha(t)$, the direction will be auto-correlated, resulting in a realistic modelling of the directionality of animal movement. It has been popularised with study of insects, explaining butterflies' flight (Kareiva and Shigesada, 1983). Where only sparse data is available, such as in fish telemetry, Lilly et al. (2022) uses CRW to understand the movement of migrating salmon in standing water. Data can also be modelled as a mixture of CRWs to distinguish different modes of behaviour in long-term telemetry data, such as by (Morales et al., 2004) in herds of elk.
- **Biased random walk** model includes a non-zero drift $\boldsymbol{\mu}$, indicating a preferred direction, while the diffusion remains uncorrelated:

$$\begin{bmatrix} dx(t) \\ dy(t) \end{bmatrix} = \begin{bmatrix} \mu_{cx} \\ \mu_{cy} \end{bmatrix} dt + \begin{bmatrix} D_x & 0 \\ 0 & D_y \end{bmatrix} \begin{bmatrix} d\Psi_x(t) \\ d\Psi_y(t) \end{bmatrix} \quad (1.7)$$

where $\boldsymbol{\mu} = \begin{bmatrix} \mu_{cx} \\ \mu_{cy} \end{bmatrix}$ is the drift coefficients along both axes, representing the directional

bias. This model is suitable for simulating animal movements that are influenced by external factors like wind or current direction or by internal states such as homing instincts or resource attraction. For example [Langrock et al. \(2012\)](#) extend approach of [\(Morales et al., 2004\)](#) to elk models with the introduction of a bias term in some models. [Avgar et al. \(2013\)](#) uses a biased random walk to incorporate memory of predation and foraging into a theoretical spatial model.

- Finally, the **Ornstein-Uhlenbeck (OU) process** ([Uhlenbeck and Ornstein, 1930](#)) is characterised by a mean-reverting drift component, models the animal returning to a specific central location (x_c, y_c) over time. The equation is given by:

$$\begin{bmatrix} dx(t) \\ dy(t) \end{bmatrix} = - \begin{bmatrix} \alpha_x(x(t) - x_c) \\ \alpha_y(y(t) - y_c) \end{bmatrix} dt + \begin{bmatrix} D_x & 0 \\ 0 & D_y \end{bmatrix} \begin{bmatrix} d\Psi_x(t) \\ d\Psi_y(t) \end{bmatrix} \quad (1.8)$$

where α_x, α_y are the reversion coefficients, and x_0, y_0 are coordinates of the central point. This model effectively captures the behaviour of animals in a variety of scenarios thanks to this mean-reversing bias term. It is the most popular description of animal movement, from capturing the trajectory of swimming whales and the circular gliding of kestrels ([Gurarie et al., 2017](#)), shoals of fish swimming ([Gautrais et al., 2012](#)) to mammals like fisher and boar ([Blackwell et al., 2016](#)). The OU process forms the basis of my investigation in Chapters 3 and 4.

The above models can be extended with the use of other stable distributions in place of Gaussian as Ψ ([Zaburdaev et al., 2015](#)). Using a heavy-tail Cauchy distribution allows to model movement as *Lévy flights* with sporadically larger displacement $d\mathbf{r}(\mathbf{t})$, matching well some animals movement ([Smouse et al., 2010](#); [Avgar et al., 2013](#)).

1.2.2.2 Eulerian Approach

By contrast to Lagrangian models, which describe movement explicitly as individual-based models (IBMs), Eulerian models are “place based”. They are better suited to tackle the questions of space use on population or group level, where sampling frequency and scale do not allow IBM to be used directly ([Smouse et al., 2010](#)). They describe patterns of appearances as a probabilistic approximation of animal appearance in a given point in space using diffusion equations. An example of such an equation is the classical diffusion equation:

$$\frac{\partial p(x, t)}{\partial t} = D \frac{\partial^2 p(x, t)}{\partial x^2} \quad (1.9)$$

where $p(x, t)$ is the probability density function representing the probability of finding the animal at point x at time t , and D is the diffusion coefficient reflecting the rate at which the probability of presence spreads out over the area. This is the generalisation of the probability density function of Brownian motion equation (Equation 1.2). Strøm et al. (2018) model long-term movement of Atlantic salmon in the ocean with Equation 1.9 providing an estimated residency distributions. Ovaskainen et al. (2008) studied movement of butterflies using capture re-capture methods, where on average, each animal was observed less than twice, suggesting the Eulerian approach due to the scarcity of individual data.

Lagrangian and Eulerian can be used interchangeably with random and direct components of an IBM equivalent to a diffusion and advection processes. To better understand the interaction of animals with the environment, more than one approach can be used at the same time to recognise the individual nature of the animal and the aggregate force of the environment on it. To model fish movement in a flow field, Gao et al. (2016) combine the Lagrangian approach for the movement of the single fish with an Eulerian approach to model the spatial field of vector flow. In a laboratory setting that provides strong support for rules of navigation based on lateral-line sensing of the currents. On a larger scale, Goodwin et al. (2006) use such a mixed approach to optimise fish passes near the hydro-electric facility, where vector fields of water flow are affecting the movement of individual fish.

1.2.2.3 State-space models

Movement parameters derived from fitting a movement model to observations are only as useful as an interpretation that can be attached to them. In most of cases, we are using different parameter sets to describe discrete modes of animal behaviour, for instance: resting, exploration or foraging that are often time and space-dependent.

The simplest way to incorporate state change in the system is to assume that only the previous state affects the probability of the transition to the next. This is known as a Markov property and simplifies inference and model fitting thanks to this assumption.

In fact, the simple random walk (Equation 1.6), or Brownian motion is a Markov process where the previous location is the only factor that influences the next location, making the future independent of any other past states. Sakiyama and Gunji (2013) use a higher-order Markov process to introduce a memory to a Levy walk (a random walk with a power-law or heavy-tail distribution) showing better food searching behaviour on simulated data than a simple Gaussian random walk. A Higher n^{th} -order Markov process is an extension, where future state depends *only* on n previous states.

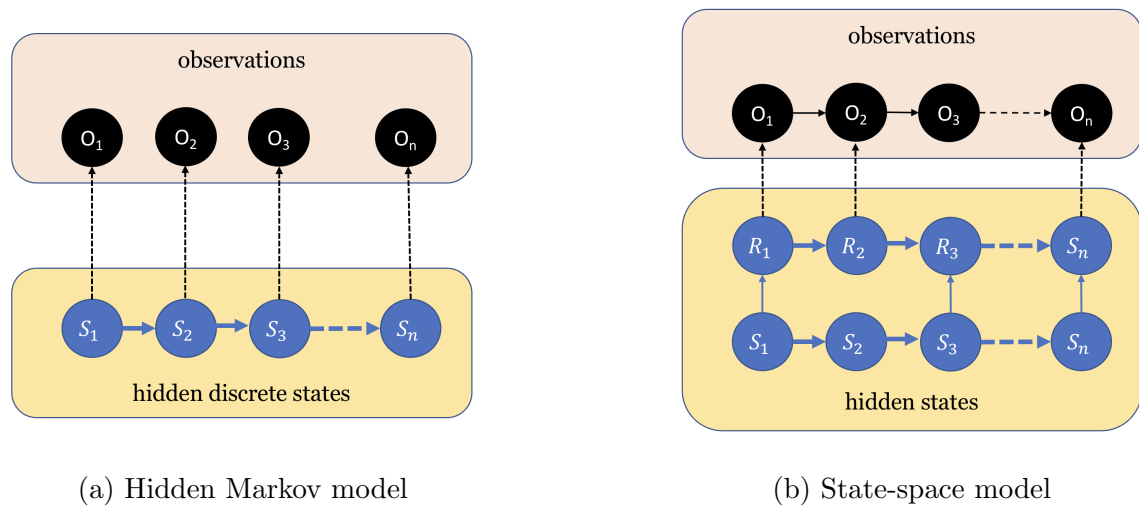


Figure 1.2: Schematics of Hidden Markov Model(a) and a more generic State-Space Model (b). In a Hidden Markov Model (a), some latent discrete states of the system S_1, S_2, \dots, S_n are changing with independent probabilities depending only on the previous step. Those states are observed with error as observations O . In general, as shown in the panel (b), process S can influence another process R (for instance observational process) at uneven intervals, either of which can assume continuous values.

When using the Markov process to model the changing of parameters of the underlying movement model (which in most cases is correlated as in CRW and OU processes), we often assume that the states of animals are a) discrete and b) latent. The modelling tool to express those assumptions is called a Hidden Markov Model (HMM), where each observation is a noisy observation of a behavioural state. In the Figure 1.2a I present a schematic of an HMM.

[Franke et al. \(2004\)](#) modelled behaviour of the movement of caribou, directly using measurement of distance and turning angle between observations to predict one of three states (bedding, feeding and relocating). [Towner et al. \(2016\)](#) used HMMs to analyse different types of swimming of white sharks with telemetry data. Using the model to accurately distinguish behavioural states allows the authors to see inter-sex differences and individual variability. The multi-year elk data from [Morales et al. \(2004\)](#) was modelled successfully with HMMs describing state-switching between types of random walks by [Langrock et al. \(2012\)](#) and different behavioural states ([Patterson et al., 2017](#)).

State-space models can be seen as a generalisation of HMMs or their continuous-time equivalent. They are a general framework where the modelling is described in a space defined by a number of states whose values change in time. Unlike HMMs, where the state value is discrete, the underlying states in the SSM take continuous values, representing the

“process” layer or a movement process. In animal movement modelling, it is also typical to add another “observational” layer (McClintock et al., 2020). Figure 1.2b presents the schematic of a complex SSM with two layers of processes with hidden states that are irregularly sampled. Dense and precise sampling of animal movement in the field is rarely possible and measurement errors are rarely truly independent. Unlike HMMs, where every observation of a hidden state has independent measurement noise, in SSMs, the observation is its own process with noise and bias, which, even though Markovian, presents another level of difficulty in fitting data to this much more realistic model.

In a previously mentioned study of butterfly dispersal (Ovaskainen et al., 2008), the sampling process has been modelled as an SSM, allowing the authors to adjust for unknown biases unavoidable in the fieldwork. Fish telemetry data, with high levels of uncertainty dependent on environmental factors show promise of increased accuracy in theoretical studies using SSMs (Campbell et al., 2024).

1.2.3 Collective behaviour

A potential key aspect of juvenile salmon migration is collective movement. Little is known about it as it is difficult to observe at the spatio-temporal scales of field research and to reproduce in a laboratory setting. In this thesis, I tackle both of those approaches. A review of collective movement is provided here to place this work in a wider context.

A stochastic movement model proposed by Vicsek et al. (1995) describe emergence of collective motion by showing a phase shift from random movement to clear alignment within the entire group. It models the alignment of velocity vectors of particles within some distance from each other with a noise term and constant speed. Another popular model based on schooling fish (Aoki, 1982) was created to describe a set of behaviours of attraction, alignment, and avoidance in the form of discrete-time simulation of otherwise random movement (Couzin et al., 2005).

1.2.3.1 Mechanisms of collective behaviour

Movement models described so far assume animals react only to sensory input from the environment. The study of social animals adds to it a response to the presence and behaviour of other agents within a sensory range.

Berdahl et al. (2017) review different mechanisms observed in migratory species both in nature and laboratory experimentation. The authors identify five primary mechanisms of collective behaviour:

- **Leadership** is an important factor in animal groups with stable social roles (for instance, elephants, horses and primates). In this case, the group relies on the superior knowledge of some individuals within a hierarchy emergent from social dynamics (Ozogány and Vicsek, 2015). Specifically, Couzin et al. (2005) show that, in theory, there is no requirement for any other physical difference between individuals to explain the spontaneous emergence of leadership in group movement. Leadership roles can be dynamic and based on specific information that an individual has, for instance, an individual sensing the predator first will initiate avoidance of the whole group of animals.
- **The many wrongs** mechanism is a well-described phenomenon where with increasing number of agents with partial knowledge, a better approximation can be found via pooling. It is hypothesized that it helps schooling fish in navigation. Assuming that each individual has a directional accuracy given by circular normal distribution Larkin and Walton (1969) show that the variance of the group’s mean accuracy will decline as $1/\sqrt{N}$ where N is a number of individuals in the shoal.
- **Emergent sensing** occurs when a response to environmental gradients is balanced by a tendency to follow the rest of the group (Berdahl et al., 2013). In the case of fish trying to follow stronger flow, individuals sensing current will initiate the movement and, after gaining enough followers, will bring ones too far away from stimuli to find the optimal direction themselves.
- **Social learning** allows for less experienced individuals to gain knowledge without direct experience by following others. This way, information can be passed across generations, for instance, about migration or other routes, as in the case of homing pigeons (Pettit et al., 2013).
- **Collective learning** means that individuals can learn from the previously mentioned many wrong mechanisms. If the group makes a particular decision multiple times, following cues leading to it can become a new taught behaviour for individuals. This way, even the more informed individuals can improve on the collective “wisdom” creating in practice a transferable culture (Sasaki and Biro, 2017).

1.2.3.2 Modelling collective behaviour

In order to quantify collective movement, we must define appropriate metrics. Many were suggested: group size, alignment, speed, turning speed, speed correlation between

individuals, directional correlation, and distance to the nearest neighbour. Based on their study of social fish, [Sumpter et al. \(2018\)](#) uses factor analysis to argue that all of those can be explained by individual characteristics of sociability and activity. These two are easier to explain using known biological mechanisms and responses.

Hydromechanical explanations were provided for the schooling of fish based on their shape and observed behaviour with theoretical models ([Weihs, 1973](#)). Once precise measurements of fish movement became possible, these models were confirmed through laboratory experiments.

Even when observations are possible, models allow for additional analysis of details that might not emerge from the empirical data model. [Croft et al. \(2015\)](#) writes on how simulated bird flocks avoid wind farm-like obstacles based on different assumptions on social rules and leadership. Their asynchronous model allows for better expression of the social interaction rules. The authors explicitly define a trade-off between social interactions and environmental awareness and explore the comparison between leaded and leaderless groups. The simulation shows situations in which strong social rules cause a worse obstacle avoidance abilities than those of a single bird, challenging an assumption that migratory birds collide with wind turbines due to sensory limitations alone.

1.2.3.3 Empirical studies of collective behaviour

The study of the behaviour of multiple animals simultaneously requires not only increase in the number of tracked animals, but also the accuracy of the method to capture differences within animals whose position is spatio-temporally correlated ([Hughey et al., 2018](#)).

By tagging enough birds in a flock of migrating white storks with high-accuracy GPS tags, [Nagy et al. \(2018\)](#) were able to show the patterns of collective sensing in birds exploiting thermal updrafts, though not identifying a simple mechanism that would explain them.

[Cooper et al. \(2018\)](#) show in a laboratory study of Sticklebacks (*Gasterosteus aculeatus*) that shoaling is a trade-off between an animal's optimal environmental conditions and the benefits of group behaviour. Temperature preference is one of those factors that can be forgone in order to move as a shoal. It is also known that standard and maximum metabolic rate influences sociability in fish ([Killen et al., 2011](#)).

[Kelley and Ouellette \(2013\)](#) leverage laboratory tools for 3D imaging of fluid dynamics to analyse the collective motion of swarms of midges (*Chironomus riparius*). As expected, they behave differently than schooling fish or flocking birds with lower levels of alignment, but their movements show some signs of local correlation.

1.2.3.4 Quantifying social and environmental factors

Often, it is difficult to disentangle the influence of social interactions on movement from environmental factors. [Calabrese et al. \(2018\)](#) define movement correlation indices to quantify the strength of social factors. The authors assume that the correlation of drift μ (as in Equation 1.4) between individuals is caused by environmental factors, whereas the correlation of diffusion D by social interactions. They define and test metrics of those correlations based on simulated and empirical data.

Modelling can be done directly on empirical data as shown by [Strandburg-Peshkin et al. \(2017\)](#) in a study of a baboon troop's movement. The study compares how different predictive models explain observed behaviour using detailed 3D environment data and basic social features, such as visual contact with a high-density of conspecifics. They found that the main predictor of movement was following previous locations of other troop members - a non-direct social interaction. The location of the sleeping site was the second most important factor, showing the importance of home range in studying some species.

Similarly, [Torney et al. \(2018a\)](#) analyses drone footage of migrating caribou extracting movement tracks and comparing different explanatory models fitted to extracted tracks. They show that alignment and attraction forces exponentially weighted with the distance between individuals provide the best explanation of movement within a herd. Due to the high resolution of the footage, they are also able to classify animals according to their life stages, finding differences in response to social cues. Calves are characterised by strong attraction but not directional alignment, which is dominant in adult individuals.

[del Mar Delgado et al. \(2018\)](#) provides a review of empirical evidence for heterogeneity in animal social behaviour. They further reinforce this theory by IBM simulations showing a variety of patterns known in collective movement, appearing more realistic when individuals exhibit some heterogeneity.

Group formation brings trade-offs between safety and coordinated movement but also limits access to resources. A study, [Fryxell and Berdahl \(2018\)](#) discusses such balance for gazelles in the context of personal fitness functions.

A mechanism to balance trade-offs between safety and coordinated movement is shown in many studies with fish. In a study by [Berdahl et al. \(2013\)](#), different sized groups of light-averse fish show the increased capability of avoiding light patches as their group's size increases in an example of collective sensing of environmental gradients. The authors compare the influence of the local light intensity gradient to social cues from other shoal members, finding greater responsiveness to social cues increases with the size of the group.

There is an increase in schooling among fish from high-predation environments (Ioannou et al., 2017) in what can be seen as an adaptation based on life history and the environment. Schooling has drawbacks as it limits food available to each fish and, in some species, might increase chances of capture (Thambithurai et al., 2018). Fish like salmon only school during particular phases of their life, possibly to optimise their energy expenditure while travelling. In general McLean et al. (2018) defines schooling in terms of energy expenditure required in different positions in the group when swimming and dependent on how recently each fish was able to feed. In the case of salmon, the effects of position in the shoal can only depend on the energy acquired before the migration season since smolts do not feed during their migration (McCormick et al., 1998).

1.3 Modern mathematical methods in biology and ecology research

The typical ecological modelling described in the previous section can benefit from important improvements in other areas of technology and science. In my work, I leverage modern data collection methods that, in turn, require the use of machine learning and simulation-based modelling due to their quantity and dimensionality. The following sections provide an introduction to these techniques.

1.3.1 Changing Data Landscape

Technological advancements over the last few decades have revolutionised how data is collected and analysed in ecological research. As the field relies on well-tested protocols and reproducible approaches, it takes time for many advancements from the fields of engineering and computer science to be adopted.

Dramatic improvements in the versatility of consumer electronics have reduced the cost of field research. Components that were once expensive and used only in industry are now produced on a mass scale at a low cost, often with simple software interfaces. These include microprocessors, batteries, transmission equipment (across various wavelengths, including satellite receivers), and different sensors such as accelerometers, temperature sensors, pressure meters, and cameras.

Inexpensive radio and acoustic transmitters allow for triangulation and reporting of the position and state of multiple animals at many points of interest. Much finer spatial and temporal data scales come without additional cost. These developments have fostered

collaborations on large-scale tracking projects, such as mapping the migration patterns of nearly two thousand salmon smolts from the British Isles (Rodger et al., 2024). Acoustic fish telemetry illustrates that areas where the application of consumer electronics is limited, are disadvantaged due to a lack of incentives to improve research tools. Precise location tracking is not possible on many telemetry systems because manufacturers limit access to the data collected with their devices (Guzzo et al., 2018).

The miniaturisation of electronics and batteries has reduced telemetry tags to a fraction of their previous size, alleviating concerns about tag burden and enabling the study of animals that were previously unfeasible to tag, such as salmon smolts (Lothian et al., 2024b). Efficient batteries allow a single tag to transmit data for months, and improvements in wearable technology set the scene for future devices that may function indefinitely. Precise GPS receivers and loggers, together with pressure sensors and accelerometers provide information on the location of animals with far greater accuracy than triangulation alone (Nathan et al., 2022). Biologgers that save temperature, pressure and acceleration data provide clues about an animal's immediate environment and its state. Images from satellites and aerial surveys allow for the analysis of animals' environments in increasing detail, unearthing information that isn't possible through observation at smaller scales (Williams et al., 2020).

Direct observation has changed with the advent of digital photography, moving from occasional observations of a single animal to constant observation at a low cost. In a laboratory setting, it allows for detailed tracking from multiple high-resolution cameras, providing detail even in darkness with infrared illumination (Lin et al., 2018). The ubiquity of high-quality imaging has effectively reversed the problem of having too few observations to having too many from which to select meaningful ones. This has led to a shift in focus towards the selection of valuable information in video tracking, described in detail in Chapter 3, where we tackle this issue in the context of observing fish movement.

Places previously inaccessible to researchers or that would cause a disturbance to the observed species can now be surveyed with remotely controlled vehicles. A camera-equipped underwater vehicle allows for undisturbed observation of fish, especially as image quality in low-light and infrared conditions has improved. Milligan et al. (2016) surveyed the density of abyssal fishes at depths of almost 5 km, providing updated density estimates compared to simpler, biased techniques based on catch data and challenging assumptions about their aggregation.

Drones can record videos of groups of animals from a distance, revealing movement patterns that cannot be distinguished from on-the-ground information. A study of Exmoor

ponies by [Kavwele et al. \(2024\)](#) automated the control of a video-recording drone, with the current GPS position provided by a collar on an individual, allowing the study of the collective aspect of its movement.

As the processing power of data-gathering devices increases, *edge computing* allows data to be pre-processed on the device, limiting the amount of raw data that must be sent across the network. This can ensure that only quality information—such as a change in behavioural state from a biologging device or an observation from a camera—triggers more resource-intensive data transmission. Developments in previously distant fields, such as sensor fusion and surveillance ([Thomas et al., 2016](#)), are becoming directly applicable to the study of animals in the wild.

The field of machine learning illustrates the dramatic improvements in the scale of data analysis and modelling that is made possible by increases in computing power. In particular, the development of Graphical Processing Units (GPUs) to perform operations on vectors of data (originally to display 3D images) has enabled breakthroughs in the development of algorithms, which are described in the following section [1.3.2](#). Recent analysis by [Sevilla et al. \(2022\)](#) shows that since the 2010s, even the impressive “Moore’s Law”, predicting the doubling of computing power every 20 months has been surpassed by the increasing capabilities of computer models. The increase in available data due to citizen science projects such as iNaturalist ([Van Horn et al., 2017](#)), Flora Incognita ([Mäder et al., 2021](#)) or Zooniverse ([Simpson et al., 2014](#)) highlights the growing importance of understanding and effectively using modern data analysis techniques to engage efficiently in ecological research.

1.3.2 Machine learning

Machine learning (ML) is a field of engineering focused on designing predictive models. Unlike statistics, which emphasizes inference and quantifying uncertainty, the primary goal in machine learning is to predict central values and generalise models from training to testing data across various real-life scenarios. This makes those techniques ill-suited to directly replace statistical modelling approaches described previously in [Section 1.2](#), but invaluable in pre-processing experimental data to extract measurement signal through automated analysis ([Valletta et al., 2017](#)).

Unsupervised machine learning methods ([1.3.2.3](#)) extract patterns aiding an interpretation of structure in the data. With the provision of annotated experimental data, supervised learning methods ([Section 1.3.2.1](#)), can automate the laborious manual process of extracting data from text, audio, images, video, and more.

I will first describe the most important supervised learning methods in Section 1.3.2.1, and more recent advances in deep learning followed by unsupervised approaches in Section 1.3.2.3. Machine learning found great success in computer vision, which I leverage in Chapter 3, where an in-depth review of modern methods of analysing visual data is presented.

1.3.2.1 Supervised learning

In supervised learning, data is typically represented in the form of a feature vector \mathbf{x} , with an associated label and a target vector \mathbf{y} . The popular problem of recognising an animal from a camera trap image, known as *image recognition*, is also a common benchmark task in the machine learning field. The knowledge to *learn* by the model is a correct choice of one of k discrete labels $\mathbf{y} \in \{1, \dots, k\}$ (e.g. species) describing the content of each single image. The input feature vector \mathbf{x} is derived from a given n by m image corresponding to a $\mathbb{R}^{n \times m}$ feature space.

The basic formulation of a machine learning problem is where the relationship between a feature vector, or an observation, \mathbf{x} and associated target \mathbf{y} is given by a function $h(\mathbf{x})$. Our goal is to find the function $f_\theta(\mathbf{x})$ which will approximate $h(\mathbf{x})$ sufficiently for practical needs with a well-chosen hyper-parameter vector θ . The simplest model used in practice is linear regression

$$f_\theta(\mathbf{x}) = \theta\mathbf{x}, \quad (1.10)$$

and logistic regression, using sigmoid function, for classification problems

$$f_\theta(\mathbf{x}) = \frac{1}{1 + e^{-\theta^T \mathbf{x}}}, \quad (1.11)$$

which can always be normalised to assume $\mathbf{y} \in (0, 1)$ (as a multi-class problem can be split into sub-problems). Those simple functions can be fitted to available data examples with their annotations $(\mathbf{x}_i, \mathbf{y}_i)$. The simple loss function based on squared error can be used

$$J(\theta, \mathbf{x}) = \sum_i (f_\theta(\mathbf{x}_i) - \mathbf{y}_i)^2, \quad (1.12)$$

and best parameters θ^* such that

$$\theta^* = \arg \min J(\theta), \quad (1.13)$$

can be found using a gradient descent algorithm.

For any problem with features $\mathbf{x} \in \mathbb{R}^n$, classification with logistic regression provides a separation with an $n - 1$ dimensional plane. High-dimensional data such as images allows for a perfect match of approximation $f_\theta(\mathbf{x}_i)$ with a target hypothesis $h(\mathbf{x}_i)$ on known training examples i . However, that does not guarantee that $f_\theta(\mathbf{x}) \approx h(\mathbf{x})$ in general, and it does not happen in practice (Hornik, 1991). Many methods have been popular to create a model f_θ that will be able to fit well to the training data but still generalise to unseen examples.

Random Forest (Scornet, 2016), Support Vector Machines (Vapnik, 1997) or Artificial Neural Networks (ANN) (Szeliski, 2022) are popular classification methods, that, in different ways, allow for the creation of a non-linear separation of data vector in ways that maximise the information gain from the classification. Random Forest is a natural extension of a Decision Tree method, a simple classification where data is repeatedly separated into binary classes based on a linear separation of the feature vector. In Random Forest, a large amount of shallow (uninformative) Decision Trees are pooled together to create a voting-like mechanism that can represent large amounts of information. Support Vector Machines transform the data into a space defined by a measure of distance between all the training data points. This increases the dimensions, allowing for a linear classification that maximises the overall separation of different classes.

ANNs are a widely used method because of recent advances in deep learning, which allowed extraordinary results to be achieved with multi-layered formulations of ANNs. These models benefit from large datasets and efficient linear algebra libraries, which enable parallelisation via Graphical Processing Unit architectures. Our Deep Predictor method described in Chapter 3 uses a Deep Neural Network.

Neural networks can be understood in the light of Universal Approximation Theory (Hornik, 1991) that provides a mathematical basis for approximating any continuous function $h(x)$. The Theorem states that for any continuous function $h(x)$ and an $\epsilon > 0$, there exists an arbitrary width $N > 0$, with weights v_i, w_i , biases b_i and bounded and non-constant function ρ such that

$$f(x) = \sum_{i \leq N} v_i \rho(w_i^T x + b_i), \quad (1.14)$$

satisfies

$$\sup_x |h(x) - f(x)| < \epsilon. \quad (1.15)$$

This formulation defines the theoretical potential of a one-layered neural network to be

used to model any complex function. The name “neural network” is owed to the inspiration taken from a biological neuron cell, which can be mathematically simplified as an activation function such as sigmoid. The input signal is weighted with w and offset with bias b to produce an output signal v if a certain threshold is reached.

For practical applications, however, it is often advantageous to employ multiple layers of such neurons. This is described by stacking L layers where each layer’s output serves as the subsequent layer’s input:

$$f(x) = f_1 \circ f_2 \circ \dots \circ f_L. \quad (1.16)$$

Such a multi-layered network gains the ability to model inputs with non-linear separation in the input space. A multi-layered network, often called “deep”, enhances the network’s ability to model more complex patterns and perform non-linear separations in the input space. Recently, [Kidger and Lyons \(2020\)](#) proved that all activation functions ρ usable in machine learning are able to approximate $h(x)$ in a deep neural network - one having a bounded width of layers and an arbitrary number of them.

A neural network $f(x)$ as defined in Equation 1.14 contains a large parameter vector θ consisting of weights, biases, and activation values for each neuron in the network. In a typical multi-layered neural network, as defined in 1.16 those parameters are large matrices with values that are specific to each application. This is contrasted with hyperparameters such as a number of layers L or type of function ρ that are set for a given architecture and do not change in training.

Some cost function J appropriate for the task can be formulated, and its minimum found using a Stochastic Gradient Descent (SGD) ([Zhang, 2004](#)). SGD is a variation of a gradient descent algorithm for such high parameter spaces where each update is performed on a randomly chosen sub-dimension of the J domain. Each parameter update step finds a gradient direction for the last layer of the network, where target y_i is compared with the current function output $f_\theta(x_i)$. To update the parameters in all layers, we need to know the corresponding gradient of J for each neuron. The backpropagation algorithm ([Goodfellow et al., 2016](#)) efficiently computes the gradient of J with respect to each parameter using the chain rule.

Using SGD and backpropagation, neural networks are able to achieve excellent fit for models in many domains. However, for a state-of-the-art performance on the benchmark task of image classification, more structural changes were required.

Traditional machine learning does not operate on raw pixel values to classify images.

For most tasks, the dimensionality would be too high to fit a model to the data. In images, information is derived from context and patterns rather than from individual pixel intensity values. This presents a challenge to the methods that cannot adapt to different, co-existing scales and transformations of objects. A variety of characteristic low-level features, such as corners and edges, are described mathematically, and the machine learning models are fitted to lower-dimensional and higher-level representations of an image. Hand-crafting of those features became an important part of image recognition work, mostly by reproducing human intuition regarding visual perception.

Thus far, we described neural networks containing *fully connected* layers. The ability to approximate any function is impeded by rigid positional connections and lack of components modelling correlation between different elements of the feature vector. It was discovered that specifically for images, we can use a convolution with arbitrary parametrised filters to allow for a low-level feature extraction. The convolution function works on image I passed in its original dimensions so that relationships between pixel values are preserved. The convolution on image I , with a convolution kernel K is defined as

$$(I * K)(x) = \sum_{\tau \in I} I(\tau)K(x - \tau), \quad (1.17)$$

and it provides a *feature heatmap* of similarity of different parts of the image with K , in a Convolutional Neural Network (CNN) there are multiple convolutional layers which act as a fully trainable filter bank. This visual data encoding is crucial from a practical perspective. Using a single fully connected layer with the input and output of a typical video camera (1080 by 720 pixels) would result in over 1 trillion parameters taking over 1TB of storage. Such a network would be almost impossible to train if only due to memory constraints. Apart from making it possible to approximate relationship $h(x)$ much better, CNNs provide a higher-level representation of common visual patterns and shapes. This property has led to the rise of *transfer learning* where weights of convolutional layers are trained on huge datasets that can then be directly copied to a network used in for a small target problem (Akçay et al., 2016). Then, just the neural networks' fully connected layers performing classification are fine-tuned to the specific tasks.

1.3.2.2 Applications of Machine learning in Ecology

Supervised machine learning allows the automation of data analysis from still images, audio field recordings and videos of animal behaviour (Valletta et al., 2017). Increasingly large datasets of ecological data are being analysed, and early examples of deep learning

applications have demonstrated their suitability for ecological research ([Christin et al., 2019](#)).

[Wijeyakulasuriya et al. \(2020\)](#) compared the use of ML algorithms of Random Forest with deep learning and analytical methods for predictive movement models of animals at different scales of gull migration and ant movements. Interestingly, the traditional ML method of Random Forest provided the best results, showing the limitations of deep learning methods when training data is limited. The authors also highlighted the lack of interpretability of those methods compared to analytical movement description that, even though having less predictive power, provides a better functional insight.

ML methods are particularly well suited to tasks involving visual data. [Torney et al. \(2019\)](#) leveraged Convolutional Neural Networks (CNNs) for a population survey of wildebeest from aerial imagery. CNNs are used to detect whales from both aerial and satellite imagery ([Guirado et al., 2019](#)) sea turtles from UAVs ([Gray et al., 2019](#)) or birds from camera traps ([Ferreira et al., 2020](#)).

As audio signals can be analysed in the form of a spectrogram, audio analysis has benefited from advancement in CNNs, resulting in their application for the detection of birds from birdsongs ([Lasseck, 2018](#)) and bat species from their echolocation calls ([Aodha et al., 2018](#)).

[Chabot et al. \(2018\)](#) compared ML methods for visual counting of large volumes of birds in breeding colonies across different conditions and environments. The authors highlight the reduction of time required to provide the same quality of counts by 90%. ML approaches have been similarly successful in counting African mammals from satellite images ([Yang et al., 2014](#); [Xue et al., 2017](#)),

As recordings of animals in the laboratory and in the field become the the standard method of the survey, so analysis of these videos becomes important. [Panadeiro et al. \(2021\)](#) describes a common video processing framework used in tracking animals in biological and ecological studies. Various machine learning and analytical methods are combined in popular software packages, where the user provides the supervision of the learning process through initial parameter tuning to specific task, and corrections to the output data thought the process.

[Banerjee et al. \(2021\)](#) developed a tool that classifies behavioural responses of fish recorded on video to ambient odour using different machine learning methods. The authors used experts to annotate the data and showed that all ML methods trained on that data exceeded the accuracy of prediction coming from manual annotations from non-experts.

In Chapter 3, I provide a further review of ML computer vision methods for object

detection and tracking.

Other sensory data can also benefit from processing with ML algorithms. Movement and location data can be modelled to infer animal behaviour. Analysis of accelerometer data from animal tags with ML provides an alternative to assess behavioural state reliably and supplement movement data analysis (Wang, 2019)

Software application Weka (Hall et al., 2009) provides access to ML algorithms for use in ecological data, for instance, analysing large-scale biodiversity data (Willcock et al., 2018) and other problems requiring a large amount of data.

1.3.2.3 Unsupervised learning

Often in ecology, we first encounter and analyse patterns before we can clearly define the mechanisms that gave rise to them. In the same way unsupervised learning is a name given to advanced statistical methods that aim to distinguish and quantify patterns in data without any explicit labelling or information provided ahead. Those methods are often a form of data pre-processing with aims such as: to select or transform exploratory variables (feature selection), to cluster data based on some commonalities, or to reduce dimensionality of data without detriment to the information in it.

Principal Component Analysis (PCA) reduces the number of dimension, or variables, in data by removing ones that are correlated. It finds such transformation of the coordinate vectors that they are ordered by the amount of variance of data explained by each. It is a common pre-processing step to reduce the the dimensionality of data for further classification with supervised learning methods (Xu and Cheng, 2017; Wijeyakulasuriya et al., 2020), or in order to observe any clustering that might not be apparent without disentangling correlated variables, such as in the analysis of movement patterns (Kays et al., 2023) or collective behaviour (Sumpter et al., 2018).

A more advanced method of dimensionality reduction, t-distributed stochastic neighbour embedding (t-SNE) is specifically designed for visualisation of multi-dimensional data to aid with visual understanding. This method was used by Valletta et al. (2017) to analyse the appearance of Wildebeest in an overhead video or by Derkarabetian et al. (2019) to illustrate genetic structure of species.

Before the development of deep learning methods, ANNs (Chon et al., 1996) and genetic algorithms (Recknagel, 2001) were used to detect patterns in species density data by creating Self-Organising Maps (Kohonen Networks) that clustered different communities together in clusters that were then explained with ecological connectivity and interdependence. The previously mentioned study of the behavioural response of fish uses an

ANN to reduce the dimensionality of data before classification by supervised ML methods (Banerjee et al., 2021).

Many algorithms for clustering exist for detections of commonalities in data (Szeliski, 2022). Franke et al. (2004) clusters observed movement observations to create discrete states for further modelling. Zhang et al. (2015) use a k-means clustering with a behavioural change point analysis of penguins' movement to find and analyse discrete types of behaviour (resting, commuting/active searching, area-restricted foraging). Gupte et al. (2022) use a custom clustering algorithm to detect and distinguish behavioural states of birds from long-term large telemetry datasets.

Clustering of visual data into background and foreground is a leading method in pre-processing of experimental imaging data in ecology. Gaussian Mixture Models (GMM) are used directly to perform background subtraction from images used in many modern methods (Panadeiro et al., 2021) by creating a probability model of pixels belonging to one of the predefined distributions. Psorakis et al. (2012) uses Gaussian mixture models to cluster behavioural data to create a network of social interactions.

Clustering approaches are particularly useful in analysing genetic data due to their very high dimensionality. Derkarabetian et al. (2019) shows clustering of high-dimensional genetic information provides delimitation of species of arachnids.

Most recently, the distinction between supervised and unsupervised learning diminishes as leaps in Generativ Artificial Intelligence (Goodfellow et al., 2016) blurs the boundaries between assumed perfect knowledge of training examples and information available just from the data context.

The extraordinary success of Large Language Models (LLMs) in retrieving information promises a revolution in many knowledge-based industries. LLMs are based on attention-based neural networks, notably transformer architecture (Vaswani et al., 2017). There are already successful applications of those techniques in areas that are based on pattern matching, such as protein understanding (Elnaggar et al., 2020) and protein folding (Jumper et al., 2021). However, their use in ecology remains rare due to the novelty of the approach. LLMs have been tested for the extraction of ecological data from literature and databases, achieving a 50-fold increase in speed while maintaining mostly high accuracy (Gougherty and Clipp, 2024). Despite their successes, in any application where scientific and statistical validity of data is required, LLMs fall short without additional manual review of the output. Indeed, the current focus of research in this area relates to improvements to reinforcement learning techniques to improve the quality of the output (Ziegler et al. (2020)).

1.4 Applications in the context of salmon migration

The aim of this thesis is to investigate the behaviour of Atlantic salmon movement during their downstream migration. It is an important question from a conservation viewpoint that affects how we should study and protect this important species and its ecosystem. It is also an interesting problem informing methods of studying other species and systems where direct observation is challenging.

Better flow sensors and investment allow for detailed mapping of the hydrological environment in potentially crucial places on the migratory route (Xu et al., 2017; Babin et al., 2020; Sridharan et al., 2023). The study of Olivetti et al. (2021) modelled smolts migration on a 500m confluence section of San Joaquin River in California. Firstly, the authors constructed a 3D computational fluid dynamic model of the reservoir using detailed flow data from a two-dimensional near-surface measurement of water flow, and river bathymetry data (depth and shape of the riverbed) from a multi-beam sonar survey. Secondly, a calibrated receiver array allowed for co-location of juvenile Chinook salmon with a sub-meter accuracy and 2-second time sampling that provided the empirical data for the calibration of a movement model of the fish within the river. With the detail flow measurements, the authors were able to calculate the precise force of drag and locomotion at every point of the studied segment. In order to model and validate a fish's response to its environment, the authors trained a deep learning model, a Long Short-Term Memory Neural Network to predict the next position of fish based on the flow, location, and the previous movement. Despite the impressive resources and detailed tracking in this study, collective behaviour was not reported on, highlighting the trade-off between the quality and quantity of data in field studies, where even with such accuracy of a method, the sample size is still limited by the laborious tagging process (424 individuals).

Holleman et al. (2022) analysed the swimming patterns from that fine-scale data, classifying movement with positive and negative flow orientation, lateral swimming, and drifting. The authors estimated the average swimming speed as lower than previously established in laboratory studies and were able to analyse and compare the movement at different depths of the water column. This flow and movement modelling has been used in another study by Sridharan et al. (2023), to develop a coarser, larger-scale model, ePTM (enhanced Particle Tracking), which allowed authors to study the migration of juvenile salmon in the context of more general river discharge and environmental conditions across the whole river system. This parallelisable agent-based model was used to describe and predict migration routes and the success of smolts in the complex river system informing

how best to design riverine structures and time the discharge of water from reservoirs.

An ordinary particle tracking model was used by [Newton et al. \(2021\)](#) to compare the direction of movement of post-smolts with the known currents in the Moray Firth, an inlet on the East Coast of Scotland. This large-scale study followed the migration of almost 800 Atlantic salmon smolts. Together with another study on the West coast of Scotland, England, and Ireland that followed over 1900 smolts ([Rodger et al., 2024](#)), those form a part of a new collaborative approach to telemetry studies. The enhanced collaboration between research organisations brings benefits from the miniaturisation of telemetry tags and cost-sharing and allows the study of much larger quantities of fish than possible otherwise.

As the efforts to consolidate data and knowledge relating to the Atlantic salmon grows, for instance, with the creation of a data hub ([Diack et al., 2022](#)), or digitisation of historical records ([Adams et al., 2022b](#)), large scale statistical modelling provides new insights. The Scottish population of juvenile salmon is now reliably mapped thanks to spatial modelling of sparse and imperfect survey data ([Malcolm et al., 2019](#)). Analysis of historical samples of salmon over almost 30 years was used to detect environmental shifts that affect the entire salmon population and wider marine ecosystem ([Vollset et al., 2022](#)).

The novel approaches to telemetry modelling incorporate movement models to test hypotheses about the smolts' movement in standing waters. Both [Hanssen et al. \(2022\)](#) in lake Evangervatnet in Norway and [Lilly et al. \(2022\)](#) in the study of movement in Loch Lomond, Scotland, use correlated random walks to model smolt movement in standing water. At every fixed length step, fish in a lake modifies the previous heading according to a zero-centred Gaussian distribution. This approach allows testing of the hypothesis of random exploration of the lake, where a lack of water flow gradient is not able to direct fish to the correct outflow.

Exploring more sophisticated statistical models with and without social interactions quantify the collective effect in salmon migration - even if its precise mechanism remains elusive. [Berdahl et al. \(2017\)](#) modelled sparse catch data of a return migration of Pacific salmon migration using two models: with and without a social component to it. The fish's probability of moving between subsequent upstream river branches was mediated by another fish's successful transition in the first model and was fully independent in the other. Inclusion of a social component provided a significantly better explanation of the catch data and the 20-year span of observations allowed averaging of any possible confounding variables such as maturation of fish, seasonal changes, etc. Using State-Space modelling, [Kururvilla et al. \(2024\)](#) conducted a a conceptually similar experiment

on downstream migrating smolts by modelling the number of smolts caught in a trap with possible social effects while taking into account all known factors influencing the timing of migration. The authors best-fitting model confirm the hypothesis of social cues influence on migration timing in juvenile Pacific salmon.

1.4.1 Outline of this thesis

This thesis casts a wide net around the problem of downstream migration of juvenile salmon, specifically trying to understand the mechanism of potential social effects. This analysis benefits from the application of modern methods at different scales, and I leverage video recording and GPU-parallelised data processing in the laboratory, simulations and the field. In laboratory experiments I consider both wild and hatchery salmon: first to measure their response to changing flow conditions, and following that, to observe their collective movement in an artificial stream. In simulation-based work, I develop improvements to a computer vision method of automatically tracking animals on video. Lastly, I develop a movement model to fit telemetry data from smolts migration.

In the first study, presented in Chapter 2, I focus on individual migrants' responses to water velocity, widely considered the most important environmental cue in their migration. I establish the baseline sensitivity of wild and hatchery smolts to the changing flow direction in an artificial river.

This experiment is supported by computer engineering, with time-synchronised cameras and image processing automation, enabling the measuring of the signal in a study otherwise requiring excessive manual work.

In Chapter 3, I develop a method of precise tracking of animals in video recording, that works robustly in cases of indistinguishable animals in crowded scenarios. This is a GPU-enabled deep learning method that is inspired by the types of data collected in my laboratory experiments and analysis in quantities not possible without high levels of automation.

In Chapter 4, I leverage the laboratory setup developed during previous experimentation and a computer vision method of automatic extraction of movement tracks to study the behaviour of Atlantic salmon migrating in groups in the artificial stream. I observe the overnight movement of wild and hatchery smolts in the presence of an obstacle and measure the collective effect on decision-making.

In the last study presented in Chapter 5, I develop a simulation-based framework for statistical analysis of field data from a study of juvenile migration. I build a GPU-accelerated movement model with an observational process to match the field-telemetry

data. The simulation accounts for presumed auto-correlation and directionality of the downstream migration, as well as for the potential collective component observed in the laboratory experimentation. I test the statistical properties of this method on two simulated scenarios, showing the validity of the approach and direct application to river telemetry data.

In the last chapter 6, I summarise the findings of my research and the implications for the future direction of research on juvenile salmon movement.

Chapter 2

Defining the water flow cues for navigation in migrating Atlantic salmon smolts

Note

The content of this chapter has been submitted to the Journal of Fish Biology under the same title and authored by Mikolaj E. Kundegorski, Hannele M. Honkanen, Alastair Stephen, Colin J. Torney, Shaun Killen, and Colin E. Adams. The manuscript was written jointly by Mikolaj Kundegorski and Hannele Honkanen based on the experiments and analysis performed solely by Mikolaj Kundegorski. All authors participated in the experimental design, conceptualisation, and revision of the manuscript.

2.1 Abstract

Successful navigation during migration is critical to fitness. In Atlantic salmon, for example, there is evidence that during migration from natal streams to the sea, passage through waters with poorly defined or mixed water velocity patterns may constrain directional navigation, causing individuals to become trapped or delayed in lakes or other bodies with slowly flowing water. In this study, we determined the minimum water velocities needed to elicit a change in the direction of holding in both wild origin and domesticated salmon smolts. Smolts required a directional flow in excess of 8.9 cm/s to show effective directional orientation toward the current. Domesticated smolts showed a similar qualitative response as wild fish but showed slightly lower minimum velocity to initiate a response. These results suggest that, in areas where the downstream migrating Atlantic salmon

smolts pass through low directional water flow, it may be possible to manipulate directional flows above this minimum threshold at least temporarily as a management tool to increase migration success. This is likely to be particularly true where smolts are passing through dams, reservoirs, or other impounded waters.

2.2 Introduction

Long distance migration is a common strategy found across a wide range of animal taxa, that often involves movement between breeding and feeding grounds (Dingle and Drake, 2007). Long distance migration is associated with a high level of risks, including predation by novel predators, exposure to disease and parasites and the chance that the migrant will not successfully reach the intended migration destination (Dingle, 2014). Overcoming this last risk is particularly challenging, especially for individuals undertaking the migration with no prior experience of the route (Adams et al., 2022a). Therefore, it is clear that successful migration is dependent upon high quality navigation ability.

Animal navigation, especially in the case of long distance migration, is hugely complicated and still not fully understood (Alerstam, 2006; Mouritsen, 2018; Putman et al., 2014). What we do know suggests that migration is only infrequently a passive process, for example where the animal relies on wind or water current to move. One of the few examples of passive migration appears to be the migration by the larvae (leptocephali) of the European eel (*Anguilla anguilla*) (Van Ginneken and Maes, 2005). However even in marine environments, where there is scope for passive movement using currents and there is a specific end goal location, variation in current patterns means that purely passive migration strategy is directionally unreliable (Putman et al., 2014). Active migration requires cues to identify the right time to start moving, an awareness of the surrounding environment, knowledge of when to stop moving and the ability to identify and interpret the correct directional cues for navigation (Åkesson et al., 2014). Some of the known mechanisms that animals use to orientate and navigate during migration include celestial, geomagnetic, visual and olfactory cues (Bolshakov et al., 2007; Cochran et al., 2004; Wikelski et al., 2015). The importance of these cues is well understood, while the required intensity of the cues needed for successful navigation is largely unknown.

Migratory Salmonidae fish use several types of cues for navigation including water flow, olfaction and geomagnetic maps (Madsen et al., 2019; Putman et al., 2014). During the early stages of marine migration, Atlantic salmon *Salmo salar* seemingly use surface currents for direction finding (Dadswell et al., 2010; Gilbey et al., 2021b; Mork et al.,

2012). Work on Chinook salmon, *Oncorhynchus tshawytscha*, and Sockeye salmon, *Oncorhynchus nerka*, has shown that these fish also use a combination of magnetic intensity and inclination angle to navigate at sea and olfactory cues during their return journey (Drenner et al., 2018; Dittman et al., 1996; Madsen et al., 2019; Putman et al., 2014). Rheotaxis, orientation to flow, is one of the main ways in which fishes respond to their environment. It is a flexible behaviour and used for many purposes, from maintaining position in flowing water, to searching for food (Coombs et al., 2020). For juvenile Atlantic salmon, in common with many other salmonids, rheotaxis has a significant role in their feeding strategy during their first few years of life when it facilitates their drift-feeding behaviour (Arnold et al., 1991; Holleman et al., 2022; Klemetsen et al., 2003). During the early stages of smolting in Atlantic salmon, this station holding behaviour alters and fish begin to lose positive rheotaxis to move downstream with the current. Initiation of the downstream migration by smolts is frequently associated with increased water flow, once a minimum temperature has been reached and day length increases (Hvidsten et al., 1995; Connor et al., 2003).

Evidence of the importance of water flow as a key navigational cue comes from investigations of Atlantic salmon smolt migration through standing waters (lakes and reservoirs). Multiple studies have shown that smolts experience very high migration failure rates and long passage times of successful migrants during lake migration compared with their passage in river channels (Aarestrup et al., 1999; Schwinn et al., 2017; Lilly et al., 2022). It has been suggested that this stems from the inability of smolts to find the outflow of lakes. This is evidenced by random and directionless swimming patterns undertaken by both smolts that migrate successfully and those that do not, in these habitats (Schwinn et al., 2017, 2018; Lilly et al., 2022; Honkanen et al., 2018, 2021; Hanssen et al., 2022). One possible explanation for the apparently random pathway patterns is that high quality directional information, that the smolts require as a cue for navigation, are missing, or at least highly reduced, in lakes (Schwinn et al., 2017). Further evidence of the likely fitness cost of lakes comes from Hutchings et al. (2019) who found that of the 72 non-anadromous salmon populations worldwide, 82% are found in catchments with lakes, suggesting that these habitats discourage migration.

Despite the well-known importance of water flow as a directional cue during the riverine component of smolt migration, there is a paucity of information on the ability of salmonids to detect current and in particular the sensitivity of current detection that allows them to orientate. It has been suggested that juvenile salmonids can sense flow change that is as low as 0.4-1.0 cm/s (Gregory and Fields, 1962; Enders et al., 2012) but there is very little

information on the minimum water velocity that can be sensed by salmonids and which will initiate a response. In one of the very few studies on this topic [Veselov et al. \(1998\)](#) tested the minimum water velocity which “elicited movement of eyes, fins, or curving of the body, and resulted in the fish orienting into the current” in Atlantic salmon. They tested alevin, fry, parr and smolt life stages by quickly accelerating the water velocity from 0 to 160-200 cm/s in a small chamber. They found that the minimum velocity that elicited such a response was ~ 4.3 cm/s for alevins (fish length 2.3-2.6 cm) but that this decreased to around 2 cm/s for fry and parr (fish length 4-8 cm) and then increased to ~ 5.5 cm/s for smolts (fish length 10-12 cm). While detailed, this study did not address a common scenario where fish have to acclimatise in, and respond to, a heterogenous flow environment.

Sensitivity and response to flow cues could be linked to their previous environment, so individuals that experience a range of naturally fluctuating flows may have a higher sensitivity threshold compared with farmed Atlantic salmon that grow in controlled hatchery conditions with very weak flows. Farmed Atlantic salmon have been subjected to domestication selection for between 10 and 20 generations and are therefore genetically distinct from the wild populations ([López et al., 2019](#)). Many studies have shown differences between wild and farmed salmon in a range of characters such as growth rates, physiology, behaviour and gene transcription ([Glover et al., 2017](#); [Einum and Fleming, 1997](#); [Fleming et al., 2002](#); [Roberge et al., 2008](#)).

Here we tested the minimum water flow rate that elicits a change in the direction of holding against the current in Atlantic salmon smolts in the seaward migration phase of their life cycle in a controlled environment experimental trial. A secondary aim was to test if Atlantic salmon of farm origin have retained the ability to use water flow as cue for orientation and at the same level of sensitivity as their wild origin counterparts. Specifically, this study aimed to answer three questions: 1) What is the behavioural response of salmon smolts to changing water velocity?; 2) What is the minimum threshold value of water velocity that elicits a change in behaviour?; 3) Do wild and farmed smolts respond differently to changing water velocity?

2.3 Methods

Behavioural trials were conducted at the Scottish Centre for Ecology and the Natural Environment (SCENE), University of Glasgow. The behavioural arena was part of an oval flume tank, 11 m long and 0.6 m wide. Water depth was ca. 20 cm and a directional

flow was created in the channel by water being drawn from a sump in the flume outside the experimental arena and pumped through directional nozzles back into the channel at the opposite end of the flume. Water in the flume tank was drawn from the nearby Loch Lomond and was maintained at ambient temperature (range 6 – 16.1° water surface temperature determined using the dataset from [Chin et al. \(2017\)](#)) during the study. Behavioural trials took place in a straight section of the flume (1.6 m long and 0.96 m²), partitioned by screens through which water could easily flow. Trials were filmed from above using two, time-synchronised Raspberry Pi computers each connected to a Full HD near-IR (day/night) camera with 15 frames per second recording frequency.

At the beginning of each trial, a single Atlantic salmon smolt was placed in the test area with a stable current (approximately 20 cm/s in the middle of channel) with flow in either a clockwise or counterclockwise direction for 20 minutes, to allow the fish to acclimatise to tank conditions and to orient to the flow. Typically, smolts would orientate head-first into the water flow during this period. At the end of the acclimation period, the water flow direction was reversed for the remaining 5 minutes of the trial. To achieve this, the direction of flow from the pumps creating the directional flow in the test arena was reversed at a single point in time. The effect in the arena was that water speed slowly decreased and then reversed direction, slowly increasing in the experimental area to a velocity that was close to the original velocity but in a direction ca 180 ° from the original current direction. Due to the size of the flume and the volume of water it contained and despite that flow velocity delivered by the pump was at a maximum from the moment of flow reversal, it took up to approximately three minutes following directional change for the flow velocity to return to its original velocity (but in the opposite direction) at the location where the fish was holding. For each test fish the lowest water velocity that initiated a behavioural flow re-orientation response in the test fish was determined (V_{min}). This was defined as the water velocity at which the smolt changed orientation (by turning 180 degree) to face into the new current direction. To measure this, the precise time at which the smolt reorientated (the reaction time) and the exact location within the trial arena where this occurred (determined from scaled coordinates taken from video footage) was recorded. Following the trial with a fish, a velocimeter (Hontzsch Flowtherm NT) was placed at the position at which the smolt in that trial was located. The change in water direction was then replicated without a fish present. V_{min} was measured as the mean water velocity measured over a 10 second period (5 seconds before and 5 after the time of the time of the initiation of the re-orientation by the test fish). The average response time was 1.5 minutes, and for most of the measured points flow stabilised in the new (opposite)

direction after about three minutes. In addition to this, the velocity of the stable current before and after flow direction change was also measured at the position where the fish was holding. All velocity measurements were made at approximately 2 cm from the bottom of the flume tank to correspond with the depth at which fish would be experiencing flow when holding at the bottom of the tank. Across all fish, in all trials, the mean velocity to which test fish were exposed during the acclimation period and following flow reversal was 12.6 cm/s (SD=5.3).

Three groups of Atlantic salmon smolts were used in the trials conducted in three separate periods; two fish groups were of fish farm origin and the third comprised wild caught fish. In the first set of trials (August 2019), farmed fish originating from an indoor aquaculture facility (supplied by MOWI's, Lochailort Hatchery) were tested. These fish (N=52 randomly selected individuals, from a larger group with mean weight of 120g (SD=22) and FL 20.7 cm (SD=1.3)) were transported to SCENE as parr and allowed to develop to the smolt stage (which as assessed using the criteria of [Gorbman et al. \(1982\)](#)) before trials were conducted (water temperature during these trials was 13.6 – 16.1°). The second set of farmed fish trials were conducted in March 2021 (water temperature during these trials was 6.0 – 6.7°), using fish originating from a freshwater lake cage farm system (supplied by MOWI: Loch Arkaig). These fish (N=58, mean weight of 44 g (SD=14), fork length 16 cm (SD =1.5)) had already reached the smolt stage or were very close to smolting on collection. Trials on farmed fish commenced once they began smolting and were acclimatised to a spring-like photoperiod (16:8), mimicking their natural migration period. We also verified the initiation of migration by observing a consistent downstream movement for fish from those groups before our trials. Initially, both farmed fish groups were raised under constant light to rapidly increase their growth, a practice diverging significantly from their wild counterparts in terms of seasonal and temperature conditions.

The third set of trials were conducted in May 2021 on wild salmon smolts collected from the River Gryffe, Scotland (55° 51.9' N; 004° 31.1' W). Smolts were captured in a rotary screw trap during the smolt run (N=31 individuals mean weight of 24 g (SD=6) and mean fork length of 13 cm (SD = 1)). These fish were transported to SCENE in oxygenated bags (transport time ~ 1 hour) after which they were placed in holding tanks in which they were held for at least 2 hours before trials. The daily temperature during those trials ranged 7.7 – 8.1°.

To account for any potential bias in directionality the initial flow direction was alternated from clockwise to counter-clockwise. The flow conditions experienced by fish during holding in the experimental area varied between experiments. This resulted from changes

in water turbidity (determined by the conditions in the water source) and for technical reasons the pump creating the flow was changed between experiments (though with the same nominal output), however in all experiments flow conditions cases provided a discernible flow resulted in fish showing positive rheotaxis when holding position. A flow profile of the flume section where experiments were conducted showed a high coefficient of variation of 0.42 (mean=18.25, SD=7.66). All of the wild fish experienced the same flow conditions except for the initial flow direction. The flow value experienced at the point where fish were holding prior to current switching varied (mean=12.9 cm/s SD=5.2, range 2.0 cm/s to 22.4 cm/s) and tested as an explanatory variable.

During the trials, four behaviours were categorised within five minutes of the flow direction change (see Table 2.1). For two of these “Swim off” and “Constant Movement” are behaviours that are uninformative in respect of the main aim of this study, which was to determine a response to flow direction and velocity. This is because both of these behaviours could be responses to other environmental or internal cues. Thus for example the behaviour “Swim off” could be a response related to investigation of a possible food item in the water column. The two behavioural categories that were informative in relation to flow cues and were thus analysed more fully were :”Change of direction” and “No reaction”. In cases where the fish was in movement throughout the experiment or initiated movement before any other response to flow direction we classify as “Other behaviours” (comprising “Swim off” and “Constant movement” and were not analysed statistically, but provided for better insight into the ranges of behaviours observed.

We analysed the data using R (Team, 2021) using generalised linear models. Seven trials were excluded where experimental measurement error occurred. A behavioural reaction to flow change in the trial was modelled as a binomial model with “Change of direction” or “No reaction” as the two outcomes. Fish type (indoor farmed, outdoor farmed and wild) and general flow conditions (direction and high/low flow strength) were considered as variables together with their interaction. “Constant Movement” and “Swim off” behavioural categories were excluded from this analysis.

The flow velocity (V_{min}) which resulted in a behavioural response was modelled for individuals which successfully changed the direction of holding as a gamma distribution with a logarithmic link function. To compare nested models we primarily used ANOVA with Likelihood Ratio Test. The Bayesian Information Criteria (BIC) and Akaike Information Criteria (AIC) were used to quantify the quality of a model fit with likelihood while penalising model complexity to compensate for overfitting. We report both values to compare the quality of fit for all models. For post-hoc analysis we used Tukey’s range

Response to Flow	Number of Samples	Name	Description
Yes	62	Change of direction	A change in fish orientation indicated by an approximately 180° switch in their holding position to a positive rheotaxis in new flow conditions.
Other behaviours	24	Swim off	The fish initiates movement away from the position where it was holding, without directional change.
	24	Constant Movement	The fish kept moving throughout the trial showing no clear response that could be related to the directional current change.
No	24	No reaction	The fish did not seem to respond behaviourally with either a change in orientation direction or by moving position.

Table 2.1: Classification of behaviour of the fish within 5 minutes from initiation of change of water flow direction. Because only one of these behaviours, Change of direction, could be clearly attributed to the flow direction change, we treat behaviour “Constant Movement” and “Swim Off” as neither responding to nor not-responding to flow (“Other behaviours”).

tests. We included fish type (smolt origin), the magnitude of stable flow at the fish location prior to change in orientation direction and their interaction as explanatory variables.

Ethical statement

These experiments were conducted under UK Home Office licence (PPL 70/8794) and the care and use of experimental animals complied with the animal welfare laws, guidelines and policies prevailing at the time of the study.

2.4 Results

Changing directional water flow caused “Change of direction” or “No reaction” in 86 fish (64% of all fish successfully tested), while for 48 fish (36%) reaction was “Other be-

haviours”. In these cases fish were either in movement during the flow reversal (“Constant Movement”) or did not change orientation when initiating a movement (“Swim off”) (see Table 2.1). None of the fish exhibited negative rheotaxis before flow reversal. Change of direction was the most common response to flow direction change across all three fish groups, displayed by 72% of the fish which behaviour was classified (62 individuals) from across all experiments (Figure 2.1). The proportion of trials where the response was “Other behaviours” was lowest in wild smolts while it was similar in both types of farmed fish (Figure 2.2). A binomial model with directional change/no reaction as the response variable, with and without fish group as an explanatory factor, showed that there was no significant effect of fish group (ANOVA: Chi-square = 3.98, $df = 2$, $p=0.137$, models fit: BIC=111 AIC=104 with fish type variable and BIC =106, AIC=104 without).

Using a Gamma-distributed GLM model we estimate the mean minimum threshold flow (V_{min}) for directional change across all three fish groups was 8.9 cm/s (95% CI: 7.7,10.4) (Figure 2). The mean V_{min} for the two groups of farmed fish were 8.5 (95% CI: 6.7,10.9) cm/s for the cage farm origin smolts and 7.3 (95% CI: 5.8,9.2) cm/s for the tank, farm origin fish. The mean V_{min} for the wild fish was slightly higher at 12.0 (95% CI: 9.2,15.6) cm/s. The full model including flow rate experienced by fish during the the initial holding period and its interactions with fish group (AIC=401, BIC=416) showed no effect of fish group on the minimum flow velocity required to initiate a re-orientation towards the new current direction. However, an ANOVA analysis with Likelihood Ratio Test implied that fish group is a significant covariate (Chi-square = 2.231, $df = 2$, $p=0.031$) while flow velocity at the point of holding and its interaction with fish type are not (Chi-square = 0.096, $df = 1$, $p=0.59$ and Chi-square = 0.451, $df = 2$, $p =0.51$, respectively).

The simpler model with fish type as the only dependent variable shows a better balance between the fit and the number of explanatory variables (AIC=396, BIC=405) and a post-hoc statistical analysis with Tukey’s range test show that the only statistical difference in flow rate required to change direction is between was between the wild fish group and the indoor farmed fish (ratio = 0.61, $p=0.031$). As some variables such as water temperature, time of the year, light and type of pumps used are highly correlated with the group of fish and thus cannot be modelled directly, we cannot rule out that fish type is only a proxy for some other variable. To examine more closely the effect of fish type (the origin of the experimental animals) whilst minimising the effect of these potentially confounding variables, we analysed a subset of 15 fish drawn from the group originating from a cage farmed and all 15 wild smolts that responded to flow change and were closest in their conditions (identical pump outputs, exposed to temperatures

within a range of 2.1 degree, no light). In this subset we found that neither previous flow conditions (Chi-square = 0.432, df = 1, p=0.23) nor type of fish (farmed or wild) (Chi-square = 0.202, df = 1, p=0.41) had a significant effect on the model. According to the Bayesian Information Criterion, the intercept-only model (AIC=396, BIC=400) provides the best balance between fit and complexity, highlighting a lack of strong evidence for differences among the groups studied.

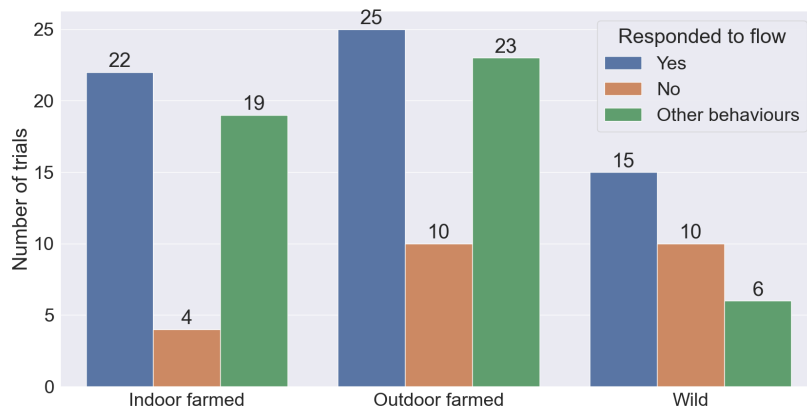


Figure 2.1: The number of trials in which fish from different origins (indoor farmed, outdoor farmed and wild) responded to the reversal of flow in the experimental area by switching direction. A clear response to flow was the most common outcome in all groups.

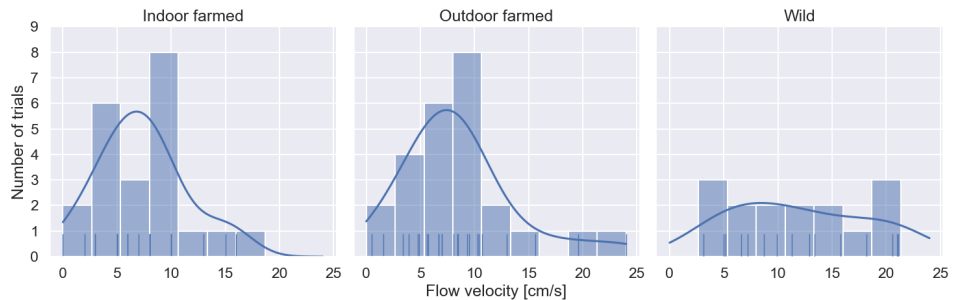


Figure 2.2: Histogram and KDE (Kernel Density Estimate) plot displaying the minimum flow velocities (V_{min} cm/s) that prompted a change in directional orientation across three fish groups. The vertical ticks along the x-axis represent individual observations contributing to the histogram formation. Each panel corresponds to one of the fish origin groups: indoor farmed, outdoor farmed, and wild.

2.5 Discussion

Here we show that the velocity required to initiate a directional change in the swimming of Atlantic salmon smolts is relatively low, with a mean V_{min} of 8.9 cm/s (~ 0.6 body length/s). Wild fish and the two groups of farmed Atlantic salmon smolts behaved similarly, although the wild fish had a slightly higher mean V_{min} value than the farmed fish, especially those from indoor facilities, were marginally more sensitive to the velocity change. The wild fish group showed the least pronounced peak in the V_{min} , that elicited a behavioural re-orientation response and there is considerable variation around the mean response for all groups (Figure 2.2). Despite this and despite the detectable (but small) differences in mean V_{min} between groups the range of responses was broadly similar ranging up to around 20 cm/s. It is self-evident that the fish in this study must be able to detect a change in direction current at a velocity lower than that at which they respond to that current. It is very possible that there is between-individual variation in the time between directional current change and a behavioural re-orientation and that this, may in part be responsible for the variation in V_{min} . Despite this however the difference between the determined mean V_{min} and the upper end of the range of V_{min} detected by a behavioural re-orientation response is only two fold difference.

It is frequently reported that migration is associated with the highest mortality rates during an animal's life cycle (Cresswell et al., 2011; Guillemain et al., 2010; Owen and Black, 1991; Sillett and Holmes, 2002; Strandberg et al., 2009). This is also true for salmonids; the downstream migration of Atlantic salmon smolts is associated with variable but relatively low survival, with mortality rates of between 0.3 and 7.0 % km⁻¹ reported during downriver migration and 0.6 to 36 % km⁻¹ during the early phases of marine migration (Thorstad et al., 2012b). Especially high mortality is observed in the river-lake confluence, likely due to predation, highlighting the necessity for reducing time spent finding the route out of the man-made reservoirs (Kennedy et al., 2018). During this initial and risky part of the Atlantic salmon migration, the evidence suggests that the most important cue for movement and migration is water flow (Otero et al., 2014; Scruton et al., 2003). Therefore, the fish's ability to detect this cue and also to react to it correctly is vitally important for successful migration. In rivers with clear and reliable water flow cues, the migration is consistently unidirectional (Thorstad et al., 2012b). However, water flow related directional cues become unreliable and poorly defined when downstream passage is through habitats that do not have strong, unidirectional currents such as lakes, reservoirs, and riverine areas near barriers (Honkanen et al., 2021). Multiple studies have shown

that the lower water discharge especially near barriers contribute to delays and failure of migration (Gauld et al., 2013; Serrano et al., 2009). In this study, Atlantic salmon smolts were clearly responding to changes in current velocities, although there was inter-individual variation (range: 0-24 cm/s). The wild fish in this study were from a population that does not have any standing waters or in-stream barriers on their migration route. It would be an interesting comparison to study populations from rivers that do and do not have a lake in them.

There is only one similar study that has investigated the flow sensitivity of juvenile Atlantic salmon in an experimental setting. Veselov et al. (1998) reported V_{min} values of ~ 5.5 cm/s for Atlantic salmon smolts. Their results show a broadly similar but a slightly lower threshold for detection than we found in the study presented here. This could however be due to a difference in the behavioural cue that was used to determine a flow change response in the experimental fish. In the Vesolov study it is slightly unclear whether they measured the directional flow as the first signs of a behavioural response occurred or when the orientation change actually took place. They also found that the minimal velocity threshold for a response (V_{min}) values were lower for fry and parr than for alevin and smolts, suggesting that V_{min} is not simply related to fish size and may be connected with development of the sensory organs and behavioural characteristics at different life stages in this species. They also found seasonal variation in the responses; with V_{min} much higher at colder temperatures (Veselov et al., 1998).

Another interesting finding from our study is that the wild and farmed fish (from indoor and outdoor farm facilities) responded to changing current in a similar way with some evidence of a slightly lower minimum velocity threshold amongst farm origin smolts. Thus, despite four or more decades of selection under domestication, farmed fish smolts have not lost the flow response that is found in wild fish. This is somewhat surprising as several studies have highlighted differences in behaviour and physiology between wild and farmed Atlantic salmon (Fleming et al., 1996; Jutila et al., 2003; Houde et al., 2010). When testing a sensory response to flow, it might be reasonable to postulate that that farmed fish might have higher V_{min} , threshold, considering that they have been reared in an environment with mostly uniform flows and arguably no fitness benefits (i.e. higher food intake, dominance) for higher flow sensitivity. Alternatively, if farmed fish are exposed to low water velocities (which might well be the case in fish from outdoor lake cages), they may be more sensitive to changes than wild fish that experience considerable variation in flow conditions in their natal rivers.

There is clear management interest in the minimum water velocity cues that are re-

quired for fish navigation and hence successful migration. Many migratory fish use rheotaxis as one of their main navigational cues during their early migration and therefore water velocities of sufficient magnitude and directional stability are required for successful migration. However, it is likely that man-made reservoirs have an added layer of complexity associated with migration with altered hydrology near the dam and the challenge of identifying any natural or man-made fish at or near the dam (Havn et al., 2018; Babin et al., 2020). This can lead directly to mortality or it may result in an additional cost incurred through a delay in migration, such as mortality via predation or smolts missing the physiologically suitable time period for entering the ocean (McCormick et al., 1998). However, where water velocities can be manipulated in standing waters, for example where there are hydropower facilities with scope for at least partially influencing the hydrological conditions within a reservoir then it may be possible to create conditions in reservoirs that facilitate successful smolt migration. This approach was demonstrated by Xu et al. (2017) who modelled flow velocities across a large reservoir in China. Using 20 cm/s as the minimum flow requirement required for migratory fish to detect, and follow, a velocity cue, they found that while most of the route through the reservoir (68%) met the minimal detection limit, there were two sections that fell below this threshold and thus constituted an invisible migration obstacle for fish. This sort of hydrological modelling in conjunction with the water velocity detection thresholds identified in our study, (that confirmed 20 cm/s flow as a minimum flow rate cue to which migrating salmon smolts will respond) has considerable potential for practical management. For example such a detection threshold may aid in predicting where and when migrating salmon smolts may be making navigation decisions based upon water flow and thus has the potential for manipulation in managed hydropower schemes.

Chapter 3

Predicting complex movement of multiple animals in simulated video recordings

Note

The content of this chapter has been written solely by Mikolaj Kundegorski on the experiments and analysis performed jointly by Mikolaj Kundegorski and Colin J. Torney. Shaun Killen, and Colin E. Adams participated in the revision of the chapter

3.1 Introduction

This chapter describes a novel method of visually tracking multiple animals in overhead video recordings. This is a deep-learning-based method inspired by work on movement analysis of juvenile salmon in an artificial stream and ungulate herds. I test this method on simulated data of complex animal movement to understand if the prediction of the next position of an animal can be robustly inferred for a wide variety of animal movements.

3.1.1 Motivation

In recent years, collective behaviour studies have benefited from drone recordings of herds of ungulates (wildebeest, blackbuck, horses) ([Rathore et al., 2023](#); [Torney et al., 2018b](#)). With improvements in technology, large quantities of video data are now available to extract position information, allowing the study of leadership, behavioural states, habits, and habitat preferences. These animals spend time foraging with minimal movements,

then rapidly accelerate in response to threats. They exhibit patterns related to social hierarchies and environmental gradients when migrating towards resources and navigating obstacles such as river crossings.

While telemetry data can explicitly provide precise location information, it lacks the detail found in video recordings. Videos can reveal an animal's behaviour, body condition, and external influences such as weather and interactions with other animals. However, to quantify those, a video recording requires the interpretation of rich visual information that is laborious and often cannot be automated with analytical methods. With sufficient equipment and recording conditions, we can achieve a sampling frequency and image quality that allow for relatively easy extraction of tracking data from the image. Laboratory experiments are often designed so that animals stand against a uniform background and are recorded with high-quality cameras (Lin et al., 2018). However, not every hardware solution can be easily deployed in the field where we want to observe animals in their natural habitat. Study sites can often be difficult to access and pose a high risk of damage or loss of equipment. Areas with changing weather, low natural light, or complete darkness requiring infra-red illumination limits the quality that can be achieved even with expensive cameras. Drone recordings often use reasonably high-quality cameras, but need to be conducted from a sufficient height not to disturb the observed herds. Most animals naturally camouflage in their natural habitats.

The next chapter (Chapter 4) of my thesis describes laboratory experiments on juvenile salmon moving in a circular flume. Fish were studied moving at night for extended periods of time, constraining the choice of camera to near-IR, the size of files that can be stored until filming completes, and network connectivity. Figure c) shows an example frame from that recording.

Our observations of salmon smolts in an artificial flume show different modes of movement. Individual fish can hold their location, swim passively oriented against the flow, or swim actively with the flow. The fish travel in various group sizes, and as they navigate the flow, their orientation and style of swimming can change. When swimming actively, they mostly perform aerobic movements that can be sustained for extended periods. However, periodically, they will perform an anaerobic burst, rapidly moving in a different direction.

Figure 3.1 illustrates the common problems in visual tracking in animal research.

- **Occlusion** Overhead footage significantly improves spatial separation of animals in the image space, yet occlusions are still unavoidable. A group of ungulates can almost entirely disappear under trees, or small animals may get partially occluded in thickets. In observations of fish in a tank, the additional difficulty arises from

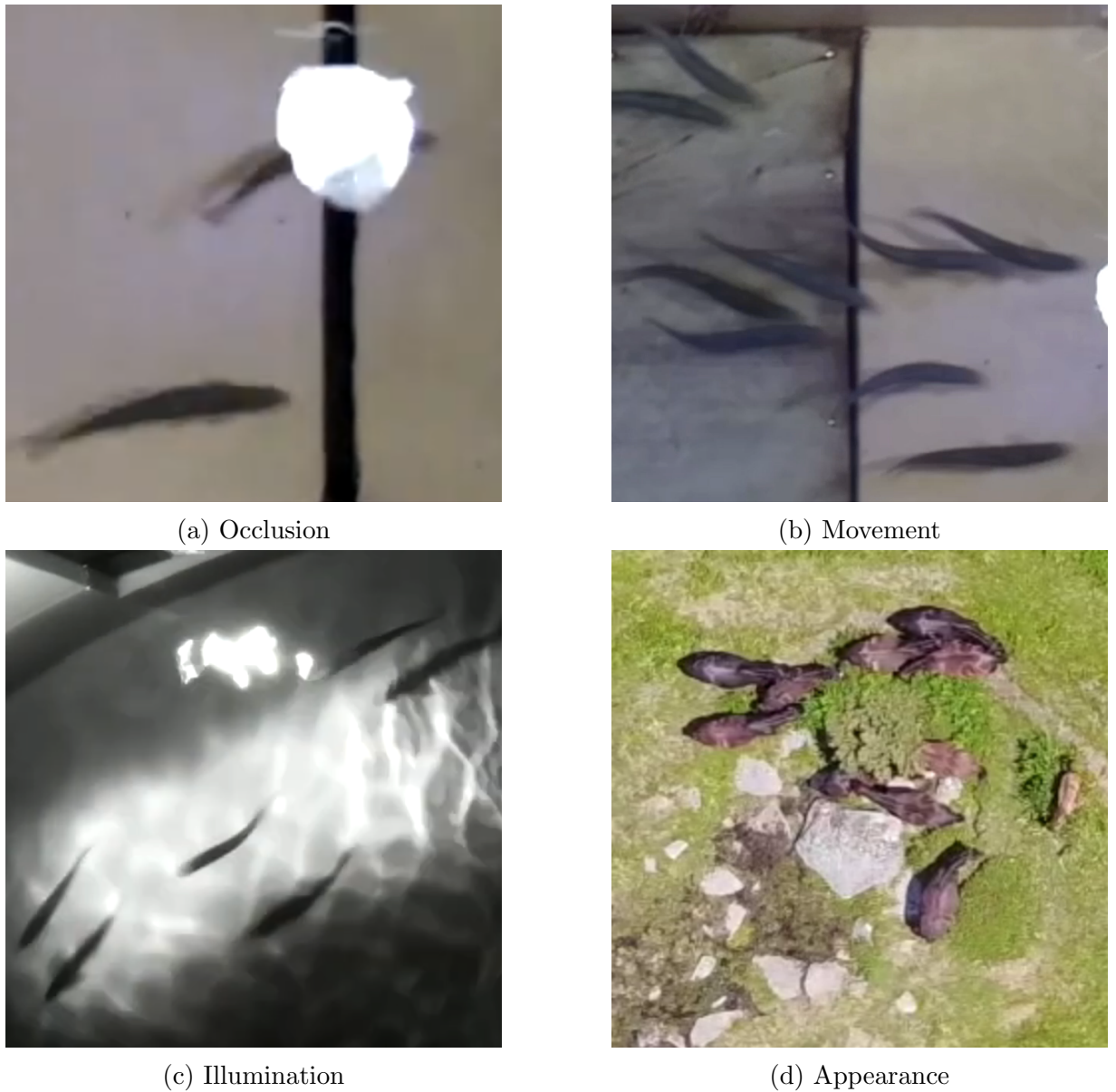


Figure 3.1: Challenges in animal tracking. Figures (a) and (b) show juvenile salmon moving in an illuminated tank, illustrating issues of occlusion and decreased image quality due to motion blur. Image (c) shows a much more challenging scenario from night-time recording with an infrared camera, where the low intensity of light limits the amount of detail registered by the camera. The last panel, (d), shows a scene with a complex background and animals that, even though not overlapping, are difficult to differentiate.

the fact that actual movement occurs in a 3D space and fish can partially or fully overlap. In Figure 3.1 a), a reflection of a lamp occludes the position of the fish almost entirely.

- **Fast movement** Rapid movement presents a dual challenge: it naturally means that the area to consider for matching the object is much larger, making the solution to the matching problem more complex. Simultaneously, with limited light, rapid movement can cause blurring and loss of visual information. Figure 3.1 b) shows an image of multiple salmon smolts travelling in a shoal. Figure 3.2 illustrates different modes of movement present in a low-light recording. The bottom row shows anaerobic movement, where a previously stationary fish performs a dynamic burst, initially bending into a “C” shape and moving quickly in an arbitrary direction. This type of movement is highly unpredictable and is useful for predator avoidance and navigating strong currents.
- **Illumination** Some field recordings occur in areas with high sun exposure, creating a large contrast between shaded and sunlit areas. Ultimately, the camera frame rate and exposure are limiting factors on the amount of light entering the sensor, and a setting that provides a good amount of visual detail in shaded areas might cause oversaturation in sunny areas. Additionally, as lighting conditions change rapidly or an animal enters a differently illuminated area, its appearance changes suddenly. Infrared cameras are particularly sensitive to this, as the amount of direct sunlight on the object contributes to most of its signal. Figure 3.1 c) shows the problem of blurred images of animals compounded by strong shadows, presenting an additional challenge.
- **Appearance and shape deformity** In the human world, the appearance of many objects—such as people in pedestrian detection or cars on the road—is different between instances and changes relatively little between frames. In contrast, in biology, conspecifics can be almost indistinguishable from recording distance, and their shape can change rapidly with movement. Additionally, animals might not conform nicely to a bounding-box approach where their shape fills one rectangle. Figure 3.1 d) shows a pack of horses from field recordings that display a variety of shapes while next to each other, making it challenging to draw clear distinctions between each of the individuals.

Modern computer vision techniques address all of those challenges and are often tested using popular benchmarks to demonstrate how well they perform in real applications. The Multiple Object Tracking Benchmark (Dendorfer et al., 2020), aimed at tracking pedestrians, is the most popular and shows vast improvements in difficult, crowded scenarios that were beyond the capabilities of simpler models. However, there is always the issue of

implementing and adjusting complex models to different scenarios. The benchmarks have limited focus and cannot guarantee the robustness of methods in unusual scenarios.

Unlike video surveillance data used for pedestrian detection or road images used for the development of autonomous driving algorithms, labelled videos from ecological and biological studies are, by comparison, in short supply. Most of it comes from experiments and is unlikely to be shared widely. Each specific domain also has unique challenges and characteristics that are not shared by others. The heterogeneity of the natural environment presents a unique challenge that varies widely between ecosystems and observed species, as highlighted in Figure 3.1.

The field of machine learning is prediction-focused, often performing well on practical tasks but without quantification of uncertainty (Ghahramani, 2015). In this work, we attempt a more methodical approach to better understand the value of using a modern deep-learning technique and its potential limitations. Particularly important is the issue of indirect learning, where the data provided for both training and evaluation of the model might lack characteristics of the real-life scenario. In our case, we investigate whether a method trained on a single animal track, which can be easily extracted and annotated, will allow generalization to multi-animal tracking—a challenging problem for data acquisition while also crucial for collective movement studies.

Recent advances in machine learning show that even without ground truth data, a lot can be learnt from the context and synthetic, also called simulated, data generation. Simulated data mimics the characteristics and structure of real-world data, in general allowing to test models under more controlled conditions. Adversarial networks - where one ML system generates synthetic data, and another is optimised to detect it - can lead to performance that vastly supersedes learning on labelled examples. The famous case of AlphaZero (Silver et al., 2017) shows that the parallel training of two neural networks playing a complex board game against each other achieved better results than the analysis of vast quantities of existing transcripts of games played by and between human opponents.

Additionally, simulation data allows for disentangling some aspects of algorithm function that would not be possible with real-world data. A common issue with limited datasets is overfitting, where, in the process of optimizing learning on a specific sample, the algorithm loses the ability to generalize to the entire population. The use of synthetic data allows us to at least partially circumvent this problem.

Machine learning techniques are contingent upon the quality and quantity of the annotated training data. *Transfer learning* allows the re-use of models trained on tasks where more data is already available and applying it to similar domains, leveraging the

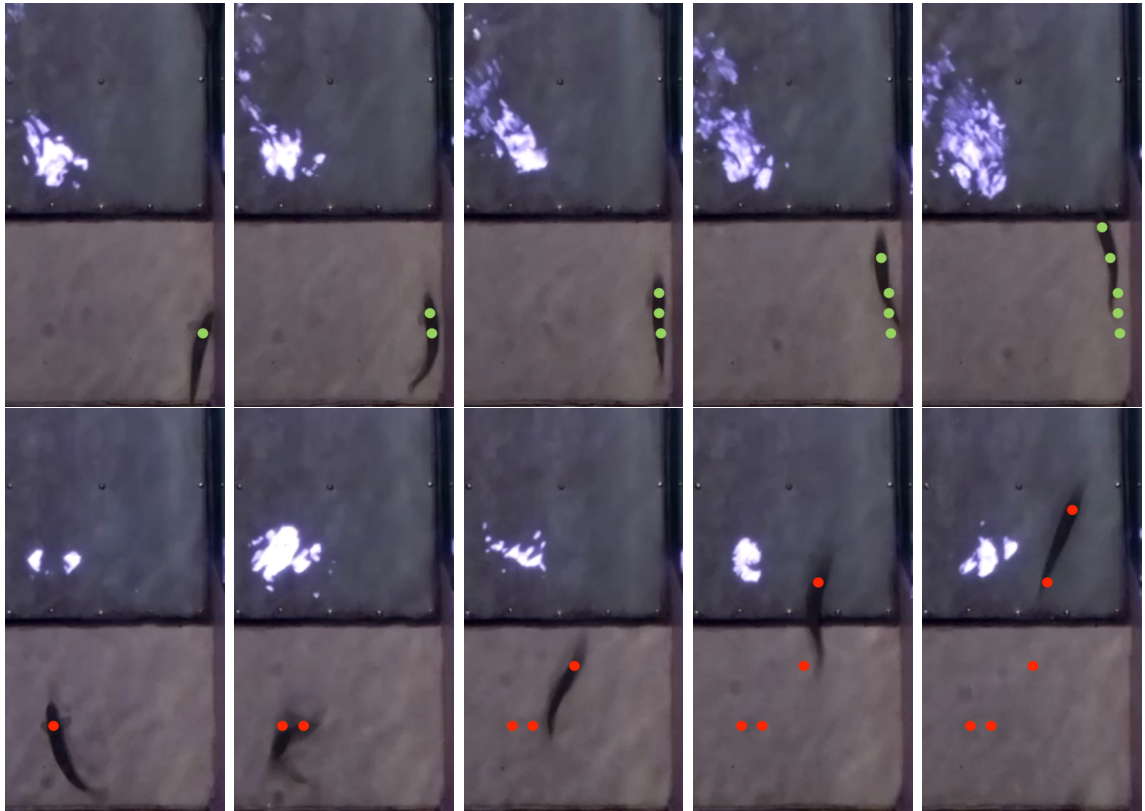


Figure 3.2: Comparison of two modes of fish movement from experiments described in Chapter 4. Each row shows subsequent frames from a low-resolution camera recording at 10 frames per second, capturing a total of 0.5 seconds of movement. The first row shows a fish swimming aerobically in a slow current. The bottom row shows anaerobic movement, where a previously stationary fish performs a dynamic burst, initially bending into a “C” shape and moving quickly in an arbitrary direction.

similarity of visual cues, for instance, between synthetic data and laboratory recording. Extraction of general image features from extensive image corpora significantly reduces the volume of subject-specific data required for annotation when adapting an object detector to a new task. However, a comprehensive framework for tracking has not yet been established, making data annotation particularly challenging due to ambiguities in the necessary level of detail for effective training. Questions arise such as whether it is possible to derive high-sample tracking from low-sample annotations, if multiple object tracking can be learned from single object annotations, and whether transfer learning can be applied across different objects exhibiting similar movement patterns.

This chapter introduces a novel approach, Deep Predictor, for location prediction in animal movement tracking. While traditional methods such as Kalman filtering are widely used and effective in many cases, they often struggle to generalise to complex movement,

which can often be the focus of animal studies. We evaluate the performance of Deep Predictor in comparison to Kalman filter-based techniques on synthetic data crafted to test the robustness and validity of our approach.

3.1.2 Contribution

In this work, we modify a step in an existing approach already adopted in ecology (Rathore et al., 2023; Torney et al., 2018b), exploring how the position prediction of animals can be improved. Specifically, we:

- Develop a new method, *Deep Predictor*, to accurately predict the bounding box of tracked animals. This method is suited to ecological applications where there is little prior tracked data for each species, as it is capable of learning both about object appearance and movement model.
- Benchmark the method against Kalman filter predictions on simulated data of complex movement, showing improved performance in all but the most trivial scenarios. In this way, we address a potential pitfall of deep learning methods applied to low-data problems that may seem to perform better on a difficult task when they are actually solving an easier one—for instance, correctly identifying individuals by appearance while failing to model their movement patterns.
- Test the robustness of the method. We demonstrate that when trained on single-object tracking, its performance does not degrade with larger animal groups. Additionally, we confirm that identical objects are tracked as effectively as distinguished ones, making the application to closely similar animals possible.

Our method builds on modern tracking techniques (Section 3.1.3.5) but replaces only one component (movement prediction) to assess the benefits and limitations of more complex tracking methods that are rarely used in ecological settings (further details in Section 3.1.3.6).

Further benefits could be achieved by implementing the latest version of the YOLO family object detector, YOLOx (Ge et al., 2021), which has been used in successful trackers (Zhang et al., 2022, 2023), and by enhancing track linking with methods like BYTE (Zhang et al., 2022). However, this lies beyond the scope of this work.

The following section summarises traditional approaches and recent developments in visual tracking.

3.1.3 Background: Visual tracking of animals

3.1.3.1 Overview

To quantify the movement of animals in a video feed, they first need to be localised as candidates for objects of interest and then classified to confirm they are the specific animal type or individual. These detections within each frame of a video need to be matched between frames to generate spatio-temporal tracks, allowing further analysis of the field or experimental data. Image recognition, described in Section 3.1.3.3, extended with algorithms to look for object candidates in the image using some method of localisation 3.1.3.2, is called *object detection*.

Observing recognised individuals over time is a problem of *object tracking* (Section 3.1.3.6). Observation of a moving animal requires the following actions to be performed across consecutive frames:

1. Localisation of candidate objects in the 1st frame
2. Classification of objects of interest in the 1st frame
3. Prediction of the position of objects of interest in the 2nd frame
4. Localisation of candidate objects in the 2nd frame
5. Classification of objects of interest in the 2nd frame
6. Linking of objects of interest between the 1st and the 2nd frames

In this work, we focus on the prediction step (step 3) to understand if our method can effectively learn a wide range of movement scenarios in providing the next position of objects of interest. The following sections, Section 3.1.3.2, 3.1.3.3, and 3.1.3.4 describe the key analytical methods used to achieve the above tasks. Recently, with computational advances, each part of the process is integrated into the same learning framework in a deep-learning technique. Following Section 3.1.3.5 presents advances in modern deep learning approaches to the problem with the theoretical underpinning of this approach in Section 1.3.2.1.

3.1.3.2 Localisation

Detecting potential objects of interest in an image frame involves separating any *foreground* objects from the *background*. This task can be trivial in laboratory settings where the

background is uniform-coloured, and objects are visually distinct. In many scenarios however, objects can appear on different scales, be static or moving, and be partially occluded. The success of classifying each object into the correct class heavily depends on the algorithm knowing where to look. There are a number of methods used to localise objects:

- Create a **sliding window** at multiple spatial scales and scan the image, performing image recognition on all extracted parts of the image. This approach is highly computationally demanding and requires a high-precision model to accommodate multiple possible configurations of background and clutter in the image, as originally proposed in Fast R-CNN ([Simonyan and Zisserman, 2015](#)).
- **Thresholding** the pixel intensity values. Assuming a smooth or reasonably uniform background, adaptive thresholding can provide candidate areas for detection by finding blobs (connected lines) distinguished by locally high gradients or intensity of pixel values. This approach can work well in very specific cases and has been widely used in semi-automated analysis of laboratory experiments, for instance, using the method of [Sridhar et al. \(2019\)](#).
- In a video feed, it is much easier to detect moving objects using **background subtraction** [Bouwmans et al. \(2008\)](#), a technique which models the subsequent values of pixels in the video as a Mixture of Gaussians. Recognising pixels that fall outside of the predicted distribution provides a foreground mask, whereas connected areas provide candidates for objects of interest. This method works reliably for stationary cameras, where the background remains static and often fails on more dynamic backgrounds, such as water surfaces. This is also a popular method in the automation of laboratory experiments where the background colour is easy to model in this way, and the camera position remains fixed ([Mönck et al., 2018](#)).
- Adding a separate regressive neural network, a **Region Proposal Network**, which performs the task of finding suitable candidates for detection. A number of successful methods use this design, such as FasterRCNN ([Ren et al., 2015](#)), which is, however, still computationally demanding.
- **Single-shot detection** leverages deep learning to incorporate the problem of finding object bounding boxes as a regression problem within an object recognition network. This method usually provides the least computational burden while sustaining high

accuracy. In our research, we use the You Only Look Once (YOLO) (Redmon and Farhadi, 2018) network to perform object detection.

3.1.3.3 Image recognition

Classifying the cropped image into one of the predefined classes is termed image classification or image recognition.

In the context of tracking a specific animal within a frame, the *class* to which the animal belongs is, for instance, a species or a visually distinguished experimental group. Depending on the the technique chosen and scenario, only the class of interest is modelled against any background clutter or different possible types of objects are explicitly modelled, providing the probability score for each class for every detected candidate object. For example, in recognising images of wildebeest in the savannah, it may also be advantageous to recognise images of zebras and trees, as this can facilitate the creation of a more robust and interpretable model.

Unlike the localisation of objects in the image, classification has always been a modelling problem and has never relied on a strictly analytical approach. Image recognition was traditionally based on a two-step process. The first step, *feature extraction*, produced a numerical representation of the image, orders of magnitude lower dimension compared to raw pixel values, to be passed to a *machine learning* algorithm for classification.

For the recognition of rigid objects of generally known shape, dense features can be used, such as Histogram of Oriented Gradients Dalal and Triggs (2005). Images of objects like pedestrians, vehicles, or faces are divided into a fixed-size grid. Each of the grid cells has a pixel intensity gradient calculated in multiple directions, hence producing a numerical vector for each cell.

This approach obviously does not work with objects that vary in their appearance, like buildings, people in general, or animals. This problem is addressed using a Bag-Of-Visual-Words approach based on bag-of-words used in text comprehension—where not the precise position but the frequency of appearance features identifies a subject (Kundegorski et al., 2016). In such cases, the image is scanned for sparse landmark points and distinguished corners, which are then described mathematically in terms of their blurred gradients at different orientations and scales. The most famous of these techniques is the Scale Invariant Feature Transform (SIFT) Lowe (1999). Then, a histogram of the appearance of different features is created using a clustering algorithm, which forms a feature vector.

Such a feature-based approach is still popular in ecology (Rey et al., 2017; Chabot et al., 2018; Banerjee et al., 2021) where it improves on manual classification approaches.

The limitations of these human-designed features are only apparent when an alternative approach is considered, where the classification and feature extraction can be optimised within one framework.

Once the image information is encoded and represented in lower dimensions, some statistical modelling techniques are used to classify the output. Various machine learning algorithms are used for image recognition, such as Random Forest (Scornet, 2016), Support Vector Machines (Vapnik, 1997), and neural networks (Szeliski, 2022). Random Forest is an ensemble classifier that pools the classification decision of a vast number of decision trees trained on small subsets of given features. Decision trees are binary tree classifiers, classifying data by assigning feature value thresholds to minimise entropy. Support Vector Machines perform a binary classification in a multidimensional space defined by an inner product of all data points. This “kernel trick” allows for easy model training once the feature space is transformed because the model to fit is still very basic.

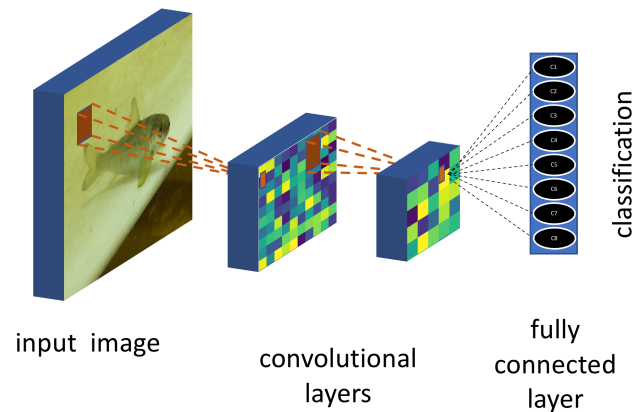


Figure 3.3: The schematic of a Convolutional Neural Network (CNN). We use convolution to reduce the dimension of the image by measuring the similarity with a custom kernel across the image space. In this schematic, the orange boxes indicate an area of an image that is multiplied by a convolution kernel, resulting in the scalar value in the next tensor. Once the image is reduced to its final feature map, a fully connected layer is used to classify an image to one of the predefined classes

Artificial Neural Networks can be described as an ensemble of interconnected binary classifiers (neurons). They have the potential to estimate a variety of non-linear models. However, the high amount of tuneable parameters meant that in the past, their optimisation using Stochastic Gradient Descent often resulted in overfitting to the training scenario data, where the network was fitting data closely but only for the provided train-

ing data or alternatively failing to model even training data well when constraints on the network complexity were introduced. This problem was difficult to overcome because of the lack of sufficiently broad training data and processing power to utilise it (Geman et al., 1992). It resulted in a period of slowdown in ANN research, commonly known as AI winter, that lasted until improvements in hardware allowed the development of new methods and training of deeper networks. In a seminal paper, Krizhevsky et al. (2012) leveraged the computational power of Graphical Processing Units for matrix operations and reformulated the optimisation problem by modifying the activation function of neurons, introducing a new type of connection between neurons: a convolutional layer. This work reported better results in image recognition than any previous technique, and since then, Convolutional Neural Networks have led in the most computer vision tasks on large benchmarks such as ImageNet (Krizhevsky et al., 2012) or PascalVOC (Everingham et al., 2015). Convolution is a localised measure of similarity. Given two functions, one representing the image I , and another, the convolution kernel k defined by trainable network parameters, convolution is formally defined as

$$(I * k)(x) = \int_{-\infty}^{\infty} I(\tau)k(x - \tau)d\tau, \quad (3.1)$$

and can be thought of as a localiser of kernel-like objects in the image I . The introduction of these layers in the network (illustrated in figure 3.3) meant that raw image data could be used as a feature vector input to a neural network classifier, and previously hand-crafted features could be learned directly from raw images. However, this requires vast datasets. With advances in data collection, they have become available in every discipline, including biology (Van Horn et al., 2017). Another approach allowing the use of neural networks in different domains is transfer learning, where network parameters of convolutional layers trained on a big dataset such as ImageNet (Krizhevsky et al., 2012), PascalVOC (Everingham et al., 2015) or COCO (Lin et al., 2015) provide a generic feature-like image representation which can be transferred to a domain-specific problem. Then, the top classification layers of the network can be retrained on the domain data providing performance better than other techniques. Such solutions are used in recognition of animals in trap cameras (Schneider et al., 2018), underwater recordings of fish (Lopez-Marcano et al., 2021) or overhead imagery (Torney et al., 2018b; Rathore et al., 2023).

More technical details on the Neural Network algorithm was provided in Section 1.3.2.1 of this thesis introduction.

The most successful image classification neural network architectures, such as AlexNet

(Krizhevsky et al., 2012), VGG (Simonyan and Zisserman, 2015), and GoogleNet (Szegedy et al., 2015), have since been used in a variety of computer vision applications. YOLO (Redmon et al., 2016) and Faster R-CNN (Ren et al., 2015) have then been the key extensions of these, enabling the object localisation task to be included in the same learning process, further reducing the need for separate algorithms at different stages of object tracking.

In this work, we are using a custom implementation of the leading deep-learning object detector YOLO, version 3 (Redmon and Farhadi, 2018), which is a popular method for fast object detection, used in real-time applications, and has been revised since the original method was proposed in Redmon et al. (2016). The YOLO architecture is still being developed with gradual improvements, currently at version 9 (Wang et al., 2024). However, newer versions lack community support and adoption within wider deep-learning frameworks that are afforded to the most popular version 3.

This approach unifies object classification and convolutional neural networks with a region proposal network that provides bounding boxes with candidates, originally introduced in Faster-RCNN (Ren et al., 2015) to simplify training and reduce inference time, compared to previous approaches where these two tasks were separate. The generation of the bounding boxes is based on the assumption that there is a finite number of objects, and the image plane is divided into a grid of *anchor boxes* which contain 9 prior shapes of bounding boxes that each of them is tasked to predict within an image.

Figure 3.4a shows the architecture of the network with three scales of features provided from a series of convolutions that have been pre-trained to detect general image features.

The authors suggest dividing an input image into a $S \times S$ grid in which each cell is responsible for providing $B = 9$ detections, each with a vector of probabilities belonging to different C classes. Figure 3.4b illustrates that concept that allows a variety of valid detections in one area of the image while keeping the total number of candidates limited. Number B corresponds to predefined anchors for bounding boxes and priors for the most commonly occurring object shapes. Each of those $S \times S \times B \times C$ detections is a vector

$$y = [t_x, t_y, w_x, w_y, P(\text{Object}), P(k|\text{Object})]^T, \quad (3.2)$$

where t_x and t_y are coordinates of the centre of a bounding box relative to the centre of a grid cell, and w_x and w_y are corrections to the prior bounding box coordinates (either linear or logarithmic). $P(k|\text{Object})$ is a probability that the object in the bounding box is of class k , given that this grid cell predicted an object.

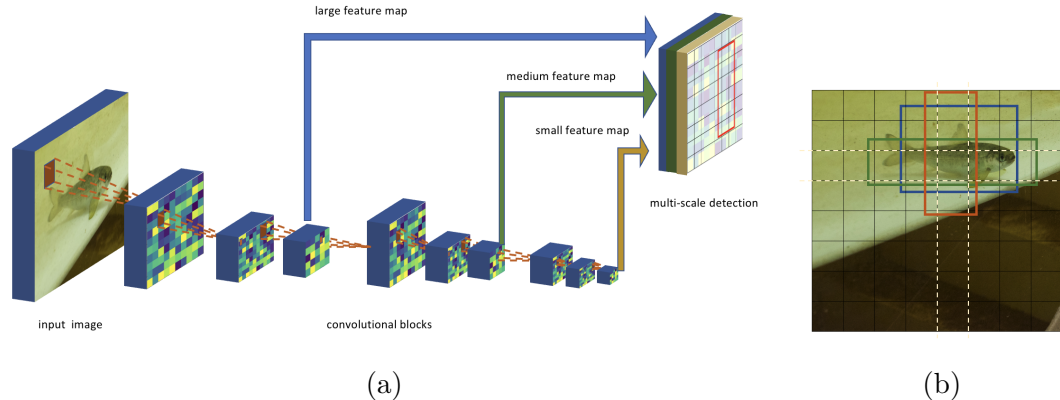


Figure 3.4: The overview of YOLO version 3 detection logic. The panel on the left shows the simplified architecture of the YOLO detector, version 3. The down-scaling of subsequent feature maps with convolution operation and extraction of those maps at different scales to allow for regression of the detector on correct bounding boxes, no matter the relative object size. The panel on the right, shows an 8×8 grid that is used to define anchor points, which can contain multiple bounding boxes with a centre inside that grid cell. In the last stage of classification, the problem is reduced to a correct prediction of object classes and their bounding boxes within a finite number of anchor points, hence making the problem easier to learn.

3.1.3.4 Track Linking

Most tasks relating to the processing of videos have real-time processing requirements. Predicting the position of tracks and matching the same object among multiple candidates across frames can be a complex problem without a valid solution—for instance, when the object becomes occluded. As improvements in hardware have simplified the problem—by providing higher image resolution and smaller absolute movement in high-frame-rate recordings—conceptually simple and fast algorithms have dominated the field.

In Section 3.2.2, I describe the principles of linear Kalman filtering, which provides the best candidate location for each tracked object (Kalman, 1960). The main drawback of this fast method is that it assumes a linear model of motion. The Extended Kalman Filter (EKF) (Welch and Bishop, 2006) allows for the approximation of non-linear dynamics by using first-order derivatives at the location of the mean. This is further improved by the Unscented Kalman Filter (UKF) (Wan and Van Der Merwe, 2000), which uses a transformation allowing the propagation of non-linear functions at deterministic points.

These methods work with prior knowledge of the functions describing the system dynamics, which are not always known when describing movement in the video; hence, the

popularity of the linear Kalman filter operating at high frame rates to approximate linear movement.

Alternatives include estimation of movement locally by shifts in pixel intensity patterns (Horn and Schunck, 1981), or using sequential Monte Carlo, also known as particle filtering (Del Moral, 1997). However, these methods generally increase the complexity of calculation while not offering an advantage in real-time applications.

Given the predicted positions of objects from the previous frame and new detections (*tracking-by-detection*), the most popular method for track association is by using the Hungarian matching algorithm (Kuhn, 1955), with the distance between predicted and detected candidates as a matching cost. This algorithm optimises the total cost iteratively and guarantees convergence on the optimal solution. It operates in polynomial time, allowing for use in real-time applications.

3.1.3.5 Modern Tracking

More recently, attempts have been made to incorporate information on the appearance of each object or even the entire movement information into the deep learning framework to eliminate the need for separate algorithms for track prediction. Appearance tracking is particularly relevant to animal movement. Unlike most of the rigid objects in our surroundings, animals have particular shape changes corresponding to the dynamics of their movement. For instance, fish conform to a C shape when they begin anaerobic swimming. Other animals would have significant change of shape, especially before rapid acceleration. Observed from overhead, most of the animals would need to visibly orientate themselves in the direction of movement before rapid speed increase. These are additional cues which would be helpful to fix problems that are of particular difficulty for Kalman filters which predict animal position based only on movement parameters.

As with object recognition, neural networks provide a unified modelling framework for object detection and tracking. Object detection networks like YOLO redefine the learning task by dividing input images into cells, each providing predictions of objects centred within it and the sizes of their bounding boxes. Figure 3.4 b) presents the concept of bounding box predictions from a single image cell as employed in the YOLO detector. The loss which is used to fit the model implicitly contains the localisation of multiple classes of objects. Such detection networks achieved considerable success in tracking benchmarks, combined with the Hungarian matching algorithm and Kalman filtering, with the most popular implementation being a SORT tracker by Bewley et al. (2016). Due to the simplicity of this approach, SORT has become a standard in a variety of real-world

applications.

Motion dynamics has long been suggested as the key to solving the problem of occlusions and similarities in targets. Defining longer tracks with temporal information has been successful on challenging datasets of tracking multiple near-identical objects by [Dicle et al. \(2013\)](#). They re-frame the problem as a generalised linear assignment of multiple tracks instead of simple 2-frame-based linear assignment to incorporate the long-term movement dynamic.

The considerable challenge still remains for tracking in crowded situations where multiple objects of the same class will occur very close to each other. To address that situation, DeepSORT algorithm ([Wojke et al., 2017](#)) uses the top layer of convolutional features of detected objects to create a similarity metric between their appearances to be used alongside distance metric for matching with the Hungarian algorithm. This metric is pre-trained on pedestrian re-identification dataset, which makes the whole method dependent on the training of not just the object detector, but also the re-identification dataset. That, however, still requires a separate algorithm for predicting the likely positions of the objects like a Kalman filter.

A very fast (although single object) tracker GoTURN ([Held et al., 2016](#)) employs a convolutional network taking two consecutive frames as input and defines a regression task (as opposed to classification) to localise the object in both frames at once. Such a tracker allows for precise tracking even when the object is partially occluded and is also conceptually simple. This approach shows the possibility for CNNs to learn visual movement information.

Following the overall shift into a unified learning framework in wider machine learning, Tracking-by-detection (TBD) is currently the main approach where all stages of the algorithm combine into one. The main focus of those methods is a high-quality object detection network, that provides the appearance and motion information that is matched between frames with a Re-Identification model. Those two parts of the network are generally trained with domain-specific data ([Feng et al., 2019](#))

In one approach, Siamese networks ([Bertinetto et al., 2016](#)) track objects passed to a network tasked with predicting their position in the next frame, given previous and current frames processed by the same convolutional pipeline. The convolutional networks share the weights and are, hence, identical in their basic feature-detection pipeline. Expanding on that approach, [Leal-Taixe et al. \(2016\)](#) enriches the association layer input with optical flow information. A novel “Detect to Track” algorithm ([Feichtenhofer et al., 2017](#)) uses the whole convolutional layer for appearance-informed matching. It creates an additional

correlation of top convolutional layers that inform feature-based motion in the frame and allows the matching of objects detected across two frames. It provides superior results in recent tracking benchmarks and massively simplifies the whole process, however, it still requires vast amounts of training data.

Some of the approaches use on-the-fly training of re-identification CNNs, such as [Chu et al. \(2019\)](#), improving the re-identification but also adding complexity both in terms of architecture and computation.

When high frame rates are available, we can rely directly on the quality of the detector itself as the absolute motion in the image spaces is limited. [Bochinski et al. \(2017\)](#) shows that without any feature-level information, high-speed tracking can be achieved using a simple approach where the problem is presented as a mere passive filter on the detector’s outputs on subsequent frames.

Even the simple approach of Tracktor ([Bergmann et al., 2019](#)) achieves high accuracy results despite using no tracking data for training. The authors use an object detection network trained on still images, applying bounding box location regression to track the object’s position from one frame to the next. This approach achieves good accuracy without increasing the complexity of training and no requirement for labelled tracking data. This method inspires our approach of trying to minimise the amount of additional complexity in tracking when a conceptually simple approach might provide sufficient accuracy.

Recent advances, such as FeatureSORT ([Hashempoor et al., 2024](#)), currently represent the best performing published tracker in the MOT20 challenge. Specifically, authors achieve enhanced results primarily due to improvements at every stage of the detection and re-identification algorithms, focusing on enhancing the features extracted for matching and re-identification, a highly domain-specific aspect.

Further enhancements are realised by simply increasing the number of available frames, although this incurs additional computational demands. [Son et al. \(2017\)](#) employ a quadruplet Siamese network to optimise both detections and the matching of objects across four consecutive video frames.

[Wang et al. \(2020\)](#) proposes combining extraction of appearance features used for matching with the detection step, increasing tracking speed while maintaining state-of-the-art accuracy.

Whereas Convolutional Neural Networks (CNNs) are useful for learning visual features, Graph Neural Networks (GNNs) are designed to model associations between objects. The architecture of the neural network layers maintains the integrity of the geometric structure of the graph, providing interpretability for tasks such as tracking. [Papakis et al. \(2021\)](#)

integrate both convolutional and graph networks into a single model, where tracking is optimised as a graph problem with an emphasis on the underlying feature appearances of objects.

Another graph-based method, the Unified Tracking Model [You et al. \(2023\)](#), suggests a tighter integration of detection, embedding, and identity association between trackers. Using Faster R-CNN, the authors detect objects, embed their features, and describe identity association as a graph-matching problem that is also resolved within the learning framework. This includes memory aggregation, where embedding information and matching are used in a feedback loop to inform future detections and track matching. The authors are able to apply parts of this system using different components. IN GNNs, the track associations can be analysed at different scales simultaneously, balancing short-term matching of closest object detections with the long-term quality of the track. In [Cetintas et al. \(2023\)](#), authors use GNNs to not only find the optimal linking of objects between subsequent frames but also to create higher-level graphs describing longer-term tracking that can then provide larger contextual information. Using such different hierarchies of graphs allows for great flexibility in the temporal scales of tracking.

The ability to work on an undefined number of previous frames has previously been achieved using recurrent neural networks, which allow for a moving-window-like approach to providing input, thus enabling the encoding of temporal information during training. Some success was achieved by incorporating the output of the detection layer into a recurrent framework, for example, by [Stewart et al. \(2016\)](#). However, since then, recurrent neural networks have mostly been superseded by approaches based on the attention model ([Vaswani et al., 2017](#)). Attention mechanisms in transformers enable the model to dynamically focus on different parts of the input sequence, significantly improving the handling of long-range dependencies compared to RNNs.

Applications of the transformer architecture to the object tracking task are beginning to emerge. Traditional detection methods use Non-Maximum Suppression (NMS) or similar algorithm to trim away multiple bounding boxes for one detection, which can suppress correct detections, especially in crowded situations. Contrary to that, transformers excel at providing a dense, non-overlapping representation of the candidates. This is because transformers, leveraging attention mechanisms, can manage multiple object representations without needing to suppress overlapping detections ([Xu et al., 2022](#); [Zhang et al., 2023](#)).

Further improvements in deep learning methods can be achieved by replacing bounding boxes with pixel-level object masks. Previously too computationally expensive, these

approaches now enable the tracking of objects with changing shapes and appearances in crowded situations, leveraging transformer architectures (Ravi et al., 2024).

The MOT challenge benchmark (Dendorfer et al., 2020) provided over many years the momentum for the advancement of tracking algorithms. However, issues of domain adaptation and generalisation remain as the more complex methods emerge and understanding of the underlying mechanisms and model robustness remains limited.

3.1.3.6 Tracking in biology and ecology research

One of the limitations of computer vision methods is that they require a specialist background and programming skills to retrain and adapt models to specific scenarios. Often, such trivial issues as the lack of a graphical interface can deter users. A recent review Panadeiro et al. (2021) compares 28 animal movement tracking software packages focused on the laboratory application. The focus of most of the tools is to allow a good procedural analysis of data with high accuracy provided by manual validation of results and tuning of the tracking process. Most of the methods use some form of background thresholding or subtraction, relying on the quality of the experimental setup. Only two of the reviewed approaches (idTracker (Pérez-Escudero et al., 2014) and Fish CNNTracker Xu and Cheng (2017)) use convolutional neural networks, but only as a specific part of the individual identification step for inter-frame matching. It is highlighted that the lack of large datasets makes the use of deep-learning methods unrealistic.

Dell et al. (2014) reviews the problems of tracking in ecology, highlighting the lack of approaches that work beyond laboratory conditions due to the breadth of data-gathering approaches, environments and types of movement. Adaptive thresholding and background subtraction are still the standard methods used in Tracktor (Sridhar et al., 2019), idTracker (Pérez-Escudero et al., 2014), ToxTrac (Rodriguez et al., 2018), FIMtrack (Risse et al., 2017), and BioTracker (Mönck et al., 2018), TRex (Walter and Couzin, 2021).

Lopez-Marcano et al. (2021) apply a modern deep learning approach to the tracking of fish in underwater imagery, with 8700 tracks of fish annotated for training and testing purposes, achieving a high accuracy.

3.2 Methods

Our tracking framework can be divided into three steps:

1. Detection of potential objects in the frame, achieved by a deep learning YOLO

detector.

2. Prediction of positions of objects observed previously, based on movement prediction using either our new method Deep Predictor or a Kalman filter.
3. Matching of objects between frames, done by a Hungarian matching algorithm [Kuhn \(1955\)](#).

We test the performance of the Deep Predictor against two formulations of the Kalman filter, addressing only the second step of our tracking framework. Often, tracking methods are tested in their entirety, but we choose to focus on the output of the second step to specifically test the value of our contribution. The failure of position prediction is often mitigated by the quality of the candidate matches. In cases where there are only a few possible detections (low false positive rate), the closest candidates will be reliably matched by the Hungarian algorithm even if the predicted position does not perfectly overlap with the candidate. As the number of candidate objects increases, the accuracy of prediction becomes more important. Testing the actual predictions overlap with the correct detections from the following frame allows us to compare the quality of this step quantifying the robustness of our approach compared to alternatives.

The next section describes the implementation details of the first step. Following that, we describe our previously used Kalman filters in Section 3.2.2 and provide a description of our method in Section 3.2.3. An introduction to testing scenarios based on complex animal movement is presented in the last section, Section 3.2.4.

3.2.1 Detection of animals

The YOLO network is trained on a dataset of 8 million images from the Common Objects in Context (COCO) dataset ([Lin et al., 2015](#)). The network already contains appropriate weights and biases describing the common appearance features of visual objects.

The loss function is used as a measure of the fit of the model to the training data at each iteration and informs the backpropagation of the weights. It is then a function of the parameters of the model, given the training dataset.

In the case of YOLO, the loss function accounts for the localisation and recognition of objects in the training images and consists of distinct parts:

- **Accuracy of object centre** with loss $\mathcal{L}_{\text{centre}}$ is defined as a sum of square differences between all objects' true coordinates (x, y) and predicted (\hat{x}, \hat{y}) coordinates:

$$\mathcal{L}_{\text{centre}} = \sum_{i=0}^{S^2} \sum_{j=0}^B \mathbf{1}_{ij}^{\text{obj}} \lambda_{\text{coord}} \left((x_i - \hat{x}_i)^2 + (y_i - \hat{y}_i)^2 \right), \quad (3.3)$$

where S^2 represents the total number of grid cells in the detection layer, B denotes the number of bounding boxes per grid cell and λ_{coord} is the weight for this part of the loss function. An indicator function $\mathbf{1}_{ij}^{\text{obj}}$ is a mask that equals 1 if the j bounding box in the i grid cell contains a detected object.

- **Accuracy of bounding box shape** is similarly defined by loss \mathcal{L}_{box} , with the values fed through a logarithm to normalise the loss across different sizes of objects,

$$\mathcal{L}_{\text{box}} = \lambda_{\text{coord}} \sum_{i=0}^{S^2} \sum_{j=0}^B \mathbf{1}_{ij}^{\text{obj}} \left((\ln w_i - \ln \hat{w}_i)^2 + (\ln h_i - \ln \hat{h}_i)^2 \right). \quad (3.4)$$

That defines the Coordinate Loss responsible for correct localisation of objects in the frame:

$$\mathcal{L}_{\text{coord}} = \mathcal{L}_{\text{centre}} + \mathcal{L}_{\text{box}}. \quad (3.5)$$

- **Accuracy of prediction** is expressed by confidence Loss ($\mathcal{L}_{\text{conf}}$) that penalises the error in the confidence predictions \hat{C} for each bounding box, distinguishing between those that are supposed to contain objects ($\mathbf{1}_{ij}^{\text{obj}}$) and those that are not ($\mathbf{1}_{ij}^{\text{no obj}}$) with a weight $\lambda_{\text{no obj}}$:

$$\mathcal{L}_{\text{conf}} = \sum_{i=0}^{S^2} \sum_{j=0}^B \left[\mathbf{1}_{ij}^{\text{obj}} (C_i - \hat{C}_i)^2 + \lambda_{\text{no obj}} \mathbf{1}_{ij}^{\text{no obj}} (C_i - \hat{C}_i)^2 \right]. \quad (3.6)$$

- **Classification Loss** $\mathcal{L}_{\text{class}}$: This component measures the squared error between the predicted probabilities $\hat{p}_i(c)$ and the true probabilities $p_i(c)$ for each class c , only in grid cells i where an object is present, with a weight λ_{class} :

$$\mathcal{L}_{\text{class}} = \sum_{i=0}^{S^2} \mathbf{1}_i^{\text{obj}} \sum_{c \in \text{classes}} \lambda_{\text{class}} (p_i(c) - \hat{p}_i(c))^2. \quad (3.7)$$

This differs from confidence loss in that each YOLO cell can only predict one object class.

Combining all the components, the total loss for the YOLO detection model is:

$$\mathcal{L} = \mathcal{L}_{\text{coord}} + \mathcal{L}_{\text{conf}} + \mathcal{L}_{\text{class}}. \quad (3.8)$$

We validate the performance of the detector on an unseen set of images coming from the simulation described later in section 3.2.4. For training, we generated 1000 images from the simulation with a single and 20 objects. We train the top layers of the object detector pre-trained on the COCO dataset (Lin et al., 2015) for 50 epochs with a learning rate of 5×10^{-4} and batch size of 16. We then fine-tune the whole network for another 50 epochs with a smaller learning rate of 10^{-4} with batch size of 4. We use optimiser Adam with $\beta_1 = 0.9, \beta_2 = 0.999, \epsilon = 10^{-8}$ and specify early stopping criteria of $\Delta_{\text{min}} = 0.01$ and patience of 5.

The detector achieves a high performance on the unseen 500 testing images, with a mean average precision (mAP) of 84.8% with an mAP threshold of 0.5, which is a good result and comparable with 79% used in a detector on recordings of fish in Chapter 4. mAP quantifies the balance between false positives and false negatives by measuring the area under the Precision-Recall curve across all detections.

3.2.2 Predicting object position with the Kalman Filter

Most of the visual tracking software in use relies on Kalman filters to aid matching of detections between frames. The Kalman filter is a basic linear predictor of state change. It can be extended to account for non-linearity but it is widely used in its basic formulation, being simple and tractable Welch and Bishop (2006). It is a two-stage algorithm where the state of a system is represented as a Gaussian distribution and each step updates the distribution parameters in accordance with the assumed transition matrix F (in our case, a movement equation) and known uncertainties. The prediction step of the Kalman filter performs a convolution of the previous state probability with the one calculated based on the state transition. This *a priori* distribution is used in Bayes' rule with new measurements to provide a posterior, which takes into account both imperfect observation and prediction. Given a state transition matrix F , which defines the assumed equation of motion, the prediction step gives a prior information of the state a in the n^{th} time step:

$$\hat{a}_n = Fa_{n-1}, \quad (3.9)$$

The uncertainty of this state estimate \hat{P}_n is updated by the prediction state:

$$\hat{P}_n = F P_n F^T + Q, \quad (3.10)$$

where Q is a matrix describing noise in the system. After the prediction step, we take a measurement z and calculate the measurement noise as:

$$\zeta_n = z_n - H \hat{b}_n, \quad (3.11)$$

where the H matrix defines which components of the state vector a are latent and which are observed. Kalman gain is then defined as

$$K = \hat{P}_n H^T [H \hat{P}_n H^T + R]^{-1}, \quad (3.12)$$

where R is a measurement noise covariance.

The posterior value of the system state and uncertainty are therefore:

$$a_n = a_{n-1} + K \zeta_n, \quad P_n = [I - KH] \hat{P}_n \quad (3.13)$$

3.2.2.1 Application of Kalman filter to image plane movement tracking

In behavioural research, we are interested in the position of an animal in the real three-dimensional world. Positions of animals moving on the ground, observed from a UAV, can be calculated with geometric transformations if the camera angle and movement are known from onboard sensors. Visual tracking is performed solely in the image space, and the position of each animal can be characterised by its bounding box.

$$b_n = [c_x, c_y, w, h], \quad (3.14)$$

where (c_x, c_y) are coordinates of the centre of the bounding box, w its width, and h its height. In this case the bounding box b_n is the observed state of the animal in the frame n of the recording. The transition matrix F can describe any linear transition between states. This allows us to create Kalman filters with constant speed, and constant acceleration of both position and the bounding box coordinates. In the next section, I describe F matrices of two popular Kalman filters for object tracking, which we benchmark against our deep learning method.

3.2.2.2 Formulation of Kalman-based methods

We compare our novel method to two formulations of the Kalman filter. The most common one, used in SORT tracker [Bewley et al. \(2016\)](#), has a state vector which tracks the position c of the middle of a bounding box, its scale s , and an aspect ratio r :

$$b_{SORT} = [c_x, c_y, s, r, \dot{c}_x, \dot{c}_y, \dot{s}]^T. \quad (3.15)$$

Another formulation comes from the work of [Torney et al. \(2018b\)](#) on visual tracking of Wildebeest on Serengeti and is formulated and tuned specifically for drone footage of animal movement where scale and ratio are less likely to change, but acceleration of movement is common:

$$b_{Accel} = [c_x, c_y, s, r, \dot{c}_x, \dot{c}_y, \ddot{c}_x, \ddot{c}_y]^T. \quad (3.16)$$

3.2.3 Deep Predictor

The high-level information about the visual scene is contained in the last convolutional layer of an object detector. The image input from three consecutive frames are processed through layers of YOLO detector extracting and encoding features at increasing scales.

Outputs of the last convolutional layers — for each of the three scales provided by the detector — is the most dense feature representation that is normally fed into a single fully connected layer in order to classify objects in the scene. We provide those top feature layers for three consecutive frames A, B and C as an input to the *Deep Predictor* together with a focal detection from the second frame B .

Figure 3.5 shows the architecture of the simple neural network that learns the appearance and movement of the animals in a features space of the YOLO detector output.

We are first applying a convolutional layer of two-spatial and one temporal dimension (3D), of 512 $3 \times 3 \times 3$ filters that is responsible for describing motion patterns across the three consecutive frames of the input.

$$x_{feats}(k, i, j) = \eta + \sum_{m=-1}^1 \sum_{n=-1}^1 \sum_{p=-1}^1 x_{in}(k+m, i+n, j+p) \cdot G(m, n, p), \quad (3.17)$$

where G is the convolution kernel, which is a matrix of weights, first initialised at random and learned during the training process and η is a bias term.

Following that, we feed the signal through two layers, also used by YOLO that are a popular choice for helping with the numerical stability of the training. As data is fed

through the training algorithm in batches, the Batch Normalisation layer helps to stabilise the learning process by normalising the outputs of the convolutional layer to have a mean close to 0 and standard deviation of 1, making it resilient to differences between different batches of training data, and reduces training time. The Batch Normalisation (Goodfellow et al., 2016) is mathematically

$$x_{norm,feat} = \gamma \left(\frac{x_{feat} - \mu}{\sqrt{\sigma^2 + \epsilon}} \right) + \beta \quad (3.18)$$

where μ and σ^2 are the mean and variance of the input of the batch and γ and β are network hyperparameters. $\epsilon = 0.001$ is a small constant added for numerical stability. Finally, we apply the activation function needed to frame the output as a classification problem. We use the Leaky Rectifier Linear Unit (Leaky ReLU) function (Goodfellow et al., 2016):

$$\phi(x) = \begin{cases} x, & \text{if } x > 0 \\ 0.1x, & \text{otherwise} \end{cases} \quad (3.19)$$

that has a small negative value where the given node is inactive, allowing for a gradient flow between layers.

Then, finally, we are applying another convolutional network with $4 \ 1 \times 1 \times 1$ filters that is essentially providing 4 values for every spatial location of the convolutional map that are interpreted as offsets, width and height of a predicted bounding box, as related to the original image coordinates.

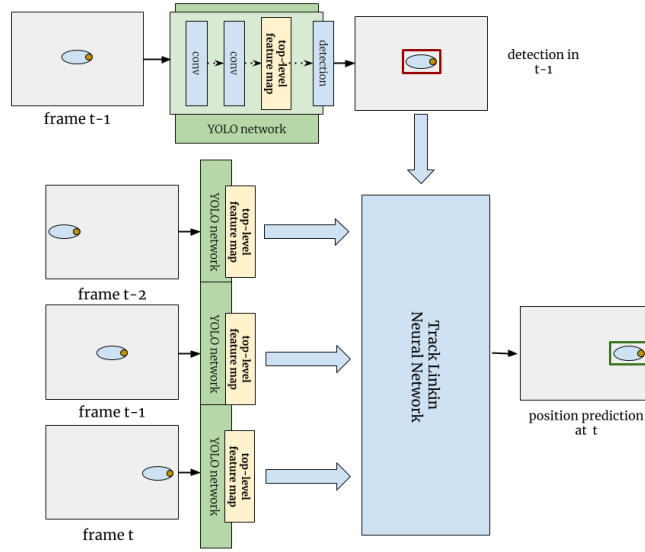


Figure 3.5: Deep Predictor takes as inputs the prediction from the frame at $t - 1$ and the feature map of all three subsequent frames, including the current frame at t . Its output is the location of a bounding box of the object detected and localised in $t - 1$ in the current frame.

Following [Bergmann et al. \(2019\)](#), we are not introducing any additional logic to the prediction step, simply fitting data as a problem of predicting location in frame C of each target object from frame B , given a feature map for frames A , B and C .

The loss function which we are optimising relies on the position of a bounding box in the final frame only and not on probabilities of detection. It is defined as a sum of square differences between all objects' true coordinates (x, y) and predicted coordinates (\hat{x}, \hat{y}) and the sum of logarithm differences between boxes' width w and height h

$$\begin{aligned} \mathcal{L}_{\text{function}} = & \lambda_{\text{coord}} \sum_{i=0}^{S^2} \sum_{j=0}^B \mathbf{1}_{ij}^{\text{obj}} [(x_i - \hat{x}_i)^2 + (y_i - \hat{y}_i)^2] \\ & + \lambda_{\text{coord}} \sum_{i=0}^{S^2} \sum_{j=0}^B \mathbf{1}_{ij}^{\text{obj}} [(\ln w_i - \ln \hat{w}_i)^2 + (\ln h_i - \ln \hat{h}_i)^2], \end{aligned} \quad (3.20)$$

where S^2 represents the total number of grid cells in the detection layer, and B denotes the number of bounding boxes per grid cell. An indicator function $\mathbf{1}_{ij}^{\text{obj}}$ is a mask that equals 1 if the j -th bounding box in the i -th grid cell contains a detected object.

The possible centre (c_x, c_y) of the predicted bounding box in frame C is limited to the same grid cell as in frame B . This limits the ability of the detector to track objects at high speed compared to their perceived size. This limitation is discussed further in the

conclusions of this chapter.

3.2.4 Simulated movement data

Our goal is to understand the limitations of Kalman-based object prediction, and compare them with a method based on deep learning which we call *Deep Predictor*.

In order to evaluate the methods on a variety of well-defined scenarios, we will use the same stochastic process that is most popular in the description of animal movement, an Ornstein-Uhlenbeck (OU) velocity process (as described in section 1.2.2). It is an autocorrelated process and mean-reverting in its usual formulation. It illustrates a range of animal behaviours and often serves as a null hypothesis when studying a behavioural response (Gurarie et al., 2017). It can be parameterised into a trivial form of constant velocity or constant acceleration motion that underlines small-scale assumptions of a Kalman filter.

Velocity in time $v(t)$ is defined by the following stochastic differential equation:

$$dv(t) = \theta(\mu - v(t)) dt + \sigma dW(t), \quad (3.21)$$

where $\theta > 0$ and $\sigma > 0$, are model parameters, μ is a mean value and $W(t)$ denotes a Wiener process of independent increments drawn from a normal distribution. Equation 3.21 can be discretised using the Euler–Maruyama method:

$$v_n = v_{n-1} + \theta(\mu - v_{n-1})\Delta t + \sigma\Delta W_{n-1}, \quad (3.22)$$

where n is a time step index and $\Delta W_n \sim \mathcal{N}(0, \Delta t)$.



Figure 3.6: An illustration showing the most basic geometrical shape, imitating the overhead appearance of an animal. This rigid object of interest is elongated to indicate the direction of movement.

We are using a trivial model of the appearance of an animal in order to control what

information is available to the deep learning methods at inference time. Overhead observation of animals can be approximated by a 2D movement with appropriate geometrical transformation of an image plane to the ground. Our example object is an ellipse-shaped animal with a feature (an eye) indicating direction-facing. It is presented in Figure 3.6 as the orientation of the animal is often the best indication of the direction of movement. Instead of modelling velocity vector $[v_x, v_y]$ as two independent OU processes, we model angular velocity ω and speed s :

$$\begin{bmatrix} \omega_n \\ s_n \end{bmatrix} = \begin{bmatrix} \theta_\omega & 0 \\ 0 & \theta_s \end{bmatrix} \left(\begin{bmatrix} \mu_\omega \\ \mu_s \end{bmatrix} - \begin{bmatrix} \omega_{n-1} \\ s_{n-1} \end{bmatrix} \right) \Delta t + \begin{bmatrix} \sigma_\omega \sqrt{\Delta t} \\ \sigma_s \sqrt{\Delta t} \end{bmatrix} \Delta W_{n-1} \quad (3.23)$$

resulting in the following equations describing the state of an animal at each data point n in terms of its orientation α , and position on a 2D plane $[z_{x,n}, z_{y,n}]$:

$$\alpha_n = \alpha_{n-1} + \omega_n \Delta t, \quad (3.24)$$

$$\begin{bmatrix} z_{x,n} \\ z_{y,n} \end{bmatrix} = \begin{bmatrix} z_{x,n-1} \\ z_{y,n-1} \end{bmatrix} + |s_n| \begin{bmatrix} \cos \alpha_n \\ \sin \alpha_n \end{bmatrix} \Delta t. \quad (3.25)$$

This formulation allows us to create simulated data of progressively more complex motion patterns resembling natural animal movement. We assume that the animals only move forward in the direction they are pointing; hence, $|s_n|$ is always positive.

3.2.4.1 Training

Difficult movement scenarios with crowded images are difficult to annotate even by hand, hence for the training of the *Deep Predictor*, we are only using single object track data with different OU sets of simple movement parameters to better match a realistic training scenario.

Table 3.1 presents the parameters of the OU movement of a single object. We are using 500 frames (of 20-frame long movements) with different coloured animals. Movement models *A* and *B* are limited to straight-line movement only, with constant and slowly changing speed. Processes *C*, *D*, and *E* are more realistic movement models with increasing dynamics.

Figure 3.7 shows the values of velocity and angular velocity, together with histograms of the processes *C* and *E* used for training of the Deep Predictor.

The training based on the same setup to the object detector training for 150 epochs with a learning rate of 10^{-4} , batch size of 8, and Adam optimiser with $\beta_1 = 0.9, \beta_2 =$

id	scenario description	μ_s	σ_s	θ_s	σ_ω	θ_ω
A	continuous speed movement in a straight line	15	0	0	0	0
B	straight line OU speed process	7	15	0.1	0	0
C	slow acceleration OU	10	0.3	0	0.05	0.5
D	OU process	8	10	0.1	0.1	0.3
E	OU process	15	3	1.8	0.1	0.5

Table 3.1: Five scenarios are used for training of the Deep Predictor. A and B are simple movements that should be easily predicted by constant a velocity filter, scenario C corresponds most closely to a constant acceleration movement, and finally, D and E are OU processes with rapid changes in speed and direction.

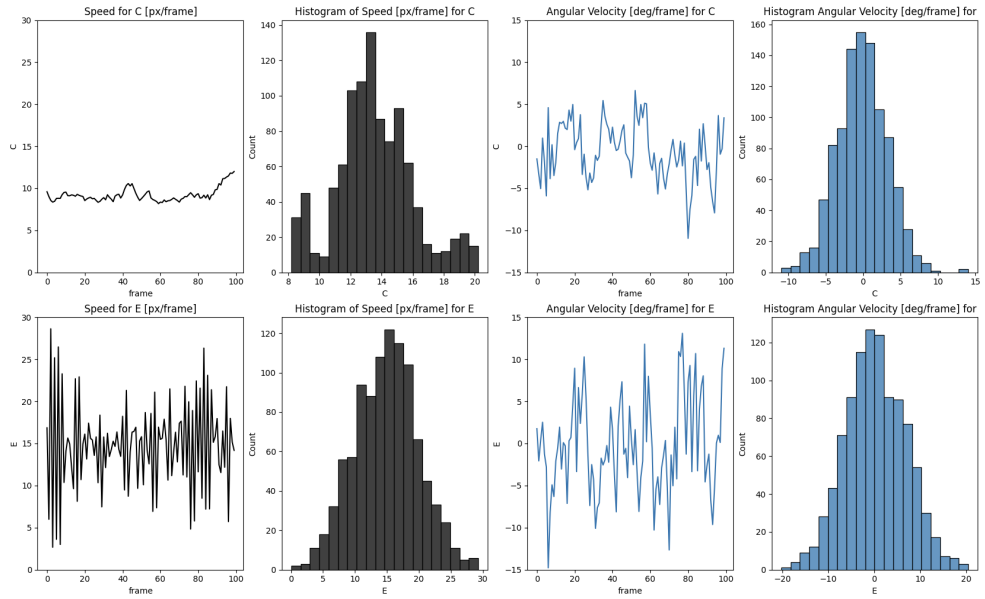


Figure 3.7: Characteristics of complex movement patterns described with an OU movement used in training of Deep Predictor. The first row shows scenario *C* as parameterised in Table 3.1 of a slow movement with gradual acceleration and frequent but small changes in heading. In contrast, scenario *E* is characterised by rapid change in speed as σ_s is ten times higher than in movement *C*.

0.999, $\epsilon = 10^{-8}$ and specify early stopping criteria of $\Delta_{min} = 0.01$ and patience of 5.

3.2.4.2 Summary of test scenarios

To test the performance of the method, we devised three scenarios of increasing complexity by the choice of different parameters μ , σ and θ in Equation 3.23 and different number of individuals. First, we investigate how the linking methods perform on trivial scenarios *A* and *B* that are the same as the ones provided for the training of Deep Predictor. The

third, most important scenario Z is an OU movement with a variety of parameters sampled randomly. Unlike scenarios used for Deep Predictor Training, where three different parameter sets were repeated multiple times in scenario Z , we are drawing a new set of parameters from the uniform distribution as presented in Table 3.2 for every vignette. Each vignette is 25 frames long, and for each number of objects in the scene 1, 3, 10 or 20, we generate 40 vignettes for scenarios A and B and 400 for scenario Z .

Figure 3.8 shows the examples of the velocity values and histograms for the selected parameters to provide some intuition on the complexity of the movement in each scenario.

id	scenario description	μ_s	σ_s	θ_s	σ_ω	θ_ω
A	continuous speed movement in a straight line	15	0	0	0	0
B	straight line OU speed process	7	15	0.1	0	0
Z	OU process	$U(0, 20)$	$U(0, 20)$	$U(0, 0.5)$	$U(0, 1)$	$U(0, 0.5)$

Table 3.2: Summary of scenarios used to evaluate the Deep Predictor’s performance on movement prediction tasks. Scenarios A and B represent simpler, more predictable movements that serve as a basis for training. Scenario Z introduces complexity with parameters drawn from uniform distributions, illustrating diverse Ornstein-Uhlenbeck (OU) processes in movements across 25-frame vignettes. The values are expressed in pixels and frames of the image sized 640×640 px.

The training of *Deep Predictor* is performed on a single object (see Section 3.2.4.1), but to test the usability of this method, we are repeating each scenario with a different number of objects to track in every frame. Figure 3.8 show the examples of the ground-truth movement of different sizes of groups and different scenarios A, B and Z.

3.2.4.3 Comparison methods

We are interested in the following questions:

- Is track linking using the Deep Predictor approach suitable to replace custom Kalman-based filters?
- is the method performance dependent on a number of tracked objects?
- Is the information about the appearance of the object an important component of linking? Or is the positional and geometrical information sufficient? (i.e. is the linker learning the appearance or something about the movement)

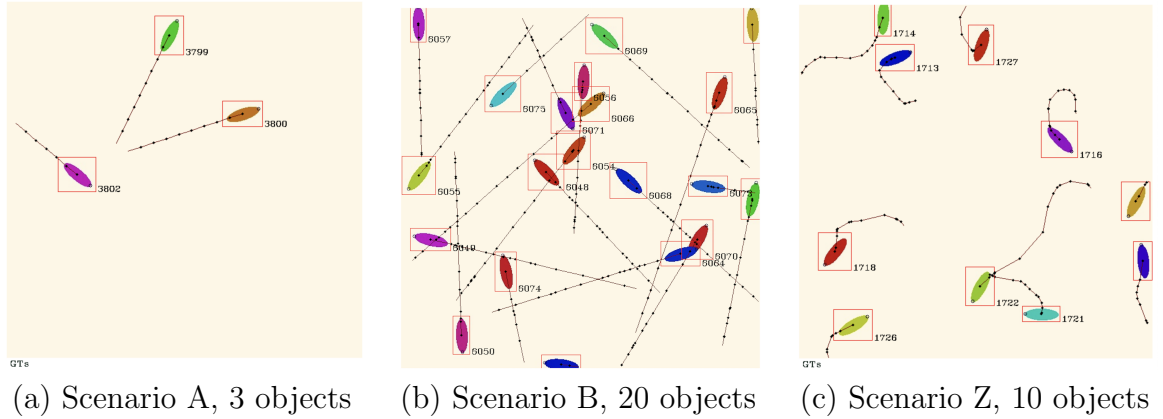


Figure 3.8: Illustration of ground-truth movement tracking in scenarios A, B, and Z with varying group sizes. Figure (a) shows scenario A with a group of 3 objects moving in a constant linear motion - the simplest multi-object example in our benchmark. In panel (b) 20 objects are moving in a straight line with a stochastically varying speed of scenario B. Panel c) shows an example of a complex movement, changing direction and velocity according to an OU process, with 10 objects tracked simultaneously.

As mentioned previously, the object prediction mechanism is one part of a multi-step process. To quantify our contribution independently from the overall tracker performance, we measure the **predicted position of a track, given two previous frames**.

As a quantitative measure, we are calculating the Intersection over Union (IoU) of the predicted position of an object bounding box with the actual position from simulated data. The IoU is usually the metric used in the cost matrix passed to the linking algorithm. We are then averaging the IoU over all the tracks in the frame. The frame score for N objects i in the frame is then given as:

$$S_f = \sum_{i=0}^N N \frac{\text{Area}(b_i \cap g_i)}{\text{Area}(b_i \cup g_i)}, \quad (3.26)$$

where b_i is the bounding box predicted from a linker, and g_i is the simulated ground truth. This score is then averaged across all the frames in a given scenario.

3.3 Results

Our experimentation shows that the algorithm of track position prediction with neural networks (Deep Predictor) can successfully learn a Kalman filter equivalent representation of movement. It performs considerably better than Kalman filters for more complex scenarios of an OU movement. Table 3.3 presents a quantitative evaluation of the track

predictions averaged over all number of tracked objects for each scenario. In the complex motion scenario Z , our method achieved an average IoU of 0.62, which was very similar in both of the easy modes of movement A and B (0.64 and 0.62 respectively). This matches our expectation that the deep-learning network is approximating all possible movements between frames equally. The Kalman filter in SORT formulation performed best on the trivial case of constant velocity movement A with an average IoU of 0.87, which was expected, and the custom Kalman Accel formulation achieved only 0.62. Figure 3.9 illustrates the performance of the trackers on the simplest scenario A , showing a tendency of the Accel method to predict slightly ahead of the actual object and the best bounding box predictions from SORT.

Scenario	Kalman (Accel)	Kalman (SORT)	Deep Predictor
constant velocity straight line (A)	0.62	0.87	0.64
complex velocity straight line (B)	0.49	0.57	0.62
complex speed angular velocity model (Z)	0.44	0.48	0.62

Table 3.3: Average Intersection of Union of all tracks, averaged across all frames for each method on different scenarios (Table 3.2). Each scenario includes between 550 and 800 different frames of movement. The standard formulation of the SORT Kalman filter gives the most accurate prediction of the next position in a simple scenario A. As the complexity of movement increases, the Kalman filter performance deteriorates, while the Deep Predictor provides robust predictions regardless of complexity.

Complex movement in a straight line, scenario B , showed a steep decline in the ability of Kalman filters to track, thus their performance dropping below that of the Deep Predictor to 0.49 for Accel and 0.57 for SORT. In the Figure 3.12 we see an example of this scenario, with rapidly accelerating objects presenting the greatest difficulty to the Kalman-based approaches.

As expected, the array of complex OU movements in scenario Z led to further deterioration of the benchmark Kalman methods, with SORT at 0.48 and Accel at 0.43. Figure 3.11 illustrates how the Kalman filter fails to compensate for a concurrent change of shape and location of a bounding box of a turning animal. The appearance of the animal provides an obvious indication of the movement direction. However, this is not in any way captured by the Kalman filtering, which needs a number of iterations to adjust the shape

of the bounding box.

In Table 3.4, we present a breakdown of results by scenario and number of objects tracked, and Figure 3.10 shows box plots of the distribution of IoU averaged between all tested frames. For all methods and scenarios, we observe decreasing performance as the number of tracked objects increases, but also a decrease in the variability of the results. This results from the more objects' IoU results being averaged in each single frame. In the complex scenario Z , Deep's performance decreases from 0.66 to 0.56, but it is still higher than single-object tracking with Kalman filters (Accel at 0.46 and SORT at 0.51).

The performance of Kalman Filters is independent of the appearance of the objects they track. We confirm that the same is true for the Deep Predictor, observing in Figure 3.14, that performance does not deteriorate in cases where the only difference in appearance can be attributed to their directional orientation. The appearance information can be used in the next matching step of tracking; however, for the location prediction, we expect the method to focus on movement-related cues.

Figure 3.13 shows the most challenging scenario with 20 objects and complex movement. In this scenario, Kalman methods achieve an average IoU of 0.41 for Accel and 0.45 for SORT, far behind the 0.57 of our method. Rapid turning of the object changes its bounding box proportion rapidly, as in real-life scenarios, where animal appearance can change faster than its location, challenging Kalman-based filters.

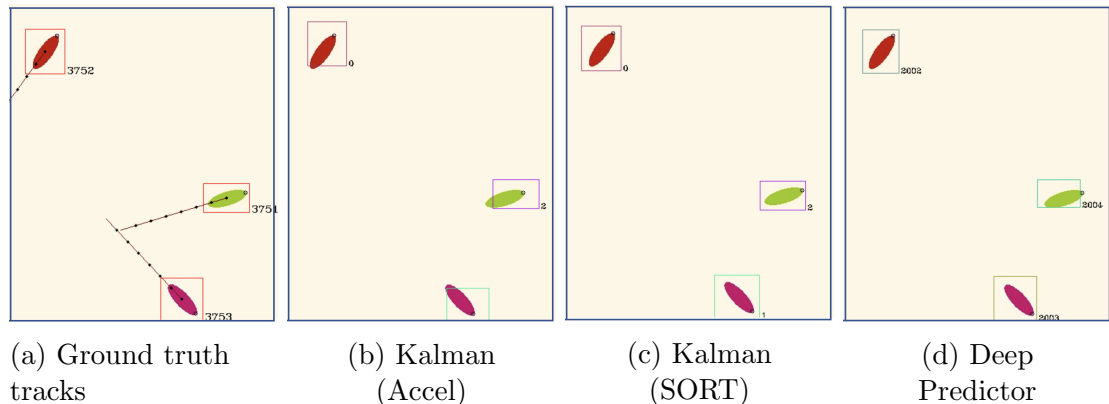


Figure 3.9: Display of the linker testing of a simple constant-velocity movement in a straight line (scenario A) with ground truth shown in panel (a). We present an object in the final frame without its bounding box prediction (for clarity). Panel (b) shows predictions from Kalman (Accel) method, showing the predicted position slightly ahead of the actual position of the animal and achieving an average IoU accuracy of 0.65. Predicted boxes from (c) Kalman (SORT) with the highest accuracy of 0.87 and (d) Deep Predictor (with 0.87 on this scenario) are both closely tracking the animal position as expected for this simplest case.

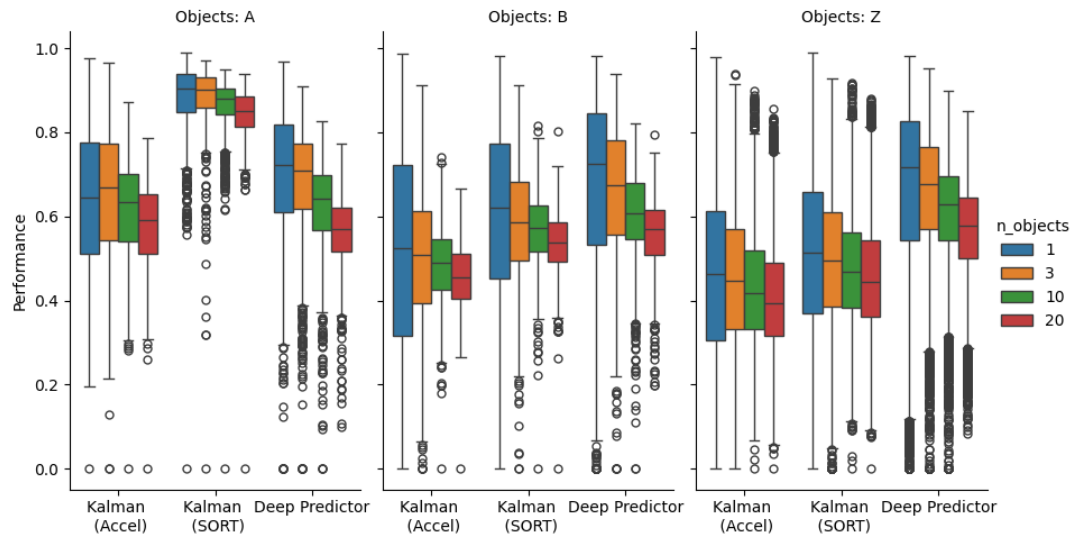


Figure 3.10: Average intersection of the union IoU of different methods with different number of objects and scenarios. The first panel shows the simple, continuous movement in the straight line, scenario A, where SORT variant performs best. On the more complex movement in the straight line, already the *Deep Predictor* performs better, and vastly outperforms Kalman-based approaches on complex OU movements in scenario Z. Our method’s performance degrades slightly with more objects in the frame, but it seems to be even across different type of movement.

3.4 Discussion

The results clearly show the advantage of using deep learning to predict the next position of an object instead of using Kalman filters, with an almost 50% improvement over the better-performing popular formulation of SORT (from 0.62 to 0.48).

In ecology, vast annotated datasets are not as readily available as in commercial areas such as surveillance or automotive sectors. For this reason, the use of deep-learning methods is limited by the risk of overfitting to specific domain data, as fewer examples for cross-validation and methodical testing exist. In cases where labelled examples differ from those encountered in the study there is a risk of introducing strong bias in observations and incorrect conclusions from extracted data.

I approached this problem by testing on simulated data to verify the robustness of the key element of the tracker, its predictor. Simulated data do not guarantee performance in real-life scenarios. However, any one set of real-life scenarios equally does not guarantee adaptation to another domain. By showing that our approach can learn complex move-

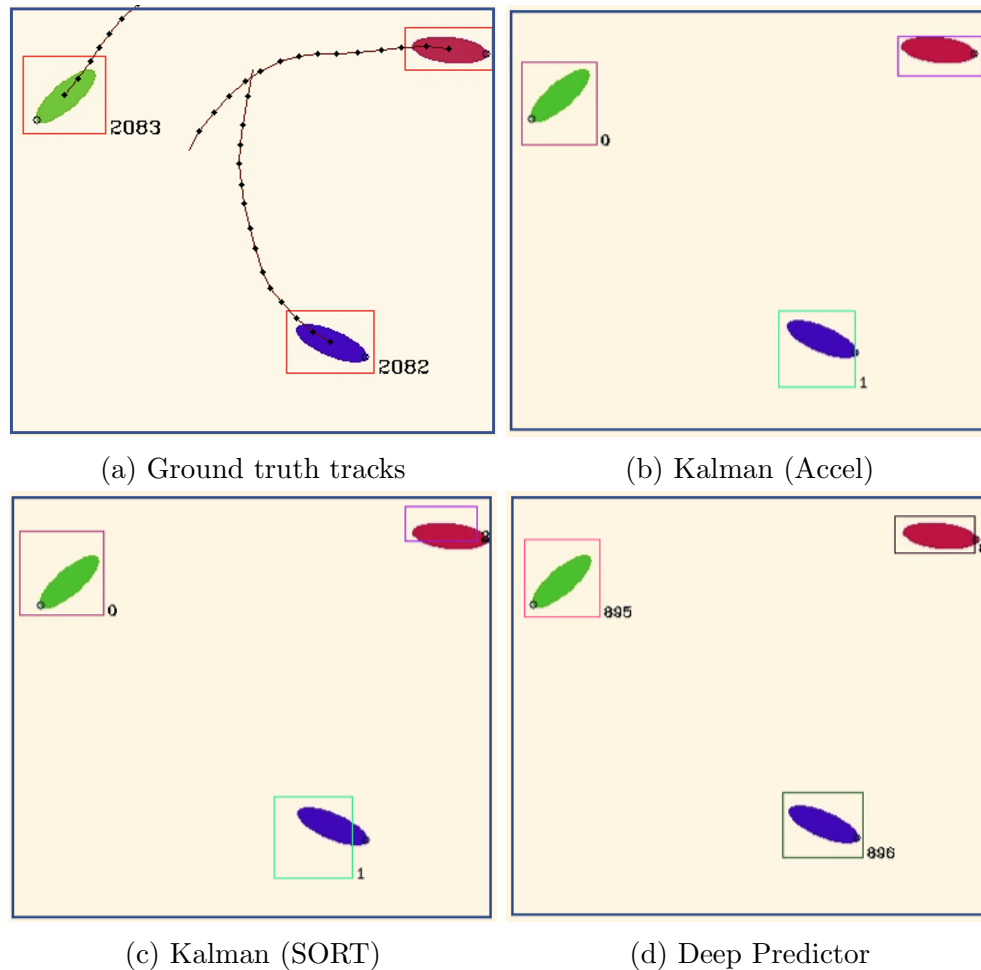


Figure 3.11: Display of the linker testing on the most realistic scenario of OU movement in directional speed and angular velocity (scenario Z) with 3 objects in the frame. The first panel (a) shows the ground truth track locations. Each panel shows a predicted location of the object by the tested methods. In panels (b) and (c), we observed Kalman-based methods failing to adjust the shape and location of the object that is rapidly changing direction, while the Deep Predictor in panel (d) is able to match the object with a bounding box despite the complexity of movement.

ment and crucially that 1) its performance does not deteriorate with a number of tracked objects and (2) That it will perform similarly on different complexities of movement, we can confidently move to domain-specific testing on real data. By simulating an array of complex OU movements that are a common description of animal movement, I have shown that the Deep Predictor can recognise movement with parameters it has seen in training data as well as generalise to those it has not. In real-world scenarios, most of the movement observed and labelled would likely come from similar experiments and be very limited. Equally important, I showed that increasing the number of animals tracked did

Scenario	no. objects	Kalman (Accel)	Kalman (SORT)	Deep Predictor
A	1	0.65	0.87	0.71
A	3	0.65	0.87	0.68
A	10	0.61	0.85	0.62
A	20	0.57	0.83	0.56
B	1	0.51	0.59	0.66
B	3	0.5	0.57	0.66
B	10	0.48	0.56	0.6
B	20	0.45	0.53	0.56
Z	1	0.46	0.51	0.66
Z	3	0.45	0.5	0.65
Z	10	0.43	0.47	0.61
Z	20	0.41	0.45	0.57

Table 3.4: Average Intersection of Union of each method on different scenarios, with a breakdown by number of objects tracked. In the simplest scenario of continuous straight-line movement A, the SORT formulation of the Kalman filter consistently provides the best results. In scenarios B (straight-line changing velocity) and Z (variety of complex OU processes), Deep Predictor provides consistently best results with less than 10% reduction in the prediction quality in tracking 20 objects (0.57) than when tracking only one (0.66).

not have much detriment, showing a decrease of 12% in average IoU from single animal tracking to a challenging scenario of 20 animals. The tracker has only been trained on single object tracks, making it especially practical, as manual labelling of multiple-track data is challenging.

As the next step, the tracker with the Deep Predictor module will be tested on existing benchmarks from the MOT20 [Dendorfer et al. \(2020\)](#) challenge to understand its performance versus the state-of-the-art trackers. The tradeoff between the quality of predictions on a benchmark needs to be weighed against the ease of application to the research problems and the robustness of this approach.

Testing complex deep-learning trackers on simulated data presented here would almost certainly result in their superior performance, but it would be impossible to distinguish the effect of superior object detection algorithms, prediction, or matching stages.

The work of [Bergmann et al. \(2019\)](#) suggests that many improvements in best-performing methods are marginal and do not always generalise to other problems. For the purpose of this project, we did not label enough movement data of animals to be able to train a complex tracker, let alone comprehensively validate it. However, knowing that the Deep

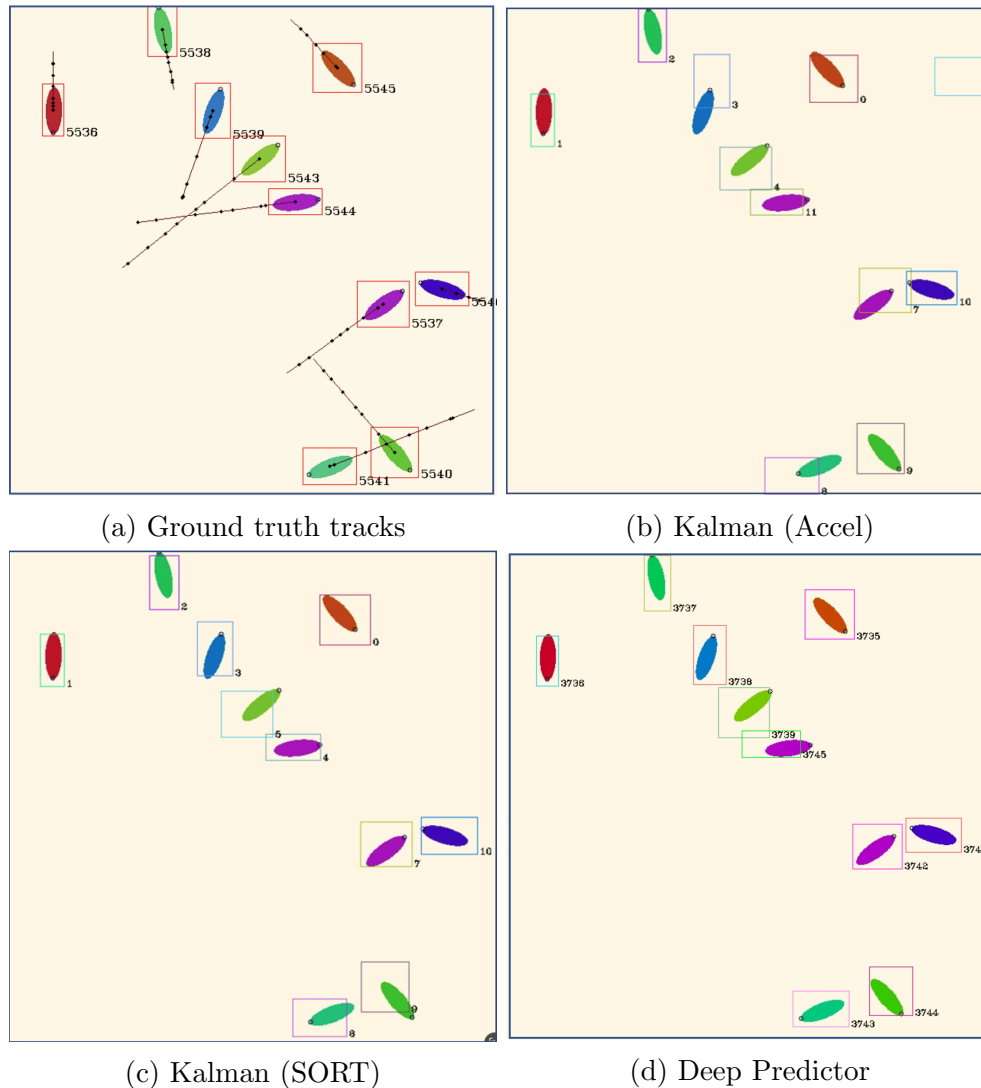


Figure 3.12: Display of the predictions of results on scenario B, a movement in a straight line with a variable speed and 10 object tracking presented in panel (a). Average performance on all frames for this scenario is 0.48 for Kalman (Accel) presented in panel (b), 0.56 for Kalman (SORT) in panel (c) and the highest result of 0.6 for Deep Predictor presented in panel (d). Empty boxes are artefacts of the track display process and do not affect the prediction score.

Predictor can generalise tracking from single object tracks, we will now re-train it on real data, using the simulated model as a starting point in transfer learning. This is to supplement the model of the movement trained on simulated data and not create one solely relating to the limited real-life datasets.

Apart from [Lopez-Marcano et al. \(2021\)](#), trackers used in animal tracking do not use deep learning detectors such as YOLO. For that reason, most of the practical difference

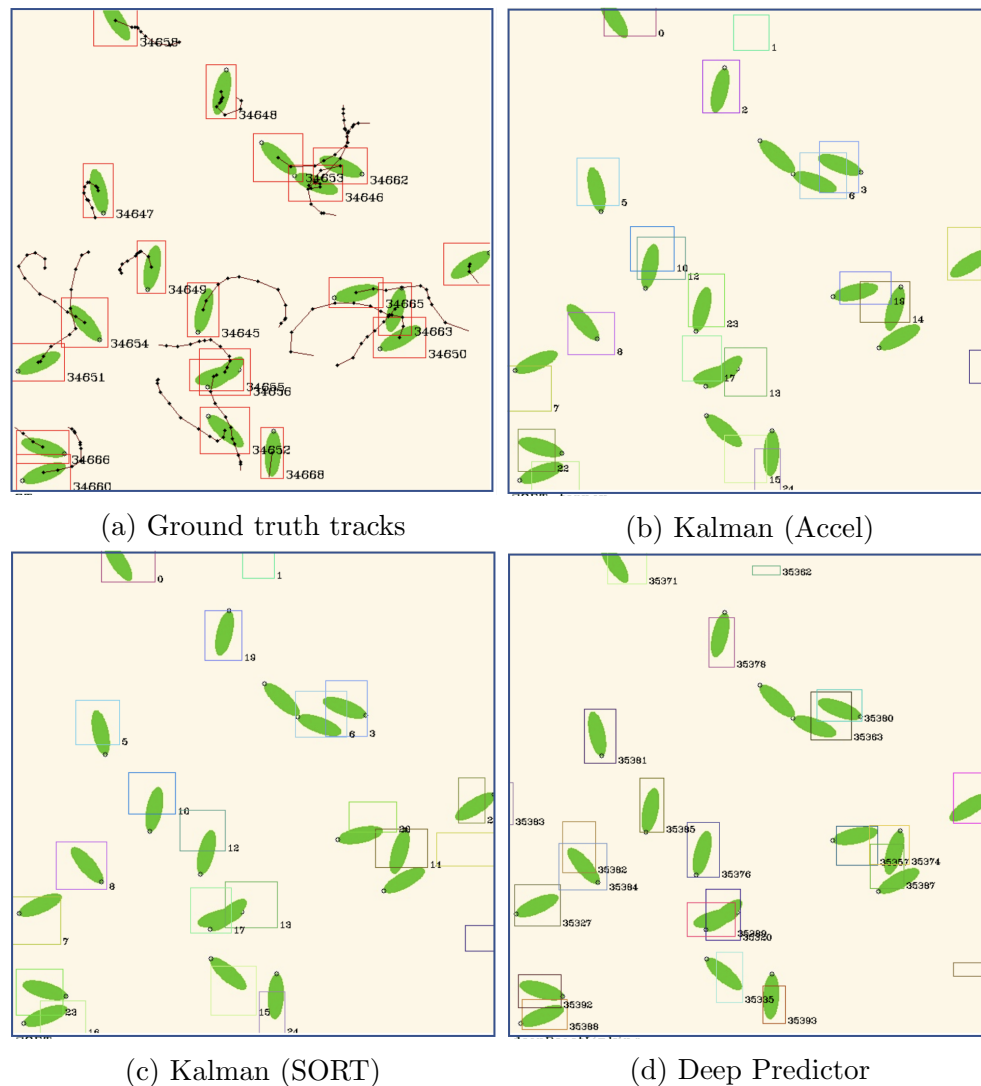


Figure 3.13: Display of the linker testing on the most complex scenario Z with 20 identical objects in the frame with the ground truth of the simulation in panel (a). Crowded scenes with minimal differences in appearance are a common problem in the visual tracking of social animals. Empty boxes are artefacts of the track display process and do not affect the prediction score. In this scenario, Kalman methods achieve an average IoU of 0.41 for Accel and 0.45 for SORT, far behind the 0.57 of Deep Predictor.

in performance between Deep Predictor and traditional animal tracking approaches would be explainable by the quality of detections, which in our case require a data-labelling exercise. In the case of [Lopez-Marcano et al. \(2021\)](#), 8700 tracks of fish were labelled, which is much more labour-intensive than annotations of still images for object detector training (as performed for Chapter 4). Without a methodical approach presented in this chapter, it is impossible to establish which part of the deep learning framework is

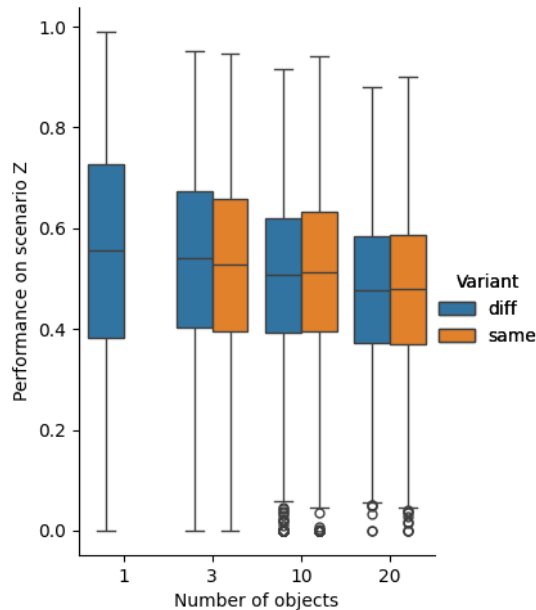


Figure 3.14: Results of Deep predictor in complex scenario Z with different number of objects and identical (orange) and distinct (blue) appearance of objects. For multiple objects performance slightly degrades for all methods, but as with Kalman filter methods that do not include appearance information, the *Deep Predictor* do not see degraded performance when objects are identical, suggesting that the orientation of the object is the sufficient information used in tracking. In the case of a single object, the appearance is irrelevant so we do not repeat this result.

responsible for superior results on a single dataset and if such an approach would scale to another application.

On this simulated data, detection quality was very high at 84% mAP on an unseen dataset. These detections are matched to predicted locations of existing tracks in every frame, and those with the highest IoU are assumed to come from the same object. We observed that even on the simplest continuous motion scenario, a constant-velocity Kalman filter (SORT) achieved a maximum of 87% on tracking of a single object. This is caused by cases where the object enters or leaves the frame but is still detected and has a deformed bounding box. These cases are very typical in real-world scenarios with many occlusions and deformations.

A formulation of the Kalman filter successfully used in tracking animals from a drone performed worse than SORT. We observed that the detections were consistently ahead of the true location of the animals, indicating a bias towards detecting accelerating animals. This makes sense because slowly moving ones are already easier to detect and, in reality,

more common. This example shows that statistical intuition about ecological observation is often more important than the quantitative result of a single method. The OU process used for testing in this chapter only modified speed, limiting scenarios to ones that can be modelled by linear velocity Kalman filter. Changes in acceleration that Kalman Accel can better model were not included in this benchmark, explaining the worse performance of that approach.

In multi-animal tracking, part of the reason for the degraded performance of Kalman filters might be related to the quality of underlying tracks. Kalman filters need at least three data points to form a model of movement but will perform better with more. The quality of earlier tracks (matched with Hungarian matching) might be the reason why it did not match single-track performance in the trivial scenario. The Deep Predictor only requires two previous frames and one prior detection to function, making it more robust and applicable in more tracking scenarios.

The Deep Predictor performs equally well in cases where simulated animals have identical colours. This confirms that the predictor provides good predictions based on the movement and directional orientation of the animal and not by matching a unique appearance.

This promising method has the potential to track animals in a variety of situations, exceeding Kalman-based approaches. It opens a new direction for further development of animal tracking software for challenging collective behaviour studies, where complex movement patterns can be incorporated explicitly into the training process without the need for excessive data labelling. This will open possibilities for studies of leadership and group decision-making that require long-term tracking of focal individuals in a group. The individual and collective reactions to threats and sudden changes in the environment can be studied in depth with arbitrary quantities of animals that can be tracked and the number of repetitions that are limited only by available data recording - not by the effort required to correct it.

Chapter 4

Collective decision making in laboratory experiment of smolt downstream migration

Note

The content of this chapter has been written solely by Mikolaj Kundegorski on the experiments and analysis performed solely by the author. Colin J. Torney, Shaun Killen, and Colin E. Adams participated in the experimental design, conceptualisation, and revision of the chapter, Adrian Bowman provided support in statistical modelling.

4.1 Introduction

Salmon migration is the critical phase of the life of Atlantic salmon. It is a dramatic shift in habitat and physiology associated with very high mortality (Thorstad et al., 2021). Migration success varies widely between populations in different river systems and within one population across individuals and different seasons. Successful navigation reduces the time juvenile salmon are subject to increased pressure and adverse environmental effects, as well as anthropogenic effects that might occur during longer journeys. Understanding factors influencing navigation is necessary for the conservation of species and ecosystems depending on the health of salmon populations.

Collective decision-making is an important aspect of decision-making in many animals. There are clear advantages to collective movement, especially in fish (Killen et al., 2011), and effect of improved obstacle and predator avoidance, as well as group sensing, has been widely observed in other species.

Some salmon species are known to travel in groups during the upstream migration (Berdahl et al., 2014) and social cues influencing the start of downstream migration has also been reported McCormick et al. (1998). Some observations suggest that juvenile salmon travels in shoals, but telemetry data is too sparse to confirm or deny, and direct observations with acoustic sonars are still very sporadic and we are not aware of observations of Atlantic salmon.

In this experiment, I test whether group size and previous group living has an effect on decision making during downstream migration of juvenile salmon. To answer this question, I designed an experiment where groups of fish in a circular tank with directional flow are presented with a choice of two channels. One channel is open and has a stronger flow, while the other is partially blocked by a small obstacle, reducing the flow and introducing an impediment to migration. We observe travelling fish on the approach to the confluence and quantify their choice in the context of proximity to other migrants ahead of them. Our study answers the following questions

1. Are smolts exhibiting migratory behaviour in the artificial stream?
2. Is the presence of an obstacle and qualitative flow differential at the entry to the choice chamber affecting fish behaviour?
3. Are fish behaving differently as part of the group than when travelling alone? We define this problem more narrowly by checking if fish is influenced by the proximity of other migrants ahead of it in the choice chamber.
4. Are wild smolts better at navigating the obstacle than farmed animals?
5. Is there a difference in group effect on the choice of a channel between fish reared in groups on a farm or previously territorial wild fish?

In the introduction of my thesis in Section 1.1.5.1, I described downstream migration, which is a critical part of the life of Atlantic salmon. After spending a number of years as parr in the fast-moving streams, salmon undergo a physiological transformation into smolts, the form that prepares them for entry into the marine environment and begin migration to the sea.

Some indirect evidence of shoaling exists from downstream movement telemetry studies in a partially controlled environment. Fernandes et al. (2015), investigated the timing and incidence of shoaling of wild salmon smolts in the south of England, showing that shoaling of the migrants is likely an adaptive response to the change in the environmental

conditions, not dependent on the kin-based structures observed in group behaviour of salmon parr. This study used PIT-tagged hatchery smolts of wild origin and assumed that smolts are shoaling if their detection time falls within 12 seconds from one another. However, an older study by [Olsén et al. \(2004\)](#) shows some aggregation (apparently as under one minute registration time) among different groups of smolts' one-time passage through a 400m length artificial stream. The authors observed some kin-structure, which was later contradicted by [Fernandes et al. \(2015\)](#), showing difficulty in drawing robust conclusions relating to group behaviour on data with low spatial or temporal resolution.

It is impractical in field studies to achieve sample sizes needed to model collective behaviour reliably. In the next chapter (Chapter 5) of my thesis, I review more closely the obstacles faced in studying collective behaviour in the wild. Most ambitious modelling studies of salmon downstream migration, such as work of [Sridharan et al. \(2023\)](#) on Pacific salmon smolts, focus on mapping precise hydrological conditions to understand the movement of individual fish without accounting for group movement.

Our approach is informed by similar observations of salmon and choice experiments on other fish aimed at understanding their response to flow and social movement.

Pacific salmon smolts were observed making a choice-chamber decision during their natural migration in rivers. In one study, individual passages of smolts were recorded with overhead infra-red cameras in various designs of culverts [Kemp and Williams \(2008\)](#), observing fish migration during both day and night. Hydraulic stimuli and lighting were found to affect the fish's swimming speed and orientation to flow. In another study, a flume was embedded within a culvert on a migratory path of different species of Pacific salmon, allowing the study of fish behaviour when presented with a choice of two channels differing in width and flow [Kemp et al. \(2005b\)](#). Fish travelled both head first and tail first, most of the time actively swimming (faster than stream velocity), showing a preference for the less turbulent water channel and sometimes actively swimming upstream out of a less preferred channel. A more recent study by [Vowles et al. \(2014\)](#) observed juvenile salmon behaviour in darkness and light in response to two channels with different flow conditions, showing differences in the behaviour of fish depending on presence of a visual signal.

Our study follows those experiments by explicitly investigating group effect in direct observation of fish choices.

[Tan et al. \(2018\)](#) presents direct measurements and modelling of a single fish (silver carp) movement in an artificial stream. A flume filled with vertical slots/obstacles had a precise flow profile measured so that repeated filmed passage of a test fish (silver carp) allowed a to model its movement. Entire visual and hydraulic cues for fish movement can

be controlled and measured, allowing a good mechanistic explanation of fish behaviour. This study does not involve any collective behaviour but provides a benchmark on what is possible with well-controlled laboratory setting and modern tracking techniques.

Schooling in fish is important to minimise the energy expenditure on swimming (Killen et al., 2011; Zhang and Lauder, 2023). For juvenile salmon that do not feed during their migration McCormick et al. (1998), the effect of shoaling would be instead related to improved migration success due to better navigation and a decrease in individual predation (Finstad and Jonsson, 2001; Kennedy et al., 2018).

A study of Miller et al. (2013) addresses the trade-off between group decision-making and individual preferences. Groups of golden shiners were trained to prefer specific channels of a three-way choice chamber in an artificial stream. The study reports that while fish in front of the shoal put equal importance on their preferences and direction chosen by other members of the group, those in the back of the shoal preferred staying within a group regardless of which choice the chamber shoal navigated towards. Swimming fish are more influenced by group members ahead of them, and that should also be true for my study subjects. When searching for potentially small effect sizes, we can focus on the effect of fish ahead of the studied individual.

Our study aims to bridge the gap between what is possible with constrained laboratory experiments and field studies. Laboratory setup offers good control of flow and detailed tracking but can only allow a limited quantity of fish shoals and poorly mimics the spatial extent of the riverine environment. However, observations in the wild are limited to a sparse number of individuals that can be tagged, and group formation might be impossible to observe.

4.1.1 Preceding work

Individual flow response In the first study presented in chapter 2, we assessed the minimum water velocities required to elicit a change in directional holding in both wild-origin and domesticated salmon smolts. Smolts needed a directional flow exceeding 8.9 cm/s to demonstrate effective directional orientation towards the current. Domesticated smolts exhibited a similar qualitative response to their wild counterparts but required slightly lower velocities to initiate a response.

Preliminary study of unobstructed movement In our preliminary experiment within the flume, we determined the smolts exhibit migratory behaviour when exposed to a stable flow (approximately 20 cm/s) for extended periods. We conducted six recordings of three

differently sized groups of fish ($n \in \{1, 5, 10\}$) throughout the night and day between the 19th of March and the 1st of May 2019. In every instance, the fish travelled downstream, forming groups and displaying migratory behaviour during extended periods, both at night and during the day. In larger groups, fish travelled head-first and at increased speeds. Additionally, we have tested the feasibility of different designs of choice chambers, observing obstacles which fish can and cannot navigate.

Given our ability to reliably observe migratory behaviour in smolts within our experimental setup and equipped with precise tools for movement data analysis, we proceeded with the experimental design detailed in the following section.

4.2 Experimental Setup

4.2.1 Salmon smolts

In this experiment, we used two batches of fish, one from a population of smolts migrating in a Scottish river, which we name “wild” and one of commercially farmed smolts of Norwegian ancestry from a freshwater hatchery which we call “farmed”. Table 4.1 presents the detailed characteristics of each studied batch. In the experiments, we used groups of 10 fish that were previously held in the same holding tank. The wild salmon smolts were collected from the River Gryffe, Scotland (55° 51.9′ N; 004° 31.1′ W), captured in a rotary screw trap during the smolt run ($N = 31$, mean weight of 24(6)g, and mean fork length of 13(1) cm). These fish were transported to the Scottish Centre for Ecology and Natural Environment (SCENE) - where experiments were conducted - in oxygenated bags (transport time approximately 1 hour) and held in holding tanks for at least 2 hours before trials. In total, we used three groups of 10 wild smolts in the experiment.

The hatchery fish were provided by MOWI from freshwater pens at Loch Arkaig in the late parr stage in March 2021. We followed industry procedure to induce smolting with constant light and used standard criteria from [Gorbman et al. \(1982\)](#) to assess smolting progress. Hatchery smolts had an average weight of 44(14)g and a fork length of 16(2) cm, and we used 5 unique groups of 10 fish held in the same holding tank prior to the experiments.

4.2.2 Artificial stream

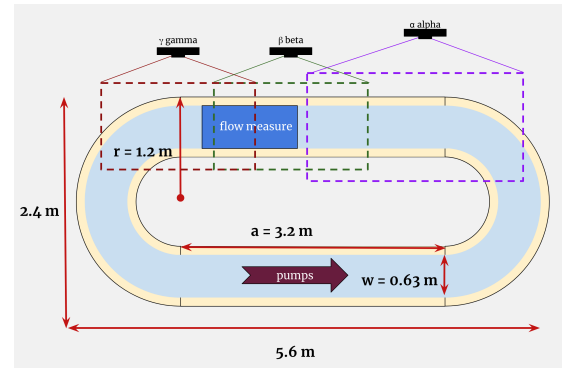
Our experiments aim to understand the downstream migration of juvenile Atlantic salmon (*Salmo salar*) better, some of which occurs in narrow, fast-moving burns. As our exper-

	farmed loch-farmed smolts	wild wild smolts
source	MOWI: Loch Arkaig	River Gryffe (55° $51.9' N$; 004° $31.1'$ W)
date experiments	March 2021	May 2021
mean weight [g]	44 (14)	24 (6)
mean fork Length [cm]	16 (2)	13 (1)

Table 4.1: Fish populations used in the experiment. Farmed fish come from a freshwater facility on Loch Arkaig, while wild smolts come from River Gryffe in Scotland. We report the mean weight and fork length of each population with standard deviation in parenthesis.



(a) The flume photograph.



(b) Dimensions of the flume

Figure 4.1: Above image (a) shows the flume used in experiments in Scottish Centre for Ecology and the Natural Environment in Rowardennan. For the duration of the experiments, all of the observation panels have been covered to limit the influence of the external environment. The laboratory itself is a room without any windows, allowing for full control of lighting conditions. The schematic of the flume in the drawing (b) shows all the relevant dimensions. The flume has the shape of a stadium with $a = 3.2$ m and $r = 1.2$ m. At the midpoint, it corresponds to 11.2 m length. The location where flow measurements were taken is marked by a blue section and the location of pump inlets and outlet in brown.

imental arena, we utilised an artificial stream (see Figure 4.1), configured as a stadium with $a = 3.2$ m and $r = 1.2$ m with a total channel length of 11.2 m and a width of 60 cm. For a fish travelling in the flume at an average observed speed, it takes approximately 40 seconds to complete the full circuit. The external mounting of the pumps facilitates unimpeded movement around the flume and is at the opposite end of the experimental area where fish are filmed and presented with the challenge.

During daytime hours, recording in the flume showed that the light at the water’s surface was 193(78) lx, while nighttime recording was conducted in complete darkness under infra-red illumination (detailed later in section 4.2.5). This corresponds to the light intensity equivalent to heavy overcast or conditions at sunrise or sunset, which is sufficient for smolts to use visual cues in a shallow tank where there is no loss of light due to depth (Fraser and Metcalfe, 1997). It is the same order of magnitude as light conditions (95 lx) used in comparison of juvenile Pacific smolts reaction to flow by Vowles et al. (2014).

In the preliminary experiments, we observed no difference in smolt behaviour between either clockwise or counter-clockwise direction of flow. Due to the limited availability of fish for repeating experiments, we opted for only one flow direction in this study (counter-clockwise).

The flume was filled with water up to about 21cm and driven at a medium speed approximately $20 \frac{cm}{s}$, corresponding to a weak flow in a natural stream. We measured the flow profile of the flume ahead of the experiments on a one-meter straight section of the flume shown in Figure 4.1. We measured 20 points on a 5×4 grid with a 15cm distance across and 20cm along the flume, repeated at depths of 7 and 14 cm. We found the flow considerably uneven with the coefficient of variation $CV = \frac{\sigma}{\mu} = 0.42$ with the mean flow of $\mu = 18.25$. Because of changes to pump output over an extended period, we relied on camera recordings of the water surface to measure flow speed during the experiments. Based on the precise measurements of the speed of air bubbles moving with the flow, we were able to measure average flow across different experimental scenarios. To verify the method, we compared the value of flow measured with a flow meter (20.4 ± 9.81 cm/s) with camera-based measurement (18.1 ± 8.78 cm/s), finding no significant difference between them. Table 4.2 shows the values of the flow measured in different variants of the experiment.

4.2.3 Choice chamber

Figure 4.2a shows a conceptual drawing of this experiment and an overhead photograph of the constructed choice chamber. We constructed the choice chamber at the opposite end of the flume from the pump inlets, at the end of the straight stretch of the tank, to minimise the impact of turbulence of the curved section on the fish as they enter the chamber. We alternate the flow at the entry to the choice chamber by placing a navigable obstacle at the other end of it. The choice chamber is 80cm long and divides the flume equally into two 31cm wide corridors. We create the “obstructed” side of the chamber by positioning a sandbag at the chamber’s downstream end, building a weir that allows

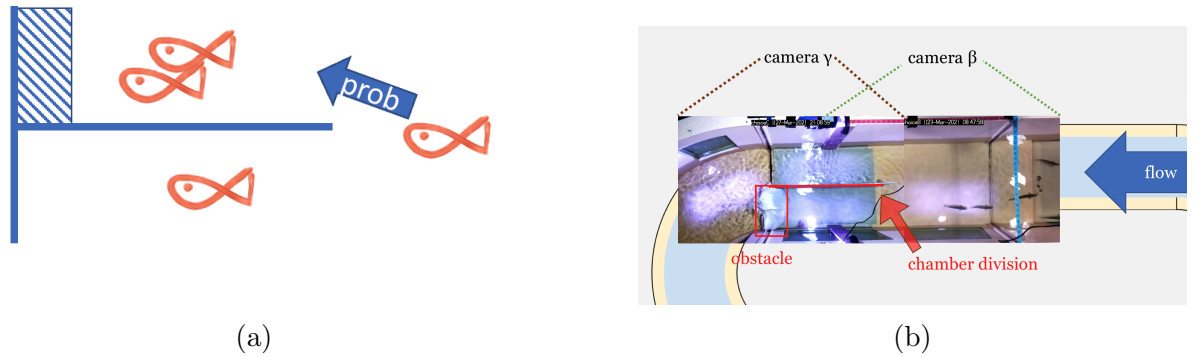


Figure 4.2: Drawing on the left presents the conceptualisation of the experimental problem. The fish travel in proximity to other conspecifics is forced to choose between channels when one of them might be impeded. Figure (b) depicts the layout of the flume, including the entire choice chamber with a highlighted entry and obstacle slowing down flow (in red) and the area ahead of it, all captured by Raspberry Pi cameras. Camera β was placed to capture fish behaviour 50 cm before the flume entrance, providing data for analysis in this chapter.

fish to swim over it but creates a discernible flow gradient at the chamber’s entrance. In description of experimental trails in table 4.2 we provide a breakdown of flow differences between each side of the choice chamber in each experimental trial.

The choice of material for the chamber proved important for both rigidity and colour. The plastic had to be strong enough to withstand turbulent water yet flexible enough for setup without permanent fixtures to the flume. We discovered that a dark floor made fish more likely to linger over it for perceived safety. Dark-coloured obstacles, such as stones, often provided good cover for holding fish. Therefore, the choice chamber was constructed from light-coloured plastic, and the obstacle was white, as in Figure 4.2b, to minimise substrate difference.

We observed the fish holding inside the choice chamber occasionally, no more frequently than in other parts of the flume. More often, fish would hold over the water outflow grid at the flume’s other end, a part of the design that was not modifiable.

4.2.4 Camera setup

We used ceiling-mounted cameras to observe the movement of fish on the straight section of the tank approaching the choice chamber and throughout the chamber, including part of the bent section beyond the chamber as presented in still frames in Figure 4.2b. In order to allow remote-controlled recording over many hours, we used Raspberry Pi NoIR second

generation camera module connected to Raspberry Pi computers set up on the local wired network. Unlike alternative USB cameras, this camera module uses a direct hardware interface with h264 encoding, allowing compression of video stream during recording, allowing high-resolution 1920 x 1080 images at 10 frame per second to be saved reliably over long time periods with a manageable file size. The resulting recordings were stored within 20GB of free space of a High-Speed SD memory card during the recording session, limiting what can be done with less optimised approaches. The direct programming interface allowed accurate reading of the time for each recorded frame (down to the millisecond), otherwise not possible with most commercial cameras. The camera uses an 8 MP Sony IMX219 CMOS sensor and a manual focus lens (aperture $f/2$) without an IR filter, allowing recording in the near-infrared. The lens was focused manually and provided a sharp image for the entire depth of the tank. The recording frame rate was reduced to 10fps from the maximum of 30 to allow a longer exposure in the most challenging IR-recording conditions.

Footage from camera β at the entry to the choice chamber channels were used to quantify fish choices by automated video analysis described in the next section.

Schematic of the flume in Figure 4.1b, illustrates the placement of all three near-infra red cameras α , β and γ used to supervise the experiment. Camera α had the largest coverage of the tank due to placement on a higher ceiling. It covered the 170cm of a straight flume section ahead of the chamber and a part of the bent section before, providing good footage for qualitative analysis of movement (presented later in the Figures 4.7a and 4.7b). Camera β covers 118cm of area ahead of the chamber and 38cm inside it. Figure 4.4 shows still images from camera β used to quantify the decision-making of fish. Camera γ shows the entire chamber area (80cm) and the turning of the flume that follows. We used this footage to validate our assumptions about fish's ability to cross the obstructed channel and other behaviours. An example of image in Figure 4.7d comes from camera γ .

The outflow grid, where fish were most often observed holding, is located at the opposite end of the flume and is not covered by any cameras. The quantitative analysis is solely based on recordings from the camera β as it covers the entry to the choice chamber. The fish was observed from late afternoon to early morning and for at least 14 hours, including 8 hrs in the night, when visible-spectrum lights were extinguished. In the darkness, recordings were facilitated by a limited set of infra-red lamps placed in a way to maximise the illumination of the most important parts of the choice chamber entry visible in Figures 4.7c 4.7d. In a low-light condition, most of the illumination reaches the camera from directly reflected light - as opposed to dispersed light - making water reflections particularly

acute. Using advanced computer vision methods allowed us to overcome the difficulties of uneven illumination.

4.2.5 Video processing

After acquiring extensive recordings of migrating salmon smolts, I utilised the existing deep learning tracker, uavTracker (<https://github.com/ctorney/uavTracker> Torney et al. (2018b)), to track fish movement. This tracker, an adaptation of SORT Bewley et al. (2016) with a YOLO detector Redmon et al. (2016), demonstrated promising results in drone footage of ungulates. The tracking framework is described in detail in Chapter 3, where it is a baseline for the investigation of our novel approaches (*not* used in this chapter). In order to use our novel Deep Predictor, a large dataset of training data is required which is only resulting from this Chapter’s work, and can be used in subsequent work. I implemented several technical modifications to simplify the training process, annotated video frames, and fine-tuned the detection network to recognize juvenile salmon. I trained the object detector on over 3 thousand annotated frames from the study, and on an unseen test set it achieved a reasonable accuracy of 79% mAP at 0.5 IoU. I adapted the detector to the challenging footage from this experiment, specifically, focusing on the night-time detections that were particularly challenging due to low luminosity, reflections and uneven illumination in near-infrared conditions. For comparison, a day-time only the detector provided an accuracy of 92% mAP - highlighting the challenge of this dataset.

Those accurate detections of fish within the camera’s image plane was used to extract temporal movement information from each fish in each camera’s recording, with technical adaptations to the uavTracker. Images in Figures 4.7c and 4.7d illustrate a high-quality detections from our system even in areas of low-contrast. Based on a qualitative assessment the tracker performs very well, in many cases detecting fish in dark areas before they are visible on the video to a researcher.

Based on real-life measurements of the flume and timestamps for each frame, we converted these tracks to real-life coordinates on a two-dimensional flume plane, disregarding the variations in the fish’s depth positions.

The fish are tracked at the recording frame rate (10 to 20 fps) within the image plane using a bounding box. The position of this bounding box is modelled with a Kalman filter, incorporating the scale and ratio of the rectangle (s and r), its position (c_x, c_y), speed, and acceleration:

$$x = [c_x, c_y, s, r, \dot{c}_x, \dot{c}_y, \ddot{c}_x, \ddot{c}_y]. \quad (4.1)$$

For subsequent analysis, the centre of each rectangle is assumed to represent the fish's position. The speed of movement is calculated at every time step to facilitate frame-wise comparisons. However, this approach is sensitive to location changes caused by the rapidly changing geometry of the bounding box, even for slow-moving fish. To mitigate this, we further filter the position using a constant velocity Kalman filter.

Any observations with an unrealistic movement speed exceeding five (5) body lengths (approximately 80 cm/s) are discarded as they commonly represent artefacts from fish accelerating rapidly and exiting the image frame.

Figure 4.4a shows examples of track traces with data points of the centre of each fish-filtered position.

Smolts prefer dark substrate for their holding position. The choice chamber has been designed to broadly match the brightness of the flume to avoid a fish-holding position inside it. The water outflow grid near the pump inlets provided a preferred location for fish resting (where modifications were not possible), but we nonetheless observed stationary fish in different parts of the flume.

In this study, our focus is on the behaviour of fish during movement, necessitating the exclusion of any non-moving tracks under the assumption that only the movement of other migratory fish will influence the behaviour of fellow migrants.

To exclude stationary fish, we are excluding movements under 5 cm/s, which corresponds to roughly 25% of the flow speed during the experiment. Including stationary tracks in the the analysis would introduce a bias from fish not being part of the migrating group.

4.2.6 Extraction of data for quantitative results

Quantifying fish's choice The flume is divided into two chambers so that fish swimming downstream are forced to choose one of the channels before facing an obstacle. Throughout the experiment, we observe only sporadic upstream movement. Figure 4.3 shows a histogram of swimming directions of all tracks visible at the entry to the choice chamber, showing an overwhelming majority of them are moving with the flow (vector 90 deg). We are excluding those tracks with an average velocity vector against the flow from the analysis.

We can only track single fish as long as it is within a field of vision of one camera, and we cannot re-identify the fish as it approaches the choice chamber again. Hence, every event of tracked fish entering a choice chamber is a pseudo-replicate where we cannot tell if it is a repeated entry of the same fish. We are confident that most of the fish migrate

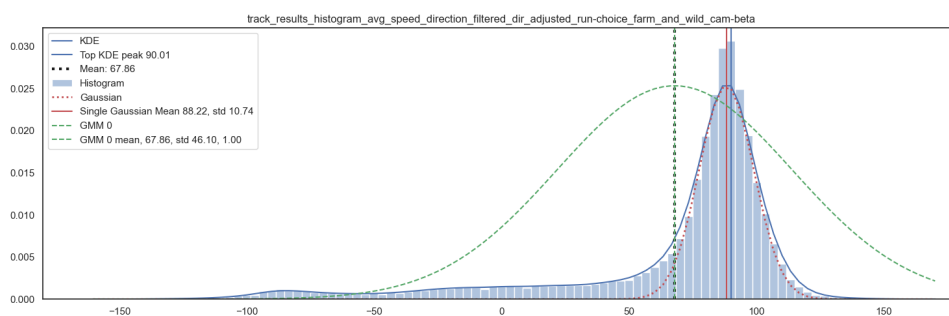


Figure 4.3: Histogram of swimming direction of all moving tracks in the choice chamber experiment. No significant peak exists for -90 deg - upstream direction. This confirms the validity of the experiment for studying migratory behaviour. For the analysis itself, we are only accounting for tracks with direction downstream to exclude any exploratory behaviour.

as we have observed the entire cohort travelling in front of the camera at the same time for most of the trials.

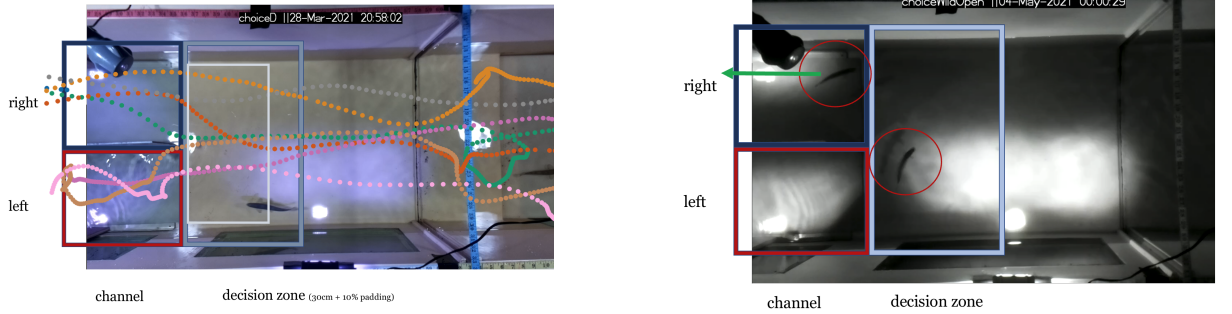
To quantify fish decisions, we define criteria for each track based on the the direction of travel and the sequence of defined areas visited.

We define an area of the entire tank width of 30 cm before the channels split as *decision area*. To allow for inaccuracies of projecting fish position to two dimensions, we are adding a 10% padding to the decision area, and similarly, we define the left and right channels of the choice chamber. Figure 4.4a shows the defined areas and examples of data points from some of the tracked fish

A track is considered to have successfully navigated the choice chamber, a **successful crossing**, if it is first registered in the decision zone and exits the frame through one of the channels, thus preventing the double counting of low-quality tracks. An exit through a given channel is recorded if we observe the fish in its area in the last second before the track disappears. This makes it a binary choice of either successfully crossing through the right channel or the left.

This means that we do not discard a data point if a fish enters one channel and later exits it to ultimately choose another. As long as the mean direction of movement of the track is downstream, we permit fish to hesitate or reconsider their decision, counting only the final choice.

Measuring group effect The most likely social effect to be observed between any two fish would be when one is following another. We will quantify this effect of one fish influencing the behaviour of another by swimming ahead of it during the crucial moment



(a) Daytime image of a fish approaching choice chamber. The fish is in the decision zone (a 30cm section ahead of the choice chamber with added padding) from which it either exits the image frame through a right or left channel of the chamber. The coloured lines overlapping the image show examples of five different track traces to illustrate a variety of tracked movement that is reduced to one behavioural decision.

(b) Nighttime recording of a fish entering the choice chamber and another fish already past the decision point. We count the number of fish that are present in the chamber channels ahead as influences for the fish in the decision zone.

Figure 4.4: Images from camera β of the approach and entry to the choice chamber illustrating our analysis of a collective aspect of decision-making.

of choosing a channel.

In order to quantify the influence of other fish for each successful crossing, we define the following:

- Entry time t_e - when a fish track is first registered in the decision zone.
- Decision time t_d - when, for the last time, fish enters the chosen chamber.
- End time t_x - when the fish exits the scene through one of the chambers.
- Decision period $\lambda_d \in (t_e, t_d)$ after the fish entered the decision zone and before it started successful crossing.

We define the number of social influences on the fish's successful crossing as

$$n_{infl} = n_{\text{right channel}}(\lambda_d) - n_{\text{left channel}}(\lambda_d), \quad (4.2)$$

where number of $n_{\text{channel}}(\lambda_d)$ is a number of fish making their own successful crossing during the period λ_d .

Additionally, we define a stricter criterion, the number of close influences on the fish’s successful crossing as

$$n_{infl}^c = n_{\text{right channel}}(t_d) - n_{\text{left channel}}(t_d), \quad (4.3)$$

where number of $n_{\text{channel}}(t_d)$ is a number of fish making their own successful crossing at the precise moment of the fish’s decision t_d .

Figure 4.4 illustrates examples of fish close to a decision time with another influencing its choice towards the right channel. The number of n_{infl} is negative when there are more fish ahead in the left-hand side channel.

4.2.7 Trials

As detailed in Table 4.2, we utilized two different batches of fish for this experiment: one farmed (“farmed”) and one wild (“wild”). The fish were left in the flume for extended periods (over 14 hours) throughout the night, during which they were recorded with IR ceiling-mounted cameras.

Every recorded group of fish was unique and naive to the flume. We excluded the first 20 minutes of each recording to allow for acclimatisation, based on our previous work on the flow response of individual fish, which showed that most smolts settle down within approximately 5 minutes.

We conducted a total of eight overnight trials with unique cohorts of ten fish each. Table 4.2 presents a summary of the flow for each trial, indicating significant variability in flow across trials of the same scenario (e.g., D and E), despite maintaining identical configurations.

4.3 Modelling framework

4.3.1 Model Formulation

We aim to understand the factors influencing the decision to choose a channel. We identify three qualitatively different scenarios: the left-hand side channel open with the right obstructed (Left Open), the right-hand channel open with the left obstructed (Right Open), and both channels open (BothOpen). In all scenarios, we model the probability of fish choosing the right channel $P(Y = \text{right_channel})$, which may vary based on the experimental scenario, the number of fish followed, and the fish’s origin. Drawing in Figure 4.2a

trial	fish type	scenario (open channel)	left cm/s	right cm/s	difference cm/s (side)
A	Farm	both	21	18	3 (left)
B	Wild	both	22	20	2 (left)
C	Wild	left	21	14	7 (left)
D	Farm	left	26	18	8 (left)
E	Farm	left	27	9	18 (left)
F	Wild	right	11	25	14 (right)
G	Farm	right	10	18	8 (right)
H	Farm	right	6	26	20 (right)

Table 4.2: Values of flow for different experiments with farmed and wild fish, measured using movement under camera observation. Each entry is uniquely named and indicates whether the left, right, or both channels were open. Notably, the left channel exhibited relatively quicker flow, despite being on the inner side, highlighting the issue of high variability and turbulence within the flume. We are **not** using actual values of flow in our model but are treating each scenario as a categorical variable for a mixed-effect model. We compared the value of flow in an unhindered movement experiment measured with a flow meter (20.4 ± 9.81 cm/s) to camera-based measurements (18.1 ± 8.78 cm/s), finding no significant difference. The flow differential between different obstructed channel scenarios C, D and G fall below the threshold established in the Chapter 2 for stationary flow response. We validate the final results by repeating analysis with those samples in Section 4.4.3.1.

illustrates the basic concept of the experiment of choice in the presence of other migrants.

We model the probability of choosing the right-hand channel $P(Y = \text{right_channel})$ as a logistic regression:

$$P(Y = \text{right_channel}) = \frac{1}{1 + e^{-z}}, \quad (4.4)$$

where z is the vector of k independent variables X_1, \dots, X_k and their coefficients β_1, \dots, β_k , plus an intercept β_0 :

$$z = \beta_0 + \beta_1 X_1 + \dots + \beta_k X_k. \quad (4.5)$$

An intuitive approach to this modelling is to rearrange the equation and expressing the logarithm of the odds ratio as vector z :

$$\ln \left(\frac{P(Y = \text{right_channel})}{1 - P(Y = \text{right_channel})} \right) = \beta_0 + \beta_1 X_1 + \dots + \beta_k X_k. \quad (4.6)$$

Alternatively, we formulate some of the variables as factorial variables, for instance, X_1 in the previous equation can be seen as having three independent categorical values A, B and C , resulting in formulation

$$\ln\left(\frac{P(Y = \text{right_channel})}{1 - P(Y = \text{right_channel})}\right) = \beta_0 + \beta_{1A}X_{1A} + \beta_{1B}X_{1B} + \beta_{1C}X_{1C} + \dots + \beta_k X_k \quad (4.7)$$

where each level of variable X_1 is modelled independently.

4.3.2 Covariates

The covariates considered to explain channel choice are presented in Table 4.3. The variation of the experiment τ_{exp} depends on which channel of the chamber is non-constricted. We encode it with one-unit symmetrical values so that the neutral scenario, when both channels are open, is coded as 0, and the coefficient of this covariate would be ignored. The origin of fish τ_{fish} is also encoded as a unit value, with farmed fish acting as the baseline. This is a natural choice, given the larger data set for farmed fish.

We consider two variables that capture potential social behaviour: n_{infl} and n_{infl}^c . Because they are related (the latter being a subset of the former), we test all models with either variable and select whichever provides a better explanation of the data (Figure 4.5). This formulation of social influence allows us to study the effect at only two discrete thresholds, as described in Section 4.2.6, enhancing the robustness of the interpretation and simplifying the analysis of fish tracks. Negative values of n_{infl} indicate that the fish is being influenced towards the left channel and positive values towards the right-hand side. A fish is not socially influenced when $n_{infl} = 0$, aligning the interpretation of this variable with τ_{exp} .

4.3.2.1 Consideration of random effects

We expect some variability between different trials that cannot be attributed to fixed effects. Random effect from id_{run} can be incorporated into logistic regression model by extending vector $z_{random_effect} = z + u_{id_{run}}$, where $u_{id_{run}} \sim \mathcal{N}(0, \sigma_{id_{run}}^2)$. Using such mixed-effect modelling provides a better fit to data, however, makes interpretation of the model somehow difficult because the combination of other variables (fish type and scenario in table 4.2 are unique for all but two out of eight trails id_{run} . For that reason, we are not considering any random effects in our modelling.

Variable	Description	Type
τ_{exp}	Variation of experiment	LeftOpen BothOpen RightOpen encoded: -1 0 1 (or as factorial)
τ_{fish}	Smolt origin	farmed wild, encoded 0 1 (or as factorial)
n_{infl}	Number of fish influencing decision towards the right-hand side channel	quantitative, integer
n_{infl}^c	Number of fish influencing decision towards the right-hand side channel at the moment t_d	quantitative, integer

Table 4.3: Description of covariates used for statistical modelling.

4.3.3 Model selection

The likelihood L represents the probability of the observed data given specific model parameters. Once a model is fitted with parameters $\theta = \{\beta_0, \beta_1, \dots, \beta_k\}$, we can calculate L to assess the closeness of fit to a set of N observations $\{y_i\}$:

$$L(\theta; y) = \prod_{i=1}^N f(y_i; \theta). \quad (4.8)$$

For computational convenience, we use the natural logarithm of the likelihood, Log-Likelihood LL:

$$LL = \ln(L). \quad (4.9)$$

As LL is negative, higher values of LL indicate a better fit to the data. However, LL does not account for the model's complexity, which can lead to overfitting and a loss of explanatory power. The goodness of fit can be adjusted using the Akaike Information Criterion (AIC), which includes the number of model parameters k :

$$AIC = 2k - 2 \ln(L) = 2k - 2LL, \quad (4.10)$$

and further, the penalty can be scaled by the dataset size N with the Bayesian Information Criterion (BIC):

$$BIC = \ln(N)k - 2LL. \quad (4.11)$$

Lower AIC and BIC scores indicate a better fit to the data while adjusting for model complexity (number of parameters).

We are evaluating all viable logistic regression models with combinations of covariates and their interactions with two variants of influence variable and use of factorial variables. Figure 4.5 shows that using n_{infl}^c provides generally better fit of the non-factorial models than n_{infl} , however for some models it results in worse performance (prominent outliers). Instead, using factorial formulation for the variables τ_{exp} provides no significant change to models fit with either choice of influence variable, while providing easier interpretability. Because τ_{fish} is a two-level factorial, coding of this variable is identical for factorial and non-factorial method. As reported in table 4.6, using close influence increases number of non-influenced fish only slightly, while providing a more reliable definition of social interaction - since the observed distance between fish has to be smaller.

We find general agreement between different modelling approaches and for the final analysis we are choosing factorial variables and numerical n_{infl}^c .

Table 4.4 presents the results of fitting of different complexity models with a subset of all available covariates using factorial formulation and n_{infl}^c . When including categorical ranked covariates, there is a compelling argument for adhering to the principle of marginality. The inclusion of interactions of any variables without the baseline of each variable itself could result in misleading coefficients, capturing the relative effects of subgroups with an arbitrary baseline as an explanation of the dependent variable.

Table 4.4 presents all fitted models sorted by log-likelihood, with values of all scores divided by 1000 and rounded for clarity. The model fit improves consistently with the inclusion of additional interactions, with the most complex model X (containing 3-way interaction) performing best on every measure (though not considerably). Figure 4.5 visualises the BIC scores, highlighting that excluding n_{infl}^c significantly reduces the model's explanatory power, increasing the BIC score from under 20 for models that include n_{infl} to over 21 for those that do not.

4.4 Results

4.4.1 Observations

We observed fish traveling both as individuals and as part of groups in all study trials, exhibiting both active and passive swimming behaviours. Figure 4.7d depicts a fish travelling head-first—an active traversal through the obstacle in the “obstructed” channel of

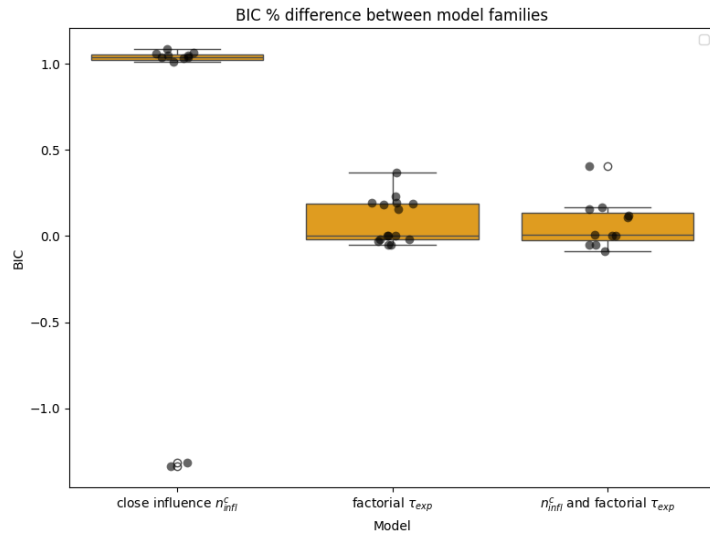


Figure 4.5: Percentage change in Bayesian Information Criterion (BIC) score for different models using n_{infl}^c instead n_{infl} as the influence variable and using factorial formulation for τ_{exp} . The box plot shows the median value for all models in the group with the quantile ranges.

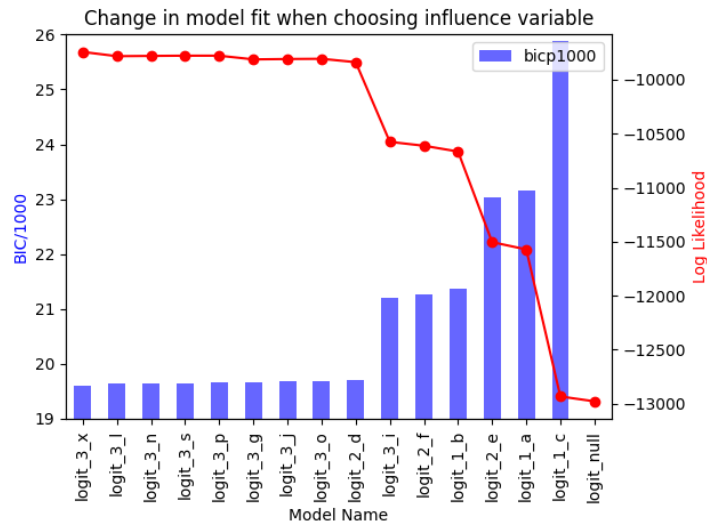


Figure 4.6: Bayesian Information Criterion (BIC) score for different models, scaled by 1000 for readability as blue bars shows all models including n_{infl}^c with close high score, with the most complex model x giving the lowest BIC score of 19.61. The red line shows the values of Log Likelihood that agree with the more complex BIC measurement and allow to compare with the null (intercept only) model.

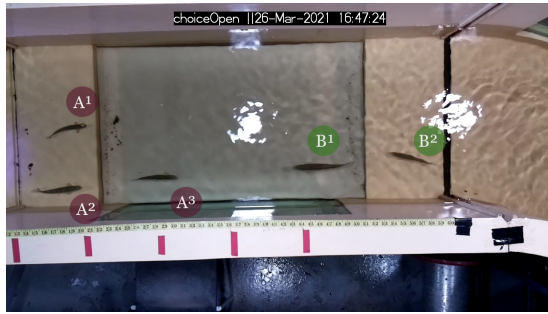
the choice chamber. The fish is tracked in the infrared recording with a bounding box. As is often the case, the fast-moving fish appears blurred due to unfavourable lighting

Model name	coefficients	LL	BIC	AIC
logit_3_x	$n_{infl}^c, \tau_{exp}, \tau_{fish}, \tau_{fish} \times$ $n_{infl}^c, \tau_{exp} \times \tau_{fish}, \tau_{exp} \times$ $n_{infl}^c, \tau_{exp} \times \tau_{fish} \times n_{infl}^c$	-9.74	19.61	19.51
logit_3_p	$n_{infl}^c, \tau_{exp}, \tau_{fish}, \tau_{fish} \times$ $n_{infl}^c, \tau_{exp} \times \tau_{fish}, \tau_{exp} \times n_{infl}^c$	-9.78	19.65	19.58
logit_3_s	$n_{infl}^c, \tau_{exp}, \tau_{fish}, \tau_{exp} \times \tau_{fish},$ $\tau_{exp} \times n_{infl}^c$	-9.78	19.65	19.57
logit_3_n	$n_{infl}^c, \tau_{exp}, \tau_{fish}, \tau_{fish} \times$ $n_{infl}^c, \tau_{exp} \times \tau_{fish}$	-9.78	19.64	19.58
logit_3_l	$n_{infl}^c, \tau_{exp}, \tau_{fish}, \tau_{exp} \times \tau_{fish}$	-9.78	19.63	19.58
logit_3_o	$n_{infl}^c, \tau_{exp}, \tau_{fish}, \tau_{exp} \times n_{infl}^c$	-9.81	19.68	19.63
logit_3_j	$n_{infl}^c, \tau_{exp}, \tau_{fish}, \tau_{fish} \times n_{infl}^c$	-9.81	19.68	19.63
logit_3_g	$n_{infl}^c, \tau_{exp}, \tau_{fish}$	-9.81	19.67	19.63
logit_2_d	n_{infl}^c, τ_{exp}	-9.84	19.72	19.68
logit_3_i	$\tau_{exp}, \tau_{fish}, \tau_{exp} \times \tau_{fish}$	-10.58	21.21	21.16
logit_2_f	τ_{exp}, τ_{fish}	-10.61	21.26	21.23
logit_1_b	τ_{exp}	-10.66	21.36	21.34
logit_2_e	n_{infl}^c, τ_{fish}	-11.50	23.04	23.01
logit_1_a	n_{infl}^c	-11.57	23.16	23.15
logit_1_c	τ_{fish}	-12.93	25.89	25.87
logit_null		-12.98	-	-

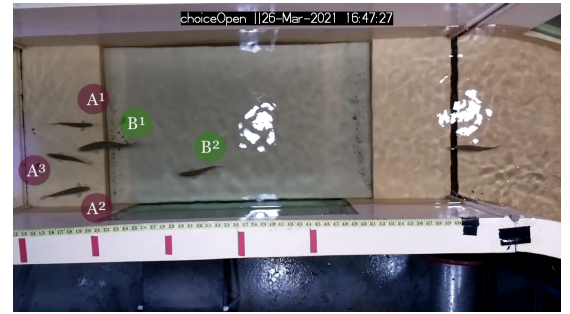
Table 4.4: Comparison of fit of Generalised Linear Models. We are using logistic regression to model how likely the fish is to choose the right-hand side channel. Both comparison using AIC and BIC, and overall The log-likelihood score shows that complex models with interactions are providing a better explanation. Overall the best fit is achieved by model X . “Logit null” represents the basic logit model with intercept only , serving as a baseline for comparison.

conditions affecting camera exposure time. In the infrared image shown in Figure 4.7c, fish are observed moving as a group with the flow direction but passively, using flow to drift tail-first and correct their direction and position in the group with gentle movements. A variety of movement patterns were observed both during the day and night, yet no clear temporal regularity was discerned.

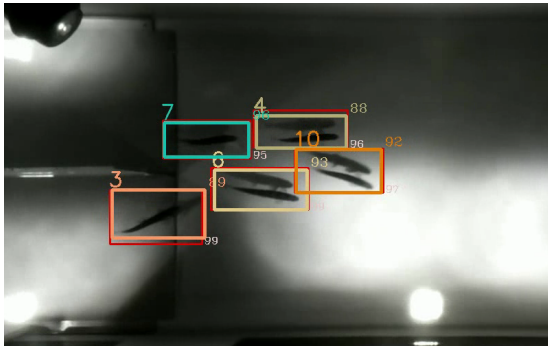
Presented in Figures 4.7a and 4.7b, we notice group formation where actively swimming fish pass over a slower-moving, passively swimming, or holding group. As fish are not observed in most of the flume area, it is impossible to determine how frequently group composition changes or even if the same group of fish is seen twice in front of the camera. However, our further analysis does not rely on such assumptions.



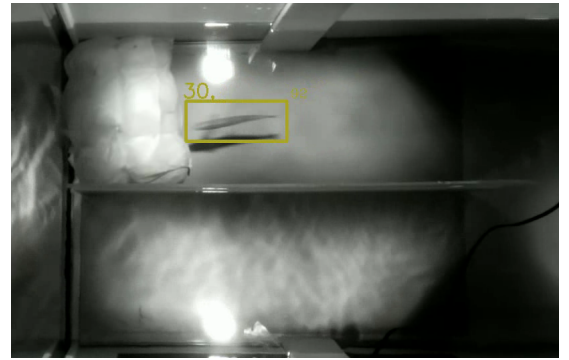
(a) Farmed fish in group A are holding or slowly passively migrating downstream while approaching group B, which is swimming actively. View from day-time observation by camera α .



(b) Continuation of group formation from (a), fish A^3 joins group B, turning and beginning swimming actively.



(c) A group of five wild smolts tracked by our tracker is swimming passively and approaching an entry to the choice chamber. View from camera β used for quantitative analysis in this study in infrared-only illumination.



(d) A single farmed fish, with a bounding box from the computer vision tracker is seen on camera γ swimming actively through the obstacle in the right-hand side channel of the choice chamber.

Figure 4.7: Illustration of different observations of group movement in the experiment with a choice chamber.

4.4.2 Frequency analysis of channel choices

For each trial, we identify the number of times and the proportion of individuals choosing either the left or right channel. Table 4.5 presents choices made by each tracked fish when traversing the choice chambers for each variant of the experiment and type of fish (“wild” and “farmed”). When both channels are open (unhindered movement), the right channel is preferred even though the flow differential can not explain that choice. This channel is on the outside of the flume with counter-clockwise flow, so the preference might be dictated by how one-directional the flume is.

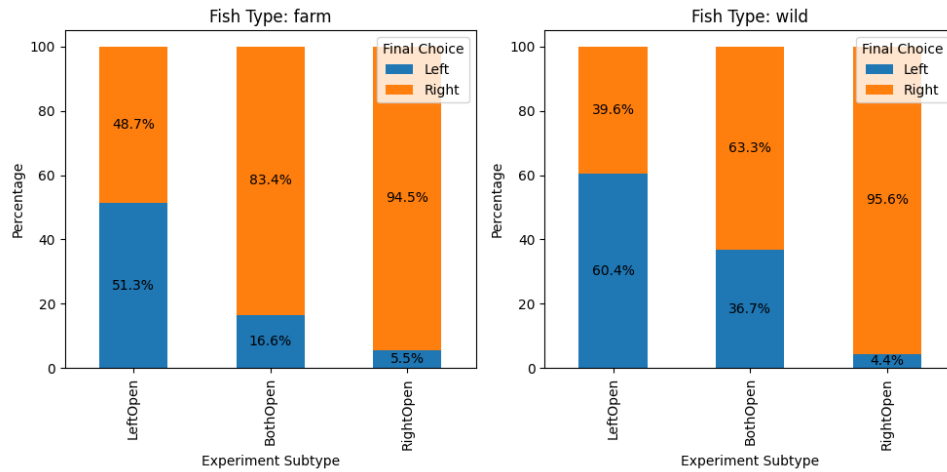


Figure 4.8: Number of choices of each channel for (a) wild and (b) farm fish in different variations of the experiment. The preference towards the right channel is apparent as well as the better ability of wild smolts to find faster moving flow, when farmed fish seem to rely more on the bias towards one side of the channel.

Variant	Channel	Wild		Farm		All	
		count	perc	count	perc	count	perc
BothOpen	left	533	36.70	279	16.60	812	25.90
BothOpen	right	920	63.30	1404	83.40	2324	74.10
LeftOpen	left	195	60.40	5412	51.30	5607	51.50
LeftOpen	right	128	39.60	5143	48.70	5271	48.50
RightOpen	left	56	4.40	286	5.50	342	5.30
RightOpen	right	1215	95.60	4879	94.50	6094	94.70
Right and Left	correct	-	88.50	-	65.50	-	67.60

Table 4.5: Choices made by each tracked fish when traversing the choice chambers for each variant of the experiment and type of fish (“wild” and “farmed”). The count provides the number of unique crossings, while the percentage value is calculated in relation to all the crossings in this scenario. When both channels are open (unhindered movement), the right channel is preferred. When presented with an obstructed channel, wild fish were much more likely to choose the better channel (88.5% to 65.5%). Overall we observed farmed fish crossings more often (total of 17403 observations to 3047 of wild fish), despite corresponding to less than twice the amount of trials.

Aggregating all crossings of the choice chamber in figure 4.8, we see a clear bias towards the right-hand side channel and differences in behaviour of fish depending on their origin. Table 4.5 shows that wild fish crosses the open channel when the other is restricted 85.5% of time while for farmed fish, it is only 65.5%. For wild fish, the number of observations is

considerably lower when the left channel is open ($N = 323$) compared to the right channel open ($N = 1271$) or both sides open ($N = 1453$). This suggests fish are less likely to migrate when their preferred route (the right channel) is unavailable.

For farmed fish, observations are lower when the right channel is open ($N = 5165$), roughly half the number observed when the left channel is open ($N = 10555$), and 50% higher per trial when both sides are open ($N = 1683$, one trial). This suggests differences in fish movement decisions; however, the experimental design does not permit a more detailed analysis of this phenomenon.

τ_{fish}	n_{infl}	zero ratio	n_{infl}^c	zero ratio
wild		0.50		0.58
farm		0.54		0.64
total		0.54		0.63

Table 4.6: Ratio of observed choice chamber decisions that were not influenced by any fish, according to two definitions of influence. Overall, wild fish are less likely to approach the chamber alone.

Fish were commonly observed travelling in groups, and the ratio of fish that were *not* influenced was a little over 50%. Table 4.6 shows the ratio of fish that were making a decision without any fish in the chamber ahead, according to two definitions of n_{infl} and n_{infl}^c . There were no stark differences in number of influences between types of fish and this effect is analysed in detailed using the statistical modelling.

4.4.3 Model interpretation

The best-performing model is the one containing all interaction terms. In table 4.7 we present model coefficients with their confidence intervals, p-values and z-scores. Coefficient of the intercept β_0 of the model has value 1.47 with a high z-score (21.08) indicating that fish have a bias towards choosing the right-hand side channel in all cases. That bias is smaller for wild fish with a comparatively small effect of type of fish τ_{fish} ($\beta = -0.89$, $Z = -9.68$), where $\tau_{fish} = 1$ for the wild fish. The odds ratio for farm fish to choose right hand side channel is 4.34 while for wild fish it is less than half of that with 1.78.

All fish respond to the opening of the left channel with covariate τ_{exp_LO} having a large negative coefficient ($\beta = -1.60$, $Z = -21.98$), resulting in 5 fold decrease in probability of fish choosing right-hand side channel. Likewise, τ_{exp_RO} ($\beta = 1.01$, $Z = 10.76$) indicates increased bias towards the other open channel as well.

There is a clear effect of social influence on the fish decision with the number of influences n_{infl} increasing the chances of choosing a channel with other fish with 6.98 times increase for each additional fish in it ($\beta = 1.94, Z = 11.07$). This covariate's effect decreases 39% for wild fish $n_{infl}^c : \tau_{fish}$ ($\beta = -0.94, Z = -4.91$), resulting in a 2.7 fold increase in the choice of a channel for each wild fish influencing it. This decrease of social effect is the baseline for the neutral case of both channels open, as the further interactions clarify the difference in the mechanism of this effect for different fish type. The effect of influence on farm fish decreases for both cases of obstructed channel $n_{infl}^c : \tau_{exp_LO}$ ($\beta = -0.98, Z = -5.49$) and $n_{infl}^c : \tau_{exp_RO}$ ($\beta = -0.92, Z = -4.45$), while for wild fish it decreases in the neutral case $n_{infl}^c : \tau_{fish}$ ($\beta = -0.94, Z = -4.91$). Meanwhile, the highest overall effect is for interactions $n_{infl}^c : \tau_{exp_LO} : \tau_{fish}$ ($\beta = 2.52, Z = 12.46$) and $n_{infl}^c : \tau_{exp_RO} : \tau_{fish}$ ($\beta = 2.36, Z = 10.56$) meaning that the wild fish responds strongly to close influence when channels are obstructed.

Interaction plot 4.9 shows that overall wild fish are slightly better at making the correct decisions while the social effect and response to the flow difference are more pronounced in the cases when one of the channels is obstructed.

Variable	Coefficient	Odds ratio	z-score	P-value	CI Lower	CI Upper
τ_{exp_LO}	-1.60	0.20	-21.98	0.00	-1.74	-1.45
β_0	1.47	4.34	21.08	0.00	1.33	1.60
n_{infl}^c	1.94	6.98	11.07	0.00	1.60	2.29
τ_{exp_RO}	1.01	2.76	10.76	0.00	0.83	1.20
τ_{fish}	-0.89	0.41	-9.68	0.00	-1.07	-0.71
$\tau_{exp_RO} : \tau_{fish}$	1.23	3.42	6.70	0.00	0.87	1.59
$n_{infl}^c : \tau_{exp_LO} : \tau_{fish}$	2.52	12.46	5.75	0.00	1.66	3.38
$n_{infl}^c : \tau_{exp_RO} : \tau_{fish}$	2.36	10.56	5.59	0.00	1.53	3.18
$n_{infl}^c : \tau_{exp_LO}$	-0.98	0.37	-5.49	0.00	-1.33	-0.63
$n_{infl}^c : \tau_{fish}$	-0.94	0.39	-4.91	0.00	-1.31	-0.56
$n_{infl}^c : \tau_{exp_RO}$	-0.92	0.40	-4.45	0.00	-1.33	-0.52
$\tau_{exp_LO} : \tau_{fish}$	0.61	1.84	3.77	0.00	0.29	0.92

Table 4.7: Logistic Regression Coefficients Ordered by Z-value. TODO

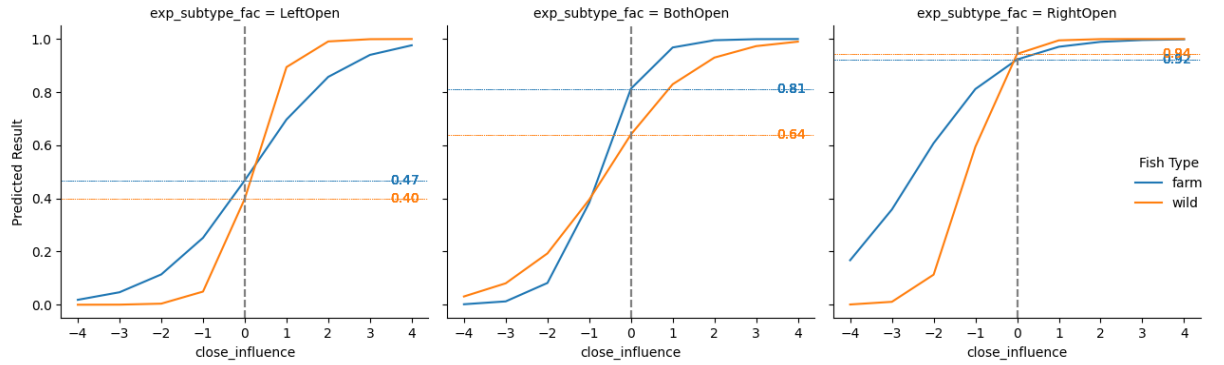


Figure 4.9: Interaction plot showing the best performing model $logit_3_x$ in three experimental scenarios τ_{exp} for a range of influences for τ_{fish} wild (blue) and farmed (orange) fish. The model predicts the probability of fish choosing the right-hand side channel. The number of influences n_{infl}^c is negative when fish influencing individual decisions is in the left-hand side channel, and positive if influencing fish is in the right. The model shows that wild fish are more responsive to the flow difference with collective decision-making reinforcing correct choices.

4.4.3.1 Comparison without trails with low-flow differential

We repeated modelling on the subset of trails, excluding C, D and E where measured flow difference (Table 4.2) fell below the threshold established in the Chapter 2 (8.9 cm/s) for stationary flow response. The best model x containing 3-way interactions cannot be fitted due to lack of data points from excluded trail C that is for wild fish with left channel open. Instead, we analyse the most complex factorial model o (with covariates n_{infl}^c , τ_{exp} , τ_{fish} , $\tau_{exp} \times n_{infl}^c$) finding agreement with the model fitted to all trials. The model shows a bias towards right hand-side with intercept $\beta_0 = 1.42$, effect of channel closure on the left τ_{exp_RO} ($\beta = -2.33$) and right τ_{exp_LO} ($\beta = 2.05$), and overall effect of close influence n_{infl}^c ($\beta = 1.20$). As with the model build on full dataset, the bias of wild fish is smaller with covariate's τ_{fish} coefficient $\beta = -0.79$, and the effect of influence decreasing for both cases of obstructed channel $n_{infl}^c : \tau_{exp_LO}$ ($\beta = -0.53$) and $n_{infl}^c : \tau_{exp_RO}$ ($\beta = -0.46$).

4.5 Discussion

We have observed fish of both wild and farmed origin exhibiting clear downstream movement indicative of migratory behaviour characteristic for their smolt phase of life.

Both origins of fish have exhibited a clear four-fold (odds ratio 4.34) bias towards the outside channel of the flume, with important differences between them (Figure 4.8). There

were four times fewer crossings observed for wild fish when the preferred, right-hand side channel was obstructed. However, when wild fish were migrating the bias towards right-hand side channel was 0.41 times smaller than for the farmed fish. This suggests that wild fish choose to migrate less when environmental conditions are unfavourable, just as when to start the migration they require an increased flow discharge in the river.

When wild fish do travel, they are better at finding a preferred route than farmed fish, with success rates of 88.5% compared to 65.5% for farmed fish (Table 4.5). This effect is confirmed in the modelling when other interactions are accounted for and illustrated with an interaction plot in Figure 4.9 This can be explained by the difference in the life history where farmed fish were never previously faced with complex navigation problems. This also implies that those navigation skills are not just inherent to the species.

We observed a significant social effect on the decision-making of salmon smolts. It was twice as strong for farmed fish in the neutral scenario when both channels were open, but more pronounced for wild fish in cases where one of the channels was obstructed (Table 4.7. This finding strongly suggests that unlike the earlier part of life when salmon parr are territorial, once they start the migration, smolts do not only “tolerate” the presence of other co-specifics but actively rely on them for their migration success.

In general, the farmed fish rely on following other fish but were less successful in finding the correct channel. Without inherent skill in navigation, it makes sense that fish of this origin rely on the shoal. This difference suggest that farmed fish are not a perfect proxy for the overall behaviour of the wild salmon. On the other hand, the difference in behaviour if well understood, can aid the study of specific phenomena. In a more challenging situation wild fish seem to relay on shoaling more, so for instance, design of fish passes can be done with a farmed fish model. That would be equivalent to modelling the worst-case scenario of a least-informed shoal. It is believed that individual heterogeneity is an important aspect of collective decision-making (Jolles et al., 2020), hence further comparison of homogeneous farmed fish with wild smolts might provide further insights into this mechanism. Further studies with wild fish originating in different environments could provide an insight on inter-population differences.

This study is unique in that it attempts to study the longitudinal behaviour of migration in a laboratory setting. Due to the size and hydraulic of the artificial flume, fine grain control of flow conditions was not possible and laminar flow was unachievable. The shape of the tank introduced a bias into the swimming patterns with considerable preference for the outside of the tank at the place of the experiment. We believe that those problems were sufficiently addressed with a modelling design that accounted for the biases. In prin-

ciple, precise measurements of flow could have been more informative, but would require a larger sample to distinguish a reliable measure of the effect as in my work in Chapter 2.

An observational study over a longer time period could tell us more about daily migration patterns, but it would be challenging to care for animals that would have to be supervised and cared for remotely.

The movement behaviour of fish in a group may change with the group size. Group size influences the kinematics (distance and direction) of response to predator attack in a study of coral reef fish, where groups of four, eight, and sixteen fish were compared (Bacchus et al., 2024). In our study, a group of ten fish might be smaller than the shoals occurring naturally in the wild, but our preliminary observations showed that with the width of choice-chamber channels, fish were already crowding on the approach. It would be interesting to quantify those social effects, but with increases in group sizes, the difficulty of conducting the study increases.

The simple choice chamber design we have used provided a good balance between the presence of an obstacle but didn't introduce a complete impediment to movement. Initially, we attempted to maximise the difference by completely blocking one side of the chamber. However, this approach led to two issues. Firstly, the dead-end channel became a perfect holding location for some fish, resulting in aggregations and making it an unsuitable location to study social effects. Secondly, if a member of a migrating group misses the entrance to the correct channel, it could not rejoin the group before it could find the way out of the dead-end which hindered the group formation. It would be preferable to observe how smolts behave on their first passage through the flume before they have the opportunity to learn any of its structure. In that case, however, it would be likely that, at first, most of the fish would pass the obstacle on their own, as that is the most commonly observed behaviour, making cases of group movement too sparse to quantify. The most feasible alternative would be deployment of cameras directly near the fish pass for longitudinal observation.

Killen et al. (2017) describes the role of physiological traits in between and within group organisation of shoaling fish. Understanding the role of leadership and social hierarchy could be possible if individual fish could be identified on camera. With farmed fish, we have investigated the use of visual markings with coloured beads or elastomer tagging, neither of which could be identified reliably on camera, even in good lighting. Without any tagging of fish, their visual similarity is too high even for the use of the most advanced deep-learning method designed to use individual appearance for that task. The PIT tags were not feasible for us due to a maximal sampling rate of 1Hz, way below the accuracy

of visual tracking.

Work of [Vowles et al. \(2014\)](#) showed avoidance of suboptimal channel of a choice chamber (with an excessively high flow) differs between day and night conditions, confirming smolts reliance on visual cues when navigating fish passes ([Haro et al., 1998](#)). Especially during the night, we observed smolts moving with the flow direction but passively, drifting tail-first. A variety of movement patterns were observed both during the day and night, yet no clear temporal regularity was discerned. Automated classification of fish orientation detection is possible and would allow us to better understand migration time patterns and swimming style. Unlike other fish that are schooling to minimise their energy expenditure on swimming against their ability to feed ([Killen et al., 2011](#); [Zhang and Lauder, 2023](#)), Juvenile salmon do not feed during their migration [McCormick et al. \(1998\)](#), and if swimming passively, likely not to gain the energetic advantage of being in a group. This implies that the benefit of schooling is limited to decision-making and overwhelming predators at synchronised passage of high-risk areas.

As shoaling helps with survival against predators, it may prove maladaptive in cases of entrapment ([Thambithurai et al., 2018](#)). Many anthropogenic obstacles on migration routes can be seen as forms of traps, and if smolts travel in larger groups, their effects might be more pronounced. Indeed, [Lemasson et al. \(2014\)](#) shows evidence from flume experimentation on juvenile palmetto bass, that actively swimming fish might be more likely to be exposed to difficult flow conditions at a downstream barrier when parts of a larger group than as individuals.

The implications of that study are important to the conservation effort, highlighting the inadequacy of considering individual fish only in the design of river infrastructure. Previous studies have shown limitations of using euthanised farmed smolts to study damage due to passage through a popular screw turbine ([Brackley et al., 2018](#)). If, as expected, fish are more likely to approach navigational obstacles as a group, the additional damage due to crowding might be underestimated.

If the group navigation plays an important role in smolts migration, then the decrease in stock in their rivers might have a non-linear relationship to the survival of following generations, making it an important factor in the modelling of the population dynamics.

Finally, a more detailed analysis of movement will be possible with use of the novel visual tracking method Deep Beast Predictor presented in Chapter 3. The data gathered during this experimentation includes validated tracks of multiple fish in variety of circumstances and can bootstrap further work on visual tracking groups of fish in the laboratory and in the wild.

Chapter 5

Individual-based modelling of salmon downstream migration using Approximate Bayesian Computation

The content of this chapter has been written solely by Mikolaj Kundegorski on the experiments and analysis performed by the author. Colin J. Torney and Jennifer R. Gaskell contributed to the experimental design, conceptualisation and revision of the chapter.

5.1 Introduction

In recent years, advances in fish telemetry allowed detailed study of new marine and freshwater ecosystems. To understand the riverine migration of Salmon on a scale exceeding single-point direct observation, the standard approach uses telemetry tags that report an animal presence in proximity to sparsely deployed river receivers. However, this is limited by low positional accuracy, high levels of noise, and biases, often on scales exceeding the observed signal.

The number of fish tagged is also very limited compared to the overall size of the migrating population. Therefore, underlying behavioural processes are impossible to quantify by modelling observed data alone with standard methods. The focus of this thesis, collective decision-making, is one of such fine-scale behavioural responses that are difficult to capture.

In this chapter, I present a likelihood-free method of Approximate Bayesian Computing (ABC) that can be used to test the hypothesis of more complex movement. It is a fast simulation-based method highly parallelisable on a Graphical Processing Unit (GPU). I

test the validity of the method on simulated telemetry data and show the possibility of extracting movement parameters, survival information and detector range from real river data of downstream salmon migration. I also investigate the possibility of quantifying the social interaction between co-specifics as an example of fine-scale behaviour that can be quantified with such an individual-based modelling approach.

5.1.1 Telemetry

Acoustic telemetry has been credited with uncovering long-term migration patterns, space use and habitat selection, as well as predator-prey interactions in aquatic environments (Matley et al., 2022).

The miniaturisation of acoustic telemetry tags allows us to study the migration of juvenile smolts without excessive increase in their mortality due to tag burden (Lothian et al., 2024b).

Technological improvements in acoustic telemetry allow detailed tracking of position - with sub-meter accuracy (Jacoby and Piper, 2023) - however practical challenges abound making it still mostly a presence-absence type of data.

As the water flow increases rapidly in Spring, salmon smolts begin their migration that lasts about one or two weeks, depending on the complexity and length of the river system. The acoustic receivers are placed in water, weeks in advance, in places that provide sufficient coverage but are also accessible and secure. In practice, some receivers will be completely lost due to a cut anchor, and currents will displace others to the less optimal parts of the river. The detection range of a receiving station can reach over a hundred meters, but in practice can be much smaller and difficult to test due to changing conditions.

Salmon traps are deployed in the higher parts of the rivers, where a number of fish are caught, tagged, and released every day. Though the direct tag-induced mortality is low, it varies widely, and the sample of migrants is effectively very low compared to the amount of fish that travel through that area every day. Acoustic tags implanted under fish scales are sending a digital ping ever 30-60 seconds at 69kHz, but transmission is prone to noise interference from turbulent water, boat engines and hydroacoustic plants. The very condition preferred by smolts, the high flow, is usually when detection quality deteriorates. Detections additionally vary on the position of the fish in relation to the receiver, occlusions and reflection of the acoustic signal from the river bed. Collisions between pings from different fish are a problem exaggerated by restricted access to raw data from the receiver stations and the seeming lack of error-correcting codes used by

manufacturers for transmission.

Unlike terrestrial telemetry, where the precise GPS location of the animal is regularly registered, underwater telemetry provides sparse registrations with no additional location information. Lack of detections are likely even if a tracked animal has appeared in proximity of a receiver.

[Whoriskey et al. \(2019\)](#) provides a review of modelling approaches in aquatic telemetry. In most of the cases telemetry location data is used to link observations at different points in the receiver array with some explanatory variables. Those variables can be environmental, such as time of the day time during migration, flow conditions, lunar cycle, tides or related to the individual: sex, size, age, condition etc. Such data, often aggregated, is then modelled using Generalised Additive Models or a similar standard approach. This approach is popular in the study of juvenile salmon migration in Scotland. [Lilly et al. \(2024\)](#) analysed the probability of successful migration through the Irish Sea dependent on smolt fork length, condition, day of the migration and distance covered by the migrant. [Newton et al. \(2021\)](#) studied migration on the East coast of Scotland and looked at the probability of smolts reaching the last array on the North Sea, depending on the size of the released group and velocity vector calculated between receivers, compared with a particle model of currents in that region. Another common way of modelling is survival analysis, where probabilities of some event, such as mortality or navigating an obstacle, are modelled in reference to time. It is used by [Lothian et al. \(2024b\)](#) to analyse the effect of tags on mortality of the smolts. Alternatively, detections can be analysed as graphs as a form of aggregation of sparse detections into a regular matrix of observations of tagged animals and receivers ([Whoriskey et al., 2019](#)). Mark-recapture models have the advantage of taking into consideration the overall catch of non-tagged individuals and help refer the analysis to the population-level data. Modelling of the spatial distribution after accounting for other environmental variables can provide insights relating to the correlation coming from social effects ([Berdahl et al., 2014](#)), or uncover other influences on the movement and habitat use based on the distribution of observations across space and time.

Telemetry data can be modelled to understand collective behaviour with the help of movement models. To better understand the behaviour of animals that produce the telemetry observations, the movement can be seen as some variation of a Random Walk (introduced in detail in Section 1.2.2 of this thesis). Commonly, data from terrestrial animals can be fitted to correlated random walks where precise location is available ([Morales et al., 2004](#); [Fryxell et al., 2008](#)). For aquatic animals, only simpler models are usually

viable: a Brownian bridge (random walk anchored at two defined locations) has been used to inform the utilisation distribution of Tiger Sharks by [Papastamatiou et al. \(2013\)](#). Movement of salmon smolts in a standing body of water was seen as a Correlated Random Walk in studies of [Hanssen et al. \(2022\)](#) and [Lilly et al. \(2022\)](#).

Telemetry location data can also be modelled with Hidden Markov Models (HMMs), where every animal's observational history is modelled as belonging to a number of hidden behavioural states. With higher computational cost, HMMs can be fitted to telemetry data with random effects, accounting better for individual variations, but this approach might still lead to biases ([McClintock, 2021](#)).

Modelling of collective movement at the level of a shoal has been attempted. Schooling of fish has been mechanistically simulated in terms of alignment, velocity correlation and optimal distance ([Aoki, 1982](#); [Reynolds, 1987](#)). Those purely theoretical models have since been used to construct stochastic models explaining emergent sensing by [Torney et al. \(2009\)](#) later confirmed by empirical study ([Berdahl et al., 2013](#)).

Some methods used to quantify collective behaviour components, such as [Dalziel et al. \(2016\)](#), do not require assumptions on the movement model that generates the observations but instead requires some form of measure of collective behaviour, such as alignment of velocity vectors of individuals. However, with acoustic river telemetry data, the resolution required for those detailed measures is not achievable.

Instead, [Calabrese et al. \(2018\)](#) developed rules for quantifying the correlation of movement between individuals from sparse field data. The authors derive their approach from the analysis of movement equations and the assumption that the correlation of the stochastic element of the equation provides the indication of collective movement. This approach assumes that every individual has its own parameters of movement equation, requiring more fine-detail data than available in our absence-presence telemetry data.

[Renardy et al. \(2023\)](#) combines modelling of flow near a hydropower plant with a manual radio telemetry of salmon smolts near a migration barrier. The animal movement and behaviour can be broadly classified based on movement between predefined areas of the water, but not in enough detail to explore underlying movement or social processes.

[Berdahl et al. \(2014\)](#) uncovers social interaction from recapture events of returning Pacific Salmon. As the fish from different natal streams move up the river, it is possible to model the time of their observations as dependent on the number of other fish moving together. During the downstream migration, branching does not occur so readily to allow this method to study the potential social effects of the juvenile population.

5.1.2 Approximate Bayesian Computation

Most of the traditional models used for the analysis of telemetry data can be fitted using likelihood methods. We can model average speed, probability of survival and other key characteristic of different river migrations with easily tractable models. In our case, however, we are modelling some non-trivial latent states which do not have an obvious relation to observations. Specifically, we have very sparse observations of a process that is largely hidden.

Approximate Bayesian Computation (ABC) is a family of methods based on Bayesian inference, which are well suited to model fitting, especially in cases where the calculation of the likelihood function is not easy or possible. In Bayesian statistics, the Bayes theorem describes how probability distribution changes in light of evidence. Unlike frequentist approach to statistics, in this paradigm, we encode what is known and unknown about the phenomena we observe in terms of probability distributions. This prior knowledge is known as a *prior* distribution $\pi(\theta)$, and can be uninformed with e.g. uniform distribution, or already centred on some initial guess about the central value with a normal distribution. The Bayes theorem defines a new distribution called *posterior* distribution $p(\theta|D)$ that is the prior updated in the light of observations D :

$$p(\theta|D) = \frac{\mathcal{L}(D|\theta)\pi(\theta)}{\mathcal{L}(D)}, \quad (5.1)$$

where $\mathcal{L}(D|\theta)$ is the likelihood of observations D given θ and $\mathcal{L}(D)$ the marginal likelihood of the observation D . In general, the difficulty arises in calculating the marginal likelihood $\mathcal{L}(D) = \int p(D|\theta)\pi(\theta)d\theta$, that might involved integrating over many dimensions of a complex function. However in simulation-based methods it can be seen as a normalising constant and ignored. If the likelihood of $\mathcal{L}(D|\theta)$ can be evaluated in some Monte Carlo-like method, the *posterior* can be revised by directly sampling from the distribution (Beaumont, 2010).

This approach is well suited to ecological studies. Solow and Smith (2009) used the ABC framework to estimate species abundance without assuming the underlying analytical distribution and instead used a more realistic sequential model. Ruiz-Suarez et al. (2020) used ABC to model movement (CRW) and investigates what temporal scale is necessary to correctly retrieve parameters of the model. Gaskell et al. (2020) used Gaussian Processes to accelerate the estimation of the synthetic likelihood function in order to allow ABC methods to be applied to IBMs at the scale allowing for population-level behaviour study.

The following two sections, introduce the basic of ABC algorithms that this study

build upon.

5.1.2.1 Sample rejection ABC

The goal of the ABC algorithm is to approximate the true distribution of parameters that produced some observations D^\dagger . A simulation model \mathcal{M} is a computer program that imitates the observed phenomena that produces observations D given set of parameters θ , we can retrieve the posterior $P(\theta|D)$ of its parameters θ using the ABC sample rejection algorithm.

We start by defining a prior of the parameters $\pi(\theta)$, which can be either uniform (ranging through a broad range of possible values) or informed, for instance, a Gaussian with mean and variance taken from estimation of probabilities from telemetry data. For instance, in our data, we can easily calculate a minimal possible value of the actual probability of survival as we know which fish survived a journey but don't know how many more missed were detected. That can be then described as a right-skewed prior distribution describing imperfect prior knowledge.

We run a simulation multiple times, every time with θ_τ coming from the prior $\pi(\theta)$. Simulation $\mathcal{M}(\theta_\tau)$ generates data D_τ . We then either accept or reject those parameters based on the distance of generated data from actual observations (target data) given tolerance threshold ϵ :

$$\rho(D_\tau - D^\dagger) < \epsilon. \quad (5.2)$$

Defining this distance function ρ directly is difficult. Most of the time D has too many dimensions and is too sparse to allow a meaningful comparison. Often, the resulting process might produce data of different dimensions making direct measures impractical.

Some form of dimensionality reduction is used to create a *summary statistic* $S(D)$, which needs to retain sufficient information about the data to guarantee that as the distance of summary statistic reduces, the simulated data is getting closer to the real observations.

The distance metric ρ can then be as simple as an Euclidean norm. However, the normalisation of a summary statistic is often necessary. In the simplest form of sample rejection, the tolerance threshold ϵ is constant. The posterior distribution of parameters is recovered as a set $\{\theta^*\}$ of parameters accepted in all iterations θ_τ :

$$p(\theta_\tau | \rho(S(D_\tau) - S(D^\dagger)) < \epsilon). \quad (5.3)$$

Which can be a good approximation of a true posterior with a sufficiently small epsilon and

a high number of repetitions. Low tolerance ϵ increases the computational effort required to find the posterior, while if it is too high, most of the samples will be accepted, and the prior will resemble the provided posterior.

5.1.2.2 Sequential Monte Carlo ABC

The sample rejection algorithm's disadvantage is that it is inefficient, sampling from the entire prior distribution, even when parameters from some parts of the parameter space are more often accepted. Some methods use Markov Chain Monte Carlo (MCMC) methods to generate the sample θ^* but because each draw depends on the previous one being rejected or accepted, they are difficult to parallelise.

An alternative is a Sequential Monte Carlo (SMC) method (Jennings and Madigan, 2017) also known as Population Monte Carlo (PMC) (Prangle, 2017) in different literature. It uses a draw of k sets of parameters θ_i , called particles and a transition kernel to decide on the randomisation of another. This allows for multiple calculations at the same time for each iteration τ for a set of particles (parameters):

1. Generate $\theta_{t,i} \sim \pi(\theta)$ for each particle $i \in k$.
2. evaluate simulation $D_i \sim \mathcal{M}(\theta_i)$
3. If $\rho(S(D_i) - S(D)) < \epsilon_0$ accept θ_i as $\theta_{i,t}^*$ else go to 1 for each particle until all accepted
4. In iteration τ , sample a new set by drawing $\theta_{i,t} \sim \mathcal{N}(\theta_{i,t-1}^*, \sigma_{t-1}^2)$ where σ is a covariance matrix between particles.
5. Repeat step 4 until simulation with new sets of parameters yields accepted θ^* .

Additionally, the tolerance ϵ is lowered as parameters converge, and weights from a transition kernel are used when calculating the covariance. What then remains as a key challenge is a design of summary statistic $S(D)$ and choice of normalisation and distance function ρ .

5.2 Methods

5.2.1 Spey river migration data

We model data from the 'Missing Salmon' project, a telemetry study of five rivers discharging into the Moray Firth on the east coast of Scotland. The data comes from rivers

in which different hypothesis about sources of smolt mortality were tested, and hence each telemetry setup is different. Rivers vary with their receiver coverage, number of confluences, man-made obstacles and varying degree of lochs and canal segments and number of smolts tagged.

We begin by analysing data from the river Spey that does not have notable confluences or loch sections and has quite evenly distributed receivers, more densely than most of other systems. Spey data will allow us to test our methods with minimal number of variables before expanding to a more generic form that can accommodate any system and strengthen potential conclusions.

The fish are caught in a rotary screw trap overnight, and a sample is selected, tagged and released into the river in batches.

Figure 5.1 shows the river Spey with 12 acoustic receiver locations and associated detection count. We can see that the number of detections varies widely, but the locations provide even coverage across the whole 48km journey of 140 individuals. As the fish swims by the receiver, it keeps being registered every time its acoustic “ping”, generated on average every 45 seconds, reaches the receiver (randomly in an interval between 30 and 60 seconds). Data corresponding to signal strength that could provide valuable information on the distance from the fish is usually not available due to equipment manufacturers’ restrictions. The number of pings generally corresponds to the length of time spent around each location but also to the probability of detection especially at a distance. Figure 5.2 shows the number of pings registered from each fish at the subsequent receivers. We can see the heterogeneity of the detection profile of every detector in its environment.

Groups of tagged fish (usually pairs) are sometimes registered at the same time at different parts of the river. Such co-occurrences might be a result of collective movement, yet the rate of those observations of fish moving independently is not known.

We calculated the time difference between the closest detection of each pair of individuals at every detector, creating a co-registration matrix. In Figure 5.3 we present the aggregate distribution of those time differences truncated at twenty minutes time.

5.2.2 Simulation of river migration

The ABC methods allow to model complex data that can be described by forward-feed (simulation) models. The rest of this section will describe the structure of the model and its GPU implementation. Following, Section 5.2.3 describes Bayesian modelling framework used for fitting and validating this simulation, presented in a schematic in the Figure 5.4.

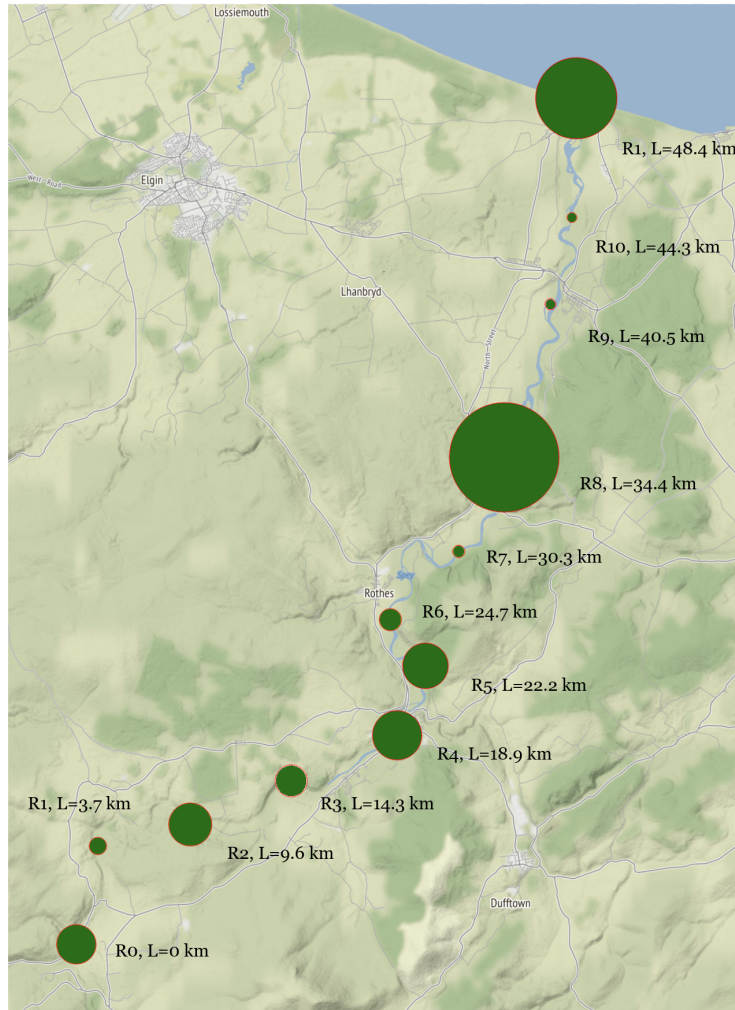


Figure 5.1: The river Spey on the east coast of Scotland. Twelve receivers R_i were deployed at distance l_i from the release site of fish tagged with acoustic receivers. The area of the dot is proportional to the number of registrations received.

5.2.2.1 Simulation

We use a discrete-time, 1D continuous space individual-based model (IBM) to approximate the smolts journey from the release site to the sea.

The model has a number of hyper-parameters that are specified according to the specific telemetry system and parameters describing movement, mortality and observations. The movement and observations are modelled as two processes. Parameters μ, α, β and γ , describe movement, P_{surv} mortality and λ observations, a total of six parameters. The overall model structure is outlined in Figure 5.5. For simplicity, $\Delta t = 1$ minute and roughly corresponds to the frequency of pings in telemetry data, which varies from 30 seconds to 1 minute. The location of fish in the river is described by a continuous variable

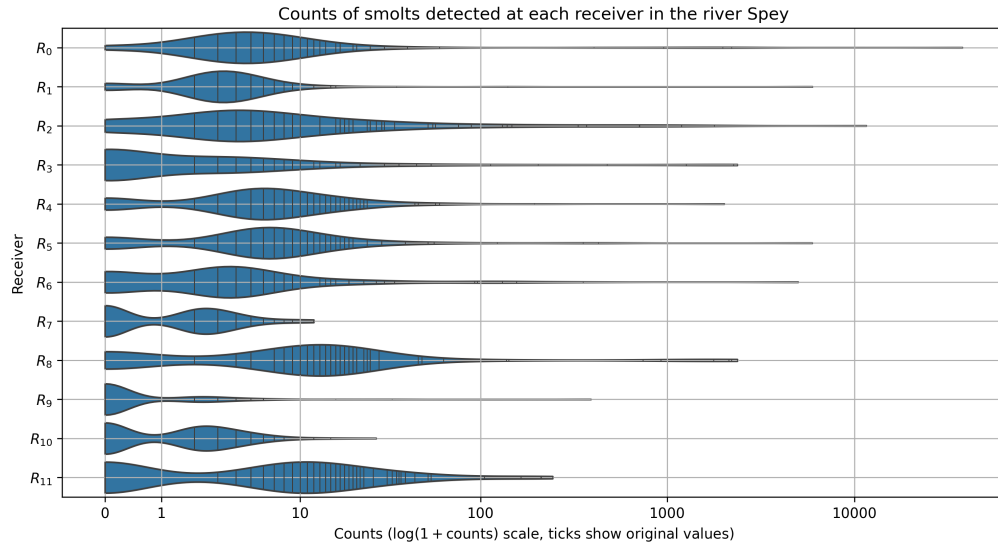


Figure 5.2: Number of pings received from each smolt registered at subsequent receivers, including 0 if a smolt was not detected. The scale is transformed with $\log(1+x)$ function, with original values marked on the scale. The median number of observations is below 10 for all but the last receiver, which corresponds to under 8 minutes of presence, but it varies largely, indicating variability in movement speed. The number of observations can also be explained by the probability of detection of fish at different distances and noisy environments.

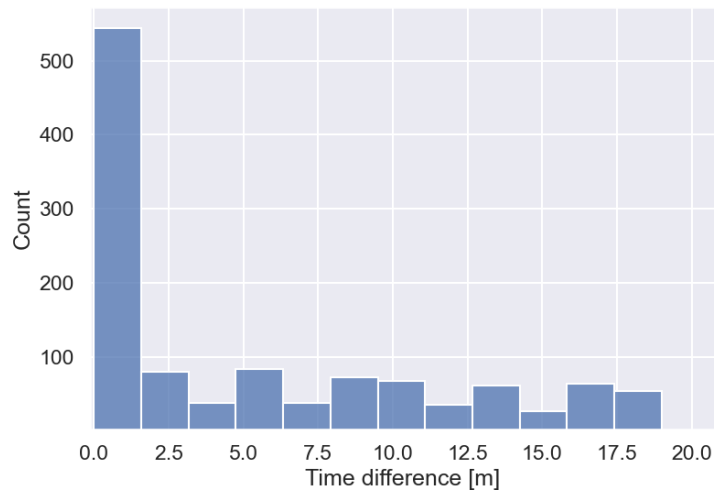


Figure 5.3: Distribution of difference in time of registration at all receivers for fish, which appeared within the 20-minute window. Over-inflation of values under 2 minutes suggest that there might be some collective effect on the movement parameters.

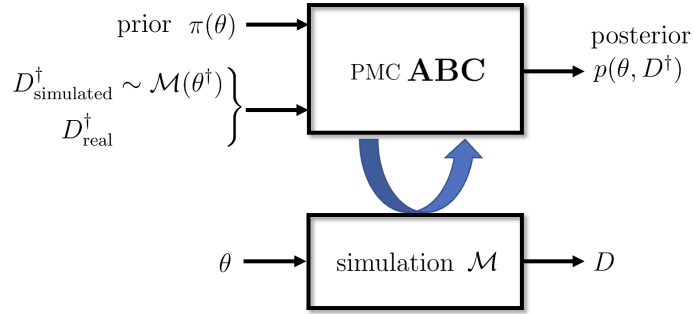


Figure 5.4: The schematic of ABC Population Monte Carlo inference. The algorithm uses a simulation \mathcal{M} to generate data based on the parameters θ coming from a set prior $\pi(\theta)$. Its goal is to estimate the true distribution of parameters underlying either the real-world, observed data $D_{\text{real}}^{\dagger}$, or simulated data $D_{\text{simulated}}^{\dagger}$ coming from a given parameter set θ^{\dagger} .

x in meters. The river length is described as l_{river} and is always the location of the last receiver. Each fish i begins movement at location $x_i \sim \mathcal{N}(0, 0.3)$, at time $t_{\text{start},i}$.

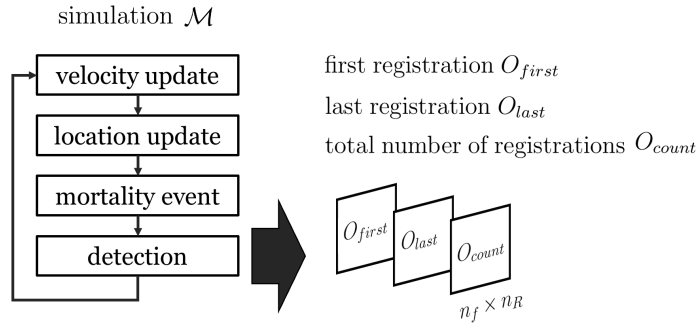


Figure 5.5: This schematic presents the logic of the simulation $\mathcal{M}(\theta)$ simulating fish movement and telemetry data observations that produce the simulation output. At every iteration, movement is updated according to Equation 5.6 and a new location of fish is also updated. Following a mortality event based on probability defined in Equation 5.7, fish are registered by the receiver array with probabilities from the equation 5.8. Those detections are aggregated in three matrices for first O_{first} , last O_{last} , and total number of registrations received O_{count} .

The main three components of the model are movement, mortality, and detection equations:

1. Movement

For each of n_f fish, the velocity $v(t)$ at time step t is modelled by a process built upon an Ornstein-Uhlenbeck mean-reverting stochastic process (described in detail in the introduction 1.2.2). It is defined by four parameters: mean speed μ , mean-reversion rate ν , stochastic component σ , and the distance of social influence γ .

We first define social influence as an averaging of the previous speeds of all fish $i, j \in N$ that fall within each other's social distance:

$$v_i^\gamma(t) = \frac{\sum_{j \in N} (\mathbb{1}_{(d_{ij} \leq \gamma)} \cdot v_j(t-1))}{\sum_{j \in N} \mathbb{1}_{(d_{ij} \leq \gamma)}}, \quad (5.4)$$

where t is a time step index, d_{ij} is the distance between fish i and j , and $\mathbb{1}_{d_{ij} \leq \gamma}$ is an indicator function that equals 1 for every fish within distance γ from fish i . For the stochastic component, we use the Euler-Maruyama discretisation of the OU process:

$$v_i(t) = v_i^\gamma(t-1) + \nu(\mu - v_i(t-1)) + \sigma \Delta W, \quad (5.5)$$

where $\Delta W \sim \mathcal{N}(0, 1)$.

In order to allow for more easily interpretable parameters we are replacing ν with $\beta = \frac{1}{\nu}$ and σ with $\alpha = \frac{\sigma^2}{2\nu}$ which corresponds to the standard deviation of the OU process. The full equation of movement for fish using i and expressed using the parameter formulation s:

$$v_i(t) = \frac{\sum_{j \in N} (\mathbb{1}_{(d_{ij} \leq \gamma)} \cdot v_j(t-1))}{\sum_{j \in N} \mathbb{1}_{(d_{ij} \leq \gamma)}} + \frac{1}{\beta}(\mu - v_i(t-1)) + \alpha \sqrt{\frac{2}{\beta}} \Delta W, \quad (5.6)$$

from which the distance $\Delta x_i(t) = v(t)\Delta t$ and the distance from the release site $x_i(t) = x_i(t-1) + \Delta x_i(t)$ are then updated.

2. Mortality

The mortality is assumed constant across the entire simulation, so at each time step, we are predicting that fish survives with probability that is a power function of the distance moved:

$$p_{surv}(t) = \left(\frac{P_{surv}}{l_{river}} \right)^{|\Delta x_i(t)|}, \quad (5.7)$$

which is based on an exponential decay function based on movement distance, where P_{surv} is the simulation parameter, the probability of survival of a journey of the river length l_{river} . This formulation does not correspond directly to the usual way of measuring mortality but to the mortality per unit distance of the full migration route.

3. **Detection** Detection depends on parameters P_{detmax}^k of each detector R_k and decay rate λ that mediates how detections become less likely with distance. We are calculating each possible detection for every fish anywhere in the river. Probability of detecting smolt i located at $x_i(t)$ at detector k located at a distance l_k from the release site is at each time step:

$$P_{det,t}^{i,k} = P_{detmax}^i e^{-\frac{|x_i(t)-l_k|}{\lambda}} \quad (5.8)$$

Optimally, both λ and P_{detmax} would be unique for each receiver, though that would much increase the number of parameters of the model. In practice, P_{detmax} is emulating the second dimension of the river because our model assumes that each fish will always swim directly by the receiver.

Parameter	Symbol	Distribution	Range	θ_A
Average velocity	μ	$U(0, 30)$	0 to $30 \frac{m}{min}$ / $50 \frac{cm}{s}$	15
Dispersion	α	$U(0, 30)$	Δv 0 to $\sqrt{2} \times 30 \frac{m}{min}$	5
Mean reversion	β	$U(1, 100)$	Mean reversion $(\frac{1}{100}, 1) \times (\mu - v(t))$	20
Detection decay	λ	$U(0, 150)$	Halving of P_{detmax} at 0 to 104 m	60
Probability of survival	P_{surv}	$U(0, 1)$	of the river length	0.5
Social influence threshold	γ	$ X , X \sim U(-10, 30)$	0 to 30 m	0 / 10

Table 5.1: Parameters, symbols, distributions, and real-world ranges of parameters used in the simulation. We sample from the provided priors to validate the method across the parameter space, as well as using set θ_A to understand the simulation at one specific point.

5.2.2.2 Model implementation

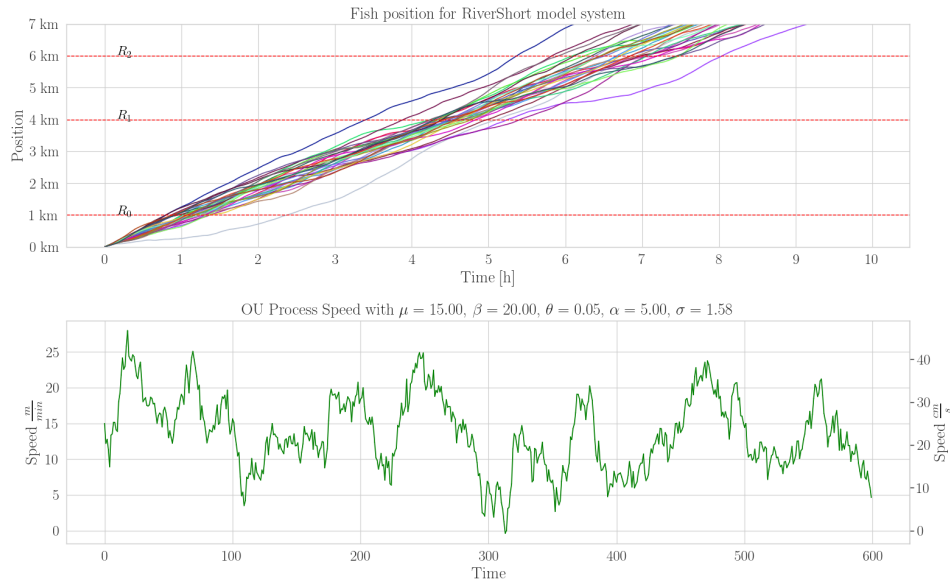


Figure 5.6: Visualisation of simulation for 30 fish moving across the length of a RiverShort system. $\beta = 20$ provides a slow mean reversion of $0.05 \frac{m}{min}$, combined with reasonably small dispersion from parameter $\alpha = 5$ gives a gentle oscillation around mean speed of $\mu = 15$. Detections at subsequent receivers are more dispersed, with over 2 hours difference in registration between some fish at R_2 at $l_2 = 6$ km.

The simulation has been written in Python in a vectorised form using the `tensorflow` library (Abadi et al., 2015), allowing for multiple simulations to be performed in parallel. It has been coded as a series of tensor operations defined as a graph function, a `tensorflow-graph` object. We define hyperparameters for two scenarios, an easy model **RiverShort** to verify the assumptions on the simplest scenario with a short river with three receivers, and **SynthSpey**, a system based on the real-world conditions of spey telemetry exercise. Table 5.2 shows the key hyperparameters for each model. We are using the same number of agents (smolts) in each model and the same release schedule. Table 5.3 shows the receiver configuration of the RiverShort scenario. The graph in Figure 5.6 shows an example movement of thirty agents in the RiverShort model with a timeline of the velocity for one of the agents.

Table 5.4 shows the configuration of receivers for the river Spey based on the telemetry study.

Model	RiverShort	SynthSpey
Number of smolts n_f	140	140
Number of receivers n_R	3	12
Simulation time t_{sim} [h]	11	438
Simulation time t_{sim} [days]	0.45	18.2
Approx. computation time for one batch t_{sim} [min]	1:30	9:00
Release: groups of 10 every 10 minutes		

Table 5.2: Comparison of smolt numbers, receiver counts, and simulation times in two models, including the common release schedule. There is a considerable difference, especially in simulation time (implied by river length).

Id	Group	Dist [km]	P_max
R_0	0	1.00	0.5
R_1	0	4.00	0.9
R_2	0	6.00	0.9

Table 5.3: Summary of receiver parameters for RiverShort model data with ID, group, distance, and maximum probability of detection.

5.2.3 Design of summary statistic

A summary statistic provides a lower dimensional representation of the outcome of simulation in a balanced way and is an application-specific challenge of the ABC approach. The output of our simulation $\mathcal{M}(\theta)$ is a list of time of detections of each of the $n_f = 140$ fish f at each of n_R receivers R with associated time t of detection. This matches the format of data coming from acoustic telemetry projects with presence tags.

We gather the output of the simulation in three matrices $n_f \times n_R$ of observations with values of first registration O_{first} , last registration O_{last} , and a total number of registrations received O_{count} .

We have three receiver-specific statistics and two that are averaged across the entire matrix. We average receiver statistics in three groups in order to make the algorithm independent of the number of river receivers.

Id	Group	Dist [km]	P_max
R_0	0	1.00	0.93
R_1	0	4.73	0.91
R_2	0	10.63	0.92
R_3	0	15.3	0.52
R_4	1	19.9	0.98
R_5	1	23.18	0.99
R_6	1	25.72	0.87
R_7	1	31.29	0.75
R_8	2	35.4	0.98
R_9	2	41.51	0.31
R_{10}	2	45.25	0.85
R_{11}	2	49.43	1.00

Table 5.4: Summary of receiver parameters for SynthSpey model data with ID, group, distance, and maximum probability of detection.

5.2.3.1 Detector based statistics

To avoid zero-inflation of many statistics, we will first define the list of all fish registered at least once at the receiver R_i as:

$$f_{obsR_i} : f_j \in O_{count}^{i,j}, O_{count}^{i,j} \neq 0, \quad (5.9)$$

and the halfway time between arrival and departure at each receiver for those fish:

$$t_{mid}^{i,j} = \frac{O_{last}^{i,j} + O_{first}^{i,j}}{2} \quad \forall f_{obsR_i}. \quad (5.10)$$

We now define three measures that are subsequently averaged and normalised to create the summary statistic:

- **median number of observations at receiver R_i :** a median number of observations of each fish at each receiver R_i , excluding fish not registered at all at the given receiver:

$$S_{observations}^i = \text{med}(f_{obs}^i). \quad (5.11)$$

- **number of unique fish observed at receiver R_i :**

$$S_{presence}^i = \sum_{f_{obs}^i} 1. \quad (5.12)$$

- **coefficient of variability of registration time at receiver** R_i adjusted by number of observations:

$$CV^i = \frac{std(t_{\text{mid}}^i)}{\bar{t}_{\text{mid}}^i \sqrt{S_{\text{presence}}^i}}, \quad (5.13)$$

where \bar{t}_{mid}^i is the average value of registration time for each receiver R_i for all fish that were registered, and $std(t_{\text{mid}}^i)$ standard deviation of that registration time.

In order to allow methods to apply to river systems with different number of receivers, we divide receiver R_i into three groups g for beginning, middle and end of the system, and average statistic between them:

$$S^g = \frac{\sum_{i \in g} S^i}{n_g} \quad \text{for } g \in \{1, 2, 3\}, \quad (5.14)$$

where n_g is the number of receivers in the group g . Tables 5.3 and 5.4 show the grouping of receivers in our experiments. If the number of receivers is even the middle group is larger by one.

5.2.3.2 General statistics

- **Median pace** we calculate the median pace of movement speed across all receivers:

$$S_{\text{pace}} = med\left(\frac{l_{R_i}}{med(t_{\text{mid}}^i)}\right), \quad (5.15)$$

where l_{R_i} is the distance of receiver R_i from the release site.

- **Average number of co-occurrences** We define a co-occurrence between two fish f_a and f_b at a receiver R_i as an instance of overlapping registrations:

$$\text{Cooccurrence}^i(f_a, f_b) = \left(\max(O_{\text{first}}^{i,a}, O_{\text{first}}^{i,b}) \leq \min(O_{\text{last}}^{i,a}, O_{\text{last}}^{i,b}) \right). \quad (5.16)$$

We then define the normalized number of co-occurrences as

$$S_{\text{co-oc}} = \frac{\sum_{i=1}^{n_R} \sum_{j=1}^{n_f} \sum_{k=1}^{n_f} \text{Cooccurrence}^i(f_j, f_k)}{\frac{1}{2} n_f (n_f - 1) n_R}. \quad (5.17)$$

5.2.3.3 Normalisation of the statistics

The statistics described above are then normalised based on observations of the simulations from the prior 5.7 to closest resemble the normal distribution as in Figure 5.8. In practice,

the skewness of some summary statistics will change depending on the hyperparameters of the modelled system and might be non-normal in the area where parameters are sampled from. We tested different families of popular normalisation functions and compared results on SynthSpey, RiverShort and real telemetry data to find transformations that, on average provide the most reasonable shapes of distributions. For each receiver group $g \in (0, 1, 2)$ we normalise receiver statistics

$$S_{rec}^g = [S_{obs}^g, \log \frac{S_{pres}^g}{1 - S_{pres}^g}, \log(1 + CV^g)]. \quad (5.18)$$

We then normalise the general statistics with the logit function:

$$S_{gen} = [\log \frac{\frac{1}{30} S_{pace}}{1 - (\frac{1}{30} S_{pace})}, \log \frac{1000 S_{co-oc}}{1 - (1000 S_{co-oc})}] \quad (5.19)$$

where the pace is additionally normalised by the maximum mean speed parameter and S_{co-oc} multiplied by large number to avoid precision issue in cases when it is a very small number.

5.2.3.4 Distance function

We use a normalised distance function to avoid any element of the summary statistic vector dominating the metric. Following the baseline approach outlined in Prangle (2017), we are first calculating the median absolute deviation (MAD) matrix of the summary statistics of a random sample of 2000 parameters from a prior. MAD has an advantage over the standard covariance matrix with regard to outliers. We use diagonal elements of the matrix as weights for the weighted Euclidean distance between each summary statistic $S^{(l)}$ and the target summary statistic S^\dagger

$$d(S^\dagger, S) = \left[\sum_{i=1}^{N_s} \{w_i (s_i^\dagger - s_i)^2\} \right]^{1/2} \quad (5.20)$$

where $N_s = 11$ is the length of the summary statistic vector, and weight $w_i = \frac{1}{\sigma_i}$ is a MAD coefficient σ_i of that element of the summary statistic.

For some values of parameters (for instance, very low survival rate), the statistics cannot be calculated. In such cases, the distance to the summary statistic of target data is set to infinity and the parameters set rejected.

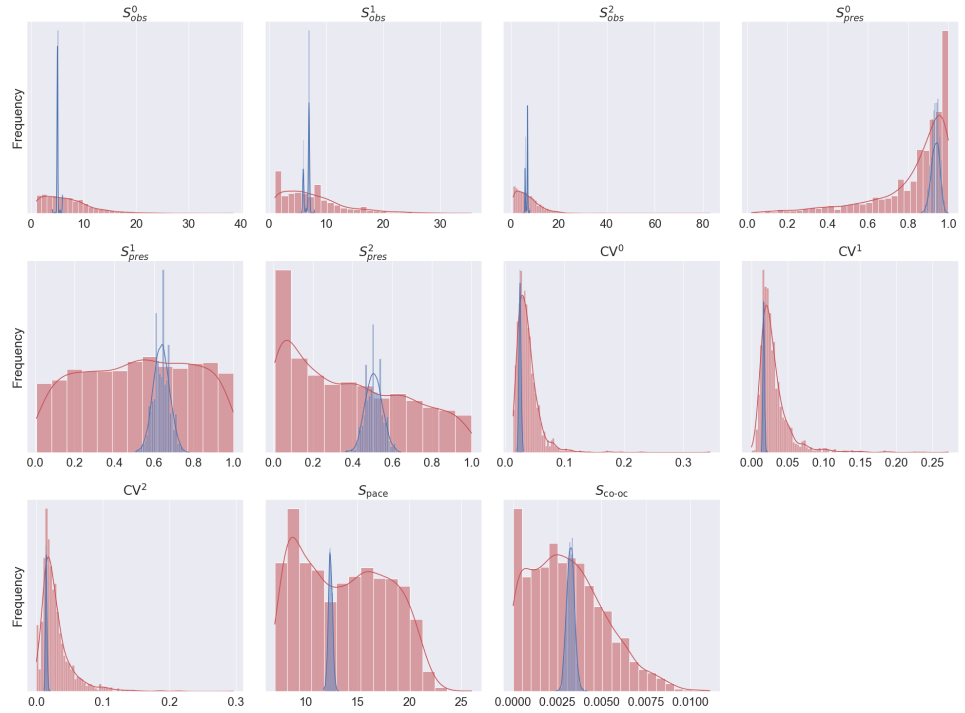


Figure 5.7: Histograms for summary statistic of simulations without normalisation for RiverShort model. The red bars show the histogram of each value of the summary statistic vector for parameters sampled 2000 times from the prior (as in table 5.1). The Coefficient of Variability of arrival time (CV) for each group is left skewed. Presence statistics S_{pres} vary from right to left skewed as the number of fish at each section of receivers depends on their mortality throughout the journey. The blue histograms overlaid are the summary statistic for 2000 repetitions of simulation from the same parameters set $\mathcal{M}(\theta_A)$.

5.2.4 ABC modelling

Our model can be a good first approximation of real fish movement behaviour, expanding on a random walk only in ways necessary to justify the persistence of downstream movement. Simulations of temporal processes do not allow constructing a likelihood function that can be analytically calculated because probabilities at each time step are conditional on the results of all the previous ones.

In this work, we estimate the posterior distribution of the true model parameters by using a Population Monte Carlo (PMC) ABC method (Prangle, 2017) adapted for batch processing on a GPU. The Monte Carlo method evaluates the model at given parameter values, so parallelisation of the model execution is the single most important improvement to the practical application of the ABC method. In our case, we are able to run simulations in batches of $B = 2000$ on a graphics card with 11GB of memory, making this modelling

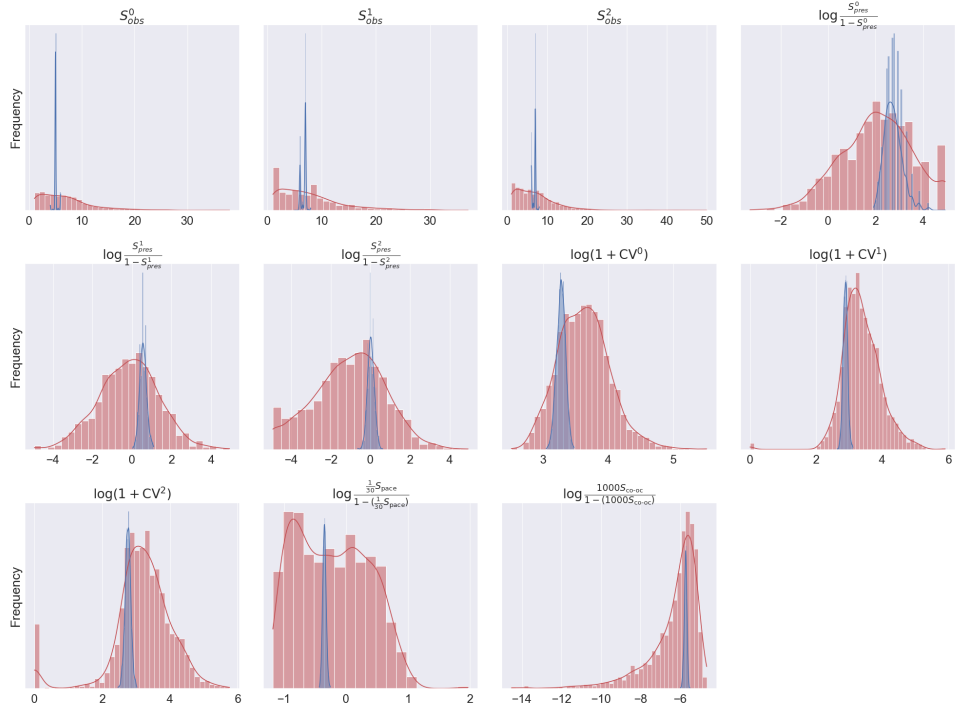


Figure 5.8: Histograms for normalised summary statistic for RiverShort model. The red bars show the histogram of each value of the summary statistic vector for parameters sampled 2000 times from the prior (as in table 5.1). Compared to 5.7 most of the statistics look much closer to the normal distribution, however the first three S_{obs} do not have a clear normalisation strategy and remain left skewed. The number of co-occurrences $S_{\text{co-oc}}$ is fairly right-skewed despite attempted normalisation. The blue histograms overlaid are the summary statistic for 2000 repetitions of simulation from the same parameters set $\mathcal{M}(\theta_A)$.

feasible.

Algorithm 1 describes the process of finding the representative sample from the estimated posterior. With every iteration τ we are sampling new parameters from a sample of L parameters θ_{t-1}^* accepted in the previous iteration using an *importance density*:

$$q_\tau(\theta) = \begin{cases} \pi(\theta) & \text{if } \tau = 1, \\ \sum_{i=1}^L w_{t-1}^i \mathcal{N}(\theta_{t-1}^{*i}, \kappa \Sigma_{w,t-1}) & \text{otherwise} \end{cases} \quad (5.21)$$

where $\kappa = 0.5$ is the scaling factor, and $\Sigma_{w,t-1}$ is a weighted covariance matrix of all L parameters θ_{t-1} , and weights w_t are defined as

$$w_\tau^i = \frac{\pi(\theta_i^t)}{q_\tau(\theta_i^t)}, \quad (5.22)$$

so that the prior knowledge is considered even at later simulation stages. This reduces the risk of converging on non-optimal parameter values due to inadequate sampling in earlier stages.

We are using an adaptive threshold h , always accepting the 10th percentile of sampled parameters. This allows the method to be more independent of specific distance distribution and gradually reduce uncertainty without introducing a threshold dependent on the application to a particular model.

Algorithm 1 describes the ABC. We repeat the main procedure 8 times, as in preliminary tests, around the 5th iteration, the average distance of accepted parameters stopped decreasing.

Algorithm 1 ABC-PMC (with the option of adaptive h_τ)

- 1: **Hyperparameters**
 - 2: $\tau = 1$, $\kappa = 0.5$, $h = 0.1$, $B = 2000$
 - 3: **Main loop**
 - 4: **repeat**
 - 5: Sample θ , B times from importance density $q_\tau(\theta)$ given in Equation 5.21 rejecting samples if $\pi(\theta) = 0$.
 - 6: Simulate y from $\mathcal{M}(\theta)$ and calculate summary statistic $S(y)$.
 - 7: Accept θ^i as θ^{i*} if $d(S, D^\dagger) \leq \text{Quantile}(d(S, S^\dagger), h)$.
 - 8: Let $w_\tau^i = \frac{\pi(\theta_\tau^i)}{q_\tau(\theta_\tau^{i*})}$.
 - 9: Increment τ to $\tau + 1$.
 - 10: **until** $\tau = 8$
 - 11: **End of loop**
-

5.2.5 Validation on simulated data

Each repetition of ABC modelling produces a posterior $p_\tau(\theta_\tau^*)$ that is expressed by its sample of L parameters θ_τ^* that were the accepted in that iteration.

We validate our method by analysing how well the resulting posterior estimate reflects the true parameter vector $\theta_i^\dagger = [\mu_i^\dagger, \beta_i^\dagger, \alpha_i^\dagger, \lambda_i^\dagger, P_{surv,i}^\dagger, \gamma_i^\dagger]$ for each of repetition i of the modelling. For each repetition, we sample the target parameter vector θ_i from a prior. Some parameter values might result in a simulation where no fish arrives at some receiver group due to very high mortality, or the detection rate is so low that no fish are registered. In such cases, the summary statistic is not defined, resulting in an invalid simulation $\mathcal{M}(\theta_i^\dagger)$ and this parameter set is not used for the experimentation.

We follow Ruiz-Suarez et al. (2020) to report absolute prediction error \mathcal{E}_{abs} between

each of the true parameter values and the median value $\hat{\theta}_i^*$ from a resulting posterior distribution over N_{rep} repetitions:

$$\mathcal{E}_{abs} = \sqrt{\frac{1}{N_{rep}} \sum_{i=1}^{N_{rep}} (\hat{\theta}_i^* - \theta_i^\dagger)^2}. \quad (5.23)$$

Next we report a relative error \mathcal{E}_{rel} for each parameter (called Dispersion Index in [Ruiz-Suarez et al. \(2020\)](#)):

$$\mathcal{E}_{rel} = \frac{1}{N_{rep}} \sum_{i=1}^{N_{rep}} \frac{|\hat{\theta}_i - \theta_i|}{\theta_i^\dagger}. \quad (5.24)$$

We discard any simulation that has a parameter set within 5% to the top or bottom of the prior parameter range to avoid biasing results by single parameters with unlikely values. We report \mathcal{E}_{abs} and \mathcal{E}_{rel} for each element of the parameter vector separately. For parameter γ , which prior goes from -10 to 30, we shift values to be positive only.

Prediction quality relates not only to the distance of the mean or median of the posterior to the true value of the parameter but also if the whole distribution correctly captures the true value. We expect that the posterior probability correctly captures the likelihood of the target value producing the simulated outcome. [Cook et al. \(2006\)](#) shows that the shape of the quantiles distribution of target values of parameters θ^\dagger should be $U(0, 1)$ if the method reliably recovers the posterior. The quantiles are defined as

$$q_i = \frac{1}{L} \sum_{l \in L} \mathbb{1}_{\theta^l > \theta_i^*}, \quad (5.25)$$

for every replication $i \in N_{rep}$ where θ_i^* is a parameter sampled L times from the posterior i .

To test how close the resulting quantile distribution is to uniform $U(0, 1)$ we calculate the p values of the χ^2 statistic of their probit distribution $\Phi^{-1}(q)$:

$$\chi^2 = \sum_1^{N_{rep}} (\Phi^{-1}(q)). \quad (5.26)$$

Further, by transforming those p-values with $\Phi^{-1}(p)$ we can produce the z_{quant} statistic that should provide an insight on the level of deviation from the perfect reproduction of the target distribution.

Those two approaches will inform how well the parameters are recovered and if the

spread of the posterior provides an accurate description of uncertainty in the model.

We repeated the ABC procedure $N_{rep} = 100$ times on different parameters from the prior on system RiverSimple and $N_{rep} = 50$ times for SynthSpey. We recognise that a social component modifying the discretised OU movement might present a particular challenge: hence we are comparing the “social” model as defined so far with one where $\gamma = 0$ and all fish swim independently (“non-social”). Additionally, we selected a parameter vector θ_A with reasonable values and repeated model fitting 25 times, seeing how reliable is the recovery of the posterior at that particular point in the parameter space. Table 5.1 provided the values chosen as an example, A . Finally, we fit our model to the observations from the telemetry study on the river Spey.

5.3 Results

5.3.1 Target parameter recovery

We tested how well can the model recover the target parameter vector θ^\dagger that has been repeatedly sampled from the prior. In Figure 5.9, \mathcal{E}_{abs} is presented for each element of the parameter vector. The absolute error depends on the scale of each parameter value but allows to compare modelling on RiverShort and SynthSpey with and without the social component γ . The mean velocity of movement has a 5.5 times larger error when modelling RiverShort ($\mathcal{E}_{abs} = 3.33$) then SynthSpey ($\mathcal{E}_{abs}=0.60$), with large difference also reported when social component γ is not fixed (2.44 to 0.68). SynthSpey seems an easier model to fit also for parameter P_{surv} with $\mathcal{E}_{abs} = 0.05$ half of that for RiverSpey $\mathcal{E}_{abs} = 0.10$. Overall, all the parameters apart from γ were recovered more accurately on SynthSpey, which shows that the method works as well with averaging over receiver groups than on a short test. For both model river systems, the error is higher when retrieving parameters λ and β in scenario with social component γ , by 20% for parameter β on RiverShort (26.81 to 20.11) to 80% for λ on SynthSpey (13.34 to 7.34). This suggests that some interaction with the social factor reduces discriminating information in summary statistic for those parameters.

In Figure 5.10 we present relative error \mathcal{E}_{rel} in the same set of scenarios. Here we observe that parameter β was the least accurate with \mathcal{E}_{rel} ranging between 0.49 for non-social model of RiverShort and 0.71 on the social model and 0.57 and 0.60 for RiverSpey. This is higher than any other observed relative error, and highlights that our summary statistic was the least informative regarding the magnitude of drift in the movement process. The

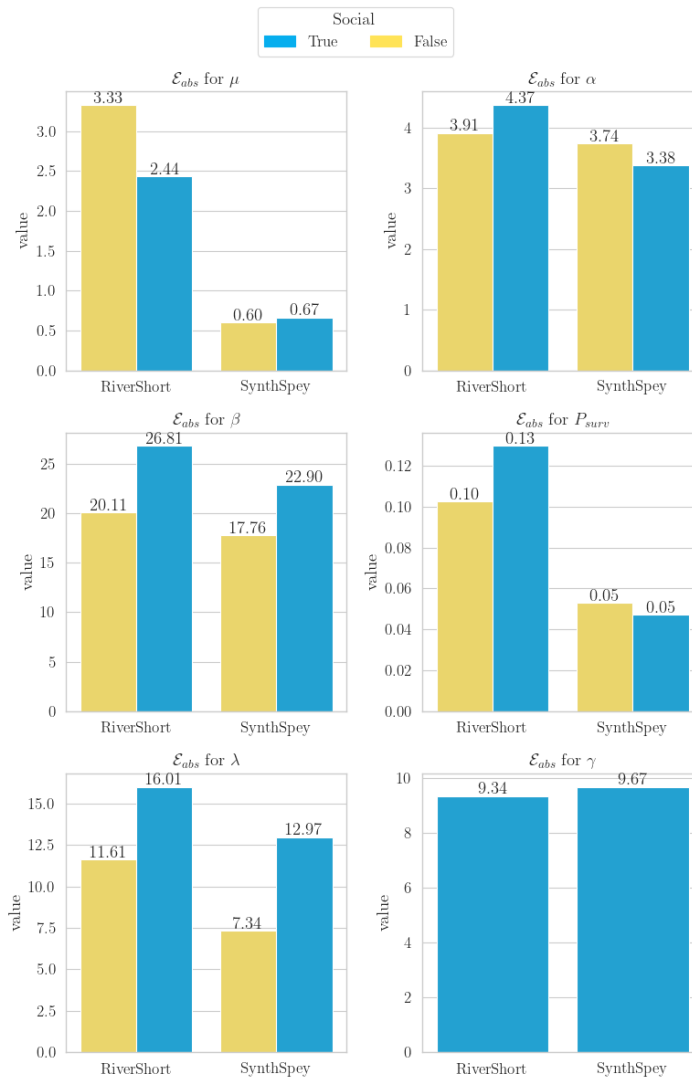


Figure 5.9: Results of absolute mean square prediction error \mathcal{E}_{abs} for each parameter for two river models RiverShort and SynthSpey, for models with and without social influence γ . For parameters μ and P_{surv} model SynthSpey provides better approximation of true parameter value. Recovery of parameters in variant with social interaction are markedly worse for parameters β and λ .

parameter γ is recovered with a large error for both SynthSpey (0.43) and RiverShort (0.39). On RiverShort, parameters α and P_{surv} are recovered slightly worse with 0.33 to 0.16 (social) and 0.28 to 0.16 (non-social) for α and 0.26 to 0.11 and 0.23 to 0.12 for P_{surv} accordingly. This can be explained by the fact that the length of RiverShort was only 6km, and sampling across the whole prior might result in fewer samples of mean speed slow enough to explore the variability of registration time provided by parameter α and registration number relevant for P_{surv} .

Apart from μ for which \mathcal{E}_{rel} is almost identical in both social and non-social scenarios, the error is higher when parameter γ is present, most by 78% for RiverShort parameter λ and 45% for β . Overall we see that parameters μ, λ, P_{surv} and α are recovered with a small error $\mathcal{E}_{rel} \leq 0.16$, while for RiverShort only μ, λ are recovered well with $\mathcal{E}_{rel} \leq 0.19$.

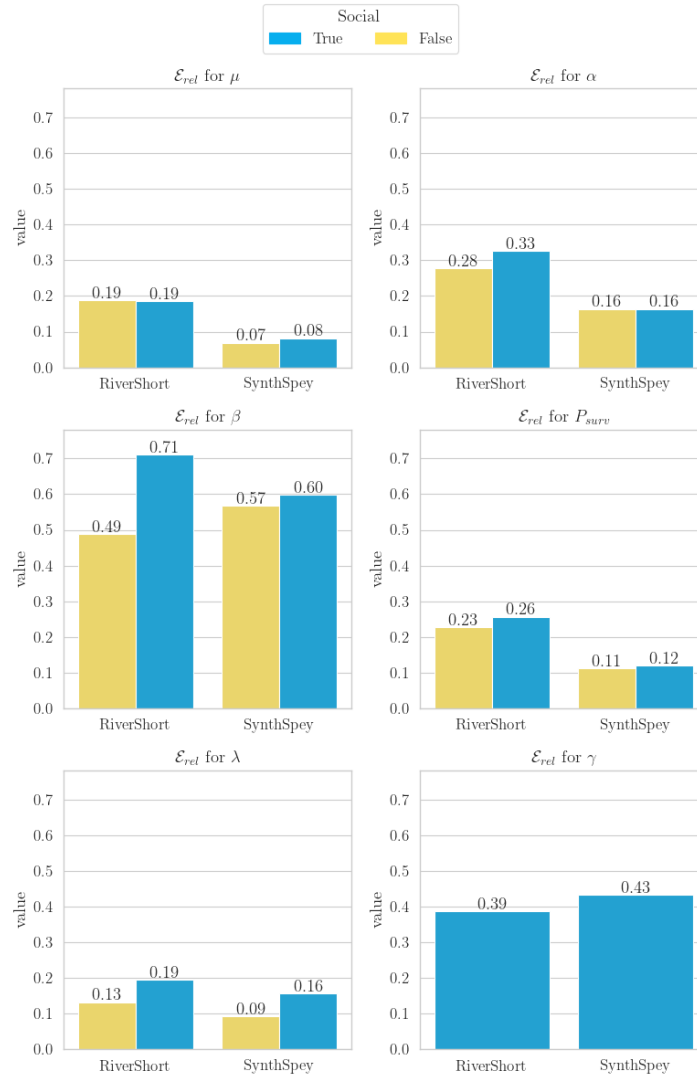


Figure 5.10: Results of relative error of prediction of target parameter \mathcal{E}_{rel} for each parameter for two river models RiverShort and SynthSpey, for models with and without social influence γ . Parameters μ, λ, P_{surv} and α are recovered with a small error $\mathcal{E}_{rel} \leq 0.16$, while for RiverShort only μ, λ are recovered well with $\mathcal{E}_{rel} \leq 0.19$. Posteriors of parameters γ and β are not recovered well by our modelling.

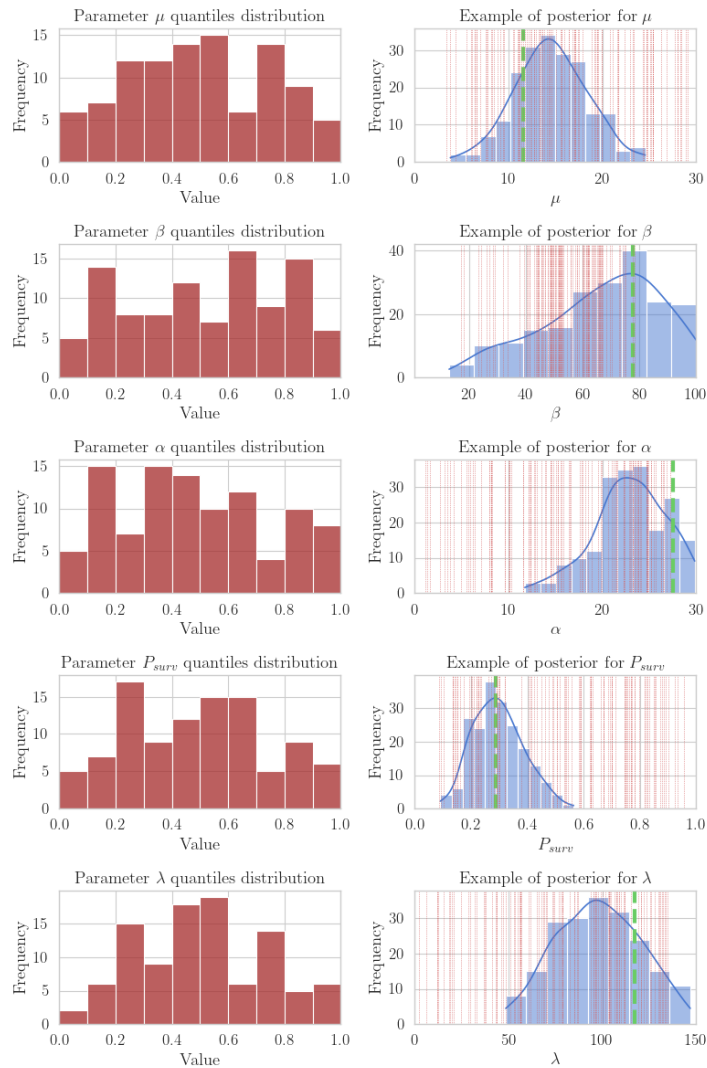


Figure 5.11: Comprehensive results of posterior estimation on the RiverShort model. The column on the left (in brown) shows the distribution of quantiles of the target value θ^\dagger sampled from the prior for each of $N_{rep} = 100$ repetitions of the algorithm. The right column shows an example from one single repetition with the true value of the parameter marked by green vertical line, the posterior distribution in blue, and predicted mean values of other repetitions in red.

5.3.2 Quantile distribution

If the predicted posterior has correct confidence intervals, the distribution of quantiles of the true value should be uniform. This assumption should be valid both when true value θ^\dagger is sampled multiple times from the prior as shown as presented in Figures 5.11 and 5.12 as well as when the process is repeated for different D^\dagger coming from the same $\mathcal{M}(\theta^\dagger)$ in

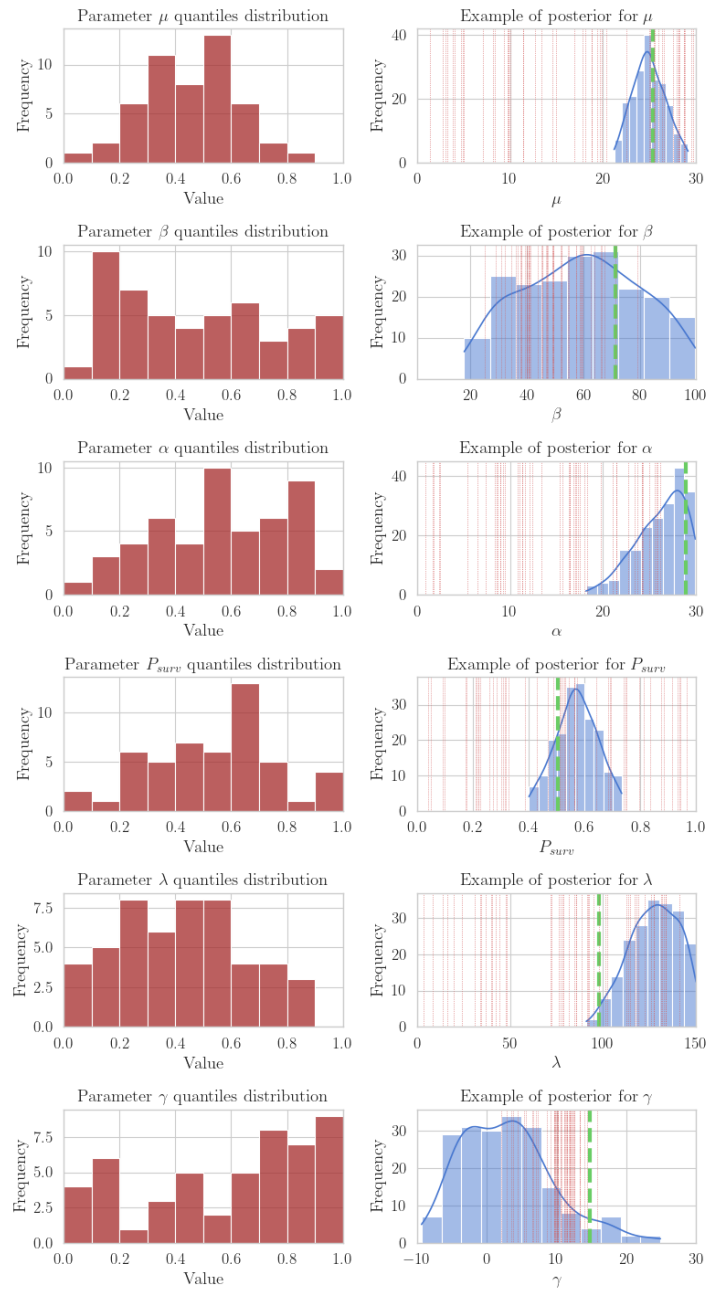


Figure 5.12: Comprehensive results of posterior estimation on the SynthSpey model. The column on the left (in brown) shows the distribution of quantiles of the target value θ^\dagger sampled from the prior for each of $N_{rep} = 50$ repetitions of the algorithm. The right column shows an example from one single repetition with the true value of the parameter marked by green vertical line, the posterior distribution in blue, and predicted mean values of other repetitions in red.

Figure 5.13. Figure 5.11 shows the results for parameter recovery for RiverShort model without social influence γ . The quantiles distribution fills the entire range 0 to 1 for all of the parameters, Under the scrutiny of the χ^2 test, quantile distributions for all parameters but α are significantly different than uniform distribution with α in RiverShort in with $p=0.07$ detailed in Table 5.5. Tables 5.5,5.6 and 5.7 provide aggregated results for all parameters, including p -value of a χ^2 test of uniformity and their z_{quant} values as defined following the equation 5.26. We provide them for completeness, however lack of apparent uniformity of quantiles suggests problems with biases in prediction of the posterior and shape of the resulting distribution that are visibly incorrect without detailed analysis of z_{quant} . z_{quant} seems incidentally under its critical value 1.96 for parameter β on SynthSpey ($p = 0.06$ for social and $p=0.03$ for non social), in Table 5.6. Also, quantiles for parameter γ in SynthSpey in table 5.7 with $p_{value} = 0.64$ suggest uniformity. Those are most likely false-positive results, caused by the simulation recovering back the prior that by definition, correctly captures the uncertainty, even if provides no additional knowledge.

The right column in Figure 5.11 shows an example posterior from one of the repetitions of the ABC algorithm with the true value generating original observations marked with green lines. We can see that for all parameters (apart from $\gamma = 0$), the posterior looks like a reasonable estimation of the target value. The red vertical lines show the mean value of the predicted posterior for all other repetitions of the algorithm, and as the true values are sampled from a prior, those two should be uniformly distributed. We can see that for parameter β , the mean values of predicted posteriors are clustered in the middle of the prior range, suggesting that predicted distribution is not very informative and close to uniform independently from the true target value.

system	social	μ				α			
		\mathcal{E}_{abs}	\mathcal{E}_{rel}	p_{value}	z_{score}	\mathcal{E}_{abs}	\mathcal{E}_{rel}	p_{value}	z_{score}
RiverShort	No	3.33	0.19	0.0	3.14	3.91	0.28	0.07	1.51
RiverShort	Yes	2.44	0.19	0.06	1.52	4.37	0.33	0.01	2.39
SynthSpey	No	0.6	0.07	0.0	6.07	3.74	0.16	1.0	5.84
SynthSpey	Yes	0.67	0.08	0.0	5.57	3.38	0.16	0.01	2.45

Table 5.5: Values of parameter approximation errors \mathcal{E}_{abs} \mathcal{E}_{rel} and p_{value} of χ^2 test of uniformity of the quantile distribution for parameters μ and α .

In Figure 5.12, we observe results for SynthSpey with the social component, similarly seeing recovery of some parameters but also clustering of mean values of distributions clustered around the centre for β and γ , explaining their high error.

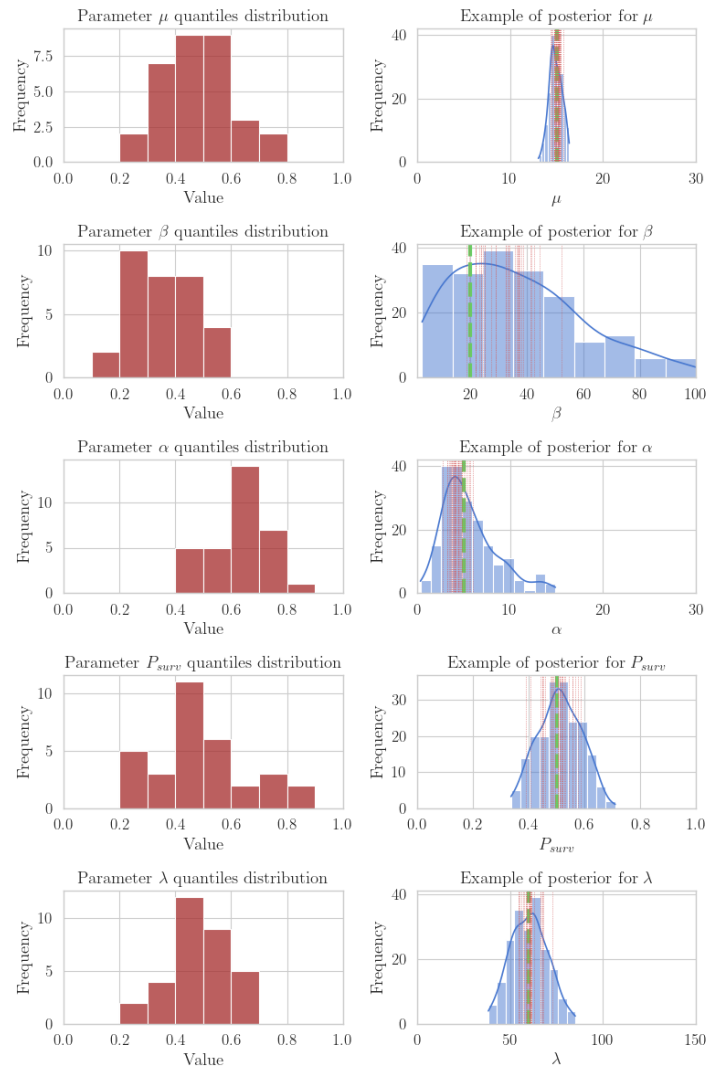


Figure 5.13: Repeated estimations of θ_A^\dagger parameter vector on RiverShort model without the social component. The column on the left (in brown) shows the distribution of quantiles of the target value θ_A^\dagger in predicted posterior for $N_{rep} = 25$ repetitions of the algorithm. The right column shows an example from one single repetition with the true value of the parameter marked by green vertical line, the posterior distribution in blue, and predicted mean values of other repetitions in red.

Alternatively, we look at the repeated ABC modelling of the posterior around the same parameter θ_A^\dagger in Figure 5.13. The quantile distribution is clearly not uniform and is centred around the middle, showing the overdispersion of the posterior as the true value of the parameter is more often in the centre of the distribution than its shape suggests. The red vertical lines on one of the predicted posteriors show the systematic bias in predicting parameter β and the broad shape of this posterior.

system	social	β				λ			
		\mathcal{E}_{abs}	\mathcal{E}_{rel}	$pvalue$	$zscore$	\mathcal{E}_{abs}	\mathcal{E}_{rel}	$pvalue$	$zscore$
RiverShort	No	20.11	0.49	0.01	2.32	11.61	0.13	0.0	4.39
RiverShort	Yes	26.81	0.71	0.01	2.5	16.01	0.19	1.0	2.75
SynthSpey	No	17.76	0.57	0.03	1.82	7.34	0.09	0.0	3.63
SynthSpey	Yes	22.9	0.6	0.06	1.55	12.97	0.16	0.0	2.71

Table 5.6: Values of parameter approximation errors \mathcal{E}_{abs} \mathcal{E}_{rel} and $pvalue$ of χ^2 test of uniformity of the quantile distribution for parameters β and λ .

system	social	P_{surv}				γ			
		\mathcal{E}_{abs}	\mathcal{E}_{rel}	$pvalue$	$zscore$	\mathcal{E}_{abs}	\mathcal{E}_{rel}	$pvalue$	$zscore$
RiverShort	No	0.1	0.23	0.0	3.41	-	-	-	-
RiverShort	Yes	0.13	0.26	0.0	3.09	9.34	0.39	0.01	2.47
SynthSpey	No	0.05	0.11	1.0	4.54	-	-	-	-
SynthSpey	Yes	0.05	0.12	0.0	3.09	9.67	0.43	0.64	0.35

Table 5.7: Values of parameter approximation errors \mathcal{E}_{abs} \mathcal{E}_{rel} and $pvalue$ of χ^2 test of uniformity of the quantile distribution for P_{surv} and γ .

5.3.3 Example of parameter recovery from real system

In Figure 5.14, we present the posteriors from ABC modelling of the data coming from a telemetry study on river Spey. We used the modelling with parameter γ as the difference in relative error on SynthSpey between social and non-social simulation. The narrow posterior for parameters μ with median value $1.94 \frac{m}{min}$ or $3.23 \frac{cm}{s}$, $\lambda = 8.29m$ and $P_{surv} = 86\%$ and $\alpha = 4.57$ suggest confidence in predicted value. The survival from analysis of the tracking data was 59.1% and differs significantly from the one we report, but that is expected, as we report intrinsic survival related to the actual movement distance. The median travel speed report from the analysis of the data was $4.2 \frac{m}{min}$ or $7 \frac{cm}{s}$. Those differences, however, are expected given different formulations of the intrinsic parameters compared to the observed data. The distribution of parameter β was very close to the provided prior (as expected based on simulated experiments). Parameter γ shows a broad distribution with a peak at a median of 14.75, which suggests possible social interaction. From previously simulated scenarios, it is clear that the posterior quality of γ is insufficient to draw conclusions about the social interactions. The width for the non-social parameters posteriors, apart from β , implies strong confidence in the predicted values.

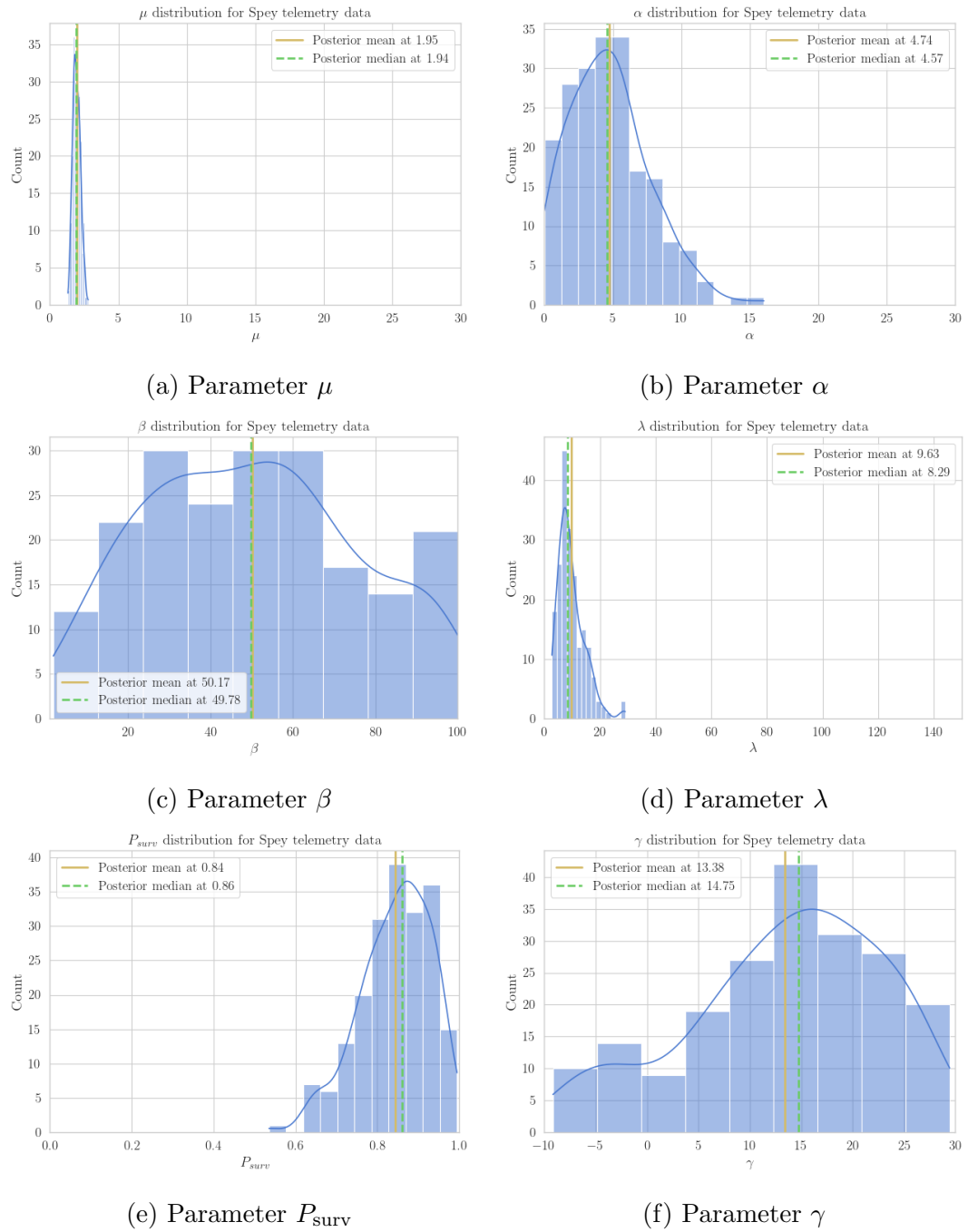


Figure 5.14: The posterior of parameters from simulation of the real data from the river Spey D_{spey}^\dagger . The narrow posterior for parameters μ with median value $1.94 \frac{m}{\text{min}}$, $\lambda = 8.29m$ and $P_{\text{surv}} = 0.86$ and $\alpha = 4.57$ suggest confidence in predicted value.

5.4 Conclusions

We presented a novel method of modelling juvenile salmon migration at a granular scale from sparse telemetry data. Presented approach provides a proof-of-concept for the direct modelling of interactions between fish, the environment and the observation process, which otherwise can only be very crude in typical acoustic telemetry modelling.

Our method was able to recover with reasonable accuracy four model parameters: mean speed μ , detectors range decay λ , probability of survival P_{surv} and dispersion α , in two simulated scenario, and from real telemetry data on river Spey.

The comprehensive testing showed significant challenges in removing bias and providing reliable confidence intervals. Promisingly, the method performed better on a realistic river model SyntSpey than on a simplified scenario RiverShort, indicating that the method scales well to larger simulations. It is important because the computation of the simulation of the RiverShort is 6 times quicker, allowing us to realistically test more design changes and hyperparameters.

The common problem with both individual-based modelling and simulation-based inference is the computational complexity. Due to the GPU parallelisable design of our algorithm, we have overcome this problem. The use of `tensorflow-graph` functional approach allowed to leverage GPU memory caching effectively and increases computation time about 2-fold. The precise execution time varies as the matrix of $N \times K \times B$, has to fit into GPU memory to be parallelised. For a representative river with $N = 140$ fish $K = 12$ receivers and batch size of $B = 2000$ on a 11GB NVIDIA 2080Ti GPU computations take approximately 3 minutes for the simulation of a week of migration, resulting in a simulation time of 0.1 seconds per single simulation.

The earlier version of this simulation used using the vectorised approach on a CPU with the numerical `numpy` library took about 10 seconds for each simulation, 100 times slower than the GPU accelerating solution. The library used for that preliminary study `astroABC` python package [Jennings and Madigan \(2017\)](#) is designed for computations on High-Performance Clusters with multiple CPUs. However, our approach offers easier parallelisation and can also be further distributed on a GPU cluster.

In our approach we try to recover specific parameters which produced given observations. The true distribution of parameters that can produce the same observation is unknown and makes it difficult to reliably quantify uncertainty. When repeatedly simulating the posterior from the same parameter vector θ_A , the quantile distribution for most parameters suggested overdispersion of the posterior (too wide confidence intervals). This

is preferable to the underdispersion that signals an underestimation of the uncertainty. Wider confidence intervals provide a solid foundation for reasoning based on the recovered parameter values and can be further revised as closer estimates are needed. Overall, the overdispersion in the case of repeated sampling of θ_A may be a result of a situation where different sets of parameters can produce similar observations and might not necessarily indicate a problem with the inference method. To provide a broader measure of how the posterior looks like for different parameters, we calculate the quantile distribution for different parameters sampled from the prior. In this case, we observed a lack of uniformity, showing the biases in the modelling that have to be better understood and accounted for to ensure better convergence. In some cases where quantile distribution looked more correct, we observed a problem highlighted by [Prangle et al. \(2014\)](#) that recovering back prior distribution leads to the false positive result of the convergence test.

Our model presented a challenge in terms of the design of the summary statistic and distance metrics. Resulting biases show that often convergence was influenced by non-informative elements of the summary statistic. As the recovered distribution differs more from the prior, the distance metric might become locally distorted. We have explored the use of the covariance matrix instead of the median absolute deviation matrix and Mahalanobis distance instead of weighted Euclidean distance, seeing detriment in both cases. One suggestion from [Prangle \(2017\)](#) is to re-calculate the co-variance matrix with every iteration of the algorithm, which is an approach that can improve the convergence of our method.

We explored different scaling parameters κ for the importance sampling and percentile acceptance threshold h . Those two parameters, when too large, lead to slower convergence without clear improvement. If reduced, they would lead to numerical instability and unrealistic multi-modal posterior distribution. Investigation regarding a more subtle decrease of distance threshold in higher iterations could lead to additional gains.

The choice of time step in the discretisation of the movement model is a balance between how realistic the model is and the computational cost. [Paun et al. \(2019\)](#) explored how the sampling in random-walk models affect the recovery of parameters in Bayesian modelling, highlighting the mismatch resulting from a low sampling rate. In our case choice of movement model sampling interval of 1 minute to match that of the observational process was dictated purely by convenience and is one of the possible explanations for biases observed in the results.

We model the imperfection of observations in the river telemetry together with the underlying movement of the fish. [Fleming et al. \(2021\)](#) highlights that biases introduced

by the registration errors can be not only severe but difficult to model without a better understanding of the process generating them. We modelled parameter λ , a distance-decay of the probability of detection from each receiver as the mean value across the whole array. Applying an informed error modelling to the telemetry data itself could provide better quality input data. Optimally both λ and P_{detmax} would be unique parameters k for each receiver and inferred from the model. However, that would make the model unique to every telemetry study and increase the complexity of fitting. The equation of detections can be improved by modelling the observation process with a hurdle model, where detections can be dense at times but still have a high rate of missed fish.

In our direct observations in chapter 4 we have seen salmon smolts moving in shoals. To prove that such behaviour occurs in the wild using sparse telemetry data hinges on many mechanistic assumptions of our simulation model. Our definition of social influence has been limited in order to retain the tensor structure of the model operations that are necessary for parallel computations.

The social distance parameter γ in our modelling seems to behave similarly to the drift component β in countering the stochastic component α . As shown by [Calabrese et al. \(2018\)](#), the correct approach to quantifying collective behaviour would instead show the correlation in the stochastic component. This presents a challenge for future work to define the correlation of velocity so that - it ties the stochastic element of movement without preventing individual variation from causing a breakup of travelling shoals. Unlike animals living in herds, the modelling of migrating shoals must allow some mechanism of periodic aggregations and dissolutions of groups. This might require an increase in the number of parameters describing both attraction and repulsion between individuals.

One of the limitations of the current model is that it assumes the same underlying parameters of movement throughout the migration. As mentioned earlier, the choice of the river Spey as the testing scenario was partially motivated by a lack of lochs or other serious obstacles that would vastly affect this assumption. In further work, we would like to explore a more complex model where a number of environments, such as lakes, rivers, canals and estuaries are modifying the movement parameters for the fish.

As observed in Chapter 4, salmon migrating in the flume exhibit different periods and propensity to migrate and choose different flow conditions across long periods. We suggest that such multiple-state behaviour can be modelled as HMM, with each of the states having its own parameters associated with it. The observations from a camera that has excellent spatial accuracy compared to telemetry data would allow us to move focus from the modelling of movement to the parameters of the collective behaviour.

The method requires no additional adaptation to use on other telemetry data from other rivers in the “Missing Salmon” project. As our understanding of parameters improves, the comparison of results between the systems might provide novel insights, especially about the stochastic component of movement in different rivers.

Chapter 6

Conclusions

Atlantic salmon is an important migratory species connected with its expansive natural environment in complex ways. As most of its populations face decline, understanding its collective behaviour and resulting population dynamic plays a crucial role in preserving Atlantic salmon and its ecosystems. Downstream migration is an important part of life history, understudied due to practical difficulties in observing the fish during that time. In this work, I focused on this aspect with a range of approaches.

In Chapter 2, I established the baseline flow value for the Atlantic salmon smolts to respond to in lacustrine environments, informing the design of river infrastructure and future studies regarding their ability to find the correct outflow or avoid dangerous water intakes of hydropower facilities.

In Chapter 4, I quantified the effect social behaviour on the navigation of an obstacle by migrating smolts, showing an advantage to the fish shoaling even when mostly passively migrating at night. The existence of social effects during the migration would be an important density-dependent effect on the species' survival and migration success, which has not yet been widely adopted in the ecological modelling of the salmon population.

In both Chapters 2 and 4 I uncovered some important differences between wild and hatchery smolts that need to be considered in the design of future studies, but can also be directly helpful in ecological engineering applications and conservation efforts. Specifically, I observed a stronger social effect on the otherwise less informed farmed fish, and a smaller threshold required by them to initiate movement than for the wild fish.

In Chapter 3, I improved the animal tracking method, which is essential for further studies of similar-looking animals, such as salmon smolts in groups with complex movement patterns.

In Chapter 5, I showed the ability of a interpretable individual-based model to partially

recover parameters from simulated and real telemetry data while achieving very high computational efficiency, opening the possibility to a new type of modelling to be applied to animal telemetry.

Understanding the fine-scale behaviour of smolts in the presence of obstacles and hazards on their migratory route is crucial in conservation efforts and sustainable river development. Hydroacoustic flow profile of the challenging bodies of water is increasingly mapped and understood, but fine-scale tracking of small fish is still impossible on the scale that can show precise levels of flow to deter or attract fish. The right amount of flow is necessary to aid the fish in navigation over standing water, that otherwise can significantly delay or even prevent the successful migration. Knowledge of what the fish experiences as excessive flow, is necessary to create a hydroacoustic barrier preventing fish from entering dangerous man-made structures, but also do not repel them from entering the fish passes.

In Chapter 2 I used smolts of three origins, in conditions that allowed the fish to find a comfortable holding location within or outside of the main flow, providing a realistic estimate of flow difference required for fish to change orientation. Large differences can be observed when measuring the same phenomena in different experimental conditions, such as smolts swimming speeds in racetracks, flumes and in the wild (Holleman et al., 2022). A similar bias is likely to apply to detection of a minimal threshold for reaction to flow change. This investigation saw a wider range of response values as it provided smolts with a more realistic environment than a smaller tank with a laminar flow would. This led to the detection of a more heterogeneous flow response, especially between fish of different origins, but likely closer to what can be expected in the field scenario where such a study would be impractical to conduct using traditional methods.

Directly observing juvenile salmon in the wild is possible but requires long-term video surveillance, such as in Kemp and Williams (2008) to monitor a culvert. Despite the improvements in imaging technology, this remains a challenge, as it requires underwater recording in infra-red illumination of small, fast-moving animals. The work presented in Chapter 3 sets a direction for visual tracking that relies on learning and predicting a movement model of each tracked animal, independent of analytical assumptions about its scale, speed or appearance.

The method does not require explicit parametrisation of the tracking model and only requires labelling of a single animal movement, which requires significantly less effort than labelling of multi-object data. Despite those minimal requirements, it is able to track multiple identical objects in crowded scenes directly applicable to studies of shoaling fish. The use of simulated data in the presented study, if confirmed by better tracking of fish

recordings can vastly improve the robustness of ecological trackers that otherwise might fail in the most crucial moments when animals are behaving unusually - responding to a threat or navigating turbulent waters. Many modern visual trackers are leveraging the rich visual detail from the high-resolution cameras that are now ubiquitous. In underwater studies, the improvements to imaging sonars are providing valuable data on fish movement, but with very low temporal and spatial resolution. The development of a system that focuses on matching tracking with the movement model addresses those limitations well by aligning the method of study with the phenomena studied.

In the design of both hydroacoustic barriers and fish passes, the velocity to which fish respond under natural conditions is difficult to measure indirectly, where the effect of group sizes is unknown as well as the effective group sizes when fish are navigating challenging scenarios. The study in Chapter 4 tackled the question of social effect in decision-making in the face of an obstacle, in laboratory conditions resembling a migration in a narrow stream.

Using the previous version of the visual tracker, it was still possible to quantify observations of fish travelling in the relatively non-turbulent area of the flume and on the aggregation that never exceeded 10 fish and usually was limited to groups of 5. In the artificial river, smolts of both farmed and wild origin exhibited clear downstream migratory behaviour and collective decision-making in the face of an obstacle. This study only analysed the decisions made by single and multiple fish approaching the obstacle from a group of 10 fish in the experimental arena over 14 hours. The night-time tracking allows observing fish as they make decisions and within a number of repetitions of the experiment, measure the influence of different flow conditions on their route selection.

As the route selection was mediated by social behaviour, we expect that the same will be true to the threshold required for reaction to flow as measured in Chapter 2. This study highlights the importance of considering group effect in the fish decision-making during the migration, and limitations of the approach that consider migrants making independent decisions.

A good body of evidence suggests the importance of social cues to migration timing (Thorstad et al., 2012b; Kururvilla et al., 2024), but the social effect on the success of migration is still difficult to quantify. Previously, it was observed that fish might shoal as a result of the presence of an obstacle to the migration (Vowles et al., 2014). It is also known that in a group, fish might be more reactive to flow as the groups' ability to sense the flow gradient increases (Torney et al., 2009; Berdahl et al., 2013). This study confirms that when presented with the ability to shoal, fish will be able to make better

decisions by following more informed individuals. Further work is needed to establish the precise mechanism. We observed that hatchery fish - though less skilled at finding the optimal migratory route - were more likely to group and were more sensitive to small flow differential.

Hatchery smolts, used in a responsible way, can play an important role in the conservation of Atlantic salmon (Lennox et al., 2021). This work shows that their utility can be high for the purpose of testing river infrastructure design. The smolts used in this experiment exhibited behaviour that was consistently different than wild smolts, which might make it easier to test hypothesis that would otherwise be too difficult to measure with limited sample and effect sizes available with wild smolts. For instance, based on the results in Chapter 4 it can be assumed that hatchery smolts, will school more readily and be worse at finding the unobstructed pathway. When designing a pathway for migration, that will allow safe passage of hatchery smolts, we can have confidence that wild fish will be able to navigate it as well. In river systems where hatchery smolts are already present, and they can be used to bootstrap studies of wild smolts such as in Fernandes et al. (2015). In such places, the design of a direct observation experiment outlined previously can be validated ahead of the migration season with the release of hatchery smolts that can be provided year-round from different facilities. A better understanding of the genetic differences between wild salmon populations and different hatchery smolts Pritchard (2023), provide another route to understand the difference between the innate abilities of juvenile salmon, and ones gained through the development of different environments Johnsson et al. (2001).

The Approximate Bayesian Computation method of modelling Atlantic salmon migration presented in Chapter 5, promises to allow testing of the collective movement hypothesis or more complex mechanism of movement within the sparse and imperfect telemetry data. The method presented partially recovered parameters of a discrete movement model inspired by an OU process. The main difficulty of this method is the design of summary statistics of the data, which will be informative but also adhere as much as possible to the normal distribution. Thanks to the the very high computational efficiency of this approach, it is possible to continue refining the simulation and its resulting statistics until the confidence in the method is reasonable for the purpose of answering a specific behavioural question - for instance, the presence of collective motion. Following the studies of Berdahl et al. (2017) and Kururvilla et al. (2024), this approach poses a question in a Bayesian context of relative evidence of different explanations of the imperfect observations. As the data availability increases, confirmation of theoretical models of the collective decision-

making becomes possible with the proposed approach.

6.1 Future work

The work described in this thesis leveraged modern technology and computational techniques and points to future research avenues. The measurement of flow value reaction in Chapter 2 can be naturally followed by such a study with multiple fish observed in a tank at the same time, to understand any possible social effects in the reaction to flow. Preliminary work done for this thesis shows that such a study would need a very high level of automation of extraction of reaction times and locations, as with the number of fish, manual labelling, and marking of positions will become too burdensome. To balance the increase in uncertainty resulting from the heterogeneity of this scenario, an increase in repetitions would be required, and possibly a study of hatchery smolts would be easier to organise. In our experimentation the smolts from freshwater pens had a reaction closer to the wild smolts than those from an indoor facility and should be preferred as a model in future studies. Given the increased social effect observed in the choice chamber experiment in Chapter 4 it would also be more likely to observe such an effect in hatchery smolts than in the wild ones if it exists.

An animal tracker with the Deep Predictor module developed in Chapter 3 would need to be tested on the tracking data developed in qualitative testing of the visual data extraction in Chapter 4. Confirming that the model works on the difficult task of the infra-red observations of fast-moving fish would open the way to perform a more detailed analysis of the collective motion already captured during the migration experiments in the flume. The basic collective metrics of group cohesion: nearest neighbour distance, average velocity vector, cosine similarity of the velocity vector, etc., can be used to analyse how different-sized effective groups are moving in the experimental river, when an obstacle does not impede their movement. With better accuracy in calculating motion, the mode of movement can be determined - whether the fish moves passively with a flow or swims with a positive or negative rheotaxis. Additional appearance classification can be easily added as part of the deep learning framework to visually distinguish the orientation of the fish. Improved tracking techniques will allow us to combine tracks across multiple cameras, in a process known as re-identification. Longer term tracks of the same individual will allow the creation of realistic movement models that can form a better basis for simulation-based analysis of telemetry data as presented in Chapter 5.

The study of collective movement presented in Chapter 4 can be repeated using an

existing fish pass or a culvert in order to study the behaviour of the wild fish during their migration. Using the same setup of network-connected, inexpensive cameras with on-board processing and data transmission should be possible for the entire period of migration at a lower cost compared to a telemetry study with a sufficient number of tagged animals for the study of collective motion. Ability to observe fish making a route choice decision in the wild, with periodic measurements of flow, temperature and other conditions would provide a valuable complement to the usual, sparse, telemetry data gathering.

Such a setup would be able to provide valuable snapshot information about the real numbers of travelling fish and their possible group structure to better inform a simulation design of movement models for the telemetry data with the ABC method. Additionally, the same ABC method can be used to model the observed fish movement directly, linking those two levels of observation with the same movement model mechanism at two different scales.

Revision of the simulation with a more realistic hurdle-based observation process, collective motion definition and introduction of parameters related to the environment, such as a river or a lake, should allow for a better fit to the experimental data.

In summary, this thesis presented diverse mathematical methods that refined our ability to test hypotheses related to Atlantic salmon downstream migration. Using different modalities of data and different spatial and temporal scales, I confirmed an important collective mechanism in smolts decision-making making and created a clear direction for the future research to quantify and incorporate the collective movement hypothesis to future scientific studies and conservation efforts.

Bibliography

- Aarestrup, K., Jepsen, N., Rasmussen, G., and Økland, F. (1999). Movements of two strains of radio tagged Atlantic salmon, *Salmo salar* L., smolts through a reservoir. *Fisheries Management and Ecology*, 6(2):97–107.
- Aas, Ø., Klemetsen, A., Einum, S., and Skurdal, J. (2011). Atlantic Salmon Ecology.
- Abadi, M., Agarwal, A., Barham, P., Brevdo, E., Chen, Z., Citro, C., Corrado, G. S., Davis, A., Dean, J., Devin, M., Ghemawat, S., Goodfellow, I., Harp, A., Irving, G., Isard, M., Jia, Y., Jozefowicz, R., Kaiser, L., Kudlur, M., Levenberg, J., Mane, D., Monga, R., Moore, S., Murray, D., Olah, C., Schuster, M., Shlens, J., Steiner, B., Sutskever, I., Talwar, K., Tucker, P., Vanhoucke, V., Vasudevan, V., Viegas, F., Vinyals, O., Warden, P., Wattenberg, M., Wicke, M., Yu, Y., and Zheng, X. (2015). TensorFlow: Large-Scale Machine Learning on Heterogeneous Distributed Systems.
- Adams, C. (1999). Does the underlying nature of polymorphism in the Arctic charr differ across the species? *ISACF Information Series*. 7. 61-69.
- Adams, C. E., Chavarie, L., Rodger, J. R., Honkanen, H. M., Thambithurai, D., and Newton, M. P. (2022a). An opinion piece: the evolutionary and ecological consequences of changing selection pressures on marine migration in Atlantic salmon. *Journal of Fish Biology*, 100(4):860–867.
- Adams, C. E., Honkanen, H. M., Bryson, E., Moore, I. E., MacCormick, M., and Dodd, J. A. (2022b). A comparison of trends in population size and life history features of Atlantic salmon (*Salmo salar*) and anadromous and non-anadromous Brown trout (*Salmo trutta*) in a single catchment over 116 years. *Hydrobiologia*, 849(4):945–965.
- Adams, C. E., Huntingford, F. A., Turnbull, J. F., and Beattie, C. (1998). Alternative competitive strategies and the cost of food acquisition in juvenile Atlantic salmon.

- Akçay, S., Kundegorski, M. E., Devereux, M., and Breckon, T. P. (2016). Transfer learning using convolutional neural networks for object classification within X-ray baggage security imagery. In *2016 IEEE International Conference on Image Processing (ICIP)*, pages 1057–1061, Phoenix, AZ, USA. IEEE.
- Åkesson, S., Boström, J., Liedvogel, M., and Muheim, R. (2014). Animal navigation. In *Animal Movement Across Scales*, pages 151–178. Oxford University Press.
- Alerstam, T. (2006). Conflicting Evidence About Long-Distance Animal Navigation. *Science*, 313(5788):791–794.
- Aodha, O. M., Gibb, R., Barlow, K. E., Browning, E., Firman, M., Freeman, R., Harder, B., Kinsey, L., Mead, G. R., Newson, S. E., Pandourski, I., Parsons, S., Russ, J., Szodoray-Paradi, A., Szodoray-Paradi, F., Tilova, E., Girolami, M., Brostow, G., and Jones, K. E. (2018). Bat detective—Deep learning tools for bat acoustic signal detection. *PLOS Computational Biology*, 14(3):e1005995.
- Aoki, I. (1982). A Simulation Study on the Schooling Mechanism in Fish. *Nippon Suisan Gakkaishi*, 48(8):1081–1088.
- Armstrong, J., Kemp, P., Kennedy, G., Ladle, M., and Milner, N. (2003). Habitat requirements of Atlantic salmon and brown trout in rivers and streams. *Fisheries Research*, 62(2):143–170.
- Arnold, G. P., Webb, P. W., and Holford, B. H. (1991). The Role of the Pectoral Fins in Station-Holding of Atlantic Salmon Parr (*Salmo Salar* L.). *Journal of Experimental Biology*, 156(1):625–629.
- Avgar, T., Deardon, R., and Fryxell, J. M. (2013). An empirically parameterized individual based model of animal movement, perception, and memory. *Ecological Modelling*, 251:158–172.
- Babin, A. B., Ndong, M., Haralampides, K., Peake, S., Jones, R., Curry, R. A., and Linnansaari, T. (2020). Migration of Atlantic salmon (*Salmo salar*) smolts in a large hydropower reservoir. *Canadian Journal of Fisheries and Aquatic Sciences*, 77(9):1463–1476.
- Bacchus, M. D., Domenici, P., Killen, S. S., McCormick, M. I., and Nadler, L. E. (2024). Kinematic performance declines as group size increases during escape responses in a schooling coral reef fish. *Frontiers in Fish Science*, 1.

- Bacon, P. J., Palmer, S. C. F., MacLean, J. C., Smith, G. W., Whyte, B. D. M., Gurney, W. S. C., and Youngson, A. F. (2009). Empirical analyses of the length, weight, and condition of adult Atlantic salmon on return to the Scottish coast between 1963 and 2006. *ICES Journal of Marine Science*, 66(5):844–859.
- Banerjee, S., Alvey, L., Brown, P., Yue, S., Li, L., and Scheirer, W. J. (2021). An assistive computer vision tool to automatically detect changes in fish behavior in response to ambient odor. *Scientific Reports*, 11(1):1002.
- Beaumont, M. A. (2010). Approximate Bayesian Computation in Evolution and Ecology. *Annual Review of Ecology, Evolution, and Systematics*, 41(1):379–406.
- Belletti, B., Garcia De Leaniz, C., Jones, J., Bizzi, S., Börger, L., Segura, G., Castelletti, A., Van De Bund, W., Aarestrup, K., Barry, J., Belka, K., Berkhuisen, A., Birnie-Gauvin, K., Bussettini, M., Carolli, M., Consuegra, S., Dopico, E., Feierfeil, T., Fernández, S., Fernandez Garrido, P., Garcia-Vazquez, E., Garrido, S., Giannico, G., Gough, P., Jepsen, N., Jones, P. E., Kemp, P., Kerr, J., King, J., Lapińska, M., Lázaro, G., Lucas, M. C., Marcello, L., Martin, P., McGinnity, P., O’Hanley, J., Olivo Del Amo, R., Parasiewicz, P., Pusch, M., Rincon, G., Rodriguez, C., Royte, J., Schneider, C. T., Tummers, J. S., Vallesi, S., Vowles, A., Verspoor, E., Wannigen, H., Wantzen, K. M., Wildman, L., and Zalewski, M. (2020). More than one million barriers fragment Europe’s rivers. *Nature*, 588(7838):436–441.
- Benhaïm, D., Leblanc, C. A., Horri, K., Mannion, K., Galloway, M., Leeper, A., Knobloch, S., Sigurgeirsson, O., and Thorarensen, H. (2020). The effect of triploidy on the performance, gut microbiome and behaviour of juvenile Atlantic salmon (*Salmo salar*) raised at low temperature. *Applied Animal Behaviour Science*, 229:105031.
- Berdahl, A., Torney, C. J., Ioannou, C. C., Faria, J. J., and Couzin, I. D. (2013). Emergent Sensing of Complex Environments by Mobile Animal Groups. *Science*, 339(6119):574–576.
- Berdahl, A., Westley, P. A., and Quinn, T. P. (2017). Social interactions shape the timing of spawning migrations in an anadromous fish. *Animal Behaviour*, 126:221–229.
- Berdahl, A., Westley, P. A. H., Levin, S. A., Couzin, I. D., and Quinn, T. P. (2014). A collective navigation hypothesis for homeward migration in anadromous salmonids. *Fish and Fisheries*, 17(2):525–542.

- Bergmann, P., Meinhardt, T., and Leal-Taixe, L. (2019). Tracking Without Bells and Whistles. In *2019 IEEE/CVF International Conference on Computer Vision (ICCV)*, pages 941–951, Seoul, Korea (South). IEEE.
- Bertinetto, L., Valmadre, J., Henriques, J. F., Vedaldi, A., and Torr, P. H. S. (2016). Fully-Convolutional Siamese Networks for Object Tracking. In *Computer Vision – ECCV 2016 Workshops*, volume 9914, pages 850–865, Cham. Springer International Publishing.
- Bewley, A., Ge, Z., Ott, L., Ramos, F., and Upcroft, B. (2016). Simple Online and Realtime Tracking. *2016 IEEE International Conference on Image Processing (ICIP)*, pages 3464–3468.
- Blackwell, P. G., Niu, M., Lambert, M. S., and LaPoint, S. D. (2016). Exact Bayesian inference for animal movement in continuous time. *Methods in Ecology and Evolution*, (7):184–195.
- Bochinski, E., Eiselein, V., and Sikora, T. (2017). High-Speed tracking-by-detection without using image information. In *2017 14th IEEE International Conference on Advanced Video and Signal Based Surveillance (AVSS)*, pages 1–6, Lecce, Italy. IEEE.
- Bolshakov, C. V., Chernetsov, N., Mukhin, A., Bulyuk, V. N., Kosarev, V., Ktitorov, P., Leoke, D., and Tsvey, A. (2007). Time of nocturnal departures in European robins, *Erithacus rubecula*, in relation to celestial cues, season, stopover duration and fat stores. *Animal Behaviour*, 74(4):855–865.
- Bouwmans, T., Baf, F. E., and Vachon, B. (2008). Background Modeling using Mixture of Gaussians for Foreground Detection - A Survey. page 20.
- Brackley, R., Lucas, M. C., Thomas, R., Adams, C. E., and Bean, C. W. (2018). Comparison of damage to live v. euthanized Atlantic salmon *Salmo salar* smolts from passage through an Archimedean screw turbine. *Journal of Fish Biology*, 92(5):1635–1644.
- Brattland, C. and Mustonen, T. (2018). How Traditional Knowledge Comes to Matter in Atlantic Salmon Governance in Norway and Finland. *ARCTIC*, 71(4):375–392.
- Calabrese, J. M., Fleming, C. H., Fagan, W. F., Rimmler, M., Kaczensky, P., Bewick, S., Leimgruber, P., and Mueller, T. (2018). Disentangling social interactions and environmental drivers in multi-individual wildlife tracking data. *Philosophical Transactions of the Royal Society B: Biological Sciences*, 373(1746):20170007.

- Campbell, J. A., Shry, S., Calles, O., and Hölker, F. (2024). Application of Animal Movement Models to Acoustic Telemetry Positioning. In *Advances in Hydraulic Research*, pages 29–41. Springer Nature Switzerland, Cham.
- Cetintas, O., Brasó, G., and Leal-Taixé, L. (2023). Unifying Short and Long-Term Tracking with Graph Hierarchies. In *2023 IEEE/CVF Conference on Computer Vision and Pattern Recognition (CVPR)*, pages 22877–22887, Vancouver, BC, Canada. IEEE.
- Chabot, D., Dillon, C., and Francis, C. (2018). An approach for using off-the-shelf object-based image analysis software to detect and count birds in large volumes of aerial imagery. *Avian Conservation and Ecology*, 13:15.
- Chavarie, L., Honkanen, H. M., Newton, M., Lilly, J. M., Greetham, H. R., and Adams, C. E. (2022). The benefits of merging passive and active tracking approaches: New insights into riverine migration by salmonid smolts. *Ecosphere*, 13(5):e4045.
- Chin, T. M., Vazquez-Cuervo, J., and Armstrong, E. M. (2017). A multi-scale high-resolution analysis of global sea surface temperature. *Remote Sensing of Environment*, 200:154–169.
- Chon, T.-S., Park, Y. S., Moon, K. H., and Cha, E. Y. (1996). Patternizing communities by using an artificial neural network. *Ecological Modelling*, 90(1):69–78.
- Christin, S., Hervet, É., and Lecomte, N. (2019). Applications for deep learning in ecology. *Methods in Ecology and Evolution*, 10(10):1632–1644.
- Chu, P., Fan, H., Tan, C. C., and Ling, H. (2019). Online Multi-Object Tracking with Instance-Aware Tracker and Dynamic Model Refreshment. *arXiv:1902.08231 [cs]*.
- Cochran, W. W., Mouritsen, H., and Wikelski, M. (2004). Migrating Songbirds Recalibrate Their Magnetic Compass Daily from Twilight Cues. *Science*, 304(5669):405–408.
- Codling, E. A. and Dumbrell, A. J. (2012). Mathematical and theoretical ecology: linking models with ecological processes. *Interface Focus*, 2(2):144–149.
- Connor, W. P., Steinhorst, R. K., and Burge, H. L. (2003). Migrational Behavior and Seaward Movement of Wild Subyearling Fall Chinook Salmon in the Snake River. *North American Journal of Fisheries Management*, 23.

- Cook, S. R., Gelman, A., and Rubin, D. B. (2006). Validation of Software for Bayesian Models Using Posterior Quantiles. *Journal of Computational and Graphical Statistics*, 15(3):675–692.
- Coombs, S., Bak-Coleman, J., and Montgomery, J. (2020). Rheotaxis revisited: a multi-behavioral and multisensory perspective on how fish orient to flow. *Journal of Experimental Biology*, 223(23):jeb223008.
- Cooper, B., Adriaenssens, B., and Killen, S. S. (2018). Individual variation in the compromise between social group membership and exposure to preferred temperatures. *Proceedings of the Royal Society B: Biological Sciences*, 285(1880):20180884.
- Couzin, I. D., Krause, J., Franks, N. R., and Levin, S. A. (2005). Effective leadership and decision-making in animal groups on the move. *Nature*, 433(7025):513–516.
- Cresswell, K. A., Satterthwaite, W. H., and Sword, G. A. (2011). Understanding the evolution of migration through empirical examples. In *Animal Migration*, pages 6–16. Oxford University Press.
- Croft, S., Budgey, R., Pitchford, J. W., and Wood, A. J. (2015). Obstacle avoidance in social groups: new insights from asynchronous models. *Journal of The Royal Society Interface*, 12(106):20150178–20150178.
- Dadswell, M. J., Spares, A. D., Reader, J. M., and Stokesbury, M. J. W. (2010). The North Atlantic subpolar gyre and the marine migration of Atlantic salmon *Salmo salar*: the ‘Merry-Go-Round’ hypothesis. *Journal of Fish Biology*, 77(3):435–467.
- Dalal, N. and Triggs, B. (2005). Histograms of Oriented Gradients for Human Detection. In *2005 IEEE Computer Society Conference on Computer Vision and Pattern Recognition (CVPR’05)*, volume 1, pages 886–893, San Diego, CA, USA. IEEE.
- Dalziel, B. D., Corre, M. L., Côté, S. D., and Ellner, S. P. (2016). Detecting collective behaviour in animal relocation data, with application to migrating caribou. *Methods in Ecology and Evolution*, 7(1):30–41.
- Darwall, W. and IUCN (2022). *Salmo salar*: The IUCN Red List of Threatened Species 2023: e.T19855A67373433.
- del Mar Delgado, M., Miranda, M., Alvarez, S. J., Gurarie, E., Fagan, W. F., Penteriani, V., di Virgilio, A., and Morales, J. M. (2018). The importance of individual variation in

- the dynamics of animal collective movements. *Philosophical Transactions of the Royal Society B: Biological Sciences*, 373(1746):20170008.
- Del Moral, P. (1997). Nonlinear filtering: Interacting particle resolution. *Comptes Rendus de l'Académie des Sciences - Series I - Mathematics*, 325(6):653–658.
- Dell, A. I., Bender, J. A., Branson, K., Couzin, I. D., de Polavieja, G. G., Noldus, L. P. J. J., Pérez-Escudero, A., Perona, P., Straw, A. D., Wikelski, M., and Brose, U. (2014). Automated image-based tracking and its application in ecology. *Trends in Ecology & Evolution*, 29(7):417–428.
- Dendorfer, P., Rezatofghi, H., Milan, A., Shi, J., Cremers, D., Reid, I., Roth, S., Schindler, K., and Leal-Taixé, L. (2020). MOT20: A benchmark for multi object tracking in crowded scenes.
- Dengler, J. and Oldeland, J. (2010). Effects of sampling protocol on the shapes of species richness curves. *Journal of Biogeography*, 37(9):1698–1705.
- Derkarabetian, S., Castillo, S., Koo, P. K., Ovchinnikov, S., and Hedin, M. (2019). A demonstration of unsupervised machine learning in species delimitation. *Molecular Phylogenetics and Evolution*, 139:106562.
- DeVries, P., Goetz, F., Fresh, K., and Seiler, D. (2004). Evidence of a Lunar Gravitation Cue on Timing of Estuarine Entry by Pacific Salmon Smolts. *Transactions of the American Fisheries Society*, 133(6):1379–1395.
- Diack, G., Bull, C., Akenhead, S. A., van der Stap, T., Johnson, B. T., Rivot, E., Patin, R., Hernvann, P.-Y., Schubert, A., Bird, T., Saunders, M., and Crozier, W. (2022). Enhancing data mobilisation through a centralised data repository for Atlantic salmon (*Salmo salar L.*): Providing the resources to promote an ecosystem-based management framework. *Ecological Informatics*, 70:101746.
- Dicle, C., Camps, O. I., and Sznaier, M. (2013). The Way They Move: Tracking Multiple Targets with Similar Appearance. In *2013 IEEE International Conference on Computer Vision*, pages 2304–2311, Sydney, Australia. IEEE.
- Dingle, H. (2014). *Migration: the biology of life on the move*. Oxford university press, New York.
- Dingle, H. and Drake, V. A. (2007). What Is Migration? *BioScience*, 57(2):113–121.

- Dittman, A. H., Quinn, T. P., and Nevitt, G. A. (1996). Timing of imprinting to natural and artificial odors by coho salmon (*Oncorhynchus kisutch*). *Canadian Journal of Fisheries and Aquatic Sciences*, 53(2):434–442.
- Doehring, K., Young, R., Hay, J., and Quarterman, A. (2011). Suitability of Dual-frequency Identification Sonar (DIDSON) to monitor juvenile fish movement at flood-gates. *New Zealand Journal of Marine and Freshwater Research*, 45(3):413–422.
- Drenner, S. M., Harrower, W. L., Casselman, M. T., Bett, N. N., Bass, A. L., Middleton, C. T., and Hinch, S. G. (2018). Whole-river manipulation of olfactory cues affects upstream migration of sockeye salmon. *Fisheries Management and Ecology*, 25(6):488–500.
- Einstein, A. (1905). On the motion of small particles suspended in liquids at rest required by the molecular-kinetic theory of heat. *Annalen der physik*, (17(549-560), 208.).
- Einum, S. and Fleming, I. A. (1997). Genetic divergence and interactions in the wild among native, farmed and hybrid Atlantic salmon. *Journal of Fish Biology*, 50(3):634–651.
- Elnaggar, A., Heinzinger, M., Dallago, C., Rehawi, G., Wang, Y., Jones, L., Gibbs, T., Feher, T., Angerer, C., Steinegger, M., Bhowmik, D., and Rost, B. (2020). ProtTrans: Towards Cracking the Language of Life’s Code Through Self-Supervised Learning.
- Enders, E. C., Clarke, K. D., Pennell, C. J., Ollerhead, L. M. N., and Scruton, D. A. (2007). Comparison between PIT and radio telemetry to evaluate winter habitat use and activity patterns of juvenile Atlantic salmon and brown trout. *Hydrobiologia*, 582(1):231–242.
- Enders, E. C., Gessel, M. H., Anderson, J. J., and Williams, J. G. (2012). Effects of Decelerating and Accelerating Flows on Juvenile Salmonid Behavior. *Transactions of the American Fisheries Society*, 141(2):357–364.
- Erkinaro, J., Mäki-Petäys, A., Huusko, A., Kuusela, J., and Niemelä, E. (2018). Low detection rate in visual observations of stream salmonids in winter. *Journal of Freshwater Ecology*, 33(1):335–345.
- Euzenat, G., Fournel, F., and Richard, A. (1999). Sea trout (*Salmo trutta* L.) in Normandy and Picardy. In Baglinière, J. L. and Maisse, G., editors, *Biology and Ecology of the Brown and Sea Trout*, pages 175–203. Springer, London.

- Everingham, M., Eslami, S. M. A., Van Gool, L., Williams, C. K. I., Winn, J., and Zisserman, A. (2015). The Pascal Visual Object Classes Challenge: A Retrospective. *International Journal of Computer Vision*, 111(1):98–136.
- Faust, C. L., Dobson, A. P., Gottdenker, N., Bloomfield, L. S. P., McCallum, H. I., Gillespie, T. R., Diuk-Wasser, M., and Plowright, R. K. (2017). Null expectations for disease dynamics in shrinking habitat: dilution or amplification? *Philosophical Transactions of the Royal Society B: Biological Sciences*, 372(1722):20160173.
- Feichtenhofer, C., Pinz, A., and Zisserman, A. (2017). Detect to Track and Track to Detect. In *2017 IEEE International Conference on Computer Vision (ICCV)*, pages 3057–3065, Venice. IEEE.
- Feng, W., Hu, Z., Wu, W., Yan, J., and Ouyang, W. (2019). Multi-Object Tracking with Multiple Cues and Switcher-Aware Classification. *arXiv:1901.06129 [cs]*.
- Fernandes, W. P., Ibbotson, A. T., Griffiths, S. W., Maxwell, D. L., Davison, P. I., and Riley, W. D. (2015). Does relatedness influence migratory timing and behaviour in Atlantic salmon smolts? *Animal Behaviour*, 106:191–199.
- Ferreira, A. C., Silva, L. R., Renna, F., Brandl, H. B., Renoult, J. P., Farine, D. R., Covas, R., and Doutrelant, C. (2020). Deep learning-based methods for individual recognition in small birds. *Methods in Ecology and Evolution*, 11(9):1072–1085.
- Finstad, B. and Jonsson, N. (2001). Factors influencing the yield of smolt releases in Norway. *Nordic Journal of Freshwater Research*, 75:37–55.
- Flávio, H., Aarestrup, K., Jepsen, N., and Koed, A. (2019). Naturalised Atlantic salmon smolts are more likely to reach the sea than wild smolts in a lowland fjord. *River Research and Applications*, 35(3):216–223.
- Fleming, C. H., Drescher-Lehman, J., Noonan, M. J., Akre, T. S. B., Brown, D. J., Cochrane, M. M., Dejid, N., DeNicola, V., DePerno, C. S., Dunlop, J. N., Gould, N. P., Harrison, A.-L., Hollins, J., Ishii, H., Kaneko, Y., Kays, R., Killen, S. S., Koeck, B., Lambertucci, S. A., LaPoint, S. D., Medici, E. P., Meyburg, B.-U., Miller, T. A., Moen, R. A., Mueller, T., Pfeiffer, T., Pike, K. N., Roulin, A., Safi, K., Séchaud, R., Scharf, A. K., Shephard, J. M., Stabach, J. A., Stein, K., Tonra, C. M., Yamazaki, K., Fagan, W. F., and Calabrese, J. M. (2021). A comprehensive framework for handling location error in animal tracking data.

- Fleming, I. A., Agustsson, T., Finstad, B., Johnsson, J. I., and Björnsson, B. T. (2002). Effects of domestication on growth physiology and endocrinology of Atlantic salmon (*Salmo salar*). *Canadian Journal of Fisheries and Aquatic Sciences*, 59(8):1323–1330.
- Fleming, I. A., Jonsson, B., Gross, M. R., and Lamberg, A. (1996). An Experimental Study of the Reproductive Behaviour and Success of Farmed and Wild Atlantic Salmon (*Salmo salar*). *The Journal of Applied Ecology*, 33(4):893.
- Flye, M. E., Sponarski, C. C., Zydlewski, J. D., and McGreavy, B. (2021). Understanding collaborative governance from a communication network perspective: A case study of the Atlantic Salmon recovery framework. *Environmental Science & Policy*, 115:79–90.
- Føre, M., Svendsen, E., Alfredsen, J., Uglem, I., Bloecher, N., Sveier, H., Sunde, L., and Frank, K. (2018). Using acoustic telemetry to monitor the effects of crowding and delousing procedures on farmed Atlantic salmon (*Salmo salar*). *Aquaculture*, 495:757–765.
- Franke, A., Caelli, T., and Hudson, R. J. (2004). Analysis of movements and behavior of caribou (*Rangifer tarandus*) using hidden Markov models. *Ecological Modelling*, 173(2-3):259–270.
- Fraser, D. J., Minto, C., Calvert, A. M., Eddington, J. D., and Hutchings, J. A. (2010). Potential for domesticated–wild interbreeding to induce maladaptive phenology across multiple populations of wild Atlantic salmon (*Salmo salar*). *Canadian Journal of Fisheries and Aquatic Sciences*, 67(11):1768–1775.
- Fraser, N. H. C. and Metcalfe, N. B. (1997). The costs of becoming nocturnal: feeding efficiency in relation to light intensity in juvenile Atlantic Salmon. *Functional Ecology*, 11(3):385–391.
- Fryxell, J. M. and Berdahl, A. M. (2018). Fitness trade-offs of group formation and movement by Thomson’s gazelles in the Serengeti ecosystem. *Philosophical Transactions of the Royal Society B: Biological Sciences*, 373(1746):20170013.
- Fryxell, J. M., Hazell, M., Borger, L., Dalziel, B. D., Haydon, D. T., Morales, J. M., McIntosh, T., and Rosatte, R. C. (2008). Multiple movement modes by large herbivores at multiple spatiotemporal scales. *Proceedings of the National Academy of Sciences*, 105(49):19114–19119.

- Gao, Z., Andersson, H. I., Dai, H., Jiang, F., and Zhao, L. (2016). A new Eulerian–Lagrangian agent method to model fish paths in a vertical slot fishway. *Ecological Engineering*, 88:217–225.
- Gaskell, J., Campioni, N., Morales, J. M., Husmeier, D., and Torney, C. J. (2020). Approximate Bayesian Inference for Individual-based Models with Emergent Dynamics.
- Gauld, N., Campbell, R., and Lucas, M. (2013). Reduced flow impacts salmonid smolt emigration in a river with low-head weirs. *Science of The Total Environment*, 458-460:435–443.
- Gautrais, J., Ginelli, F., Fournier, R., Blanco, S., Soria, M., Chaté, H., and Theraulaz, G. (2012). Deciphering Interactions in Moving Animal Groups. *PLoS Computational Biology*, 8(9):e1002678.
- Ge, Z., Liu, S., Wang, F., Li, Z., and Sun, J. (2021). YOLOX: Exceeding YOLO Series in 2021.
- Geman, S., Bienenstock, E., and Doursat, R. (1992). Neural networks and the bias/variance dilemma. *Neural computation*.
- Ghahramani, Z. (2015). Probabilistic machine learning and artificial intelligence. *Nature*, 521(7553):452–459.
- Gilbey, J., Mcgregor, H., Gilbey, J., Malcolm, I., Cauwelier, E., Millidine, K., Sampayo, J., Morris, D., and Jackson, F. (2021a). A national assessment of the influence of farmed salmon escapes on the genetic integrity of wild Scottish Atlantic salmon populations. Technical report, Marine Scotland Science.
- Gilbey, J., Utne, K. R., Wennevik, V., Beck, A. C., Kausrud, K., Hindar, K., Garcia De Leaniz, C., Cherbonnel, C., Coughlan, J., Cross, T. F., Dillane, E., Ensing, D., García-Vázquez, E., Hole, L. R., Holm, M., Holst, J. C., Jacobsen, J. A., Jensen, A. J., Karlsson, S., Ó Maoiléidigh, N., Mork, K. A., Nielsen, E. E., Nøttestad, L., Primmer, C. R., Prodöhl, P., Prusov, S., Stevens, J. R., Thomas, K., Whelan, K., McGinnity, P., and Verspoor, E. (2021b). The early marine distribution of Atlantic salmon in the North-east Atlantic: A genetically informed stock-specific synthesis. *Fish and Fisheries*, 22(6):1274–1306.

- Glover, K., Solberg, M., McGinnity, P., Hindar, K., Verspoor, E., Coulson, M., Hansen, M., Araki, H., Skaala, Ø., and Svåsand, T. (2017). Half a century of genetic interaction between farmed and wild Atlantic salmon: Status of knowledge and unanswered questions. *Fish and Fisheries*, 18(5):890–927.
- Godfrey, J. D., Stewart, D. C., Middlemas, S. J., and Armstrong, J. D. (2015). Depth use and migratory behaviour of homing Atlantic salmon (*Salmo salar*) in Scottish coastal waters. *ICES Journal of Marine Science*, 72(2):568–575.
- Goodfellow, I., Bengio, Y., and Courville, A. (2016). *Deep Learning*. MIT Press.
- Goodwin, R. A., Nestler, J. M., Anderson, J. J., Weber, L. J., and Loucks, D. P. (2006). Forecasting 3-D fish movement behavior using a Eulerian–Lagrangian–agent method (ELAM). *Ecological Modelling*, 192(1-2):197–223.
- Gorbman, A., Dickhoff, W. W., Mighell, J. L., Prentice, E. F., and William Waknitz, F. (1982). Morphological indices of developmental progress in the parr-smolt coho salmon, *Oncorhynchus kisutch*. *Aquaculture*, 28(1-2):1–19.
- Gougherty, A. V. and Clipp, H. L. (2024). Testing the reliability of an AI-based large language model to extract ecological information from the scientific literature. *npj Biodiversity*, 3(1):13.
- Gray, P. C., Fleishman, A. B., Klein, D. J., McKown, M. W., Bézy, V. S., Lohmann, K. J., and Johnston, D. W. (2019). A convolutional neural network for detecting sea turtles in drone imagery. *Methods in Ecology and Evolution*, 10(3):345–355.
- Green, A., Honkanen, H. M., Ramsden, P., Shields, B., Del Villar-Guerra, D., Fletcher, M., Walton, S., Kennedy, R., Rosell, R., O’Maoiléidigh, N., Barry, J., Roche, W., Whoriskey, F., Klimley, P., and Adams, C. E. (2022). Evidence of long-distance coastal sea migration of Atlantic salmon, *Salmo salar*, smolts from northwest England (River Derwent). *Animal Biotelemetry*, 10(1):3.
- Greene, C. M., Hall, J. E., Guilbault, K. R., and Quinn, T. P. (2010). Improved viability of populations with diverse life-history portfolios. *Biology Letters*, 6(3):382–386.
- Gregory, R. W. and Fields, P. E. (1962). Discrimination of low water velocities by juvenile silver (*Oncorhynchus kisutch*) and Chinook salmon (*Oncorhynchus tshawytscha*). Technical Report 52 to U.S. Army Corps of Engineers, Seattle, University of Washington, College of Fisheries,.

- Grünbaum, D. (2012). The logic of ecological patchiness. *Interface Focus*, 2(2):150–155.
- Guillemain, M., Bertout, J.-M., Christensen, T. K., Pöysä, H., Väänänen, V.-M., Triplet, P., Schricke, V., and Fox, A. D. (2010). How many juvenile Teal *Anas crecca* reach the wintering grounds? Flyway-scale survival rate inferred from wing age-ratios. *Journal of Ornithology*, 151(1):51–60.
- Guirado, E., Tabik, S., Rivas, M. L., Alcaraz-Segura, D., and Herrera, F. (2019). Whale counting in satellite and aerial images with deep learning. *Scientific Reports*, 9(1):14259.
- Gupte, P. R., Beardsworth, C. E., Spiegel, O., Lourie, E., Toledo, S., Nathan, R., and Bijleveld, A. I. (2022). A guide to pre-processing high-throughput animal tracking data. *Journal of Animal Ecology*, 91(2):287–307.
- Gurarie, E., Fleming, C. H., Fagan, W. F., Laidre, K. L., Hernández-Pliego, J., and Ovaskainen, O. (2017). Correlated velocity models as a fundamental unit of animal movement: synthesis and applications. *Movement Ecology*, 5(1):13.
- Guzzo, M. M., Van Leeuwen, T. E., Hollins, J., Koeck, B., Newton, M., Webber, D. M., Smith, F. I., Bailey, D. M., and Killen, S. S. (2018). Field testing a novel high residence positioning system for monitoring the fine-scale movements of aquatic organisms. *Methods in Ecology and Evolution*, 9(6):1478–1488.
- Hall, M., Frank, E., Holmes, G., Pfahringer, B., Reutemann, P., and Witten, I. H. (2009). The WEKA data mining software: an update. *ACM SIGKDD Explorations Newsletter*, 11(1):10–18.
- Hampson, K., Dushoff, J., Cleaveland, S., Haydon, D. T., Kaare, M., Packer, C., and Dobson, A. (2009). Transmission Dynamics and Prospects for the Elimination of Canine Rabies. *PLoS Biology*, 7(3):e1000053.
- Handegard, N. O. and Williams, K. (2008). Automated tracking of fish in trawls using the DIDSON (Dual frequency IDentification SONar). *ICES Journal of Marine Science*, 65(4):636–644.
- Hansen, L. P. and Quinn, T. P. (1998). The marine phase of the Atlantic salmon (*Salmo salar*) life cycle, with comparisons to Pacific salmon. 55.

- Hanssen, E. M., Vollset, K. W., Salvanes, A. G. V., Barlaup, B., Whoriskey, K., Isaksen, T. E., Normann, E. S., Hulbak, M., and Lennox, R. J. (2022). Acoustic telemetry predation sensors reveal the tribulations of Atlantic salmon (*Salmo salar*) smolts migrating through lakes. *Ecology of Freshwater Fish*, 31(2):424–437.
- Haraldstad, T., Forseth, T., Olsen, E. M., Haugen, T. O., and Höglund, E. (2022). Empirical support for sequential imprinting during downstream migration in Atlantic salmon (*Salmo salar*) smolts. *Scientific Reports*, 12(1):13736.
- Haro, A., Odeh, M., Noreika, J., and Castro-Santos, T. (1998). Effect of Water Acceleration on Downstream Migratory Behavior and Passage of Atlantic Salmon Smolts and Juvenile American Shad at Surface Bypasses. *Transactions of the American Fisheries Society*, 127(1):118–127.
- Hashempoor, H., Koikara, R., and Hwang, Y. D. (2024). FeatureSORT: Essential Features for Effective Tracking.
- Havn, T. B., Thorstad, E. B., Teichert, M. A. K., Sæther, S. A., Heermann, L., Hedger, R. D., Tambets, M., Diserud, O. H., Borchering, J., and Økland, F. (2018). Hydropower-related mortality and behaviour of Atlantic salmon smolts in the River Sieg, a German tributary to the Rhine. *Hydrobiologia*, 805(1):273–290.
- Held, D., Thrun, S., and Savarese, S. (2016). Learning to Track at 100 FPS with Deep Regression Networks. In *Computer Vision – ECCV 2016*, volume 9905, pages 749–765. Springer International Publishing, Cham.
- Hendry, K., Cragg-Hine, D., O’Grady, M., Sambrook, H., and Stephen, A. (2003). Management of habitat for rehabilitation and enhancement of salmonid stocks. *Fisheries Research*, 62(2):171–192.
- Hiedanpää, J., Saijets, J., Jounela, P., Jokinen, M., and Sarkki, S. (2020). Beliefs in Conflict: The Management of Teno Atlantic Salmon in the Sámi Homeland in Finland. *Environmental Management*, 66(6):1039–1058.
- Holleman, R. C., Gross, E. S., Thomas, M. J., Rypel, A. L., and Fangue, N. A. (2022). Swimming behavior of emigrating Chinook Salmon smolts. *PLOS ONE*, 17(3):e0263972.
- Honkanen, H. M., Boylan, P., Dodd, J. A., and Adams, C. E. (2019). Life stage-specific, stochastic environmental effects overlay density dependence in an Atlantic salmon population. *Ecology of Freshwater Fish*, 28(1):156–166.

- Honkanen, H. M., Dodd, J. A., Fordyce, J. R., Boylan, P., and Adams, C. E. (2017). Density- and species-dependent errors in single-pass timed electrofishing assessment of riverine salmonids. *Ecology of Freshwater Fish*, 27(1):98–102.
- Honkanen, H. M., Orrell, D. L., Newton, M., McKelvey, S., Stephen, A., Duguid, R. A., and Adams, C. E. (2021). The downstream migration success of Atlantic salmon (*Salmo salar*) smolts through natural and impounded standing waters. *Ecological Engineering*, 161:106161.
- Honkanen, H. M., Rodger, J. R., Stephen, A., Adams, K., Freeman, J., and Adams, C. E. (2018). Counterintuitive migration patterns by Atlantic salmon *Salmo salar* smolts in a large lake. *Journal of Fish Biology*, 93(1):159–162.
- Hooten, M. B., Johnson, D. S., McClintock, B. T., and Morales, J. M. (2017). *Animal movement: statistical models for telemetry data*. CRC Press, Taylor & Francis Group, Boca Raton London New York.
- Horn, B. K. P. and Schunck, B. G. (1981). Determining optical flow. *Artificial Intelligence*, 17(1):185–203.
- Hornik, K. (1991). Approximation capabilities of multilayer feedforward networks. *Neural Networks*, 4(2):251–257.
- Houde, A. L. S., Fraser, D. J., and Hutchings, J. A. (2010). Reduced anti-predator responses in multi-generational hybrids of farmed and wild Atlantic salmon (*Salmo salar* L.). *Conservation Genetics*, 11(3):785–794.
- Hughey, L. F., Hein, A. M., Strandburg-Peshkin, A., and Jensen, F. H. (2018). Challenges and solutions for studying collective animal behaviour in the wild. *Philosophical Transactions of the Royal Society B: Biological Sciences*, 373(1746):20170005.
- Hutchings, J. A., Ardren, W. R., Barlaup, B. T., Bergman, E., Clarke, K. D., Greenberg, L. A., Lake, C., Piironen, J., Sirois, P., Sundt-Hansen, L. E., and Fraser, D. J. (2019). Life-history variability and conservation status of landlocked Atlantic salmon: an overview. *Canadian Journal of Fisheries and Aquatic Sciences*, 76(10):1697–1708.
- Hvidsten, N., Jensen, A. J., Vivas, H., Bakke, D., and Heggberget, T. G. (1995). Downstream migration of Atlantic salmon smolts in relation to water flow, water temperature, moon phase and social behaviour. *Nordic J Freshw. Res.*, (70):38–48.

- Ioannou, C. C., Ramnarine, I. W., and Torney, C. J. (2017). High-predation habitats affect the social dynamics of collective exploration in a shoaling fish. *Science Advances*, 3(5):e1602682.
- Jacoby, D. M. P. and Piper, A. T. (2023). What acoustic telemetry can and cannot tell us about fish biology. *Journal of Fish Biology*, page jfb.15588.
- Jennings, E. and Madigan, M. (2017). astroABC: An Approximate Bayesian Computation Sequential Monte Carlo sampler for cosmological parameter estimation. *Astronomy and Computing*, 19:16–22.
- Johnsson, J. I., Höjesjö, J., and Fleming, I. A. (2001). Behavioural and heart rate responses to predation risk in wild and domesticated Atlantic salmon. *Canadian Journal of Fisheries and Aquatic Sciences*, 58(4):788–794.
- Jolles, J. W., King, A. J., and Killen, S. S. (2020). The Role of Individual Heterogeneity in Collective Animal Behaviour. *Trends in Ecology & Evolution*, 35(3):278–291.
- Jumper, J., Evans, R., Pritzel, A., Green, T., Figurnov, M., Ronneberger, O., Tunyasuvunakool, K., Bates, R., Žídek, A., Potapenko, A., Bridgland, A., Meyer, C., Kohli, S. A. A., Ballard, A. J., Cowie, A., Romera-Paredes, B., Nikolov, S., Jain, R., Adler, J., Back, T., Petersen, S., Reiman, D., Clancy, E., Zielinski, M., Steinegger, M., Pacholska, M., Berghammer, T., Bodenstein, S., Silver, D., Vinyals, O., Senior, A. W., Kavukcuoglu, K., Kohli, P., and Hassabis, D. (2021). Highly accurate protein structure prediction with AlphaFold. *Nature*, 596(7873):583–589.
- Jutila, E., Jokikokko, E., Kallio-Nyberg, I., Saloniemä, I., and Pasanen, P. (2003). Differences in sea migration between wild and reared Atlantic salmon (*Salmo salar* L.) in the Baltic Sea. *Fisheries Research*, 60(2-3):333–343.
- Kalman, R. E. (1960). A New Approach to Linear Filtering and Prediction Problems. *Journal of Basic Engineering*, 82(1):35–45.
- Kareiva, P. M. and Shigesada, N. (1983). Analyzing insect movement as a correlated random walk. *Oecologia*, 56(2-3):234–238.
- Karppinen, P. and Erkinaro, J. (2009). Using motion-sensitive radio tags to record the activity and behavioural patterns of spawning Atlantic salmon. *Ecology of Freshwater Fish*, 18(2):177–182.

- Karppinen, P., Hynninen, M., Vehanen, T., and Vähä, J.-P. (2021). Variations in migration behaviour and mortality of Atlantic salmon smolts in four different hydroelectric facilities. *Fisheries Management and Ecology*, 28(3):253–267.
- Kavwele, C. M., Hopcraft, J. G. C., Davy, D., and Torney, C. J. (2024). Automated and repeated aerial observations of GPS-collared animals using UAVs and open-source electronics. *Ecosphere*, 15(4):e4841.
- Kays, R., Crofoot, M. C., Jetz, W., and Wikelski, M. (2015). Terrestrial animal tracking as an eye on life and planet. *Science*, 348(6240):aaa2478.
- Kays, R., Hirsch, B., Caillaud, D., Mares, R., Alavi, S., Havmøller, R. W., and Crofoot, M. (2023). Multi-scale movement syndromes for comparative analyses of animal movement patterns. *Movement Ecology*, 11(1):61.
- Kelley, D. H. and Ouellette, N. T. (2013). Emergent dynamics of laboratory insect swarms. *Scientific Reports*, 3(1):1073.
- Kemp, P. S., Armstrong, J. D., and Gilvear, D. J. (2005a). Behavioural responses of juvenile Atlantic salmon (*Salmo salar*) to presence of boulders. *River Research and Applications*, 21(9):1053–1060.
- Kemp, P. S., Gessel, M. H., and Williams, J. G. (2005b). Fine-Scale Behavioral Responses of Pacific Salmonid Smolts as They Encounter Divergence and Acceleration of Flow. *Transactions of the American Fisheries Society*, 134(2):390–398.
- Kemp, P. S. and Williams, J. G. (2008). Response of migrating chinook salmon (*Oncorhynchus tshawytscha*) smolts to in-stream structure associated with culverts. *River Research and Applications*, 24(5):571–579.
- Kennedy, R. J., Rosell, R., Millane, M., Doherty, D., and Allen, M. (2018). Migration and survival of Atlantic salmon *Salmo salar* smolts in a large natural lake. *Journal of Fish Biology*, 93(1):134–137.
- Kerr, J. R. and Kemp, P. S. (2018). Masking a fish’s detection of environmental stimuli: application to improving downstream migration at river infrastructure. *Journal of Fish Biology*.
- Kidger, P. and Lyons, T. (2020). Universal Approximation with Deep Narrow Networks.

- Killen, S. S., Marras, S., Nadler, L., and Domenici, P. (2017). The role of physiological traits in assortment among and within fish shoals. *Philosophical Transactions of the Royal Society B: Biological Sciences*, 372(1727):20160233.
- Killen, S. S., Marras, S., Steffensen, J. F., and McKenzie, D. J. (2011). Aerobic capacity influences the spatial position of individuals within fish schools. *Proceedings of the Royal Society B: Biological Sciences*, 279(1727):357–364.
- King, S. L., Schick, R. S., Donovan, C., Booth, C. G., Burgman, M., Thomas, L., and Harwood, J. (2015). An interim framework for assessing the population consequences of disturbance. *Methods in Ecology and Evolution*, 6(10):1150–1158.
- Klemetsen, A., Amundsen, P.-A., Dempson, J. B., Jonsson, B., Jonsson, N., O’Connell, M. F., and Mortensen, E. (2003). Atlantic salmon *Salmo salar* L., brown trout *Salmo trutta* L. and Arctic charr *Salvelinus alpinus* (L.): a review of aspects of their life histories. *Ecology of Freshwater Fish*, 12(1):1–59.
- Kochalski, S., Riepe, C., and Arlinghaus, R. (2022). Perceived socio-cultural ecosystem services provided by wild Atlantic Salmon populations in four European countries. *Aquatic Ecosystem Health & Management*, 25(3):12–21.
- Koene, J. P., Elmer, K. R., and Adams, C. E. (2020). Intraspecific variation and structuring of phenotype in a lake-dwelling species are driven by lake size and elevation. *Biological Journal of the Linnean Society*, 131(3):585–599.
- Krizhevsky, A., Sutskever, I., and Hinton, G. E. (2012). ImageNet classification with deep convolutional neural networks. *Communications of the ACM*, 60(6):84–90.
- Kuhn, H. W. (1955). The Hungarian method for the assignment problem. *Naval Research Logistics Quarterly*, 2(1-2):83–97.
- Kundegorski, M., Akcay, S., Devereux, M., Mouton, A., and Breckon, T. (2016). On using Feature Descriptors as Visual Words for Object Detection within X-ray Baggage Security Screening. In *7th International Conference on Imaging for Crime Detection and Prevention (ICDP 2016)*, pages 12 (6 .)–12 (6 .), Madrid, Spain. Institution of Engineering and Technology.
- Kururvilla, M., Quinn, T. P., Anderson, J. H., Miller, E. M., Berger, A. G., Okasaki, C., McMillan, J. R., Pess, G. R., Westley, P. A. H., and Berdahl, A. M. (2024). Social influences complement environmental cues to stimulate migrating juvenile salmon.

- Langrock, R., King, R., Matthiopoulos, J., Thomas, L., Fortin, D., and Morales, J. M. (2012). Flexible and practical modeling of animal telemetry data: hidden Markov models and extensions. *Ecology*, 93(11):2336–2342.
- Larkin, P. A. and Walton, A. (1969). Fish School Size and Migration. page 5.
- Lasseck, M. (2018). Audio-based Bird Species Identification with Deep Convolutional Neural Networks.
- Leal-Taixe, L., Canton-Ferrer, C., and Schindler, K. (2016). Learning by Tracking: Siamese CNN for Robust Target Association. pages 33–40.
- Leander, J., Klaminder, J., Jonsson, M., Brodin, T., Leonardsson, K., and Hellström, G. (2020). The old and the new: evaluating performance of acoustic telemetry systems in tracking migrating Atlantic salmon (*Salmo salar*) smolt and European eel (*Anguilla anguilla*) around hydropower facilities. *Canadian Journal of Fisheries and Aquatic Sciences*, 77(1):177–187.
- Lemasson, B. H., Haefner, J. W., and Bowen, M. D. (2014). Schooling Increases Risk Exposure for Fish Navigating Past Artificial Barriers. *PLoS ONE*, 9(9):e108220.
- Lennox, R. J., Alexandre, C. M., Almeida, P. R., Bailey, K. M., Barlaup, B. T., Bøe, K., Breukelaar, A., Erkinaro, J., Forseth, T., Gabrielsen, S.-E., Halfyard, E., Hanssen, E. M., Karlsson, S., Koch, S., Koed, A., Langåker, R. M., Lo, H., Lucas, M. C., Mahlum, S., Perrier, C., Pulg, U., Sheehan, T., Skoglund, H., Svenning, M., Thorstad, E. B., Velle, G., Whoriskey, F. G., and Vollset, K. W. (2021). The quest for successful Atlantic salmon restoration: perspectives, priorities, and maxims. *ICES Journal of Marine Science*, 78(10):3479–3497.
- Lilly, J., Honkanen, H. H., Rodger, J. R., Del Villar, D., Boylan, P., Green, A., Pereiro, D., Wilkie, L., Kennedy, R., Barkley, A., Rosell, R., Maoiléidigh, N. Ó., O’Neill, R., Waters, C., Cotter, D., Bailey, D., Roche, W., McGill, R., Barry, J., Beck, S. V., Henderson, J., Parke, D., Whoriskey, F. G., Shields, B., Ramsden, P., Walton, S., Fletcher, M., Whelan, K., Bean, C. W., Elliott, S., Bowman, A., and Adams, C. E. (2024). Migration patterns and navigation cues of Atlantic salmon post-smolts migrating from 12 rivers through the coastal zones around the Irish Sea. *Journal of Fish Biology*, 104(1):265–283.
- Lilly, J., Honkanen, H. M., McCallum, J. M., Newton, M., Bailey, D. M., and Adams, C. E. (2022). Combining acoustic telemetry with a mechanistic model to investigate

- characteristics unique to successful Atlantic salmon smolt migrants through a standing body of water. *Environmental Biology of Fishes*, 105(12):2045–2063.
- Limburg, K. E., Landergren, P., Westin, L., Elfman, M., and Kristiansson, P. (2001). Flexible modes of anadromy in Baltic sea trout: making the most of marginal spawning streams. *Journal of Fish Biology*, 59(3):682–695.
- Lin, K., Zhou, C., Xu, D., Guo, Q., Yang, X., and Sun, C. (2018). Three-dimensional location of target fish by monocular infrared imaging sensor based on a L–z correlation model. *Infrared Physics & Technology*, 88:106–113.
- Lin, T.-Y., Maire, M., Belongie, S., Bourdev, L., Girshick, R., Hays, J., Perona, P., Ramanan, D., Zitnick, C. L., and Dollár, P. (2015). Microsoft COCO: Common Objects in Context. *arXiv:1405.0312 [cs]*.
- Llewellyn, M. S., McGinnity, P., Dionne, M., Letourneau, J., Thonier, F., Carvalho, G. R., Creer, S., and Derome, N. (2016). The biogeography of the atlantic salmon (*Salmo salar*) gut microbiome. *The ISME Journal*, 10(5):1280–1284.
- López, M. E., Linderoth, T., Norris, A., Lhorente, J. P., Neira, R., and Yáñez, J. M. (2019). Multiple Selection Signatures in Farmed Atlantic Salmon Adapted to Different Environments Across Hemispheres. *Frontiers in Genetics*, 10.
- Lopez-Marcano, S., L. Jinks, E., Buelow, C. A., Brown, C. J., Wang, D., Kusy, B., M. Ditria, E., and Connolly, R. M. (2021). Automatic detection of fish and tracking of movement for ecology. *Ecology and Evolution*, 11(12):8254–8263.
- Lothian, A. J., Newton, M., Barry, J., Walters, M., Miller, R. C., and Adams, C. E. (2018). Migration pathways, speed and mortality of Atlantic salmon (*Salmo salar*) smolts in a Scottish river and the near-shore coastal marine environment. *Ecology of Freshwater Fish*, 27(2):549–558.
- Lothian, A. J., Rodger, J., Wilkie, L., Walters, M., Miller, R., Conroy, C., Marshall, S., MacKenzie, M., and Adams, C. E. (2024a). Smolting in post-sexually mature male Atlantic salmon (*Salmo salar* L.) parr in the wild. *Ecology of Freshwater Fish*, 33(2):e12755.
- Lothian, A. J., Rodger, J., Wilkie, L., Walters, M., Miller, R., Muller, K., and Adams, C. E. (2024b). A comparison of acoustic tag sizes on wild Atlantic salmon *Salmo salar* L. smolt migration success and behaviour. *Ecology of Freshwater Fish*, page e12798.

- Lowe, D. (1999). Object recognition from local scale-invariant features. In *Proceedings of the Seventh IEEE International Conference on Computer Vision*, pages 1150–1157 vol.2, Kerkyra, Greece. IEEE.
- Mäder, P., Boho, D., Rzanny, M., Seeland, M., Wittich, H. C., Deggelmann, A., and Wäldchen, J. (2021). The Flora Incognita app – Interactive plant species identification. *Methods in Ecology and Evolution*, 12(7):1335–1342.
- Madsen, S. S., Winther, S. S. T., Bollinger, R. J., Steiner, U., and Larsen, M. H. (2019). Differential expression of olfactory genes in Atlantic salmon (*Salmo salar*) during the parr–smolt transformation. *Ecology and Evolution*, 9(24):14085–14100.
- Maitland, P. (1995). World status and conservation of the Arctic charr *Salvelinus alpinus*. *Nordic Journal of Freshwater Research*, 71:113–127.
- Malcolm, I. A., Millidine, K. J., Glover, R. S., Jackson, F. L., Millar, C. P., and Fryer, R. J. (2019). Development of a large-scale juvenile density model to inform the assessment and management of Atlantic salmon (*Salmo salar*) populations in Scotland. *Ecological Indicators*, 96:303–316.
- Matley, J. K., Klinard, N. V., Barbosa Martins, A. P., Aarestrup, K., Aspillaga, E., Cooke, S. J., Cowley, P. D., Heupel, M. R., Lowe, C. G., Lowerre-Barbieri, S. K., Mitamura, H., Moore, J.-S., Simpfendorfer, C. A., Stokesbury, M. J., Taylor, M. D., Thorstad, E. B., Vandergoot, C. S., and Fisk, A. T. (2022). Global trends in aquatic animal tracking with acoustic telemetry. *Trends in Ecology & Evolution*, 37(1):79–94.
- McCleave, J. D., Power, J. H., and Rommel, S. A. (1978). Use of radio telemetry for studying upriver migration of adult Atlantic salmon (*Salmo salar*). *Journal of Fish Biology*, 12(6):549–558.
- McClintock, B. T. (2021). Worth the effort? A practical examination of random effects in hidden Markov models for animal telemetry data. *Methods in Ecology and Evolution*, 12(8):1475–1497.
- McClintock, B. T., Langrock, R., Gimenez, O., Cam, E., Borchers, D. L., Glennie, R., and Patterson, T. A. (2020). Uncovering ecological state dynamics with hidden Markov models. *Ecology Letters*, 23(12):1878–1903.
- McCormick, S. D., Hansen, L. P., Quinn, T. P., and Saunders, R. L. (1998). Movement, migration, and smolting of Atlantic salmon (*Salmo salar*). 55:16.

- McIlvenny, J., Youngson, A., Williamson, B. J., Gauld, N. R., Goddijn-Murphy, L., and Del Villar-Guerra, D. (2021). Combining acoustic tracking and hydrodynamic modelling to study migratory behaviour of Atlantic salmon (*Salmo salar*) smolts on entry into high-energy coastal waters. *ICES Journal of Marine Science*, 78(7):2409–2419.
- McLean, S., Persson, A., Norin, T., and Killen, S. S. (2018). Metabolic Costs of Feeding Predictively Alter the Spatial Distribution of Individuals in Fish Schools. *Current Biology*, 28(7):1144–1149.e4.
- Miller, N., Garnier, S., Hartnett, A. T., and Couzin, I. D. (2013). Both information and social cohesion determine collective decisions in animal groups. *Proceedings of the National Academy of Sciences*, 110(13):5263–5268.
- Milligan, R. J., Morris, K. J., Bett, B. J., Durden, J. M., Jones, D. O. B., Robert, K., Ruhl, H. A., and Bailey, D. M. (2016). High resolution study of the spatial distributions of abyssal fishes by autonomous underwater vehicle. *Scientific Reports*, 6(1).
- Milner, N., Elliott, J., Armstrong, J., Gardiner, R., Welton, J., and Ladle, M. (2003). The natural control of salmon and trout populations in streams. *Fisheries Research*, 62(2):111–125.
- Mönck, H. J., Jörg, A., von Falkenhausen, T., Tanke, J., Wild, B., Dormagen, D., Piotrowski, J., Winklmayr, C., Bierbach, D., and Landgraf, T. (2018). BioTracker: An Open-Source Computer Vision Framework for Visual Animal Tracking.
- Moore, A., Potter, E. C. E., Milner, N. J., and Bamber, S. (1995). The migratory behaviour of wild Atlantic salmon (*Salmo salar*) smolts in the estuary of the River Conwy, North Wales. *Canadian Journal of Fisheries and Aquatic Sciences*, 52(9):1923–1935.
- Morales, J. M., Haydon, D. T., Frair, J., Holsinger, K. E., and Fryxell, J. M. (2004). Extracting More Out of Relocation Data: Building Movement Models as Mixtures of Random Walks. *Ecology*, 85(9):2436–2445.
- Morales, J. M., Moorcroft, P. R., Matthiopoulos, J., Frair, J. L., Kie, J. G., Powell, R. A., Merrill, E. H., and Haydon, D. T. (2010). Building the bridge between animal movement and population dynamics. *Philosophical Transactions of the Royal Society B: Biological Sciences*, 365(1550):2289–2301.
- Mork, K. A., Gilbey, J., Hansen, L. P., Jensen, A. J., Jacobsen, J. A., Holm, M., Holst, J. C., Ó Maoiléidigh, N., Vikebø, F., McGinnity, P., Melle, W., Thomas, K., Verspoor,

- E., and Wennevik, V. (2012). Modelling the migration of post-smolt Atlantic salmon (*Salmo salar*) in the Northeast Atlantic. *ICES Journal of Marine Science*, 69(9):1616–1624.
- Morton, J., Ariza, E., Halliday, M., and Pita, C. (2016). Valuing the wild salmon fisheries of Scotland: The social and political dimensions of management. *Marine Policy*, 73:35–45.
- Mouquet, N., Lagadeuc, Y., Devictor, V., Doyen, L., Duputié, A., Eveillard, D., Faure, D., Garnier, E., Gimenez, O., Huneman, P., Jabot, F., Jarne, P., Joly, D., Julliard, R., Kéfi, S., Kergoat, G. J., Lavorel, S., Le Gall, L., Meslin, L., Morand, S., Morin, X., Morlon, H., Pinay, G., Pradel, R., Schurr, F. M., Thuiller, W., and Loreau, M. (2015). Predictive ecology in a changing world. *Journal of Applied Ecology*, 52(5):1293–1310.
- Mouritsen, H. (2018). Long-distance navigation and magnetoreception in migratory animals. *Nature*, 558(7708):50–59.
- Nagy, M., Couzin, I. D., Fiedler, W., Wikelski, M., and Flack, A. (2018). Synchronization, coordination and collective sensing during thermalling flight of freely migrating white storks. *Philosophical Transactions of the Royal Society B: Biological Sciences*, 373(1746):20170011.
- Nakagawa, S. and Freckleton, R. P. (2011). Model averaging, missing data and multiple imputation: a case study for behavioural ecology. *Behavioral Ecology and Sociobiology*, 65(1):103–116.
- Nathan, R., Monk, C. T., Arlinghaus, R., Adam, T., Alós, J., Assaf, M., Baktoft, H., Beardsworth, C. E., Bertram, M. G., Bijleveld, A. I., Brodin, T., Brooks, J. L., Campos-Candela, A., Cooke, S. J., Gjelland, K. Ø., Gupte, P. R., Harel, R., Hellström, G., Jeltsch, F., Killen, S. S., Klefoth, T., Langrock, R., Lennox, R. J., Lourie, E., Madden, J. R., Orchan, Y., Pauwels, I. S., Říha, M., Roeleke, M., Schlägel, U. E., Shohami, D., Signer, J., Toledo, S., Vilck, O., Westrelin, S., Whiteside, M. A., and Jarić, I. (2022). Big-data approaches lead to an increased understanding of the ecology of animal movement. *Science*, 375(6582):eabg1780.
- Newton, M., Barry, J., Lothian, A., Main, R., Honkanen, H., Mckelvey, S., Thompson, P., Davies, I., Brockie, N., Stephen, A., Murray, R. O., Gardiner, R., Campbell, L., Stainer, P., and Adams, C. (2021). Counterintuitive active directional swimming behaviour by

- Atlantic salmon during seaward migration in the coastal zone. *ICES Journal of Marine Science*, 78(5):1730–1743.
- Newton, M., Dodd, J. A., Barry, J., Boylan, P., and Adams, C. E. (2018). The impact of a small-scale riverine obstacle on the upstream migration of Atlantic Salmon. *Hydrobiologia*, 806(1):251–264.
- Olivetti, S., Gil, M. A., Sridharan, V. K., and Hein, A. M. (2021). Merging computational fluid dynamics and machine learning to reveal animal migration strategies. *Methods in Ecology and Evolution*, 12(7):1186–1200.
- Olsén, K. H., Petersson, E., Ragnarsson, B., Lundqvist, H., and Järvi, T. (2004). Downstream migration in Atlantic salmon (*Salmo salar*) smolt sibling groups. *Canadian Journal of Fisheries and Aquatic Sciences*, 61(3):328–331.
- Otero, J., L’Abée-Lund, J. H., Castro-Santos, T., Leonardsson, K., Storvik, G. O., Jonsson, B., Dempson, B., Russell, I. C., Jensen, A. J., Baglinière, J.-L., Dionne, M., Armstrong, J. D., Romakkaniemi, A., Letcher, B. H., Kocik, J. F., Erkinaro, J., Poole, R., Rogan, G., Lundqvist, H., MacLean, J. C., Jokikokko, E., Arnekleiv, J. V., Kennedy, R. J., Niemelä, E., Caballero, P., Music, P. A., Antonsson, T., Gudjonsson, S., Veselov, A. E., Lamberg, A., Groom, S., Taylor, B. H., Taberner, M., Dillane, M., Arnason, F., Horton, G., Hvidsten, N. A., Jonsson, I. R., Jonsson, N., McKelvey, S., Næsje, T. F., Skaala, Ø., Smith, G. W., Sægvog, H., Stenseth, N. C., and Vøllestad, L. A. (2014). Basin-scale phenology and effects of climate variability on global timing of initial seaward migration of Atlantic salmon (*Salmo salar*). *Global Change Biology*, 20(1):61–75.
- Ovaskainen, O., Luoto, M., Ikonen, I., Rekola, H., Meyke, E., and Kuussaari, M. (2008). An Empirical Test of a Diffusion Model: Predicting Clouded Apollo Movements in a Novel Environment. *The American naturalist*, 171:610–9.
- Owen, M. and Black, J. M. (1991). The importance of migration mortality in non-passerine birds. In *Bird Population Studies: Relevance To Conservation And Management*, page 0. Oxford University Press.
- Ozogány, K. and Vicsek, T. (2015). Modeling the Emergence of Modular Leadership Hierarchy During the Collective Motion of Herds Made of Harems. *Journal of Statistical Physics*, 158(3):628–646.

- Panadeiro, V., Rodriguez, A., Henry, J., Wlodkovic, D., and Andersson, M. (2021). A review of 28 free animal-tracking software applications: current features and limitations. *Lab Animal*, 50(9):246–254.
- Papakis, I., Sarkar, A., and Karpatne, A. (2021). GCNNMatch: Graph Convolutional Neural Networks for Multi-Object Tracking via Sinkhorn Normalization.
- Papastamatiou, Y. P., Meyer, C. G., Carvalho, F., Dale, J. J., Hutchinson, M. R., and Holland, K. N. (2013). Telemetry and random-walk models reveal complex patterns of partial migration in a large marine predator. *Ecology*, 94(11):2595–2606.
- Patterson, T. A., Parton, A., Langrock, R., Blackwell, P. G., Thomas, L., and King, R. (2017). Statistical modelling of individual animal movement: an overview of key methods and a discussion of practical challenges. *AStA Advances in Statistical Analysis*, 101(4):399–438.
- Paun, I. A., Husmeier, D., and Torney, C. (2019). A study on discrete-time movement models.
- Pearson, K. (1905). The Problem of the Random Walk. *Nature*, 72(1867):342–342.
- Pérez-Escudero, A., Vicente-Page, J., Hinz, R. C., Arganda, S., and de Polavieja, G. G. (2014). idTracker: tracking individuals in a group by automatic identification of unmarked animals.
- Perry, W. B., Solberg, M. F., Besnier, F., Dyrhovden, L., Matre, I. H., Fjelldal, P. G., Aylton, F., Creer, S., Llewellyn, M., Taylor, M. I., Carvalho, G., and Glover, K. A. (2019). Evolutionary drivers of kype size in Atlantic salmon (*Salmo salar*): domestication, age and genetics. *Royal Society Open Science*, 6(4):190021.
- Persson, L., Kagervall, A., Leonardsson, K., Royan, M., and Alanära, A. (2019). The effect of physiological and environmental conditions on smolt migration in Atlantic salmon *Salmo salar*. *Ecology of Freshwater Fish*, 28(2):190–199.
- Persson, L., Leonardsson, K., and Alanära, A. (2018). Manipulation of the energetic state of Atlantic salmon *Salmo salar* juveniles and the effect on migration speed: *s. salar* energetic state and smolt migration. *Journal of Fish Biology*, 92(4):961–978.
- Pettit, B., Flack, A., Freeman, R., Guilford, T., and Biro, D. (2013). Not just passengers: pigeons, *Columba livia*, can learn homing routes while flying with a more experienced conspecific. *Proceedings of the Royal Society B: Biological Sciences*, 280(1750):20122160.

- Prangle, D. (2017). Adapting the ABC Distance Function. *Bayesian Analysis*, 12(1).
- Prangle, D., Blum, M. G. B., Popovic, G., and Sisson, S. A. (2014). Diagnostic tools for approximate Bayesian computation using the coverage property. *Australian & New Zealand Journal of Statistics*, 56(4):309–329.
- Preisler, H. K., Ager, A. A., Johnson, B. K., and Kie, J. G. (2004). Modeling animal movements using stochastic differential equations. *Environmetrics*, 15(7):643–657.
- Pritchard, V. (2023). Project to Establish the Genetic Composition of Contemporary Wild and Farmed Atlantic Salmon Populations in the Loch Ness, Garry, Arkaig, Lochy and Shiel Catchments of Northern Scotland. Phase 1: Genetic Baseline. Technical report, Institute for Biodiversity and Freshwater Conservation, UHI Inverness.
- Psorakis, I., Roberts, S. J., Rezek, I., and Sheldon, B. C. (2012). Inferring social network structure in ecological systems from spatio-temporal data streams. *Journal of The Royal Society Interface*, 9(76):3055–3066.
- Putman, N. F., Scanlan, M. M., Billman, E. J., O’Neil, J. P., Couture, R. B., Quinn, T. P., Lohmann, K. J., and Noakes, D. L. (2014). An Inherited Magnetic Map Guides Ocean Navigation in Juvenile Pacific Salmon. *Current Biology*, 24(4):446–450.
- Rand, P. (2010). IUCN Red List of Threatened Species: *Oncorhynchus nerka*. *IUCN Red List of Threatened Species*.
- Rathore, A., Sharma, A., Shah, S., Sharma, N., Torney, C., and Guttal, V. (2023). Multi-Object Tracking in Heterogeneous environments (MOTHe) for animal video recordings. *PeerJ*, 11:e15573.
- Ravi, N., Gabeur, V., Hu, Y.-T., Hu, R., Ryali, C., Ma, T., Khedr, H., Rädle, R., Rolland, C., Gustafson, L., Mintun, E., Pan, J., Alwala, V., Carion, N., Wu, C.-Y., Girshick, R., Dollár, P., and Feichtenhofer, C. (2024). SAM 2: Segment Anything in Images and Videos.
- Recknagel, F. (2001). Applications of machine learning to ecological modelling. *Ecological Modelling*, 146(1-3):303–310.
- Redmon, J., Divvala, S., Girshick, R., and Farhadi, A. (2016). You Only Look Once: Unified, Real-Time Object Detection. In *2016 IEEE Conference on Computer Vision and Pattern Recognition (CVPR)*, pages 779–788, Las Vegas, NV, USA. IEEE.

- Redmon, J. and Farhadi, A. (2018). YOLOv3: An Incremental Improvement. *arXiv:1804.02767 [cs]*.
- Ren, S., He, K., Girshick, R., and Sun, J. (2015). Faster R-CNN: Towards Real-Time Object Detection with Region Proposal Networks. *arXiv:1506.01497 [cs]*.
- Renardy, S., Ciraane, U. D., Benitez, J.-P., Dierckx, A., Archambeau, P., Piroton, M., Erpicum, S., and Ovidio, M. (2023). Combining fine-scale telemetry and hydraulic numerical modelling to understand the behavioural tactics and the migration route choice of smolts at a complex hydropower plant. *Hydrobiologia*, 850(14):3091–3111.
- Rey, N., Volpi, M., Joost, S., and Tuia, D. (2017). Detecting animals in African Savanna with UAVs and the crowds. *Remote Sensing of Environment*, 200:341–351.
- Reynolds, C. W. (1987). Flocks, herds and schools: A distributed behavioral model. In *Proceedings of the 14th annual conference on Computer graphics and interactive techniques*, SIGGRAPH '87, pages 25–34, New York, NY, USA. Association for Computing Machinery.
- Rikardsen, A. H., Righton, D., Strøm, J. F., Thorstad, E. B., Gargan, P., Sheehan, T., Økland, F., Chittenden, C. M., Hedger, R. D., Næsje, T. F., Renkawitz, M., Sturlaugsson, J., Caballero, P., Baktoft, H., Davidsen, J. G., Halttunen, E., Wright, S., Finstad, B., and Aarestrup, K. (2021). Redefining the oceanic distribution of Atlantic salmon. *Scientific Reports*, 11(1):12266.
- Risse, B., Berh, D., Otto, N., Klämbt, C., and Jiang, X. (2017). FIMTrack: An open source tracking and locomotion analysis software for small animals. *PLOS Computational Biology*, 13(5):e1005530.
- Roberge, C., Normandeau, É., Einum, S., Guderley, H., and Bernatchez, L. (2008). Genetic consequences of interbreeding between farmed and wild Atlantic salmon: insights from the transcriptome. *Molecular Ecology*, 17(1):314–324.
- Rodger, J. R., Lilly, J., Honkanen, H. M., Del Villar, D., Kennedy, R., Maoiléidigh, N. Ó., Boylan, P., Rosell, R., Morris, D. J., O'Neill, R., Waters, C., Cotter, D., Wilkie, L., Barkley, A., Green, A., Beck, S. V., Ribbens, J., Henderson, J., Parke, D., Kettle-White, A., Ballantyne, L., Marshall, S., Hopper, P., Gauld, N., Godfrey, J. D., Chapman, L. E., Thorburn, J., Drumm, A., Whoriskey, F., Shields, B., Ramsden, P., Barry, J., Millane, M., Roche, W., Armstrong, J. D., Wells, A., Walton, S., Fletcher, M., Bailey, D. M.,

- Whyte, B., McGill, R., Bilsby, M., Whelan, K., Bean, C. W., and Adams, C. E. (2024). Inshore and offshore marine migration pathways of Atlantic salmon post-smolts from multiple rivers in Scotland, England, Northern Ireland, and Ireland. *Journal of Fish Biology*, page jfb.15760.
- Rodriguez, A., Zhang, H., Klaminder, J., Brodin, T., Andersson, P. L., and Andersson, M. (2018). *ToxTrac* : A fast and robust software for tracking organisms. *Methods in Ecology and Evolution*, 9(3):460–464.
- Ruiz-Suarez, S., Leos-Barajas, V., Alvarez-Castro, I., and Morales, J. M. (2020). Using approximate Bayesian inference for a "steps and turns" continuous-time random walk observed at regular time intervals. *PeerJ*, 8:e8452.
- Sakiyama, T. and Gunji, Y.-P. (2013). Emergence of an optimal search strategy from a simple random walk. *Journal of The Royal Society Interface*, 10(86):20130486.
- Samways, K. M. and Cunjak, R. A. (2015). Increases in benthic community production and metabolism in response to marine-derived nutrients from spawning Atlantic salmon (*Salmo salar*). *Freshwater Biology*, 60(8):1647–1658.
- Sasaki, T. and Biro, D. (2017). Cumulative culture can emerge from collective intelligence in animal groups. *Nature Communications*, 8(1):15049.
- Schindler, D. E., Scheuerell, M. D., Moore, J. W., Gende, S. M., Francis, T. B., and Palen, W. J. (2003). Pacific salmon and the ecology of coastal ecosystems. *Frontiers in Ecology and the Environment*, 1(1):31–37.
- Schmolke, A., Thorbek, P., DeAngelis, D. L., and Grimm, V. (2010). Ecological models supporting environmental decision making: a strategy for the future. *Trends in Ecology & Evolution*, 25(8):479–486.
- Schneider, S., Taylor, G. W., and Kremer, S. C. (2018). Deep Learning Object Detection Methods for Ecological Camera Trap Data. *arXiv:1803.10842 [cs]*.
- Schwinn, M., Aarestrup, K., Baktoft, H., and Koed, A. (2017). Survival of Migrating Sea Trout (*Salmo trutta*) Smolts During Their Passage of an Artificial Lake in a Danish Lowland Stream. *River Research and Applications*, 33(4):558–566.
- Schwinn, M., Baktoft, H., Aarestrup, K., Lucas, M. C., and Koed, A. (2018). Telemetry observations of predation and migration behaviour of brown trout (*Salmo trutta*) smolts negotiating an artificial lake. *River Research and Applications*, 34(8):898–906.

- Scornet, E. (2016). Random forests and kernel methods. *IEEE Transactions on Information Theory*, 62(3):1485–1500.
- Scruton, D. A., McKinley, R. S., Kouwen, N., Eddy, W., and Booth, R. K. (2003). Improvement and optimization of fish guidance efficiency (FGE) at a behavioural fish protection system for downstream migrating Atlantic salmon (*Salmo salar*) smolts. *River Research and Applications*, 19(5-6):605–617.
- Serrano, I., Rivinoja, P., Karlsson, L., and Larsson, S. (2009). Riverine and early marine survival of stocked salmon smolts, *Salmo salar* L., descending the Testebo River, Sweden. *Fisheries Management and Ecology*, 16(5):386–394.
- Sevilla, J., Heim, L., Ho, A., Besiroglu, T., Hobbhahn, M., and Villalobos, P. (2022). Compute Trends Across Three Eras of Machine Learning.
- Sillett, T. S. and Holmes, R. T. (2002). Variation in survivorship of a migratory songbird throughout its annual cycle. *Journal of Animal Ecology*, 71(2):296–308.
- Silver, D., Schrittwieser, J., Simonyan, K., Antonoglou, I., Huang, A., Guez, A., Hubert, T., Baker, L., Lai, M., Bolton, A., Chen, Y., Lillicrap, T., Hui, F., Sifre, L., van den Driessche, G., Graepel, T., and Hassabis, D. (2017). Mastering the game of Go without human knowledge. *Nature*, 550(7676):354–359.
- Simonyan, K. and Zisserman, A. (2015). Very Deep Convolutional Networks for Large-Scale Image Recognition.
- Simpson, R., Page, K. R., and De Roure, D. (2014). Zooniverse: observing the world’s largest citizen science platform. In *Proceedings of the 23rd International Conference on World Wide Web, WWW ’14 Companion*, pages 1049–1054, New York, NY, USA. Association for Computing Machinery.
- Smouse, P. E., Focardi, S., Moorcroft, P. R., Kie, J. G., Forester, J. D., and Morales, J. M. (2010). Stochastic modelling of animal movement. *Philosophical Transactions of the Royal Society B: Biological Sciences*, 365(1550):2201–2211.
- Solow, A. R. and Smith, W. K. (2009). Estimating species number under an inconvenient abundance model. *Journal of Agricultural, Biological, and Environmental Statistics*, 14(2):242–252.

- Son, J., Baek, M., Cho, M., and Han, B. (2017). Multi-object Tracking with Quadruplet Convolutional Neural Networks. In *2017 IEEE Conference on Computer Vision and Pattern Recognition (CVPR)*, pages 3786–3795, Honolulu, HI. IEEE.
- Soto, D., Trueman, C., Samways, K., Dadswell, M., and Cunjak, R. (2018). Ocean warming cannot explain synchronous declines in North American Atlantic salmon populations. *Marine Ecology Progress Series*, 601:203–213.
- Sridhar, V. H., Roche, D. G., and Gingsins, S. (2019). Tracktor: Image-based automated tracking of animal movement and behaviour. *Methods in Ecology and Evolution*.
- Sridharan, V. K., Jackson, D., Hein, A. M., Perry, R. W., Pope, A. C., Hendrix, N., Danner, E. M., and Lindley, S. T. (2023). Simulating the migration dynamics of juvenile salmonids through rivers and estuaries using a hydrodynamically driven enhanced particle tracking model. *Ecological Modelling*, 482:110393.
- Stewart, R., Andriluka, M., and Ng, A. Y. (2016). End-to-End People Detection in Crowded Scenes. In *2016 IEEE Conference on Computer Vision and Pattern Recognition (CVPR)*, pages 2325–2333, Las Vegas, NV, USA. IEEE.
- Stockwell, C. L., Filgueira, R., and Grant, J. (2021). Determining the Effects of Environmental Events on Cultured Atlantic Salmon Behaviour Using 3-Dimensional Acoustic Telemetry. *Frontiers in Animal Science*, 2:701813.
- Stoilova, V. (2024). Behavioural Guidance Systems for Downstream Migrating Fish: A Mini-review. In *Advances in Hydraulic Research*, pages 385–396. Springer Nature Switzerland, Cham.
- Strandberg, R., Klaassen, R. H., Hake, M., Olofsson, P., and Alerstam, T. (2009). Converging migration routes of Eurasian hobbies *Falco subbuteo* crossing the African equatorial rain forest. *Proceedings of the Royal Society B: Biological Sciences*, 276(1657):727–733.
- Strandburg-Peshkin, A., Farine, D. R., Crofoot, M. C., and Couzin, I. D. (2017). Habitat and social factors shape individual decisions and emergent group structure during baboon collective movement. *eLife*, 6.
- Strøm, J. F., Thorstad, E. B., Hedger, R. D., and Rikardsen, A. H. (2018). Revealing the full ocean migration of individual Atlantic salmon. *Animal Biotelemetry*, 6(1):2.

- Sumpter, D. J. T., Szorkovszky, A., Kotrschal, A., Kolm, N., and Herbert-Read, J. E. (2018). Using activity and sociability to characterize collective motion. *Philosophical Transactions of the Royal Society B: Biological Sciences*, 373(1746):20170015.
- Szegedy, C., Liu, W., Jia, Y., Sermanet, P., Reed, S., Anguelov, D., Erhan, D., Vanhoucke, V., and Rabinovich, A. (2015). Going Deeper With Convolutions. pages 1–9.
- Szeliski, R. (2022). *Computer Vision: Algorithms and Applications, 2nd Edition*. Springer.
- Tan, J., Tao, L., Gao, Z., Dai, H., and Shi, X. (2018). Modeling Fish Movement Trajectories in Relation to Hydraulic Response Relationships in an Experimental Fishway. *Water*, 10(11):1511.
- Team, R. C. (2021). R: A Language and Environment for Statistical Computing.
- Thambithurai, D., Hollins, J., Van Leeuwen, T., Rácz, A., Lindström, J., Parsons, K., and Killen, S. S. (2018). Shoal size as a key determinant of vulnerability to capture under a simulated fishery scenario. *Ecology and Evolution*, 8(13):6505–6514.
- Thomas, P. A., Marshall, G., Faulkner, D., Kent, P., Page, S., Islip, S., Oldfield, J., Breckon, T. P., Kundegorski, M. E., Clark, D. J., and Styles, T. (2016). Toward sensor modular autonomy for persistent land intelligence surveillance and reconnaissance (ISR). page 983108, Baltimore, Maryland, United States.
- Thorstad, E., Uglem, I., Arechavala-Lopez, P., Økland, F., and Finstad, B. (2011). Low survival of hatchery-released Atlantic Salmon smolts during initial river and fjord migration. *Boreal Environment Research*, 16:115–120.
- Thorstad, E. B., Bliss, D., Breau, C., Damon-Randall, K., Sundt-Hansen, L. E., Hatfield, E. M., Horsburgh, G., Hansen, H., Maoiléidigh, N. Ó., Sheehan, T., and Sutton, S. G. (2021). Atlantic salmon in a rapidly changing environment—Facing the challenges of reduced marine survival and climate change. *Aquatic Conservation: Marine and Freshwater Ecosystems*, 31(9):2654–2665.
- Thorstad, E. B., Uglem, I., Finstad, B., Chittenden, C. M., Nilsen, R., Økland, F., and Bjørn, P. A. (2012a). Stocking location and predation by marine fishes affect survival of hatchery-reared Atlantic salmon smolts. *Fisheries Management and Ecology*, 19(5):400–409.

- Thorstad, E. B., Whoriskey, F., Uglem, I., Moore, A., Rikardsen, A. H., and Finstad, B. (2012b). A critical life stage of the Atlantic salmon *Salmo salar*: behaviour and survival during the smolt and initial post-smolt migration. *Journal of Fish Biology*, 81(2):500–542.
- Torney, C., Neufeld, Z., and Couzin, I. D. (2009). Context-dependent interaction leads to emergent search behavior in social aggregates. *Proceedings of the National Academy of Sciences*, 106(52):22055–22060.
- Torney, C. J., Hopcraft, J. G. C., Morrison, T. A., Couzin, I. D., and Levin, S. A. (2018a). From single steps to mass migration: the problem of scale in the movement ecology of the Serengeti wildebeest. *Philosophical Transactions of the Royal Society B: Biological Sciences*, 373(1746):20170012.
- Torney, C. J., Lamont, M., Debell, L., Angohiatok, R. J., Leclerc, L.-M., and Berdahl, A. M. (2018b). Inferring the rules of social interaction in migrating caribou. *Philosophical Transactions of the Royal Society B: Biological Sciences*, 373(1746):20170385.
- Torney, C. J., Lloyd-Jones, D. J., Chevallier, M., Moyer, D. C., Maliti, H. T., Mwita, M., Kohi, E. M., and Hopcraft, G. C. (2019). A comparison of deep learning and citizen science techniques for counting wildlife in aerial survey images. *Methods in Ecology and Evolution*, 10(6):779–787.
- Torrissen, O., Olsen, R. E., Toresen, R., Hemre, G. I., Tacon, A. G., Asche, F., Hardy, R. W., and Lall, S. (2011). Atlantic Salmon (*Salmo salar*): The “Super-Chicken” of the Sea? *Reviews in Fisheries Science*, 19(3):257–278.
- Towner, A. V., Leos-Barajas, V., Langrock, R., Schick, R. S., Smale, M. J., Kaschke, T., Jewell, O. J. D., and Papastamatiou, Y. P. (2016). Sex-specific and individual preferences for hunting strategies in white sharks. *Functional Ecology*, 30(8):1397–1407.
- Tušer, M., Frouzová, J., Balk, H., Muška, M., Mrkvička, T., and Kubečka, J. (2014). Evaluation of potential bias in observing fish with a DIDSON acoustic camera. *Fisheries Research*, 155:114–121.
- Uhlenbeck, G. E. and Ornstein, L. S. (1930). On the Theory of the Brownian Motion. *Physical Review*, 36(5):823–841.
- Valletta, J. J., Torney, C., Kings, M., Thornton, A., and Madden, J. (2017). Applications of machine learning in animal behaviour studies. *Animal Behaviour*, 124:203–220.

- Van Ginneken, V. J. T. and Maes, G. E. (2005). The European eel (*Anguilla anguilla*, Linnaeus), its Lifecycle, Evolution and Reproduction: A Literature Review. *Reviews in Fish Biology and Fisheries*, 15(4):367–398.
- Van Horn, G., Mac Aodha, O., Song, Y., Cui, Y., Sun, C., Shepard, A., Adam, H., Perona, P., and Belongie, S. (2017). The iNaturalist Species Classification and Detection Dataset. *arXiv:1707.06642 [cs]*.
- Vapnik, V. N. (1997). The Support Vector method.
- Vaswani, A., Shazeer, N., Parmar, N., Uszkoreit, J., Jones, L., Gomez, A. N., Kaiser, L. u., and Polosukhin, I. (2017). Attention is All you Need. In Guyon, I., Luxburg, U. V., Bengio, S., Wallach, H., Fergus, R., Vishwanathan, S., and Garnett, R., editors, *Advances in Neural Information Processing Systems*, volume 30. Curran Associates, Inc.
- Veselov, A., Kazakov, R., Sysoyeva, M., and Bahmet, I. (1998). Ontogenesis of rheotactic and optomotor responses of juvenile Atlantic salmon. *Aquaculture*, 168(1-4):17–26.
- Vicsek, T., Czirok, A., Ben-Jacob, E., Cohen, I., and Sochet, O. (1995). Novel type of phase transition in a system of self-driven particles. *Physical Review Letters*, 75(6):1226–1229.
- Vollset, K. W., Urdal, K., Utne, K., Thorstad, E. B., Sægrov, H., Raunsgard, A., Skagseth, Ø., Lennox, R. J., Østborg, G. M., Ugedal, O., Jensen, A. J., Bolstad, G. H., and Fiske, P. (2022). Ecological regime shift in the Northeast Atlantic Ocean revealed from the unprecedented reduction in marine growth of Atlantic salmon. *Science Advances*, 8(9):eabk2542.
- Vowles, A. S., Anderson, J. J., Gessel, M. H., Williams, J. G., and Kemp, P. S. (2014). Effects of avoidance behaviour on downstream fish passage through areas of accelerating flow when light and dark. *Animal Behaviour*, 92:101–109.
- Wagner, M. A. and Reynolds, J. D. (2019). Salmon increase forest bird abundance and diversity. *PLOS ONE*, 14(2):e0210031.
- Walter, T. and Couzin, I. D. (2021). TRex, a fast multi-animal tracking system with markerless identification, and 2D estimation of posture and visual fields. *eLife*, 10:e64000.
- Wan, E. and Van Der Merwe, R. (2000). The unscented Kalman filter for nonlinear estimation. In *Proceedings of the IEEE 2000 Adaptive Systems for Signal Processing, Communications, and Control Symposium (Cat. No.00EX373)*, pages 153–158, Lake Louise, Alta., Canada. IEEE.

- Wang, C.-Y., Yeh, I.-H., and Liao, H.-Y. M. (2024). YOLOv9: Learning What You Want to Learn Using Programmable Gradient Information. In *arXiv.org*.
- Wang, G. (2019). Machine learning for inferring animal behavior from location and movement data. *Ecological Informatics*, 49:69–76.
- Wang, Z., Zheng, L., Liu, Y., Li, Y., and Wang, S. (2020). Towards Real-Time Multi-Object Tracking. In *Computer Vision – ECCV 2020*, volume 12356, pages 107–122. Springer International Publishing, Cham.
- Ween, G. B. and Colombi, B. J. (2013). Two Rivers: The Politics of Wild Salmon, Indigenous Rights and Natural Resource Management. *Sustainability*, 5(2):478–495.
- Weihs, D. (1973). Hydromechanics of Fish Schooling. *Nature*, 241(5387):290–291.
- Welch, G. and Bishop, G. (2006). An Introduction to the Kalman Filter. page 16.
- Whoriskey, K., Martins, E. G., Auger-Méthé, M., Gutowsky, L. F. G., Lennox, R. J., Cooke, S. J., Power, M., and Mills Flemming, J. (2019). Current and emerging statistical techniques for aquatic telemetry data: A guide to analysing spatially discrete animal detections. *Methods in Ecology and Evolution*, 10(7):935–948.
- Wijeyakulasuriya, D. A., Eisenhauer, E. W., Shaby, B. A., and Hanks, E. M. (2020). Machine learning for modeling animal movement. *PLOS ONE*, 15(7):e0235750.
- Wikelski, M., Arriero, E., Gagliardo, A., Holland, R. A., Huttunen, M. J., Juvaste, R., Mueller, I., Tertitski, G., Thorup, K., Wild, M., Alanko, M., Bairlein, F., Cherenkov, A., Cameron, A., Flatz, R., Hannila, J., Hüppop, O., Kangasniemi, M., Kranstauber, B., Penttinen, M.-L., Safi, K., Semashko, V., Schmid, H., and Wistbacka, R. (2015). True navigation in migrating gulls requires intact olfactory nerves. *Scientific Reports*, 5(1):17061.
- Willcock, S., Martínez-López, J., Hooftman, D. A., Bagstad, K. J., Balbi, S., Marzo, A., Prato, C., Sciandrello, S., Signorello, G., Voigt, B., Villa, F., Bullock, J. M., and Athanasiadis, I. N. (2018). Machine learning for ecosystem services. *Ecosystem Services*, 33:165–174.
- Williams, H. J., Taylor, L. A., Benhamou, S., Bijleveld, A. I., Clay, T. A., de Grissac, S., Demšar, U., English, H. M., Franconi, N., Gómez-Laich, A., Griffiths, R. C., Kay, W. P., Morales, J. M., Potts, J. R., Rogerson, K. F., Rutz, C., Spelt, A., Trevail, A. M.,

- Wilson, R. P., and Börger, L. (2020). Optimizing the use of loggers for movement ecology research. *Journal of Animal Ecology*, 89(1):186–206.
- Wilson, A. J., Gíslason, D., Skúlason, S., Snorrason, S. S., Adams, C. E., Alexander, G., Danzmann, R. G., and Ferguson, M. M. (2004). Population genetic structure of Arctic Charr, *Salvelinus alpinus* from northwest Europe on large and small spatial scales. *Molecular Ecology*, 13(5):1129–1142.
- Wojke, N., Bewley, A., and Paulus, D. (2017). Simple Online and Realtime Tracking with a Deep Association Metric. *arXiv:1703.07402 [cs]*.
- Xu, Y., Ban, Y., Delorme, G., Gan, C., Rus, D., and Alameda-Pineda, X. (2022). TransCenter: Transformers with Dense Representations for Multiple-Object Tracking.
- Xu, Z. and Cheng, X. E. (2017). Zebrafish tracking using convolutional neural networks. *Scientific Reports*, 7(1).
- Xu, Z., Yin, X., Sun, T., Cai, Y., Ding, Y., Yang, W., and Yang, Z. (2017). Labyrinths in large reservoirs: An invisible barrier to fish migration and the solution through reservoir operation. *Water Resources Research*, 53(1):817–831.
- Xue, Y., Wang, T., and Skidmore, A. K. (2017). Automatic Counting of Large Mammals from Very High Resolution Panchromatic Satellite Imagery. *Remote Sensing*, 9(9):878.
- Yang, Z., Wang, T., Skidmore, A. K., Leeuw, J. d., Said, M. Y., and Freer, J. (2014). Spotting East African Mammals in Open Savannah from Space. *PLOS ONE*, 9(12):e115989.
- You, S., Yao, H., Bao, B.-k., and Xu, C. (2023). UTM: A Unified Multiple Object Tracking Model with Identity-Aware Feature Enhancement. In *2023 IEEE/CVF Conference on Computer Vision and Pattern Recognition (CVPR)*, pages 21876–21886, Vancouver, BC, Canada. IEEE.
- Zaburdaev, V., Denisov, S., and Klafter, J. (2015). Lévy walks. *Reviews of Modern Physics*, 87(2):483–530.
- Zhang, J., O’Reilly, K. M., Perry, G. L. W., Taylor, G. A., and Dennis, T. E. (2015). Extending the Functionality of Behavioural Change-Point Analysis with k-Means Clustering: A Case Study with the Little Penguin (*Eudyptula minor*). *PLOS ONE*, 10(4):e0122811.

- Zhang, T. (2004). Solving large scale linear prediction problems using stochastic gradient descent algorithms. In *Twenty-first international conference on Machine learning - ICML '04*, page 116, Banff, Alberta, Canada. ACM Press.
- Zhang, Y. and Lauder, G. V. (2023). Energetics of collective movement in vertebrates. *Journal of Experimental Biology*, 226(20):jeb245617.
- Zhang, Y., Sun, P., Jiang, Y., Yu, D., Weng, F., Yuan, Z., Luo, P., Liu, W., and Wang, X. (2022). ByteTrack: Multi-Object Tracking by Associating Every Detection Box.
- Zhang, Y., Wang, T., and Zhang, X. (2023). MOTRv2: Bootstrapping End-to-End Multi-Object Tracking by Pretrained Object Detectors. In *2023 IEEE/CVF Conference on Computer Vision and Pattern Recognition (CVPR)*, pages 22056–22065, Vancouver, BC, Canada. IEEE.
- Ziegler, D. M., Stiennon, N., Wu, J., Brown, T. B., Radford, A., Amodei, D., Christiano, P., and Irving, G. (2020). Fine-Tuning Language Models from Human Preferences.